

IN-15
110799

NASA Technical Memorandum 104752

P.213

LifeSat Engineering In-House Vehicle Design

A. Adkins, G. Badhwar, L. Bryant, J. Caram, G. Conley, T. Crull, P. Cuthbert, E. Darcy, P. DeLaune, M. Edeen, J. Engler, P. Fink, B. Gadd, M. Golightly, M. Gulizia, L. Hood, G. Jackson, J. Keller, M. Kilbourn, J. Kowal, C. Kroll, K. Kroll, L. Ling, A. Loomis, C. Madden, B. McCleary, R. Meyerson, C. Miller, R. Nuss, M. Richardson, E. Robertson, D. Rodriguez, D. Rogers, G. Roset, P. Shack, R. Spann, W. Stevens, B. Teasdale, M. Tigges, D. Tuckness, N. Wilks

July 1992

(NASA-TM-104752) LIFESAT
ENGINEERING IN-HOUSE VEHICLE DESIGN
(NASA) 213 p

N92-34080

Unclass

NASA

G3/15 0110799



LifeSat Engineering In-House Vehicle Design

G. Badhwar, L. Bryant, J. Caram, G. Conley, P. Cuthbert, E. Darcy, P. DeLaune, M. Edeen, P. Fink, M. Golightly, L. Hood, G. Jackson, M. Kilbourn, J. Kowal, K. Kroll, L. Ling, C. Madden, R. Meyerson, R. Nuss, M. Richardson, E. Robertson, D. Rodriguez, P. Shack, R. Spann, B. Teasdale, M. Tigges, N. Wilks
Lyndon B. Johnson Space Center
Houston, Texas

A. Adkins, J. Engler, B. Gadd, M. Gulizia, J. Keller, C. Kroll, C. Miller, D. Rogers, G. Roset, W. Stevens, D. Tuckness
Lockheed Corporation
Houston, Texas

T. Crull, B. McCleary
McDonnell Douglas Corporation
Houston, Texas

A. Loomis
Computer Sciences Corporation
Houston, Texas

National Aeronautics and Space Administration
Lyndon B. Johnson Space Center
Houston, Texas

July 1992

CONTENTS

Section		Page
1	<u>BACKGROUND</u>	1
1.1	PHASE A LIFESAT STUDY.....	1
1.2	PHASE B LIFESAT STUDY.....	1
2	<u>INTRODUCTION</u>	3
2.1	GALACTIC COSMIC RADIATION (GCR) ISSUES.....	3
2.2	JSC LIFESAT DESIGN TEAM.....	3
2.3	REVISED LIFESAT SCIENCE WORKING GROUP REQUIREMENTS.....	4
2.4	EVOLUTION OF LIFESAT MASS PROPERTIES.....	6
3	<u>LIFESAT PROJECT REQUIREMENTS FOR VEHICLE PERFORMANCE</u>	8
3.1	REQUIREMENTS SYNTHESIS.....	8
3.2	REQUIREMENTS DEVELOPMENT.....	8
3.3	FUNCTIONAL DECOMPOSITION.....	8
3.4	ADDITIONAL PRODUCTS OF THE LIFESAT FUNCTIONAL DECOMPOSITION.....	9
4	<u>RADIATION ENVIRONMENT</u>	10
4.1	INTRODUCTION.....	10
4.2	RADIATION EXPOSURE AND DEORBIT PERFORMANCE.....	10
4.3	CONCLUSIONS.....	13
4.4	RADIATION ENVIRONMENT SIMULATION.....	13
5	<u>CONFIGURATION DESCRIPTION</u>	15
5.1	EXPENDABLE LAUNCH VEHICLE PERFORMANCE.....	15
5.2	SPACECRAFT EXTERNAL CONFIGURATION.....	16
5.2.1	<u>Atmospheric Entry Trajectory</u>	16
5.2.2	<u>External Moldline</u>	16
5.2.3	<u>Sizing</u>	17
5.3	SPACECRAFT INTERNAL CONFIGURATION.....	17
5.4	PAYLOAD MODULE AND AUXILIARY PAYLOADS.....	18
5.5	MASS PROPERTIES.....	19
5.6	COMMUNICATION AND TRACKING (C&T).....	24
5.6.1	<u>Introduction</u>	24
5.6.2	<u>C&T Hardware</u>	24
5.6.2.1	Orbits.....	24
5.6.2.2	Data Throughput Required.....	24
5.6.2.3	Tracking Requirements.....	25
5.6.3	<u>C&T System</u>	25
5.6.3.1	Communications Hardware Options.....	25
5.6.3.1.1	<u>Option 1 - DSN</u>	25
5.6.3.1.2	<u>Option 2 - TDRSS</u>	27
5.6.3.1.3	<u>Option 3 - DSN on orbit TDRSS backup</u>	27
5.6.3.2	GPS Hardware.....	28
5.6.3.2.1	<u>Highly elliptical orbit</u>	28
5.6.3.2.2	<u>Effect of vehicle spinrate on antennas</u>	29
5.6.3.2.3	<u>Other issues</u>	29
5.6.3.2.4	<u>GPS size, weight and power estimate</u>	29
5.6.3.3	Antennas.....	30
5.6.3.3.1	<u>Fore/aft hemispherical antenna option</u>	30

Section		Page
5.6.3.3.2	<u>Circumferential belts option</u>	31
5.6.3.4	Summary and Recommendation	32
5.6.4	<u>Analysis</u>	33
5.6.4.1	Communications and Tracking Radio Frequency Coverage	33
5.6.4.1.1	<u>Sun visibility analysis</u>	33
5.6.4.1.2	<u>Deep Space Network ground station coverage</u>	34
5.6.4.1.2.1	Single LifeSat vehicle	34
5.6.4.1.2.2	Dual LifeSat vehicles	35
5.6.4.1.3	<u>TDRS East and TDRS West Coverage</u>	36
5.6.4.1.4	<u>Global Positioning System constellation coverage</u>	37
5.6.4.2	Link Margin Analysis	38
5.6.4.3	Service Comparison	38
5.6.5	<u>60-Day Elliptical Orbit</u>	39
5.6.5.1	Link Margin Analysis	39
5.6.5.2	Antennas	41
5.6.5.3	Conclusion	41
5.6.6	<u>Interfaces</u>	42
5.6.6.1	Power	42
5.6.6.2	Guidance, Navigation, and Control (GN&C)	42
5.6.6.3	Data Management System (DMS)	42
5.6.6.3.1	<u>Command and telemetry data</u>	42
5.6.6.3.2	<u>Control and monitoring</u>	42
5.6.6.3.2.1	Equipment control	42
5.6.6.3.2.2	Antenna management	42
5.6.6.3.2.3	Health and status	43
5.6.6.4	Thermal	43
5.6.6.5	Ground	43
5.6.6.6	Deep Space Network or Tracking and Data Relay Satellite System Network	44
5.6.7	<u>Conclusion</u>	44
5.7	GUIDANCE, NAVIGATION, AND CONTROL	45
5.7.1	<u>LifeSat Subsystem Description</u>	45
5.7.1.1	Guidance	45
5.7.1.2	Navigation	46
5.7.1.3	Control	46
5.7.2	<u>LifeSat Guidance, Navigation, and Control Avionics Design</u>	47
5.7.2.1	Introduction	47
5.7.2.2	Components	48
5.7.2.2.1	<u>Navigation system</u>	48
5.7.2.2.2	<u>Control system</u>	48
5.7.2.3	Architecture	49
5.7.2.4	Power Requirements	52
5.7.2.5	Design Conclusions and Issues	53
5.7.3	<u>Navigation State Integrator Model Comparison</u>	54
5.7.4	<u>Momentum Wheel Sizing</u>	54
5.8	PROPULSION	56
5.8.1	<u>Introduction</u>	56
5.8.2	<u>Fault Tolerance</u>	56
5.8.3	<u>Thrust Determination</u>	56
5.8.4	<u>Propellant Quantity</u>	57
5.8.5	<u>System Sizing</u>	58
5.8.6	<u>Power</u>	59
5.9	THERMAL PROTECTION SYSTEM	59
5.9.1	<u>Thermal Analysis</u>	60

Section		Page
5.9.2	<u>Results</u>	61
5.9.2.1	Thermal Protection System	61
5.9.2.2	Passive Thermal Control System.....	62
5.9.3	<u>Conclusions</u>	63
5.10	THERMAL CONTROL SYSTEM	70
5.10.1	<u>Cooling System Requirements and Goals</u>	71
5.10.2	<u>Development of the Cooling System</u>	72
5.10.2.1	Determination of Vehicle Heat Loads	72
5.10.2.1.1	<u>Vehicle-generated heat loads</u>	72
5.10.2.1.2	<u>Environmental heat loads</u>	72
5.10.2.2	Development of a Numerical Model of the TCS	73
5.10.2.2.1	<u>Development of the basic model</u>	73
5.10.2.2.2	<u>Radiator model development</u>	75
5.10.2.2.3	<u>Fluid Selection</u>	77
5.10.2.2.4	<u>Results of the modeling process</u>	77
5.10.2.3	Cooling System Modifications for the Redundancy Requirements	78
5.10.2.4	Thermal Storage System.....	80
5.10.2.5	PM Refrigeration System.....	81
5.10.3	<u>Weight, Volume, and Cost Estimates</u>	81
5.10.4	<u>Summary and Conclusions</u>	82
5.10.5	<u>Recommendations for Future Work</u>	82
5.11	ELECTRICAL POWER REQUIREMENTS	84
5.11.1	<u>Introduction</u>	84
5.11.2	<u>Assumptions</u>	84
5.11.2.1	Timeline.....	84
5.11.2.2	Subsystems.....	85
5.11.3	<u>Results</u>	86
5.11.4	<u>Design Options</u>	87
5.11.4.1	Primary Battery	87
5.11.4.2	Primary Fuel Cell.....	87
5.11.4.3	Hybrid (Primary and Secondary)	87
5.11.5	<u>Baseline System</u>	88
5.11.5.1	Primary Nonrechargeable Battery.....	88
5.11.5.2	PV/Secondary Battery	88
5.11.5.3	Distribution and Control.....	88
5.11.5.4	Estimated Cost.....	88
5.11.6	<u>Conclusions</u>	90
5.12	DATA SYSTEM	90
5.12.1	<u>Data Management Subsystem</u>	90
5.12.2	<u>Data Management System Components</u>	90
5.12.2.1	Central Processing Unit.....	91
5.12.2.2	Mass Storage	91
5.12.3	<u>Interfaces</u>	91
5.12.3.1	Guidance, Navigation, and Control.....	92
5.12.3.2	Payload.....	92
5.12.3.3	Communications and Tracking	92
5.12.3.4	Radiation Detectors	92
5.12.3.5	Power and Propulsion.....	92
5.13	SOFTWARE.....	93
5.13.1	<u>LifeSat Flight Software Conceptual Design and Development</u> <u>Planning Assumptions</u>	93
5.13.2	<u>Purpose</u>	93
5.13.3	<u>Software Functional Decomposition</u>	94
5.13.4	<u>Cost Estimate Methodology</u>	94

Section		Page
5.13.5	<u>Software Estimate Abstract</u>	95
5.14	LIFE SUPPORT SYSTEM.....	95
5.14.1	<u>Requirements</u>	95
5.14.2	<u>Life Support System Conceptual Design</u>	97
5.14.3	<u>Water Vapor Removal Options</u>	99
6	<u>MISSION DESCRIPTION</u>	100
6.1	DESIGN REFERENCE MISSIONS.....	100
6.2	LIFESAT TRAJECTORY OVERVIEW.....	100
6.3	OPERATIONAL PHASES.....	100
6.4	PRELAUNCH PHASE.....	101
6.5	LAUNCH PHASE.....	102
6.6	STEADY-STATE OPERATION PHASE.....	104
6.7	LANDING PHASE.....	105
6.8	POSTLANDING PHASE.....	106
7	<u>FLIGHT DYNAMICS</u>	107
7.1	BALLISTIC ENTRY DYNAMICS.....	107
7.1.1	<u>Entry Profile Dynamics</u>	107
7.1.2	<u>Analysis</u>	108
7.1.3	<u>Results</u>	109
7.1.4	<u>Conclusions</u>	112
7.2	CENTRIFUGE DYNAMICS.....	113
7.2.1	<u>Effects of the Moving Mice on the Centrifuge</u>	113
7.2.1.1	Worst Case CG Offset.....	113
7.2.1.2	Effect of Moving Mice on LifeSat Angular Velocity.....	114
7.2.2	<u>Vibration Analysis for an Unbalanced Centrifuge</u>	115
7.2.3	<u>Conclusions</u>	116
7.3	TAPE DRIVE DYNAMICS.....	117
7.3.1	<u>Tape Drive Start Up and Stop Transient Effects in Microgravity</u>	117
7.3.1.1	Characteristics of Tape Drives and Vehicle.....	117
7.3.1.2	Effects on the Micro-g of Experiment.....	117
7.3.1.3	Results.....	118
7.3.1.4	Conclusions.....	119
8	<u>LANDING ANALYSIS</u>	122
8.1	LANDING OPPORTUNITIES FROM CIRCULAR ORBITS.....	122
8.1.1	<u>Assumptions and Background</u>	122
8.1.2	<u>Methodology</u>	123
8.1.3	<u>Empirical Results</u>	124
8.1.4	<u>Theoretical Discussion</u>	127
8.1.5	<u>Conclusions</u>	129
8.2	ENTRY FOOTPRINT ANALYSIS.....	129
8.2.1	<u>Mission Scenarios</u>	130
8.2.2	<u>Footprint Analysis Assumptions</u>	131
8.2.2.1	Vehicle and Environment Assumptions.....	132
8.2.2.2	Monte Carlo Dispersions.....	132
8.2.3	<u>Footprint Analysis Results</u>	133
8.2.3.1	Proposed Landing Areas.....	133
8.2.3.2	Monte Carlo Analysis.....	135
8.2.3.3	Nominal Atmospheric Entry.....	137
8.2.3.4	Landing Footprint Sensitivities.....	141
8.2.4	<u>Conclusions</u>	142

Section		Page
9	<u>REFERENCES</u>	143
APPENDIX A	<u>LIFESAT ENGINEERING BASELINE REQUIREMENTS FOR VEHICLE PERFORMANCE</u>	A-1
APPENDIX B	<u>FUNCTIONAL DECOMPOSITION</u>	B-1
APPENDIX C	<u>MASS AND DESIGN DETAILS</u>	C-1
APPENDIX D	<u>LIFESAT GN&C AVIONICS COMPONENTS</u>	D-1
APPENDIX E	<u>NAVIGATION STATE INTEGRATOR MODEL COMPARISON</u>	E-1
APPENDIX F	<u>THERMAL PROTECTION SYSTEM</u>	F-1
APPENDIX G	<u>ENVIRONMENTAL HEAT LOADS</u>	G-1
APPENDIX H	<u>SUBSYSTEM COMPONENT DUTY CYCLE ASSUMPTIONS</u>	H-1
APPENDIX I	<u>DETAILED LOC AND COMPLEXITY ESTIMATE</u>	I-1
APPENDIX J	<u>LAUNCH AND LANDING ACTIVITIES</u>	J-1

TABLES

Table	Page
4-1 RADIATION DOSAGE, DEORBIT PERFORMANCE, ABORT CAPABILITY	11
5-1 ATLAS II SERIES PAYLOAD PERFORMANCE FOR THE BEO	16
5-2 JSC LIFESAT MASS PROPERTIES STATEMENT	23
5-3 OPTION 1 - DSN	27
5-4 OPTION 2 - TDRSS	27
5-5 OPTION 3 - DSN/TDRSS	28
5-6 GPS RECEIVER	30
5-7 FORE/AFT HEMISPHERICAL OPTION	31
5-8 CIRCUMFERENTIAL BELTS OPTION	32
5-9 C&T OPTIONS SUMMARY	33
5-10 PERCENTAGES OF TIME SUN IS IN AND OUT OF VIEW OF LIFESAT	34
5-11 COVERAGE STATISTICS BETWEEN LIFESAT AND THE DSN GROUND STATIONS	35
5-12 ON-ORBIT COVERAGE ANALYSIS TO TDRS EAST AND WEST	37
5-13 SERVICE COMPARISON	39
5-14 SUMMARY OF RESULTS	40
5-15 C&T POWER REQUIREMENTS	42
5-16 THERMAL REQUIREMENTS FOR C&T EQUIPMENT	43
5-17 LIFESAT MOMENTUM WHEEL SIZING RESULTS	55
5-18a PROPELLANT USAGE SCENARIO	58
5-18b PROPULSION SYSTEM MASS SUMMARY	59
5-18c PROPULSION SYSTEM POWER SUMMARY	59
5-19 TPS CHARACTERISTICS FOR NOMINAL HEATING AND 300°F STRUCTURE TEMPERATURE LIMIT	64
5-20 EFFECT OF STRUCTURE TEMPERATURE LIMIT AND HEATING ON TPS WEIGHT	64
5-21 TPS CHARACTERISTICS FOR ESTIMATED 60-DAY ORBIT TRAJECTORY AND 300°F STRUCTURE TEMPERATURE LIMIT	64
5-22 TPS WEIGHT FOR ESTIMATED 60-DAY ORBIT TRAJECTORY	64
5-23 DEFINITION OF LIFESAT MISSION PHASES USED IN ELECTRICAL LOAD ANALYSIS	84
5-24 RODENT MODULE DESIGN REQUIREMENTS	96
5-25 WEIGHT, POWER, AND VOLUME REQUIREMENTS	98
5-26 WATER VAPOR REMOVAL COMPARISON	99
7-1 AERODYNAMIC FORCE COEFFICIENTS	110
7-2 MASS PROPERTIES	111
7-3 RESULTS OF DISK DRIVES MICRO-G ANALYSIS	120
8-1 TYPICAL ENTRY TIMELINE (900 km CIRCULAR ORBIT)	130
8-2 VEHICLE AND PARACHUTE AERODYNAMIC COEFFICIENTS	132
8-3 AERODYNAMIC AND MASS DISPERSION MAGNITUDES	133
8-4 MONTE CARLO NOMINAL AND DISPERSED PERFORMANCE	138
8-5 CONTRIBUTORS TO FOOTPRINT MAGNITUDE - 900 km MISSION	141
8-6 MISS DISTANCE SENSITIVITIES, OPEN LOOP DEORBIT GUIDANCE - 900 km MISSION	142
E-1 INTEGRATOR/STEPSIZE COMPARISONS (IN ORDER OF SPEED- FASTEST TO SLOWEST)	E-2

Table		Page
G-1	LIFESAT NONORBIT HEAT BUDGET	G-4
G-2	THERMAL STORAGE SYSTEM WEIGHTS.....	G-4
G-3	WEIGHT, VOLUME AND COST ESTIMATES FOR THE LIFESAT VEHICLE.....	G-5
G-4	PAYLOAD MODULE REFRIGERATION SYSTEM ESTIMATES	G-5
J-1	DELTA II PRELAUNCH ACTIVITIES.....	J-1
J-2	THE RRS PRELAUNCH TIMELINE	J-2
J-3	THE RRS LAUNCH TIMELINE	J-3
J-4	THE RRS LANDING PHASE TIMELINE	J-4
J-5	THE RRS POSTLANDING PHASE TIMELINE.....	J-5

FIGURES

Figure		Page
2-1	Reusable Reentry Satellite Mass Comparison.....	7
4-1	Van Allen Belt and LifeSat Elliptical Orbit Polar Orientation.....	12
4-2	Van Allen Belt and LifeSat Elliptical Orbit Aligned for Landing	12
4-3	Performance and Radiation Versus Argument of Perigee.....	13
5-1	LifeSat External View - Operational Mode.....	20
5-2	Potential LifeSat Delta II Launch Configurations.....	20
5-3	LifeSat Internal View - Solar Arrays Blanked	21
5-4	Proposed LifeSat Landing Configuration	21
5-5	Payload Module Interior Layout.....	22
5-6	Option 1 Block Diagram.....	26
5-7	Typical Ground Track for 275 km Altitude Circular Orbit	34
5-8	Functional Block Diagram	49
5-9	Avionics Architecture - Option 3.....	51
5-10a	Power Requirements.....	52
5-10b	ACS Thruster Arrangement.....	57
5-10c	Propulsion System Schematic.....	58
5-11	Preliminary Entry Trajectory	65
5-12	Thermal Analysis Body Point Locations.....	66
5-13	Thermal Protection System Thermal Math Model.....	66
5-14	Passive Thermal Control System Thermal Math Model.....	67
5-15	Preliminary TPS Configuration.....	67
5-16	Internal Insulation Requirements (Nose Region)	68
5-17	Internal Insulation Requirements (Cone Region).....	68
5-18	Internal Insulation Requirements (Base Region).....	69
5-19	Internal Insulation Requirements (Cone Region).....	69
5-20	Internal Insulation Requirements (Cone Region).....	70
5-21	Schematic of the Flow Network.....	73
5-22	Schematic of the SINDA/FLUINT Model.....	75
5-23	Sectional View of a Radiator Panel	76
5-24	SINDA/FLUINT Representation of a Radiator Flow Passage.....	77
5-25	SINDA/FLUINT Representation of a Radiator Wall Panel	77
5-26	Schematic of the TCS Including Redundancy Requirements.....	79
5-27	Schematic of the Pump Monitoring System	80
5-28	LifeSat Average Power Loads	86
5-29	Hybrid Power System Concept.....	89
5-30	DMS Block Diagram (one string of the two-string system).....	91
5-31	Conceptual Design of the LifeSat Life Support System.....	97
6-1	An Event Overview of the Phases.....	101
6-2	A Delta II 7920 Mission Profile.....	103
7-1	Processor Analysis Flow.....	108
7-2	LifeSat Orientation Parameters.....	110
7-3	Nominal Entry Trajectory Plots	111
7-4	Dispersed CG Trajectory.....	112
7-5	Scenario for Worst Case CG Offset in Centrifuge.....	114
7-6	Inertial and Relative Coordinate Systems for the Vehicle and Experiment	119
7-7	G-load Contour for Case d	121
8-1	Possible Groundtrack Shifts for a 275 km Orbit.....	123

Figure		Page
8-2	Landing Opportunity Availability for One Hypothetical Mission	124
8-3	Lighting Conditions for WSMR Landings	125
8-4	Lighting Conditions for Landings Near Canberra, Australia	126
8-5	Landing Opportunity Availability as a Function of Additional Propellant	127
8-6	Landing Opportunity Availability for Sites to 32.5 Degree Latitude	128
8-7	LifeSat Mission Scenario Categories for Footprint Analysis	131
8-8	Sketch of White Sands Missile Range	135
8-9	Example of Monte Carlo Landing Locations for 900 km Mission	136
8-10	Total Footprint Downrange Distance Versus Nominal Entry G-Load	136
8-11	Nominal Entry Trajectories (Page 1 of 2)	139
8-11	Nominal Entry Trajectories (Page 2 of 2)	140
B-1	LifeSat Level One Functional Flow	B-7
B-2	LifeSat Level One Functional Interface N**2	B-8
B-3	LifeSat Level One Functional Flow	B-9
B-4	LifeSat Level One Functional Interface N**2	B-10
G-1	Sectional View of the Vehicle	G-1

ACRONYMS AND SYMBOLS

ACS	Attitude Control System
AFRSI	Advanced Flexible Reusable Surface Insulation
AOS	Acquisition of Signal
ATCO	Ambient Temperature Catalytic Oxidizer
BEO	Big Elliptical Orbit
BTU	British Thermal Unit
CCSDS	Consultative Committee for Space Data Systems
Cd	Coefficient of drag
CG	Center of Gravity
CMG	Control Moment Gyro
CPU	Central Processing Unit
CRIT-1	Criticality-1
CSC	Computer Software Component
CSCI	Computer Software Configuration Item
C&T	Communications and Tracking
dB	Decibels
deg	Degrees
DMS	Data Management System
DOD	Department of Defense
DPPG	Commercial Delta II: Payload Planners Guide
DRM	Design Reference Mission
DSN	Deep Space Network
ECLSS	Environmental Control and Life Support System
EI	Entry Interface
EIRP	Effective Isotropic Radiated Power
ELV	Expendable Launch Vehicle
EMI	Electromagnetic Interference
EPDC	Electrical Power Distribution Control
ETR	Eastern Test Range
F-	Flight minus (days)
FLUINT	Fluid Integrator
FRCI-12	Fibrous Refractory Composite Insulation
FRSI	Flexible Reusable Surface Insulation
ft	Feet
g	Gravity Constant
GBM	General Biology Module
GCEM	Ground Control Experiment Module
GCR	Galactic Cosmic Radiation
GE	General Electric
GMT	Greenwich Mean Time
GN&C	Guidance, Navigation, and Control
GPS	Global Positioning System

GRAMM-88	Global Reference Atmospheric Model
GSE	Ground Support Equipment
GSTDN	Ground Space Tracking and Data Network
HRSI	High-Temperature Reusable Surface Insulation
IFMU	Integrated Flight Management Units
IMU	Inertial Measurement Unit
INS	Inertial Navigation System
JPL	Jet Propulsion Laboratory
JSC	Johnson Space Center
JUNC	Junction
Kbps	Kilobits per second
km	Kilometer
KSC	Kennedy Space Center
lbf	Pounds Force
lbm	Pounds Mass
LEO	Low Earth Orbit
LI-900	Lockheed Insulation, 9 pcf density
LI-2200	Lockheed Insulation, 22 pcf density
LifeSat	Life Sciences Satellite
LOC	Lines of Code
LOS	Loss of Signal
LSS	Life Support System
LSSWG	LifeSat Science Working Group
M	Mach number
MA	Multiple Access
Mb	Megabits
Mbps	Megabits per second
MECO	Main Engine Cutoff
MET	Mission Elapsed Time
MFRSET	Mass Flow Rate Set
MLI	Multi-Layer Insulation
MSL	Mean Sea Level
MST	Missile Service Tower; gantry
nm	Nautical Mile
PI	Principal Investigator
PLEN	Plenum
PLF	Payload Fairing
PLS	Personnel Launch System
PM	Payload Module
PRD	Project Requirements Document

PTCS	Passive Thermal Control System
PV	Photovoltaic
rad	Radiation Absorbed Dosage
RCG	Reaction Cured Glass
RF	Radio Frequency
RFI	Radio Frequency Interference
RPM	Revolutions per Minute
RRS	Reusable Reentry Satellite
RSI	Reusable Surface Insulation
RSS	Root-Sum-Square
s	Standard Deviation
SA	Single Access
SAIC	Science Applications International Corporation
SARAT	Search and Rescue Antenna
SARSAT	Search and Rescue Satellite
SCSI	Small Computer System Interface
SDIO	Strategic Defense Initiative Organization
sec	Second
SECO	Stage Two Engine Cutoff
SEP	Spherical Error Probability
SINDA	Systems Improved Numerical Differencing Analyzer
SMA	S-Band Multiple Access
SOW	Statement of Work
SPS	Standard Positioning Service
sq ft	Square Feet
SR&QA	Safety, Reliability and Quality Assurance
SSA	S-Band Single Access
SSF	Space Station Freedom
TBD	To Be Determined
TCS	Thermal Control System
TDRS	Tracking and Data Relay Satellite
TDRSS	Tracking and Data Relay Satellite System
TMM	Thermal Math Model
TPS	Thermal Protection System
TSS	Thermal Synthesizer System
WBS	Work Breakdown Structure
WFOV	Wide Field-of-View
WRT	With Respect To
WSMR	White Sands Missile Range
XMIT	Transmit
XPNDR	Transponder
ZOE	Zone of Exclusion
a	Albedo
F _{ij}	View Factor

k	Conductivity
L	Length of Thickness
$Q_{\text{conduction}}$	Conduction Heat Flux
Q_{Earth}	Earth Emitted Flux
Q_{emitted}	Reradiated Vehicle Heat Flux
$Q_{\text{absorbed - Earth}}$	Absorbed Radiated Flux From Earth
$Q_{\text{absorbed - sun}}$	Absorbed Radiated Flux From the Sun
Q_{solar}	Solar Flux
T_{int}	Internal Temperature
T_s	Surface Temperature
α	Absorptivity
ϵ	Emissivity
σ	Stefan-Boltzmann Constant

CONTRIBUTORS

Adkins, Antha	(LESC/C80)	Kroll, Ken	(NASA/EP4)
Badhwar, G. D./PHD	(NASA/SN31)	Ling, Lisa	(NASA/ET4)
Bryant, Lee	(NASA/ET4)	Loomis, Audrey	(CSCSSD)
Caram, Joe	(NASA/EG3)	Madden, Christopher	(NASA/ES3)
Conley, Gary	(NASA/ET3)	McCleary, Bret	(MDCA/2MK)
Crull, Tim	(MDCA219)	Meyerson, Rob	(NASA/EG3)
Cuthbert, Pete	(NASA/ET4)	Miller, Chuck	(LESC/C07B)
Darcy, Eric	(NASA/EP5)	Nuss, Ray	(NASA/EE6)
DeLaune, Paul	(NASA/EK6)	Richardson, Michael	(NASA/IA151)
Edeen, Marybeth	(NASA/EC7)	Robertson, Ed	(NASA/ET2)
Engler, J.	(LESC/C87)	Rodriguez, David	(NASA/ET3)
Fink, Pat	(NASA/EE3)	Rogers, Dick	(LESC/CO3)
Gadd, Bill	(LESC/C80)	Roset, Gerry	(LESC/C18)
Golightly, Mike	(NASA/SN31)	Shack, Paul	(NASA/EE3)
Gulizia, Mike	(LESC/C87)	Spann, Robert	(NASA/IA151)
Hood, Laura	(NASA/EE7)	Stevens, William	(LESC/CO3)
Jackson, Gary L.	(NASA/NB5)	Teasdale, Bill	(NASA/EE)
Keller, John/PHD	(LESC/C70)	Tigges, Mike	(NASA/ET4)
Kilbourn, Max	(NASA/ET3)	Tuckness, D. G./PHD	(LESC/C87)
Kowal, John	(NASA/ES3)	Wilks, Nancy	(NASA/ET3)
Kroll, Chip	(LESC/C80)		

SECTION 1 BACKGROUND

(Prepared by Edward Robertson)

The LifeSat program was initiated at the NASA/Ames Research Center in 1988 to research the effects of microgravity and cosmic radiation on living organisms. The effects of long-term human exposure to free-space radiation fields over a range of gravitational environments has long been recognized as one of the primary design uncertainties for human space exploration. Ground-based research cannot adequately simulate a space radiation environment, which provides simultaneous exposure to a wide spectrum of photon and particle radiation, nor can it adequately simulate reduced gravity fields. The Reusable Reentry Satellite (RRS), or LifeSat concept, was proposed to provide relatively frequent and "inexpensive" scientific access to a space environment for periods of up to 60 days.

1.1 PHASE A LIFESAT STUDY

NASA/Ames conducted a Phase A feasibility study (NASA TM 101043, "A Conceptual Design Study of the Reusable Reentry Satellite," October 1988) which focused on spacecraft designs satisfying the top-level LifeSat science requirements. Included in the top-level documentation were the requirements for a payload module (PM) to support up to 12 rodents ranging in mass from 24 to 600 grams and a general biology module (GBM) supporting lower life forms for an on-orbit duration of up to 60 days. At the end of the mission, the spacecraft would deorbit and perform a soft landing in the continental United States to facilitate quick access to the payload contents. The design emphasized the reuse of recovered spacecraft hardware for subsequent missions. The intended flight rate was set at three flights per year over a 10-year period using a Delta II-class expendable launch vehicle (ELV).

The Phase A study produced a spacecraft conceptual design resembling a Discoverer configuration with a total weight of approximately 2800 pounds. The spacecraft would carry a 525-pound PM 45 inches in diameter and 36 inches long.

1.2 PHASE B LIFESAT STUDY

In August of 1988, the LifeSat project management responsibility was transferred to the Johnson Space Center (JSC), and the Phase A study results were incorporated into a Phase B statement of work. In January of 1989, NASA/JSC released "A Request for Proposal" for a LifeSat Phase B design effort. The first of two contracts was awarded to General Electric (GE) Aerospace with subcontract support by Lockheed Missiles and Space Company. The second contract, awarded much later in the Phase B study, was

given to Science Applications International Corporation (SAIC) with subcontract support by Fairchild Space. Each contract was funded at \$1M over a period of 9 months.

The two prime contractors, GE Aerospace and SAIC, produced Phase B reports in FY 1990 emphasizing gravitation research in a circular low Earth orbit (LEO) with integrated rodent modules capable of supporting 18 rats for up to 60 days. Both contractors selected an axisymmetric spacecraft outer moldline and a ballistic atmospheric entry trajectory with ablator thermal protection. The GE design was derived from the proven Discoverer geometry while the SAIC design used a larger forebody cone angle and a smaller nose radius. The contractors split on their concepts for producing artificial gravity. GE used a more traditional design, spinning the spacecraft about its longitudinal axis, while SAIC opted for a lower RPM, end-over-end rotation using a deployable, 100-foot Astromast truss. The contractors also varied in their approach toward power generation. GE relied solely on lithium thionyl chloride (Li-SOCl₂) primary batteries supplying 127W average power over a 60-day mission. The SAIC design supplied approximately 200W average power using a combination of body-mounted gallium arsenide/germanium (GaAs/Ge) solar arrays and nickel-hydrogen (Ni-H₂) secondary batteries. The contractors considered both steerable parafoil main parachutes and Apollo-type ringsail parachutes for the terminal descent phase. GE baselined steerable parachute technology because of its potential to provide crossrange control and to reduce the magnitude of the ground impact velocity by employing a flare maneuver. SAIC baselined ringsail parachutes because of their proven flight performance and design simplicity, accepting a penalty both in footprint size and impact velocity as compared to proposed parafoil designs.

The GE and SAIC Phase B conceptual designs focused on gravitation biology requirements and only briefly addressed the design impacts of the shift toward radiobiological science that occurred during the latter half of the Phase B studies. The LifeSat Science Working Group (LSSWG) provided a revised requirements document to NASA/JSC in the second quarter of FY 1991.

SECTION 2

INTRODUCTION

(Prepared by Edward Robertson)

The objective of the JSC LifeSat Project Office was to provide a smooth transition for the LifeSat program from a Phase B to a Phase C/D status at the beginning of FY 1992. The engineering team was tasked to support the Project Office in the evaluation of the LifeSat design requirements and the release of a statement of work (SOW) in the first quarter of FY 1992. The in-house reference design generated during the study would be used for the evaluation of Phase C/D contractor proposals.

2.1 GALACTIC COSMIC RADIATION (GCR) ISSUES

A critical design issue in the radiation biology requirements was the lack of definition of the minimum radiation absorbed dosage (rad) required to produce statistically meaningful data. During a rodent radiation experiment there would be a number of cells killed, a number of cells wounded and subsequently killed by the immune system of the organism, and a number of cells that would exhibit a radiation-induced mutation and survive. At low dose rates and low total absorbed dosage, it can be difficult to statistically separate the radiation-induced effects from the background level of mutagenesis exhibited by a control group of organisms. The difficulty is increased by the large number of confounding variables present in a space-based experiment.

For GCR experimentation, the desired radiation dosage for statistically meaningful data was perceived to be in the range of 10 rads, depending on both the number of specimens and the "purity" of the radiation field. Since the maximum achievable GCR dosage is approximately 1.5 rads per month in free space, a mission of at least 200 days would be required to accumulate the desired level of exposure. In the highly elliptical orbit chosen for the GCR missions, the dosage is approximately 60 percent of the free space rate, and the absorbed radiation includes a significant amount of trapped proton and electron radiation from repeated passages through the Van Allen Belts.

2.2 JSC LIFESAT DESIGN TEAM

The JSC design team was assembled in March of 1991 with membership from the LifeSat Project Office, the Life Sciences Directorate, the Engineering Directorate, and Safety, Reliability and Quality Assurance (SR&QA). Systems integration techniques were applied during the design process to promote the goals of simplicity in design and operation and overall mission cost-effectiveness under the LSSWG design requirements.

The inclusion of SR&QA personnel on the preliminary design team was a test of concurrent design techniques for NASA/JSC. Traditionally SR&QA personnel have been involved much later in the design process, resulting in costly program delays for redesign and reevaluation. The concurrent design experience revealed some shortcomings in the definition of SR&QA safety policies and their engineering application in the preliminary design process.

SR&QA safety policy, derived largely from JSC experience in manned spaceflight, calls for a minimum of two-fault tolerance (three-string redundancy) on Criticality-1 (CRIT-1) spacecraft functions (those involving possible loss of human life), although a waiver may be granted on the basis of demonstrated subsystem reliability. Criticality-2 (CRIT-2) functions (related to mission success) call for single-fault tolerance (two-string redundancy). The safety and reliability policies do not address unique design situations, such as propulsion system design, in which hardware redundancy may actually decrease overall system reliability. Also, no distinctions are made between the immediate safety risks involved with the operation of a manned spacecraft and the indirect safety risks associated with the reentry and landing of a robotic spacecraft. In the latter case, the robotic spacecraft would not only have to miss its intended landing footprint, but also strike in proximity to a human being in order to threaten human life.

The subsystem design engineers initially found the SR&QA safety policies to be highly restrictive. At the preliminary design stage, many of the engineers were more familiar with designing on a subsystem level rather than a functional level. In the face of mass and volume limitations, however, it was not reasonable to simply triple the mass and volume estimates of a single-string system to approximate a three-string system. Designing for redundant hardware and operations on a functional level resulted in a more mass-efficient design solution.

The engineers also found that in many cases a CRIT-1 function, such as the LifeSat deorbit burn, had roots in several spacecraft subsystems, leading to widespread three-string redundancy. The avionics, power, and thermal control subsystems were particularly subject to the cascading effect of functional redundancy. However, with close cooperation between subsystem engineers and SR&QA personnel, the team met the safety requirements using a combination of hardware redundancy and contingency spacecraft operations. Despite initial difficulties, early SR&QA inputs were of significant benefit during the preliminary design process and resulted in a higher quality product.

2.3 REVISED LIFESAT SCIENCE WORKING GROUP REQUIREMENTS

Early in the JSC study, several critical requirements were identified by the design team within the revised requirements document. Of particular importance was the addition of a requirement for a high apogee elliptical orbit, initially specified at 350 by 35,000 km altitude. The high apogee orbit was added to provide payload exposure to GCR with the intention of matching the

free space GCR spectrum (including the particle mass distribution, particle energy distribution, and particle flux) as closely as possible. The high apogee orbit indirectly constrained the allowable mass of the spacecraft due to the payload performance limits of the Delta II 7925 ELV selected during the contractor Phase B studies. Even at the 350 by 20,600 km orbit selected to maximize useful GCR exposure, the Delta II 7925 is limited to less than 3500 lbm of payload. Compounding the effect of the loss in ELV payload capacity was an increase in the thermal protection system (TPS) mass of the spacecraft. The 20,600 km apogee orbit produced higher atmospheric entry velocities and higher stagnation temperatures than the Phase B circular LEO, resulting in a thicker layer of ablative TPS. Even the lightweight GE Phase B design proposal, when modified for the highly elliptical orbit, would exceed the launch capacity of the Delta II 7925 to the highly elliptical orbit.

The high apogee orbit also affected the selection of avionics components. The lack of global positioning system (GPS) coverage above approximately 4000 km altitude forced the addition of an independent system to support the deorbit maneuver. An inertial navigation system (INS) was used to propagate the spacecraft velocity vector from the time of the last GPS update to the initiation of the deorbit burn occurring near apogee. A final GPS update was used to evaluate the necessity for trim burns prior to reaching Earth entry interface.

In the Phase B studies, the contractors emphasized the use of integrated PMs containing both the pressurized experiment vessel and the life support hardware and consumables (i.e. the "rodent module"). In the revised requirements the LSSWG shifted the responsibility for life support from the PM to the spacecraft and modified the requirements for the GBM. The GBM was defined to support mixed payloads containing cell and tissue samples and populations of organisms. The experiment packages would obtain life support gases from the ambient PM atmosphere as needed and dump waste gases and thermal energy back into the air flow. The spacecraft assumed the functions of atmospheric temperature, mixture and humidity control, and waste gas removal which increased the number of spacecraft/PM interfaces and the complexity of the vehicle integration task. Under the revised requirements, mice became the organisms of primary interest rather than the rats baselined in the Phase B studies, a concession to the scientific need for mixed payloads and larger rodent populations to be housed under the GBM mass, volume and power allocations.

Under the revised requirements, the GBM was defined to provide a minimum of 1.0 m³ of internal volume, housing a 1.0 meter diameter centrifuge and three STS-equivalent middeck lockers. The GBM requirements resulted in a PM with approximately twice the usable payload volume of the rodent modules designed in the Phase B study. The design volume of the JSC spacecraft was enlarged to accommodate the larger PM, increasing the mass of the primary structure and the TPS.

Under the revised LSSWG specifications, the JSC spacecraft was required to supply an average power of 150W to the GBM in addition to the power supplied

for environmental control, with 225W peaks of 30 minutes duration allowed every 2 hours and transient peaks of 500W. The GE and SAIC designs supplied 40W and 96W to their rodent modules, respectively, which included the operational power for their life support systems. As a result, the JSC power system was designed to produce an average total power of 600W. In comparison, the GE and SAIC spacecraft produced average power levels of 127W and 200W, respectively.

The requirement for a large centrifuge to be housed within the pressurized PM was also a significant impact to the JSC design. The large centrifuge or "Bioreactor" was added to enable LifeSat to simultaneously provide an artificial gravity (artificial-g) environment and a microgravity environment. A primary design concern was the continuous transfer of angular momentum from the centrifuge to the spacecraft via internal aerodynamic drag and mechanical friction over a period of 60 days.

2.4 EVOLUTION OF LIFESAT MASS PROPERTIES

Figure 2-1 is a graphical representation of the mass properties evolution of LifeSat from Phase A through the JSC design effort. The growth from the 2800 lbm Phase A design to the 3500 lbm GE Aerospace Phase B design was due to a 600 lbm increase in the mass of the PM and a corresponding increase in the mass of usable propellant.

Between the two contractor Phase B concepts, the difference in total mass can be attributed primarily to variations in specific design solutions. The SAIC use of an Astromast and deployed module, for instance, resulted in a structural mass penalty of approximately 225 lbm as compared to the GE design. The SAIC design also allocated more mass for avionics and TPS.

The masses of the JSC and the contractor spacecraft differ primarily in the areas of avionics, power, propulsion and landing systems. JSC realized a substantial mass savings in its power system by using stationary paddle solar arrays, high-efficiency secondary battery technology and a sun-pointing spacecraft attitude. The JSC mass estimates for usable propellant and avionics and landing system hardware were comparatively higher than the contractor estimates, however.

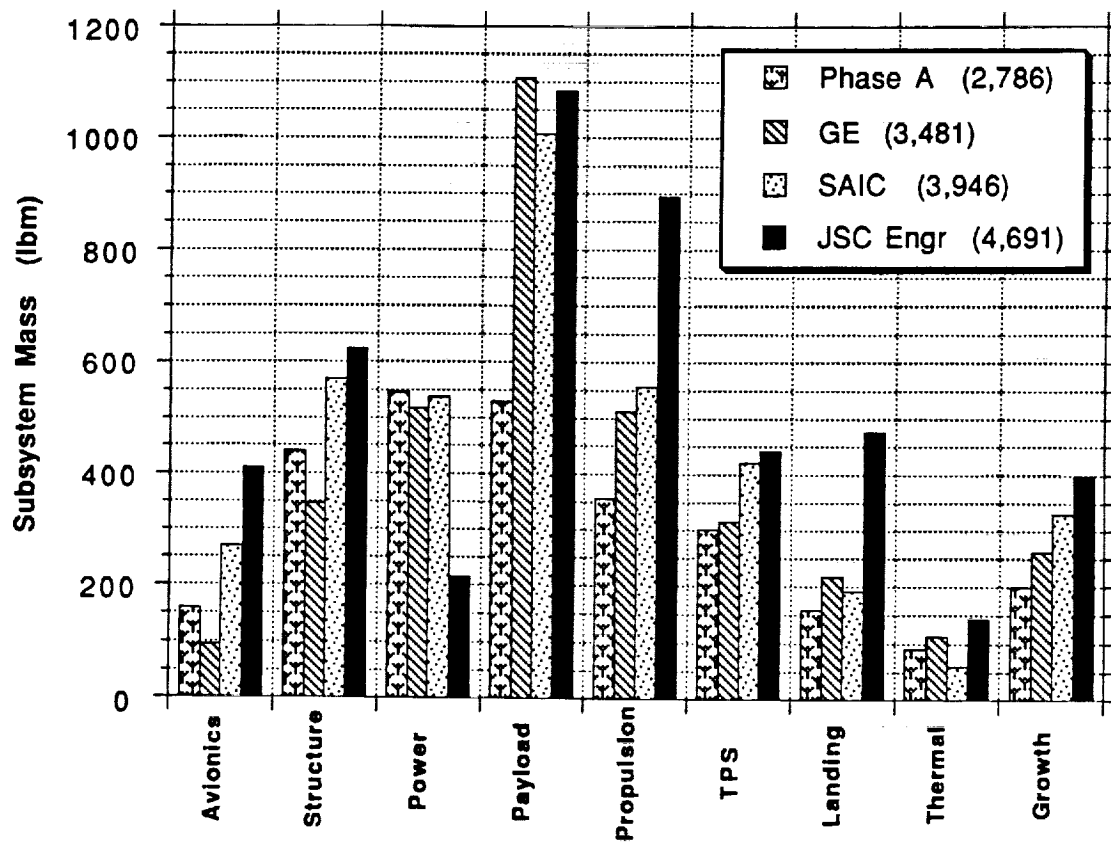


Figure 2-1. Reusable Reentry Satellite Mass Comparison

SECTION 3 LIFESAT PROJECT REQUIREMENTS FOR VEHICLE PERFORMANCE

(Prepared by Chuck Miller)

The following is a brief history of the development of the vehicle performance requirements. The requirements are presented in appendix A and are organized as an initial level B requirements document for the vehicle.

3.1 REQUIREMENTS SYNTHESIS

The initial requirements set was derived through synthesis based on requirements presented in the LifeSat Level A/B System Design Contract Statement of Work as contained in the respective Request for Proposal, results of both formal and informal discussions with the science community, and program/project management decisions. These requirements were refined during meetings with representatives from the science community and the project offices and through technical reviews conducted by the JSC Engineering Directorate.

3.2 REQUIREMENTS DEVELOPMENT

An engineering design team was formed in the Engineering Directorate once the LifeSat project office began formalizing the project requirements. This team, consisting of representatives from the various engineering disciplines, began to hold regular meetings to assist in refinement of the project technical requirements. As a direct result of these meetings, a verifiable set of project requirements was eventually provided to the Engineering Directorate by the LifeSat Project Management Office.

3.3 FUNCTIONAL DECOMPOSITION

A functional decomposition of the project requirement was performed. This process is described in appendix B. This effort resulted in dividing the project requirements into vehicle specific and, subsequently, in the assignment of decomposed and derived functional requirements to specific vehicle subsystems. A detailed analysis of these functional requirements by the engineering team resulted in the definition of the vehicle performance requirements that are presented in appendix A. Additionally, functional flows of all vehicle and LifeSat elements were developed with their respective interfaces. These were provided to the engineering team to ensure that all interfaces between the various subsystems which comprised the LifeSat vehicle were properly identified. Coordination between representatives from the several engineering disciplines comprising the engineering team resulted in negotiating responsibility for defining the vehicle interfaces.

3.4 ADDITIONAL PRODUCTS OF THE LIFESAT FUNCTIONAL DECOMPOSITION

Several other products were produced as a result of the requirements definition and functional decomposition process. Two of these products were provided to the LifeSat Project Office to assist in overall project management. A hierarchical tree of the project requirements was developed as a result of the functional decomposition. This was forwarded to the project office and formed the basis of the project work breakdown structure. Also, a requirements traceability matrix was developed that allowed the science community requirements to be traced with the project requirements down to the requirements for each of the subsystems. This matrix was also forwarded to the project office for use in the project management plan.

SECTION 4 RADIATION ENVIRONMENT

(Prepared by Lee Bryant)

4.1 INTRODUCTION

During Phase A and the first part of Phase B, the LifeSat objective was to provide a resource to study the effect of a microgravity environment on the immune systems of various life forms. To accomplish this objective, the vehicle would be placed in LEO for up to 60 days and then recovered. During the latter half of Phase B, the science community changed emphasis to radiation biology (radiation from the Van Allen Belt and GCR). The orbits required to support the radiation biology were established by the science community and determined by a small amount of analysis near the end of Phase B performed by the contractors.

To expose the specimens to the Van Allen Belt, which consists largely of protons and some electrons, the orbital altitude is about 900 km. This circular orbit did not pose much of a problem to the project. But the science community recommended an elliptical orbit which would allow the vehicle to spend as much time as possible at apogee while being exposed to GCR. The orientation of the elliptical orbit was recommended to be polar where the GCR comes through the doughnut hole due to the Van Allen Belt's equatorial alignment.

During a 60-day mission, the orbit orientation of an elliptical orbit will rotate due to the Earth's oblateness. For the altitudes recommended, 20,600 by 350 km, the line of apsis (the line connecting apogee and perigee) will rotate approximately 24° . Therefore, an orbit with a polar orientation will not be aligned with the landing site at the end of mission. To perform the deorbit maneuver (which also must rotate the line of apsis) will require an additional amount of propellant proportional to the rotation required.

4.2 RADIATION EXPOSURE AND DEORBIT PERFORMANCE

It is desirable for the life forms to be exposed to one type of radiation during the duration of the mission. This can easily be accomplished for the missions with the proton radiation objective but is not easily accomplished for the GCR missions. The elliptical orbits suggested by the science community had large dosages of protons (613 rads) and a very low dosage of GCR (see table 4-1 102.2°). This is due to the vehicle passing through the proton region at least once every revolution and can be seen in figure 4-1. Proton and electron radiation levels are computed from the AP8 model.

**TABLE 4-1. RADIATION DOSAGE, DEORBIT PERFORMANCE,
ABORT CAPABILITY**

60 Day Flt 90 Deg Incl	Perigee Latitude	AP8 p+	AP8 e-	GCR	Ratio of GCR	Delta Velocity (ft/sec)	Days Abort Coverage
200 km by 20000 km	-90.0	768	2.26	1.62	0.21	7115	0
	-60.0	440	2.60	1.62	0.36	Large	0
	-30.0	33	6.30	1.68	4.10	Large	0
	0.0	1.2	13.50	1.76	10.69	4746.6	0
	30.0	23.0	9.70	1.71	4.97	2359.4	0
	60.0	190	3.60	1.64	0.84	436.7	12
	90.0	736	2.24	1.63	0.22	3024.7	0
350 km by 20600	55	125	4.40	1.65	1.26	150.0	24
	102.2	613	2.0	1.63	0.26	3830.2	0
	167.7	31	13.0	1.75	3.83	150.0	24
350 km circ	NA	1.8	0.02	0.75	29.53	440.0	NA

The orientation of the orbit greatly affects the amount of proton exposure which the specimens receive, and placing the line of apsis nearer the equator can reduce the proton dosage to 1.2 rad. However, the orientation which is fuel-efficient for deorbit is slightly above the equator and receives 31 rads of protons (table 4-1 167.7°). This orientation allows the vehicle to pass below the proton region around perigee and above the proton region at apogee (figure 4-2).

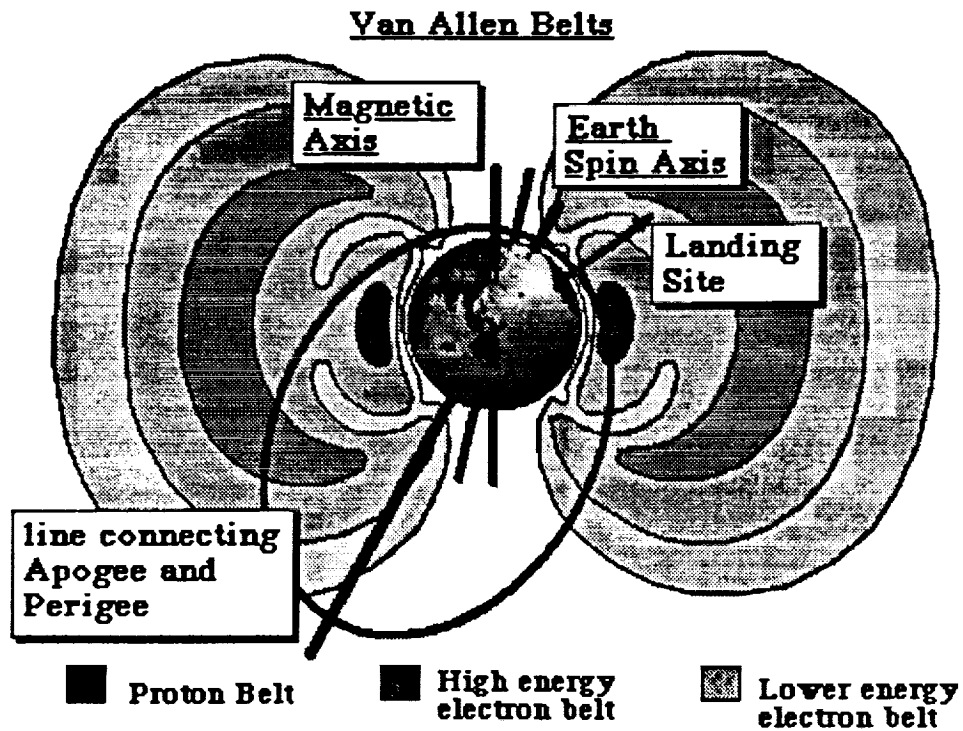


Figure 4-1. Van Allen Belt and LifeSat Elliptical Orbit Polar Orientation

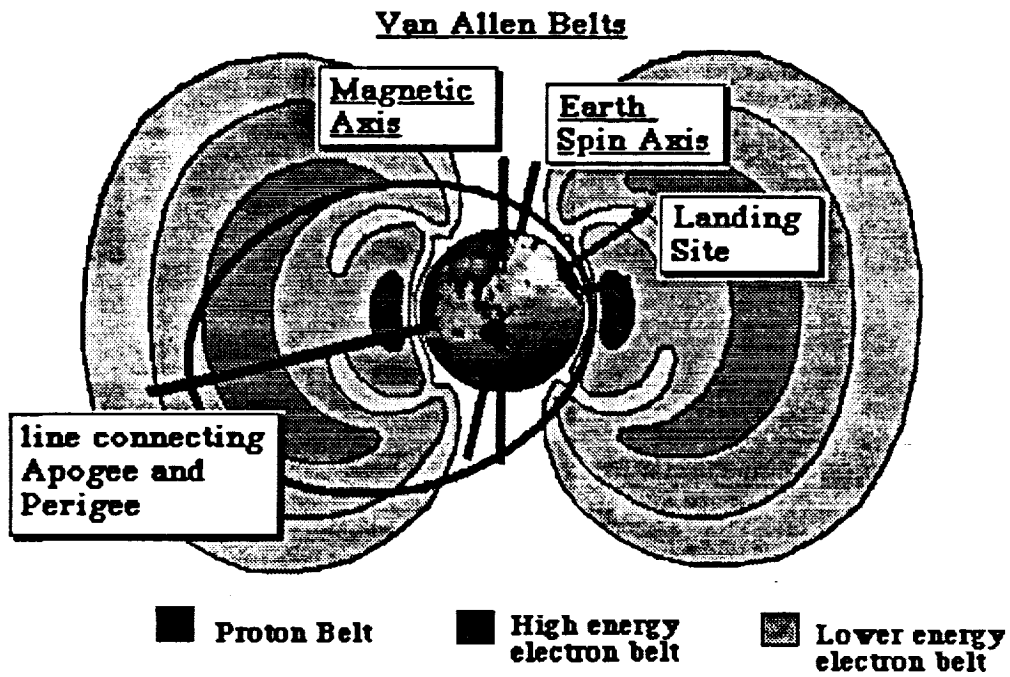


Figure 4-2. Van Allen Belt and LifeSat Elliptical Orbit Aligned for Landing

One measure of goodness is the ratio of GCR to the total dosage. The table indicates this ratio is highest for low altitude circular orbits. However, the GCR dose is very low and may not have a complete spectrum. If the protons are to be minimized, the orbit must be oriented near the equator as stated earlier. The region around the equator up to the fuel minimum deorbit is presented in figure 4-3.

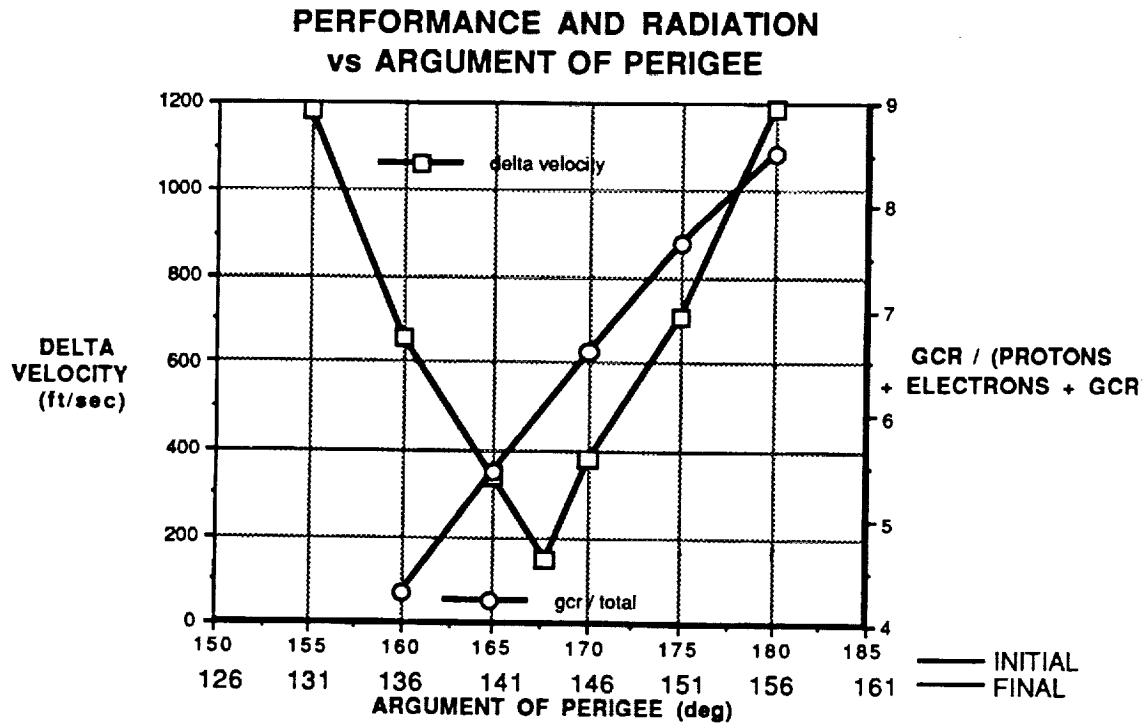


Figure 4-3. Performance and Radiation Versus Argument of Perigee

4.3 CONCLUSIONS

The science community decided that statistically meaningful GCR data could not be obtained from the orbits listed in table 4-1 due to the low dosage of GCR and the amount of proton contamination. For this reason, it is recommended that GCR missions only be flown much above the Van Allen Belt. To achieve a mission which leaves Earth passing through the Van Allen Belt only once, receiving GCR for 60 days, then returning through the belts, requires an apogee more than twice the distance to the Moon.

4.4 RADIATION ENVIRONMENT SIMULATION (Prepared by Gary Conley)

A prototype was developed on the Silicon Graphics workstation to demonstrate how orbital trajectory design and analysis tools would benefit by using modern 3-D graphics and animation. Benefits include orbital trajectory visualization to

enhance engineering analysis and the easy information exchange with other engineers and management. Complex orbital motions (such as the shape of the orbit, inclination, apsidal rotation, and nodal regression) can be easily visualized. Major features of the prototype include a well defined rotating Earth model, a model of Van Allen Belt, an orbiting satellite, and VCR-like user input controls (play, fast forward, freeze). Plans are being discussed to extend this prototype into a general tool for doing engineering analysis. A video is being prepared to document the entire LifeSat scenario (ascent, on orbit, and entry) and will be available in the near future.

SECTION 5 CONFIGURATION DESCRIPTION

(Prepared by Edward Robertson)

5.1 EXPENDABLE LAUNCH VEHICLE PERFORMANCE

The LifeSat Phase A and Phase B vehicle concepts were designed to provide controlled proton environments for biological payloads in circular LEOs ranging from 350 km to 900 km in altitude. The two-stage Delta II 7920 provides the capability to simultaneously launch two Phase B spacecraft with a combined mass in excess of 8000 lbm. The three-stage Delta II 7925, which consists of a STAR-48B orbit insertion stage (OIS) in addition to the Delta II 7920 booster, was not required for the circular LEO missions [5].

The evolution of LifeSat during the JSC design study resulted in a vehicle mass growth from the Phase B range of 3500 to 4000 lbm to approximately 4700 lbm. Despite the growth in the gross vehicle mass, the Delta II 7920 ELV provides sufficient performance to enable a dual launch of the JSC concept to the Phase B set of circular LEO missions. As noted in section 2.3, however, the scientists expanded the mission set during the JSC study to include a highly elliptical orbit (350 x 20,600 km) for GCR experimentation. The 350 x 20,600 km orbit was a compromise between the payload performance of the launch vehicle (which improves with reduced apogee altitudes) and the purity of the GCR field. Even with the aid of the STAR-48B OIS, however, the Delta II 7925 lacks the performance to insert the JSC vehicle into a 350 x 20,600 km orbit.

Late in the JSC design study, the LSSWG became interested in extremely high apogee orbits (60-day period) to avoid the contamination of the GCR field by particles trapped in the Van Allen Belts. The Atlas II series of ELVs was examined as a possible alternative to the Delta II for a big elliptical orbit (BEO) ($C_3 = -0.62 \text{ km}^2/\text{sec}^2$). The non-optimized payload data for the Atlas II series launch vehicles is shown in table 5-1 for a 28.5 degree orbit inclination and three σ (99.9 percent) flight performance reserves using the large (4.2 m diameter) payload firing (PLF). The reference trajectory uses a two-burn upper stage maneuver without the STAR-48B OIS and a one-burn maneuver with the OIS [6]. Commercial Atlas representatives indicated that varying the launch inclination up to approximately 35° would have little effect on the payload capacity of the Atlas II series of ELVs. Using the medium (3.3 m diameter) PLF rather than the large PLF, however, can provide a separated payload mass increase of approximately 110 kg to a $C_3=0$.

TABLE 5-1. ATLAS II SERIES PAYLOAD PERFORMANCE FOR THE BEO

Expendable Launch Vehicle	Separated Payload Mass (kg / lbm)
Atlas II	1800 / 3970
Atlas II w/OIS	2060 / 4550
Atlas IIA	1880 / 4150
Atlas IIA w/OIS	2120 / 4680
Atlas IIAS	2470 / 5450
Atlas IIAS w/OIS	2490 / 5500

5.2 SPACECRAFT EXTERNAL CONFIGURATION

5.2.1 Atmospheric Entry Trajectory

Lift vector control for the reentry vehicle was considered for the JSC in-house design. A lifting entry trajectory has several advantages over a ballistic entry trajectory: lower peak deceleration loads, lower heating rates, and potential crossrange capability. But entry simulations for the 20,600 km apogee orbit showed that a Discoverer-shaped ballistic spacecraft could land in the desired footprint at the White Sands Missile Range (WSMR) while remaining under the 15-g peak load limitation specified in the LSSWG requirements. The simplicity and lower estimated costs of a ballistic entry body and guidance system proved to be the deciding factors in the selection of a ballistic spacecraft entry trajectory.

5.2.2 External Moldline

A wide variety of spacecraft configurations have been developed and tested for aerodynamic performance during atmospheric entry. The Crew Emergency Return Vehicle study completed in August 1988 lists performance data for four blunt reentry shapes: the Apollo command module, Moses (or Discoverer), Scram (a Viking derivative), and a simple hemisphere [7].

The Discoverer shape tends to be more statically stable than the other shapes for a given longitudinal center of gravity (CG) location and exhibits relatively small changes in angle-of-attack and lift-to-drag ratio with respect to CG offsets from the spacecraft centerline. The almost cylindrical shape also has an excellent volume-to-surface area ratio which yields structural and TPS mass efficiencies and provides packaging flexibility for payloads and subsystems.

A disadvantage of the Discoverer shape is its low drag coefficient, compared with the Apollo and Viking configurations, which yields a larger ballistic coefficient for a given spacecraft diameter and mass. A larger ballistic coefficient translates to higher peak stagnation heating and higher peak g-loads during atmospheric entry. The larger nose radius of the Discoverer shape, however, partially offsets the adverse thermal effects of its higher ballistic coefficient.

Because of its volumetric efficiency and aerodynamic stability, the Discoverer shape was chosen for the JSC reference design (figure 5-1). However, with the recent emphasis on very high apogee elliptical orbits (beyond lunar orbit), the operational and programmatic trades between ballistic and lifting trajectories should be reevaluated. An alternative shape, such as a scaled personnel launch system (PLS) biconic, may provide a highly functional platform for LifeSat operations and simultaneously provide a test-bed for automated targeting lift vector reentry and land recovery systems.

5.2.3 Sizing

The maximum diameter of the spacecraft was initially determined from a combination of Phase B trajectory information, Delta II performance data, and the estimated dimensions of the PM. The GE Phase B design, which also employed the Discoverer shape (79" diameter), had a ballistic coefficient of approximately 130 lbf/ft². Using the same ballistic coefficient, the JSC design required a maximum diameter of 95" for a reentry mass of 4250 lbm. The standard Delta II 9.5 ft (2.9m) diameter PLF can accommodate a single 95" LifeSat in the two- or three-stage mode. A dual launch of the Delta II would require the 10.0-foot diameter PLF in the two-stage mode (figure 5-2). A scale check using a solid model generated using SDRC I-DEAS software indicated that a 95" diameter spacecraft would accommodate a 1-cubic meter PM.

5.3 SPACECRAFT INTERNAL CONFIGURATION

The first step in the configuration design was to model the primary structure, launch vehicle attach fitting, and TPS. An axisymmetric skin-stringer primary structure was roughly modeled to carry the launch and reentry loads (figure 5-3). The payload attach fitting was placed on the aft end of the spacecraft, resulting in a nose-up attitude during launch (figure 5-2). The TPS materials and thickness distributions were calculated based on the estimated ballistic coefficient of the spacecraft, a 300°F temperature limit of the aluminum primary structure, and the entry trajectories/footprint analysis at WSMR. Ablation of the nose results in a gradual distortion of the aerodynamic moldline from the Discoverer shape.

The second step in the configuration design was the location of the largest internal components: the propellant and pressurant tanks, the PM, and the parachute cannisters (figure 5-3). Because the six hydrazine tanks and two

pressurant tanks will be nearly empty after the deorbit burn, they were placed in the aft region of the spacecraft. This location also had the advantage of placing the tanks and the engines in close proximity, reducing the length of the propellant lines. The cylindrical PM was placed toward the nose of the spacecraft along its axis of symmetry. This placement provided quick access to the PM upon recovery of the spacecraft and promoted a stable CG location for atmospheric entry. The centerline placement also enabled the generation of an axisymmetric artificial gravity field within the PM by spinning the spacecraft. The three main parachute cannisters were located axisymmetrically at the aft end of the spacecraft. In the landing configuration displayed in figure 5-4, the nose TPS is jettisoned to enable the deployment of the stabilization legs. An airbag in the nose (not shown) attenuates the majority of the impact loads. An advantage of this landing configuration is the availability of air for convective cooling after touchdown. Thermal soakback from a closed TPS configuration would severely compromise the effectiveness of the TPS during the 4-hour recovery period.

The two solar arrays and deployment mechanisms are located 180° apart on the exterior of the cone TPS near the nose/cone interface. The thermal radiator, consisting of eight individual panels, is located on the aft end of the spacecraft around the four deorbit engines. The designs of both the solar array and the thermal radiator were simplified by the continuous Sun-pointing alignment of the spacecraft nose during the on-orbit phase. The Sun-pointing alignment eliminates the need for solar array gimbaling and provides a favorable radiative environment in the aft region. The remaining subsystem components were placed around the circumference of the PM toward the nose. The forward location provides excellent access during spacecraft assembly and integration and improves the stability of the vehicle during atmospheric entry.

5.4 PAYLOAD MODULE AND AUXILIARY PAYLOADS

The GBM in the JSC design is 1.16 m in diameter and 1.40 m long, providing a usable internal volume slightly in excess of 1 m³. The GBM is designed to house a rodent facility supporting approximately 50 mice, a bioreactor for culturing cell samples, and a limited volume of auxiliary payloads (figure 5-5). Multiple interfaces are required between the spacecraft subsystems and the PM to provide the necessary coolant fluid, life support functions, electrical power, and data transmission.

The ESA Biopan, a self-contained biological experiment container, was mounted on the aft end of the spacecraft. The Biopan provides its own thermal protection for atmospheric entry by closing its hinged outer shell. The radiation detector/carousel specified in the LSSWG requirements was mounted on the wall of the conical spacecraft section near the aft end. This location provides a minimum of material interference with the measured radiation spectrum.

5.5 MASS PROPERTIES

The mass properties format for the JSC LifeSat reference design (table 5-2) was adopted from reference 8. The format provides several levels of data: the design mass summary (top level), mass properties (second level), and mass and design details (third level and beyond are in appendix C). Each level is subdivided into 13 functional system codes to ensure a logical, uniform tabulation of the mass and design data for subsystem hardware, consumables, expendables, and propellants composing the spacecraft dry mass, inert mass, and gross mass.

The Excel mass properties spreadsheet used within the JSC Systems Definition Branch is designed to be filled out at the detailed (third) level. The mass values are automatically propagated to the mass properties and summary levels using embedded functions. It is also possible to iteratively converge upon a component or fluid mass as a function of other vehicle data. The usable propellant mass, for instance, is typically expressed as a function of the vehicle inert and gross masses using the rocket equation. Reserve and residual propellant masses, in turn, can be expressed as a percentage of the usable propellant mass.

Three systems level approximations were made in the LifeSat mass statement.

- First, the primary structural mass was estimated from historical reentry vehicle data obtained from the JSC Systems Definition Branch. The body structure areal density estimate of 3.0 lbm/ft² was extracted from the minimum manned correlation of the ESTFOR14 plot. A finite element study was initiated by the JSC engineering team to refine the structural mass estimate. However, the LifeSat program was cancelled before the structural analysis could be completed.
- Second, a mounting and attach structure factor of 20 percent of the individual component masses was included within the first eight functional codes which, when combined with growth, form the vehicle dry mass.
- Third, a factor of 15 percent of the spacecraft dry mass was included to account for the mass growth (ninth functional code) that historically accompanies the evolution of a vehicle concept during the design process.

The component and fluid masses tabulated within each functional category were obtained from detailed design studies conducted at JSC. A concerted effort was made to promote data exchange and compromise among the subsystem designers. Within the boundaries of the LSSWG requirements, vehicle operational parameters were selected to promote favorable functional interfaces and a mass-efficient spacecraft design.

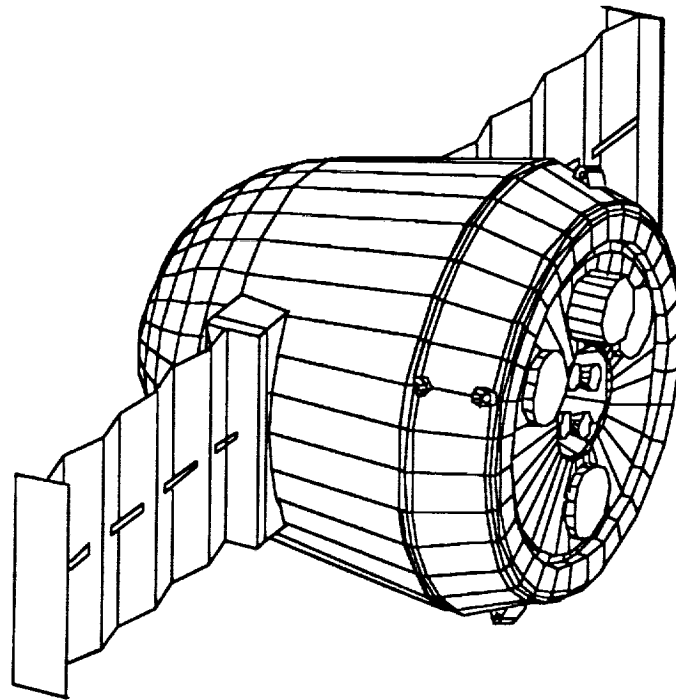
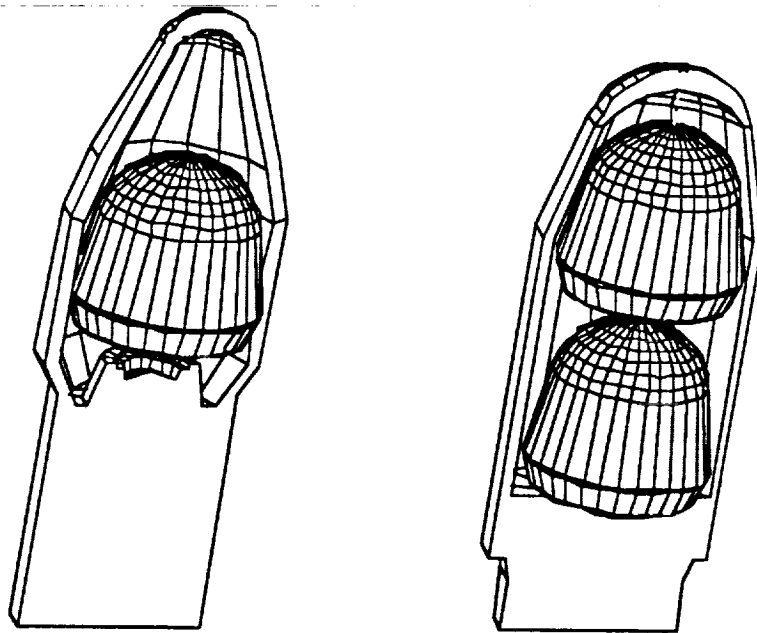


Figure 5-1. LifeSat External View - Operational Mode



9.5-foot Diameter PLF 10.0-foot Diameter PLF
Three-stage Configuration Two-stage Configuration

Figure 5-2. Potential LifeSat Delta II Launch Configurations

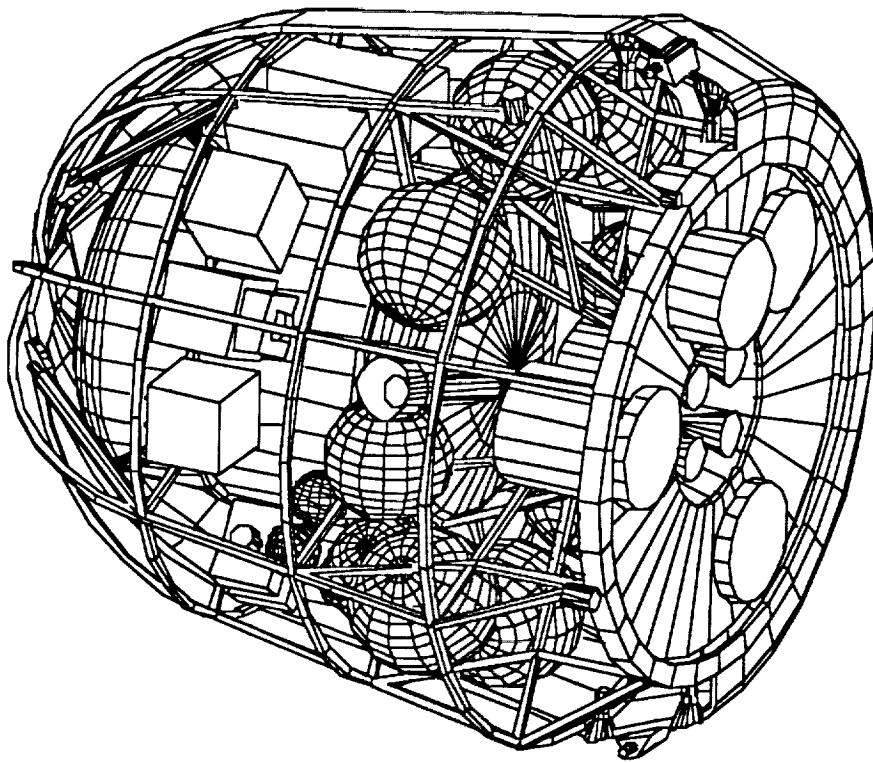


Figure 5-3. LifeSat Internal View - Solar Arrays Blanked

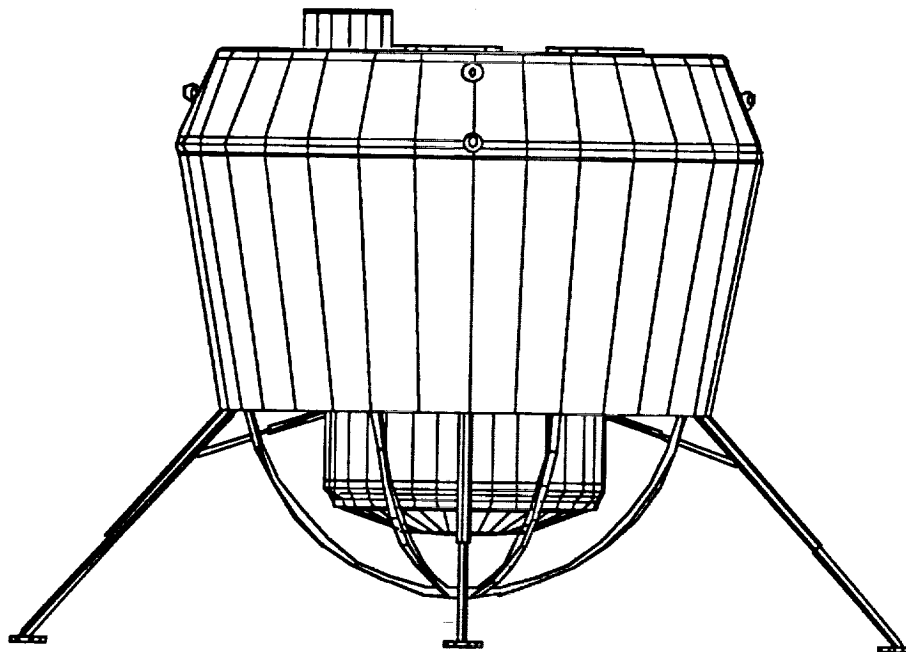


Figure 5-4. Proposed LifeSat Landing Configuration

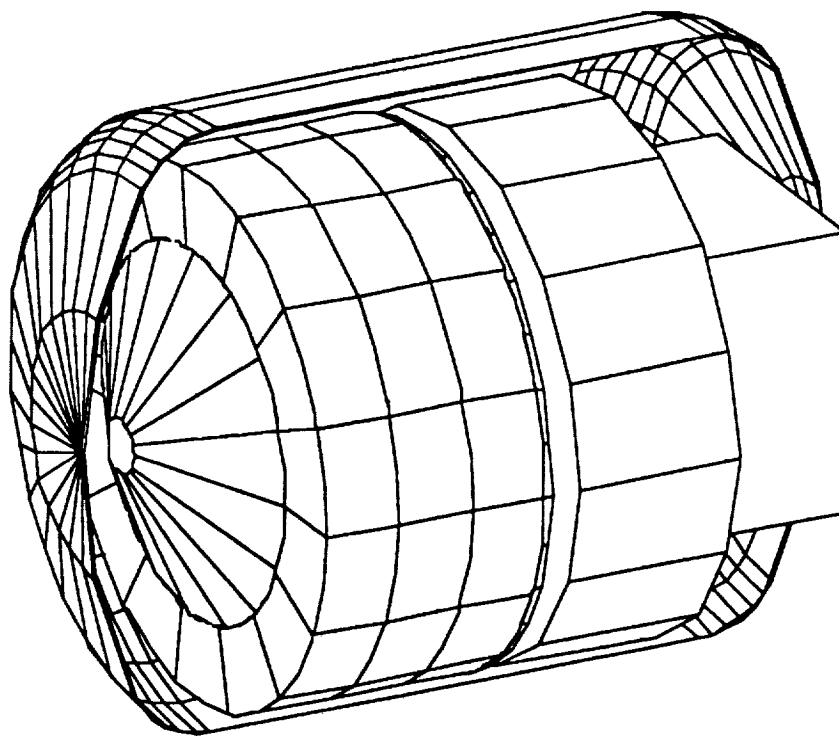
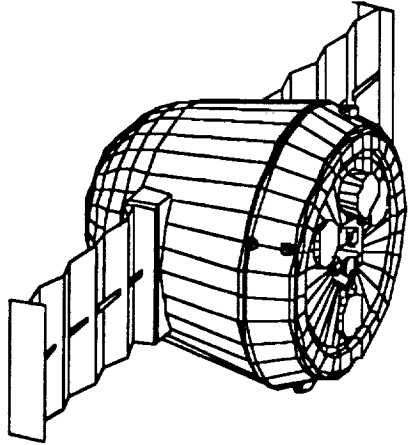


Figure 5-5. Payload Module Interior Layout

TABLE 5-2. JSC LIFESAT MASS PROPERTIES STATEMENT

Design Mass Summary

FUNCTIONAL SUBSYSTEM CODE	Reusable Reentry Satellite	Payload Attach Fitting	TOTAL	On-Orbit External View
1.0 STRUCTURE	624	6306*		
2.0 PROTECTION	444			
3.0 PROPULSION	227			
4.0 POWER	215			
5.0 AERO CONTROLS	0			
6.0 AVIONICS	376			
7.0 ENVIRONMENT	246			
8.0 LANDING/RECOV	475			
9.0 GROWTH	391			
DRY MASS	2,998			<p>* Optional PAFs include the 6019, 6915 and 6306</p> <p>NOTES:</p> <p>S/C max diameter is 95" which will fit in the Delta II 9.5 foot PLF</p> <p>6306 PAF: max 5512 lb @ 101.5" above S/C separation plane 2" maximum offset from the centerline</p> <p>Nose radius = 3.35 ft (42.3% of base diameter)</p> <p>Cone half-angle = 10 degrees</p> <p>Length from nose to max diameter = 82% of base diameter</p>
10.0 NON-CARGO	149			
11.0 CARGO	883			
INERT MASS	4,030			
12.0 NON-PROPELLANT	57			
13.0 PROPELLANT	632			
GROSS MASS	4,719	110	4,829	

Mass Properties

LifeSat	Mass (lbs)		Mass (lbs)
1.0 Structure <ul style="list-style-type: none">- Primary Body Structure- Subsystem Mounting Structure (information only)	624	8.0 Landing and Recovery	475
	624		
	329	9.0 Growth (15% of Dry Mass)	391
2.0 Protection <ul style="list-style-type: none">- Thermal Protection System- Insulation (TBD)	444		
	444	LifeSat Dry Mass	2,998
	0	10.0 Non-Cargo	149
3.0 Propulsion <ul style="list-style-type: none">- Orbital Maneuvering System- Attitude Control System	227	- Reserve and Residual Fluids	74
	211	- Active Thermal Control Fluids	75
	16	11.0 Cargo	883
4.0 Power <ul style="list-style-type: none">- Generation- Electrical Pwr Dist. & Control (EPDC)	215	- Pressure Vessel, Structure and Fittings	258
	172	- Centrifuge, Middeck Lockers & Freezer	600
	43	- Radiation Detectors	25
6.0 Avionics <ul style="list-style-type: none">- Guidance, Navigation & Control (GNC)- Data Management System (DMS)- Instrumentation- Communications & Tracking (C&T)		LifeSat Inert Mass	4,030
	376	12.0 Non-Propellant (Consumables)	57
	209	13.0 Propellant	632
7.0 Environment <ul style="list-style-type: none">- Life Support System (LSS)- Thermal Control System (TCS)	80	- Usable OMS and ACS Propellant	632
	14		
	63	LifeSat Gross Mass	4,719
	246		
	96		
	150		

5.6 COMMUNICATION AND TRACKING (C&T)

5.6.1 Introduction

This section contains the C&T system design for LifeSat. It includes the requirements and assumptions for the design, equipment selection (weight, size and power), radio frequency (RF) coverage analysis and link analysis, operations of C&T, and interfaces with other systems. Several missions, with several different possible orbits, will be flown. Paragraph 5.6.5 contains additional link margin analysis on the C&T quick look of the 60-day elliptical orbit. More detailed information is contained in NASA Memo TBD LifeSat C&T System Design.

5.6.2 C&T Assumptions

(Prepared by Laura Hood)

5.6.2.1 Orbits

The orbits investigated in this report are the:

Highly Elliptical Orbit 350 km x 20,600 km (Perigee Latitude 167.7; table 4-1.)

Low Earth Orbit 34° inclination 275 km circular

Low Earth Orbit 34° inclination 900 km circular

Dual LifeSat Orbits: 34° 350 km LEO and 34° 900 km LEO, 34° 900 km LEO
and 34° 700 km LEO

60-day elliptical orbit

5.6.2.2 Data Throughput Required

It was assumed that 300 Mb/day of unformatted data will be transmitted. Consultative Committee for Space Data Systems (CCSDS) data formats will probably be required; but, it is not known at this time the level of CCSDS compliance needed, so the amount of overhead is unknown. The breakdown of the 300 Mb/day is as follows.

<u>Science Data</u>	<u>Mb/day</u>
Biological experiment	25
Radiological	80
Video*	95
Vehicle*	100

* Assumed values

A 1 kbps uplink of commands and file transfers will be received by LifeSat during communication contacts when needed.

5.6.2.3 Tracking Requirements

The on-orbit position accuracy requirement for LifeSat is 3 km, in order to periodically align the inertial measurement units (IMUs). For entry and in order to hit the footprint at WSMR, the state vector will be updated at the last opportunity before deorbit to provide trim burns as accurately as possible.

5.6.3 C&T System

(Prepared by Paul Shack and Laura Hood)

Three options for the LifeSat communications system have been investigated. Selection of a particular configuration will depend on the final requirements for communications coverage during specific mission phases. The options investigated include communications via NASA Deep Space Network (DSN) ground stations for all data, communication via the Tracking and Data Relay Satellite System (TDRSS) for all data, and a combination of the two with the TDRSS providing a low data rate capability only in support of reentry, landing, and contingencies.

Each of the three options can be implemented using currently available equipment. The main component of each is either the NASA Standard Near Earth Transponder or the NASA Standard TDRSS Transponder (both manufactured by Motorola). These units are space-qualified and have been used successfully on a number of spacecraft. Single-fault tolerance is maintained throughout the communication system with the exception of the antennas and the RF distribution network. The effect of single failures in these typically high reliability areas needs to be traded off against the complexity of working around the single fault points. GPS redundancy would be required to achieve dual-fault tolerance for reentry.

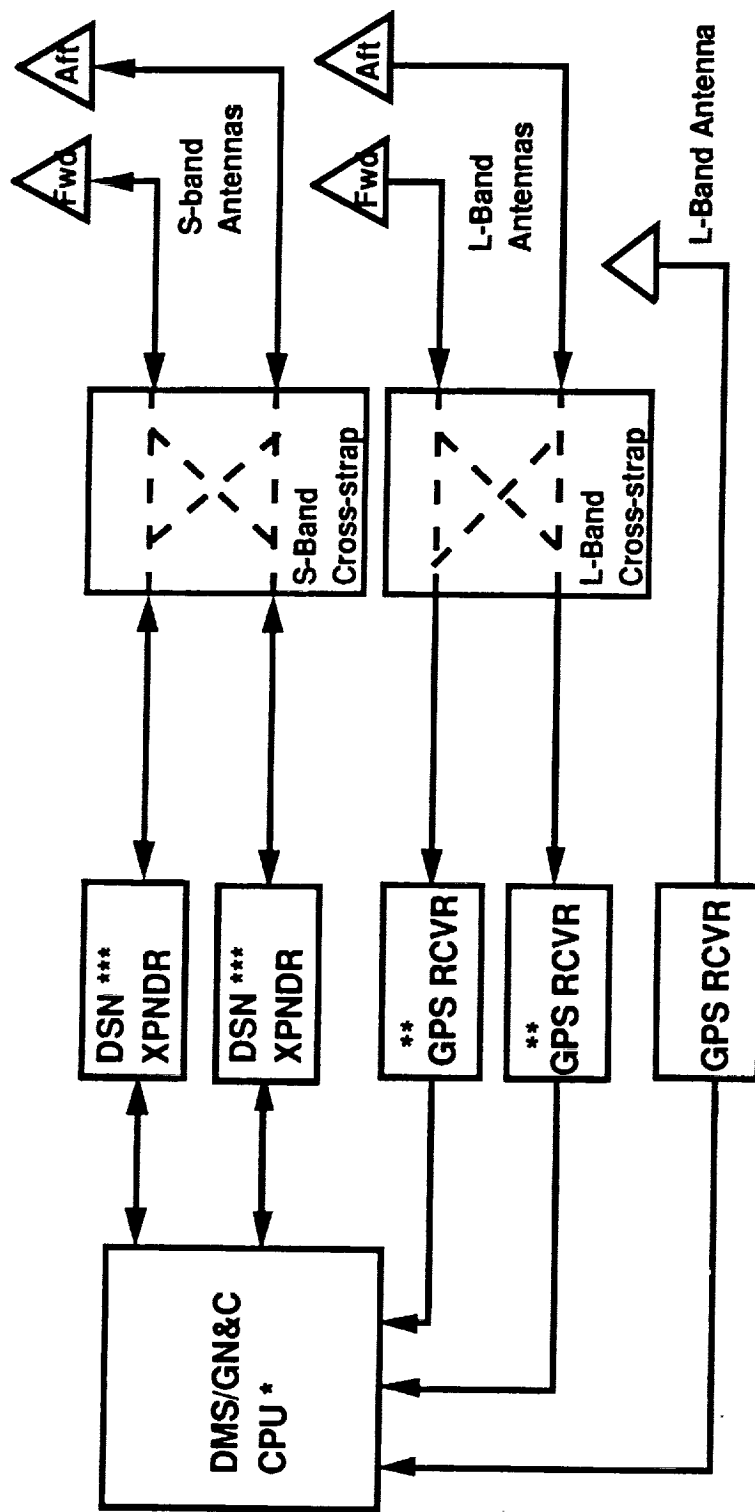
5.6.3.1 Communications Hardware Options

Figure 5-6 is a block diagram of design option 1. Option 2 is the same except that the DSN transponder is replaced by a DSN/TDRSS transponder and a high-power amplifier is inserted after the transponder. Option 3 is the same as option 1 except that the DSN transponder is replaced by the DSN/TDRSS transponder.

5.6.3.1.1 Option 1 - DSN. Option 1 is based on communications being provided only with ground stations, specifically the NASA DSN. This option would have the least impact for size, weight, and power, as well as having the minimum cost of the three options. The size, weight and power for this communications option are in table 5-3.

In addition, with this option the onboard systems would be compatible with the Ground Space Tracking and Data Network (GSTDN). Entry and descent

Option 1 DSN Prime Comm & Backup Tracking, GPS Prime Tracking



* CPU is part of data management system and will perform the following functions for C&T: data buffering, data multiplexing, antenna switching algorithm, etc.

** Only one string of GPS is powered on at one time. The third GPS receiver is for reentry redundancy and its antenna will be placed in the best location for reentry.

*** Only one string of Communication equipment is powered on at one time

Figure 5-6. Option 1 Block Diagram

TABLE 5-3. OPTION 1 - DSN

COMPONENT	QUANTITY	WT	VOLUME	SIZE (IN)	POWER
NEAR EARTH XPNDR (2.5 WATT RF)	2	7.2 LBS PER UNIT INCLUDING DIPLEXER	230 CU IN	7.8 x 8.3 x 3.5	7 WATTS RECEIVE 24 WATTS XMIT/RCV

coverage could, if required, be provided by the Salinas Peak tracking station. This station is located on WSMR and would provide coverage to near landing.

5.6.3.1.2 Option 2 - TDRSS. Option 2 provides the capability to support all required mission data communications via TDRSS. In addition, the NASA Standard Transponder can provide communications with both DSN and the GSTDN ground stations. This option has the most impact for size and weight and requires significantly more power. It is also the most expensive of the three options. The low data rate to which the TDRSS link is constrained by the distances involved requires long periods of transmitter on time. This is further discussed in paragraph 5.6.4.2. The size, weight and power for this option are in table 5-4.

TABLE 5-4. OPTION 2 - TDRSS

COMPONENT	QUANTITY	WT	VOLUME	SIZE (IN)	POWER
NEAR EARTH /TDRSS XPNDR (2.5 WATT RF)	2	16 LBS PER UNIT INCLUDING DIPLEXER	397 CU IN	13.5 x 6.4 x 4.6	17 WATTS RECEIVE 36 WATTS XMIT/RCV

5.6.3.1.3 Option 3 - DSN on orbit TDRSS backup. Option 3 provides the capability to support all on-orbit communications via the DSN. It also uses the TDRSS capability of the NASA Standard TDRSS Transponder to provide limited low data rate (1 kbps) backup communications. This option would have approximately the same impact for size, weight, and hardware cost as the TDRSS option. It would have power requirements slightly greater than the DSN option but significantly less than the TDRSS option. The link between TDRSS and the LifeSat cannot be maintained when the altitude of the spacecraft is greater than 10,000 km. Therefore, backup communications will be available only under limited conditions. The size, weight and power for this option are in table 5-5.

TABLE 5-5. OPTION 3 - DSN/TDRSS

COMPONENT	QUANTITY	WT	VOLUME	SIZE (IN)	POWER
NEAR EARTH /TDRSS XPNDR (2.5 WATT RF)	2	16 LBS PER UNIT INCLUDING DIPLEXER	397 CU IN	13.5 x 6.4 x 4.6	17 WATTS RECEIVE 36 WATTS XMIT/RCV

5.6.3.2 GPS Hardware (Prepared by Ray Nuss)

In considering design options for a GPS receiver on the vehicle, several issues must be studied before a configuration can be chosen. These issues arise first because of the possible highly elliptical orbit taking the satellite above the orbit of the GPS satellites, and second because of the possible spin rate of 42 RPM or greater.

5.6.3.2.1 Highly elliptical orbit. The problem comes from the relatively narrow beamwidth of the GPS satellite antennas. The antennas are designed to cover only a region below the GPS satellite on (or very near) the earth. A GPS receiver in a high orbit can only see a GPS satellite which is on the opposite side of the earth and within a narrow view angle (approximately 7°) from the earth. This greatly reduces the ability of the GPS receiver to track GPS satellites and thus compute an accurate position. Some simulations have been performed which show that a GPS receiver located in a geosynchronous orbit can achieve a position solution accurate to about 2000 feet after 2 to 6 hours; another set of simulations show an accuracy of 100 meters after 2 days of tracking. Position determination relies on appropriate software and knowledge of the LifeSat orbit, within the GPS receiver, as well as whether selective availability is being implemented on the GPS satellites.

GPS accuracy has been described in various ways by different users and government agencies. When an accuracy is specified, it is important to associate that accuracy with dimensions and percentiles. The Department of Defense (DOD) defines the GPS Standard Positioning Service (SPS) accuracy as 100 meters 2dRMS (2 dimensions, root mean square) and 76 meters SEP (spherical error probability). Interpreted, the 100 meter 2dRMS value means that a 100-meter radius circle about a point will contain at least 95 percent of all possible position fixes obtained with a system at that point. The 76 meter SEP value means that a 76-meter radius sphere about a point will contain at least 50 percent of all possible position fixes obtained with a system at that point. For 1-sigma accuracy, the SEP (a 49-meter radius sphere about a point) will contain at least 19 percent of all possible position fixes obtained with a system at that point. The footprint analysis used 50-meter error in each axis and 1-σ accuracy which means that the accuracy of GPS will be better than this.

LifeSat requirements call for 100-meter accuracy just prior to the deorbit burn, which occurs at the highest point of the vehicle orbit (apogee). Special software

to simulate the orbit would be required to determine the length accuracy a GPS receiver on LifeSat could achieve. Also, specially designed software would have to be developed for the GPS receiver. Use of a high gain antenna with INS aiding would greatly improve position determination.

5.6.3.2.2 Effect of vehicle spinrate on antennas. Two possible basic designs are proposed to accommodate the vehicle spin. The first design would be to place one or two GPS antennas on the sides of the vehicle. For one antenna, testing would have to be performed to determine the feasibility of position determination with the GPS receiver receiving satellite signals on and off at the vehicle spinrate. For two antennas, an RF combiner could be used, or an RF switch driven by appropriate logic to switch between the two antennas. The RF switch could be internal to the GPS receiver. A receiver with two antenna ports could be used, with each port having a dedicated receiver channel.

The second design would be to place two antennas near the LifeSat spin axis at opposite ends of the LifeSat. Here a combiner could possibly be used to connect the two antennas to a single GPS receiver. This configuration would leave an area a few degrees wide around the LifeSat where the two antenna patterns would overlap with a difference of only about 6 dB. A study and testing program would have to be performed to determine the effects of this 6 dB difference in signal levels. Again, to avoid this possible problem, a switch could be used with appropriate logic to connect the GPS receiver to the antenna with the strongest signal. A dedicated channel receiver could also be used.

5.6.3.2.3 Other issues. GPS redundancy would be required to achieve dual-fault tolerance for reentry. A third GPS receiver would be provided for this redundancy, and its antenna positioned for reentry coverage. To minimize signal loss and noise input, the GPS receiver should be as close as possible to the antennas.

Environmental specifications of current GPS receivers are not known, but should be very similar to other avionics equipment (temperatures of 0 to 120°F and pressures of 12.4 to 15.2 psia). Radiation susceptibility is a concern since GPS receivers rely heavily on imbedded software and memory.

Currently several GPS receivers are built for space applications. One (Motorola GPS Explorer Platform) is scheduled to be launched as early as January 1992. Current receivers would have to be modified for LifeSat. However, several vendors have space-qualified designs in work or proposed. Today, GPS receivers weigh from 5 to 100 pounds, and use from 5 to 70W of power. However, weight and power are highly dependent on the capabilities of the GPS receiver. As of this writing, the NASA Standard GPS Program is not considering the requirements of LifeSat because of the late scheduled delivery of the NASA GPS (~1996) versus the earlier requirement for LifeSat (~1995).

5.6.3.2.4 GPS size, weight and power estimate. Table 5-6 has the estimated size, weight and power for the GPS receiver.

TABLE 5-6. GPS RECEIVER

COMPONENT	QUANTITY	WT (LBS)	VOL	SIZE (IN)	POWER
GPS RECEIVER	3	10 LBS PER UNIT	336 CU IN	6 x 7 x 8	15 WATTS

5.6.3.3 Antennas (Prepared by Pat Fink)

Two antenna configurations are being examined. Each configuration attempts to achieve hemispherical coverage at minimal power consumption.

Configuration one (fore/aft hemispherical option) consists of one S-band and one L-band patch antenna on the nose and one S-band and one L-band patch antenna aft. Configuration two consists of two circumferential belt antennas (one S-band and one L-band) near to the aft end of the satellite.

5.6.3.3.1 Fore/aft hemispherical antenna option. Table 5-7 lists the size, weight, and power of the fore/aft hemispherical option. The antenna coverage for the fore/aft antenna configuration is approximately 84 percent with reduced coverage around the midsection of the vehicle.

Advantages:

- More power efficient for low to moderate power requirements (which is likely)
- Antenna construction is simpler and likely to be much less expensive (unless thermal protection becomes prohibitive)

Disadvantages:

- Less coverage (approximately 84 percent)
- Thermal protection on nose may not be feasible
- Requires aft space (dimensions attached)

TABLE 5-7. FORE/AFT HEMISPHERICAL OPTION

COMPONENT	QUAN	WEIGHT LBS	SIZE INCHES	VOL CU IN	POWER WATTS
POWER AMP *	2	2.0 EA	6 x 4.5 x 4	108.0	125.0 XMIT ONLY
CABLES	5	0.504 EA	4.0 FT/CABLE		
**SWITCH	2	1.0 EA	2 x 3 x 3	18.0	2.0 PULSE
L-BAND ANTENNA GPS	3	4.4	8.12 SQ x 1.1 DEEP	72.5	
S-BAND ANTENNA (for command and telemetry)	2	2.0	5.35 SQ x 1.1 DEEP	30.5	
TOTAL WITHOUT POWER AMP		21.7		314.5 CU IN + 20 FT CABLE	2 WATTS DURING SWITCHING

* Power Amplifier is for TDRSS Only Option. Totals are 25.7lbs, 530.5 cu in + 16 ft of cable, and 125W with the power amplifier.

** 1 L-band and 1 S-band

5.6.3.3.2 Circumferential belts option. Table 5-8 lists the size, weight, and power of the circumferential belts option. The antenna coverage for this option is approximately full coverage with reduced coverage at the nose and aft ends of the vehicle.

Advantages

- Greater coverage (-1 dBi over >95 percent)
- Easier thermal protection
- Additional redundancy - graceful degradation
- More power efficient for high power requirements
- Requires no aft space

Disadvantages:

- Increased complexity
- More expensive
- May not be compatible with deployable solar panels

- May not be compatible with landing air bag deployment concept
- Precedent not yet found on satellite even though used on missiles and rockets

TABLE 5-8. CIRCUMFERENTIAL BELTS OPTION

COMPONENT	QUAN	WEIGHT LBS	SIZE INCHES	VOL CU IN	POWER WATTS
POWER AMP *	8	1.19 EA	4 x 3.5 x 1	14.0	1.13 **
CABLES	16	0.536 EA	4.25 FT/CABLE		
COMBINER	1	0.188	4 x 1.5 x 1	6.0	
DIVIDER	1	0.188	4 x 1.5 x 1	6.0	
ANTENNAS	1 S-BAND 1 L-BAND	17.2 TOTAL	25 FT x 4.8 IN x 0.125 IN TOTAL	180.0	
TOTAL		35.6		304 CU IN + 68 FT CABLE	9.04

- * For TDRSS Only Option, higher power is needed.
The power amplifier changes to 1.56 lbs, 4.5 x 4.5 x 1 inches, 20.25 cu in, and 11.3W.
The total changes to 38.6 lbs, 354 cu in + 68 ft cable + antenna belt, and 90.4W.
- ** The power is for transmit only.

5.6.3.4 Summary and Recommendation

The characteristics of the three options are summarized in table 5-9. The first option with the fore/aft antenna design, which uses the DSN for all communications, represents the minimum size, weight, power, and cost impacts.

Unless other drivers are identified, the DSN option is the recommended baseline configuration. With the addition of the requirement for TDRSS coverage during the deorbit burn, option 3 would become the recommended option.

TABLE 5-9. C&T OPTIONS SUMMARY

OPTION	VOL (CU IN)	WEIGHT (LB)	PEAK/STBY (WATT)	DUTY CYCLE (HRS/DAY) CIRC/ELL
OPTION 1/FA	1793	66.6	26 / 7	0.25/0.4 COM
OPTION 1/CIR	1783	81	35/7	2/4 GPS
OPTION 2/FA	2343	88.2	161 / 17	4 / 5 COM
OPTION 2/CIR	2166	101	126/17	2/4 GPS
OPTION 3/FA	2127	84.2	38 / 17	0.25 /0.4 COM
OPTION 3/CIR	2117	99	47/17	2/4 GPS

FA - Fore/Aft antenna design

CIR - Circumferential antenna design

5.6.4 Analysis

5.6.4.1 Communications and Tracking Radio Frequency Coverage (Prepared by Bill Gadd)

There is a requirement for a minimum of two contacts per day with LifeSat. Coverage analysis was performed for LifeSat to the TDRSS, the DSN ground stations, and the GPS constellation to determine if the contact requirement is met. Coverage analysis was performed for three LifeSat orbits.

- Circular Orbit - 34° inclination, 275 km altitude
- Circular Orbit - 34° inclination, 900 km altitude
- Elliptical Orbit - 20,600 km apogee, 350 km perigee

Figure 5-7 shows the ground track for the 275 km circular orbit. Analysis was performed for both on-orbit and reentry. The trajectory data was provided by the Performance Analysis Branch of the Systems Engineering Division at JSC.

5.6.4.1.1 Sun visibility analysis. To minimize battery power drainage, it was proposed that LifeSat transmit data during daylight hours only. The main issue concerns the amount of time LifeSat will be blocked from the Sun during the 60-day mission. A simulation was performed on a 60-day mission for both the circular orbits and the elliptical orbit described above. Table 5-10 shows the amount of time the Sun is in and out of view of LifeSat.

TABLE 5-10. PERCENTAGES OF TIME SUN IS IN AND OUT OF VIEW OF LIFESAT

	275 km Circular	900 km Circular	Elliptical Orbit
In View	59.3	66.2	94.0
Out of View	40.7	33.8	6.0

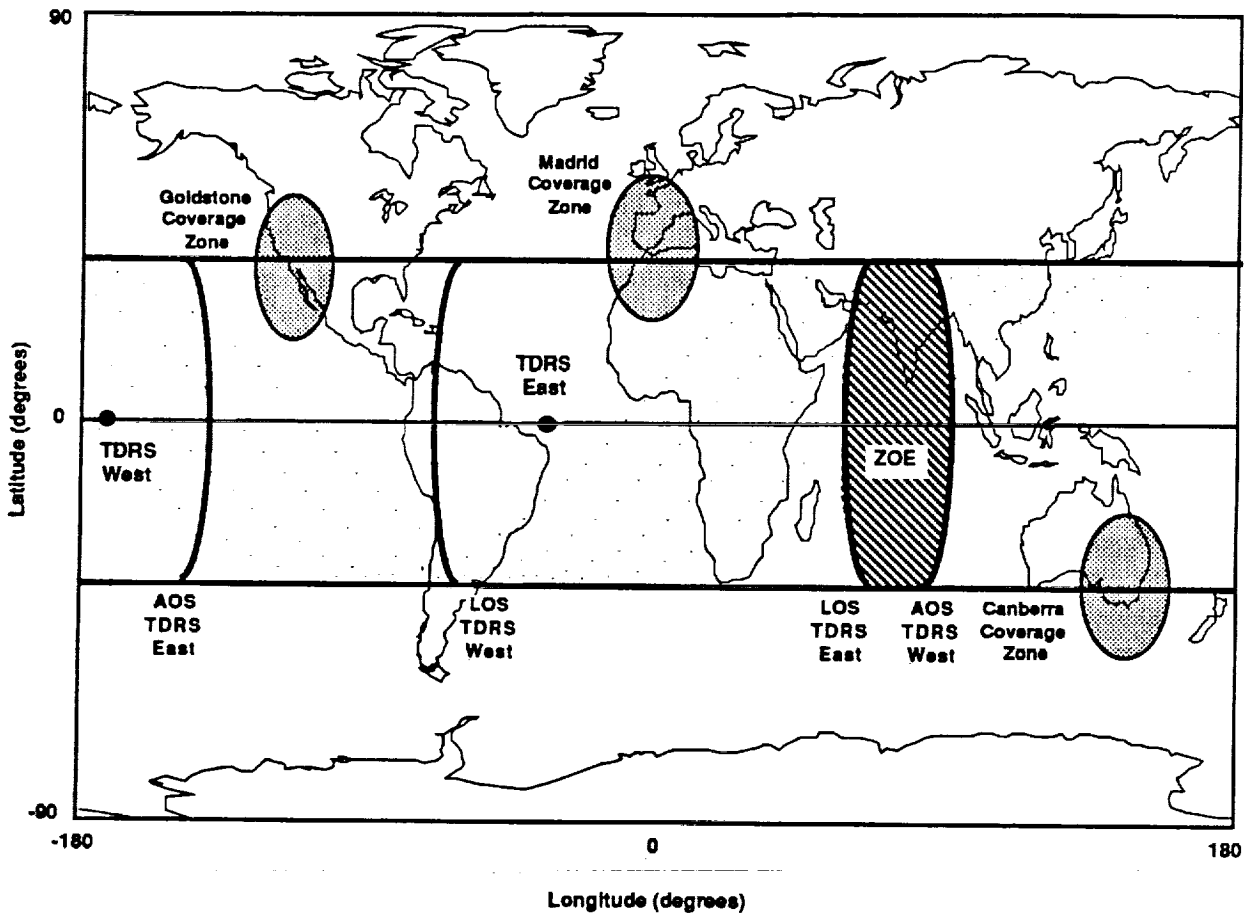


Figure 5-7. Typical Ground Track for 275 km Altitude Circular Orbit

5.6.4.1.2 Deep Space Network ground station coverage. Analysis was also performed to determine the coverage to the DSN 26 m subnet ground stations in Madrid, Spain, Goldstone, California, and Canberra, Australia.

5.6.4.1.2.1 Single LifeSat vehicle: A statistical average was determined of the number of times per day LifeSat was in view of any of the three DSN ground

stations. Also, the minimum and maximum duration time that LifeSat was in view of any of the DSN ground stations was computed. The criteria for LifeSat contact with a DSN ground station is as follows:

- Must be at least 7° above the horizon of the ground station
- Must be simultaneously in view of the Sun

The second criterion was included to prevent transmitting data in the darkness. Table 5-11 shows the on-orbit coverage to the DSN.

TABLE 5-11. COVERAGE STATISTICS BETWEEN LIFESAT AND THE DSN GROUND STATIONS

	Circular 275 km	Circular 900 km	Elliptical Orbit
Avg. # of Contacts Per Day	3	6	4
Maximum Duration	6 min	14 min	140 min
Minimum Duration	5 min	5 min	5 min
Min/Max Contacts Per Day	3/4	4/8	3/8

The results show that DSN coverage is adequate for all three types of orbits.

The reentry analysis shows that for the 275 km circular orbit, there is no reentry coverage from any of the three DSN ground stations. Canberra provides a few minutes of coverage at deorbit burn for the 900 km orbit, and Goldstone provides a few minutes coverage before landing. Canberra provides excellent coverage at deorbit burn for the elliptical orbit and for approximately 1.8 hours after the burn. After Canberra loses sight of LifeSat, no other coverage is available to and including final landing.

5.6.4.1.2.2 Dual LifeSat vehicles: There was concern that two LifeSat vehicles, orbiting simultaneously, could experience some interference when transmitting data because they both transmit at the same frequency. Interference would not occur between the two vehicles because the DSN can track only one vehicle at a time and the other vehicle transmitter can be turned off.

Analysis was performed for two vehicles in orbit at the same time to determine if there were at least two contacts per day with any of the three DSN ground stations. Two orbits were analyzed:

- Vehicle 1 at 350 km, Vehicle 2 at 900 km, circular orbits
- Vehicle 1 at 700 km, Vehicle 2 at 900 km, circular orbits

A 60-day mission was simulated to determine the frequency and duration of contacts. The analysis criteria was as described in paragraph 5.6.4.1.2.1. Results are summarized below.

350 km/900 km orbit:

The requirement for the two contacts per day with any of the three DSN ground stations was met. The two vehicles pass over the same ground station simultaneously at least once per day with a maximum time of about 9 minutes.

700 km/900 km orbit:

The requirement for the two contacts per day with any of the three DSN ground stations was met. The two vehicles pass over the same ground station simultaneously at least once per day with a maximum time of about 14 minutes.

The two contacts per day requirement was easily met by both orbital scenarios. Thus, the DSN can be used to support the LifeSat mission.

5.6.4.1.3 TDRS East and TDRS West Coverage. The first analysis performed was coverage to both TDRS East and TDRS West for both S-Band single access (SSA) and S-Band multiple access (SMA). The SMA and SSA have antenna tracking limits as defined in "The Space Network (SN) Users' Guide - Revision 6," GSFC, September 1988. The procedure for SMA consisted of first checking to see if a TDRS was above the horizon of LifeSat and then checking to see if LifeSat was within the 13° half-cone limit of the TDRS antenna. The procedure for the SSA case was the same except the TDRS coverage limit was a rectangular region -31° to 31° North-South and -22.5° to 22.5° East-West. The analysis did not include having the Sun in view. A 60-day mission was simulated to produce statistical coverage data. Table 5-12 shows the coverage results for the on-orbit analysis.

TABLE 5-12. ON-ORBIT COVERAGE ANALYSIS TO
TDRS EAST AND WEST

	Circular 275 km	Circular 900 km	Elliptical Orbit
%Total Coverage (SSA)	90.9*	98.4*	82.3*
%Total Coverage (SMA)	90.9*	98.4*	15.1*
Maximum Time in TDRS East Pass	59 min.	79 min.	—
Minimum Time in TDRS East Pass	54 min.	71 min.	—
Maximum Time in TDRS West Pass	59 min.	79 min.	—
Minimum Time in TDRS West Pass	54 min.	71 min.	—
Maximum Coverage Time Per Orbit	94 min.	121 min.	—
Minimum Coverage Time Per Orbit	93 min.	103 min.	—
Maximum Time in Zone of Exclusion (ZOE)	12 min.	5 min.	—
Minimum Time in ZOE	7 min.	0 min.	—

* Coverage is for combination of both TDRS East and TDRS West.

For both the circular orbits and the SSA mode of the elliptical orbit, the coverage is excellent; coverage is poor for the elliptical orbit in SMA mode.

For reentry, a state vector update is needed to perform the proper reentry burn. Another state vector update is needed about halfway down the reentry to determine if a corrective burn is needed. The reentry analysis shows that coverage is more favorable for the elliptical orbit. At deorbit burn over Perth, Australia, the SSA results show that LifeSat is in view and inside the half-cone limit of both TDRSs until landing at WSMR. The SMA results show that LifeSat is in view of both TDRSs but is outside the TDRS half-cone limit for about 90 minutes after the burn. If TDRS is needed for an emergency state vector update at deorbit burn, the SSA mode should be used if available.

A problem occurs for reentry from the circular orbits: The deorbit burn occurs in the ZOE. Because of the stringent landing footprint, the most current state vectors are needed to determine if corrective burns are needed. Delaying the burn a few minutes will allow TDRS West to come into view and provide coverage all the way to WSMR. If the burn cannot be delayed, other means of communication (such as a mobile ground station) must be investigated if communication is required during the burn.

5.6.4.1.4 Global Positioning System constellation coverage. The final analysis consisted of LifeSat coverage to the GPS constellation. To provide an accurate state vector, 4 of the 21 GPS satellites available during the LifeSat mission must be in view of LifeSat. Below is the procedure used to determine the number of GPS satellites in view of LifeSat at a given time.

- a. For a GPS satellite to be selected it had to be at least 5° above the Earth's limb (horizon).
- b. If the GPS satellite met criteria A, then it was determined if the LifeSat was within the 42.8° full coverage cone limit of the GPS satellite antenna. If so, the GPS satellite was selected.

For the elliptical orbit, GPS coverage of apogee, when deorbit burn occurs, is inadequate, with only one or two GPS satellites in view. GPS coverage becomes acceptable at or below an altitude of 6000 km. For the circular orbits, GPS coverage is excellent throughout the mission.

5.6.4.2 Link Margin Analysis (Prepared by Antha Adkins)

Link margins were calculated for the return link from LifeSat to the DSN 26 m subnet, the TDRSS SMA service, and the TDRSS SSA service. The margins were calculated for a 275 km circular orbit, a 900 km circular orbit, and a 20,600 km apogee elliptical orbit. The TDRSS parameters were taken from the "Space Network (SN) User's Guide," Revision 6; and the DSN parameters were taken from the "Deep Space Network/Flight Project Interface Design Handbook," 810-5, Revision D.

The maximum data rate used was 1.2 Mbps, which is the maximum data rate that the current DSN 26 m configuration can support. The minimum data rate for TDRSS links is 1 kbps, as specified by the SN User's Guide.

5.6.4.3 Service Comparison

Table 5-13 provides a comparison of the three possible services for the three orbits chosen. The DSN 26 m subnet and the TDRSS SSA service are able to support a 300 Mb/24 hour downlink for any of the orbits examined, but the TDRSS SMA service is unable to support this throughput for any orbit. However, scheduling the TDRSS SSA service for the period of time needed may be difficult. Furthermore, it takes 2.5W to transmit to the DSN, but 25W to transmit all of the data through the TDRSS. It also takes several hours to transmit the data through the TDRSS, but only several minutes to transmit the data through the DSN for the circular orbit. So it takes much less power and time to transmit the data through the DSN, making the DSN the better choice for the daily data transmissions. However, for times when less data is required and when the DSN is not available (for example at deorbit), a low power link to TDRSS might be a good option.

TABLE 5-13. SERVICE COMPARISON

ORBIT	LINK/SERVICE	POWER	TIME TO TRANSMIT 300 Mb
275 km circular	DSN	2.5 W	4.2 min
	TDRSS SMA	2.5 W	no link
	TDRSS SMA	25 W	181 Mb in 24 hours
	TDRSS SSA	2.5 W	181 Mb in 24 hours
	TDRSS SSA	25 W	3.8 hours
900 km circular	DSN	2.5 W	4.2 min
	TDRSS SMA	2.5 W	no link
	TDRSS SMA	25 W	173 Mb in 24 hours
	TDRSS SSA	2.5 W	181 Mb in 24 hours
	TDRSS SSA	25 W	3.9 hours
20600 km elliptic	DSN	2.5 W	24 min
	TDRSS SMA	2.5 W	no link
	TDRSS SMA	25 W	173 Mb in 24 hours
	TDRSS SSA	2.5 W	138 Mb in 24 hours
	TDRSS SSA	25 W	5.2 hours

5.6.5 60-Day Elliptical Orbit

An analysis to support a 60-day elliptical orbit was performed. The maximum distance between LifeSat and the Earth will be 1.3 million km.

5.6.5.1 Link Margin Analysis

Link margins were calculated for the return link from LifeSat to the DSN 34 m subnet. This subnet was used instead of the 26 m subnet that was used for the near-Earth trajectories because the ranging capabilities of the 26 m subnet would be exceeded when LifeSat is at its maximum range. The maximum ranging capability of the 26 m subnet is 644,000 km. The DSN parameters were taken from the "Deep Space Network/Flight Project Interface Design Handbook," 810-5, Revision D.

Although physical coverage of the 60-day elliptical orbit trajectory is near-continuous, the DSN will probably be dedicated to the LifeSat mission only a certain percentage of time. For different percentages of time used for communication between the DSN and LifeSat, the data rate needed to transmit 300 Mb/24 hours was calculated. Then the LifeSat effective isotropic radiated power (EIRP) needed to transmit that data rate was calculated. Finally, the

antenna gain needed to produce that EIRP for a series of different RF transmit powers was calculated.

The data rate needed to transmit 300 Mb/24 hours was calculated for 100 percent, 50 percent, 25 percent, and 10 percent of the time used for communication, where 100 percent equals 24 hours. The actual amount of time scheduled for LifeSat by the DSN needs to be worked out between LifeSat and JPL. Finally, the antenna gain needed to generate the EIRP was calculated for 2.5W, 25W, 50W, and 100W of transmit power. A 1 dB circuit loss was assumed. See table 5-14.

TABLE 5-14. SUMMARY OF RESULTS

% Time used for Contact	Data Rate for 300 Mb/24 hours (kbps)	Antenna Gain Needed with the Transmit Power			
		2.5 W	25 W	50 W	100 W
100	3.5	10.1 dB	0.1 dB	-2.9 dB	-5.9 dB
50	7.0	13.2 dB	3.2 dB	0.2 dB	-2.8 dB
25	13.9	16.1 dB	6.1 dB	3.1 dB	0.1 dB
10	34.8	20.1 dB	10.1 dB	7.1 dB	4.1 dB

Based on these results, a basic configuration can be developed. It will be assumed that 10 percent of the time will be used for communication. The 25W power amplifier and 10.1 dB gain antenna will be used. This power amplifier was used in previous studies for communication with the TDRSS, and its total power consumption is 125W. For the near-Earth orbits, no power amplifier was required to communicate to the DSN. Therefore, this orbit drives the system to consume more power, weight, and size than the previous orbits studied. Furthermore, for the near-Earth orbits, an antenna with a -1 dBic gain was used. This trajectory would require a 10.1 dB gain antenna, which is no longer hemispherical. Because hemispherical coverage is desired, the antenna design will be more complicated than that for the near-Earth orbit designs. If LifeSat is spinning at the proposed rate of 42 rpm, the antenna design will be further complicated.

Some additional changes could be made to the system that would reduce the amount of antenna gain or transmit power required. One possibility would be to add coding, which could provide a 4 to 7 dB improvement. Another possibility would be to reduce the amount of data that needs to be sent.

5.6.5.2 Antennas

The Electromagnetic Systems Branch at JSC provided two possible antenna configurations for the near-Earth orbits.

- (1) A pair of patch antennas, one on the fore of the spacecraft and one on the aft
- (2) A circumferential belt antenna

For the 60-day elliptical orbit trajectory, four antenna configurations were discussed.

- (1) Six horn antennas around the circumference of the spacecraft and one on the aft
- (2) One horn antenna on the aft, steerable by gimbals
- (3) A planar phased array on the aft
- (4) A circumferential phased array belt

For the 60-day elliptical orbit trajectory, configuration 1 is the simplest and would be recommended for a nonspinning spacecraft. If the spacecraft is spinning, however, neither configuration 1 nor configuration 2 would be feasible; a steerable antenna will be needed. Electronically steerable antennas (such as configurations 3 and 4) are believed to be more reliable than mechanically steerable antennas (such as configuration 2). Configuration 4, the circumferential phased array belt, would give the most coverage, but it is a custom design and will be very expensive. Therefore, for a spinning vehicle, configuration 3, a planar phased array on the aft of the spacecraft, is the preferred option.

Each of these options for the 60-day elliptical orbit trajectory is more complicated than either of the options for the near-Earth missions. This extra complication means that the antenna design for the 60-day elliptical orbit trajectory will cost and weigh more than the near-Earth options.

5.6.5.3 Conclusion

Communication support of the 60-day elliptical orbit trajectory is possible. However, because of the distance involved, the communication system design will be more costly and complicated than that for a near-Earth trajectory. For 10 percent of the time used for contact, an extra power amplifier and a much more complicated antenna design are required than those for near-Earth orbits.

5.6.6 Interfaces

(Prepared by Laura Hood)

5.6.6.1 Power

Table 5-15 summarizes the power requirements of the C&T system.

TABLE 5-15. C&T POWER REQUIREMENTS

Communication Link	275 km Orbit	900 km Orbit	HEO Orbit	Power (Watts) Peak/Standby
DSN (Option 1)	15 min/day	15 min/day	24 min/day	26/7
TDRSS (Option 2)	3.8 hrs/day	3.9 hrs/day	5.2 hrs/day	161/17
DSN (Option 3)	15 min/day	15 min/day	24 min/day	38/17
GPS	2 hrs/day	2 hrs/day	4 hrs/day	15
SARSAT	12 hrs	12 hrs	12 hrs	17

5.6.6.2 Guidance, Navigation, and Control (GN&C)

The tracking measurements from the GPS receiver shall be sent to GN&C. The IMU state vector from GN&C shall be sent to the GPS receiver to aid GPS acquisition.

5.6.6.3 Data Management System (DMS)

5.6.6.3.1 Command and telemetry data. The DMS shall send telemetry data to the C&T transponder with the data formatted for transmission. This includes formatting the data packets into CCSDS transfer frames.

DMS shall receive uplink commands from C&T transponder and process them.

5.6.6.3.2 Control and monitoring. DMS computer shall provide a control and monitoring interface to C&T to control equipment configuration, manage the antenna, and monitor C&T equipment health and status.

5.6.6.3.2.1 Equipment control: DMS shall provide control of C&T equipment to power ON equipment and configure equipment in appropriate modes. The scheduling of power ON/OFF times can be calculated on board or uplinked from the ground. If the transponder has both DSN and TDRSS capability, the appropriate command must be sent to the transponder to configure it.

5.6.6.3.2.2 Antenna management: DMS shall send antenna switch commands based on line of sight to communications site (ground station, TDRSS). Information to compute this line of sight may be provided by GN&C.

5.6.6.3.2.3 Health and status: C&T equipment shall send health and status measurements to DMS to format for telemetry.

5.6.6.4 Thermal

Antennas shall be mounted on the spacecraft so that any material that covers them is RF transparent. If this is not possible, antennas will be mounted external to the thermal material and jettisoned before reentry.

Table 5-16 contains the amount of heat generated by C&T equipment and operating temperatures for the equipment. The equipment is designed to operate in a nonpressurized environment, but it requires a temperature range between -10 C and +55 C. For the transponders, virtually all the input power is dissipated as heat in the unit. For the power amplifier used with the TDRSS option, 100W is dissipated as heat and 25W is RF energy which is radiated from the antennas.

TABLE 5-16. THERMAL REQUIREMENTS FOR C&T EQUIPMENT

COMPONENT	OPTION	TEMPERATURE RANGE	HEAT DISSIPATED (WATTS) PEAK/STANDBY
DSN TRANSPONDER	DSN (Option 1)	-10 C TO +55 C	24/7
DSN/TDRSS TRANSPONDER	TDRSS (Option 2) OR DSN/TDRSS (Option 3)	-10 C TO +55 C	38/17
GPS	ALL OPTIONS	-10 C TO +55 C	15
SARSAT	ALL OPTIONS	-10 C TO +55 C	17 (REENTRY)
HIGH POWER AMPLIFIER	TDRSS ONLY (OPTION 2)	-10 C TO +55 C	100

5.6.6.5 Ground

Commands to control LifeSat equipment or LifeSat payloads shall be uplinked via the communications uplink when necessary. File transfers shall be uplinked via the communications uplink when necessary. Telemetry from the spacecraft will be divided into payload data and spacecraft data, with payload data being forwarded to science data destination and spacecraft data being used to verify health and status of vehicle.

5.6.6.6 Deep Space Network or Tracking and Data Relay Satellite System Network

Interface between LifeSat and TDRSS must be compatible with specifications in "Space Network (SN) User's Guide," Revision 6. Interface between LifeSat and DSN must be compatible with specifications in the "Deep Space Network/Flight Project Interface Design Handbook," 810-5, Revision D.

5.6.7 Conclusion

The RF coverage analysis and link margin analysis for LifeSat was performed for communications with the DSN and the TDRSS. It was assumed that 300 Mb/day of telemetry (payload and spacecraft) was required. Communication coverage to the DSN was found to be adequate for the current proposed orbits of 275 km circular, 900 km circular, and 350 km x 20,600 km elliptical.

Two options were investigated for the antenna design which will work on a spinning spacecraft. For the first option, the antennas are located on the nose and aft of the vehicle near the spin axis of the vehicle to avoid interruptions due to spinning. The antenna on the nose is still questionable because the ablator material used for thermal protection is not RF transparent. It may be possible to mount the nose antenna external to the TPS and jettison the antenna before reentry. The second option is a circumferential antenna around the side of the vehicle. Since the thermal protection on the side of the vehicle is RF transparent, the circumferential antenna does not have a problem with the TPS. The disadvantages to this design are increased size, weight, and power and the possibility of obscuration if deployable solar arrays are used.

Coverage analysis and link margin analysis were performed to study the best system to support LifeSat. Coverage analysis to the DSN, TDRSS, and GPS was performed for both on-orbit and reentry cases. Link calculations were performed to the DSN and TDRSS. The link calculations and coverage analysis were used to determine the best option for the LifeSat communications system.

Coverage analysis was performed to determine what support was available for reentry. The DSN provides little to no coverage of the deorbit burn for the circular orbits, but it provides excellent coverage during and after the burn for the elliptical orbit. Similarly, the TDRSS provides coverage of the deorbit burn for the elliptical orbit, but the deorbit burn occurs in the ZOE for the two circular orbits. If TDRSS coverage was desired for the circular orbits, the deorbit burn could be delayed for a few minutes until LifeSat is in view of the TDRSS. RF coverage analysis was performed for the GPS. GPS coverage is excellent below 6000 km in altitude, but it is limited at altitudes above this. The actual GPS receiver may be integrated with other GN&C or avionics equipment.

The link calculations showed that much more power and time are required to transmit the daily data through the TDRSS SSA service than through the DSN

26 m subnet for the orbits examined. Therefore, the DSN should be used as the primary network to receive the LifeSat telemetry data. The TDRSS could still be used as a backup service for the DSN, but a power amplifier would be needed; and the amplifier adds additional mass, size, and power consumption to the communication system. If the power amplifier were removed, a low data rate link to the TDRSS could still be used for backup during critical phases (such as deorbit) and emergencies. A communication system design using the DSN 26 m subnetwork for the daily telemetry downlink of 300 Mb and the TDRSS services for critical phases and emergencies could be used if the additional size, weight, power, and cost of the TDRSS/DSN transponder can be justified for this purpose.

5.7 GUIDANCE, NAVIGATION, AND CONTROL (Prepared by Mike Gulizia)

5.7.1 LifeSat Subsystem Description

5.7.1.1 Guidance

For all of LifeSat's mission scenarios, a guidance scheme would be needed primarily for the deorbit phase. On-orbit guidance would also be used for any orbit adjustments necessary.

The deorbit phase would begin with a deorbit burn calculation and continue with an orbital trim burn (if necessary) and atmospheric entry. The selection of a liquid propulsion system (see paragraph 5.8) enables the deorbit guidance to be closed loop. Closed loop guidance is not a major impact to vehicle software and avionics requirements, and it vastly reduces the landing footprint, compared to open loop guidance. (See paragraph 8.2 for details.)

During the powered flight portions of the deorbit phase, namely the deorbit and orbital trim burns, the thrust vector pointing direction and the burn cutoff time are computed based on the current state vector and the target position vector until the desired velocity is converged upon.

The entry portion of the deorbit phase, which occurs in the sensible atmosphere until parachute deployment, is ballistic. A constant entry roll rate of 25°/sec was used to null out CG dispersions and cancel lift. Ballistic entry simplifies guidance and control requirements and results in a reasonably small landing footprint. (See paragraph 8.2 for details.)

5.7.1.2 Navigation

A variety of navigation techniques are available for LifeSat. The two parameters needed from a navigation system are state vector (the translational portion) and attitude. The state vector, which includes the vehicle's position and velocity vectors, is needed for targeting to a landing sight. The vehicle attitude, or orientation, is needed to direct the deorbit thrust vector, as well as for Sun pointing and communication.

The primary navigation sensor, used throughout the entire mission, is used to maintain knowledge of both state vector and attitude. Several types of IMUs are available for this purpose and were selected as primary navigation sensor options. IMU accelerometer biases and gyro drift rates cause errors to accumulate in the state vector, so external navigation sensor updates are necessary.

Knowledge of the true state vector is determined with GPS receivers. Orbit determination may also be done with DSN receivers.

A linear covariance analysis was performed to determine the frequency of GPS updates required to maintain position estimation accuracies on the order of 3 to 10 km. It was found that GPS updates every 6 hours for 350 km circular orbits provided sufficient accuracy for on-orbit coast mission phases. However, due to unavailability of GPS above 4000 to 6000 km, expected position estimate accuracies were degraded (to about 25 to 30 km) for 350 x 20,600 km elliptical orbits. It is expected that errors of this size can be removed during the deorbit phase via a final GPS update before entry and an orbital trim burn. The use of GPS for an orbiting vehicle is still under investigation.

Attitude determination can be achieved with a combination of horizon and Sun sensors. Horizon sensors determine the angle between the center of the Earth and the spin axis (of the sensor in nonspinning vehicles, or of the spacecraft in spinning vehicles). Sun sensors measure the angle between the Sun and the spin axis. Alternatively, star trackers may be used to determine vehicle attitude. For missions beyond geosynchronous orbit, horizon sensors are ineffective and star trackers (or star scanners) would be required.

Details of the components of the LifeSat navigation and control system and the avionics architecture options studied are in paragraph 5.7.2.

5.7.1.3 Control

A method of controlling LifeSat is required for both microgravity and artificial gravity payload environments on orbit, as well as for the deorbit and entry phases of the missions. For microgravity missions, three-axis stabilization is accomplished with momentum wheels. For artificial gravity missions, spin stabilization is used.

The attitude control system (ACS) (see paragraph 5.8) is used for the deorbit phase, on-orbit burns, and momentum wheel desaturation.

An analysis of the disturbance torques affecting the vehicle's attitude dynamics was conducted to size the momentum wheels and determine the frequency of momentum desaturation maneuvers. Momentum wheels were sized using the new configuration with solar panels as well as the Phase B design without solar panels. Details of the momentum wheel sizing study are in paragraph 5.7.4.

5.7.2 LifeSat Guidance, Navigation, and Control Avionics Design

5.7.2.1 Introduction

A variety of navigation techniques are available for LifeSat. As a result of the variety of possible mission scenarios discussed, including low altitude circular orbits of 275 km, 350 km, 700 km, and 900 km, elliptical orbits of 350 x 20,600 km, and two large elliptical orbits, and a 60-day elliptical orbit, several different avionics designs were investigated.

Option 1: Incorporating current state-of-the-art technology with off-the-shelf avionics components.

Option 2-3: Incorporating future state-of-the-art (with 1993 - 1994 production initiation dates) technology. This includes future IMUs, attitude sensor(s), etc.

Option 4-6: Incorporating the wide field-of-view (WFOV) star tracker camera needed for the large elliptical missions.

Accuracy requirements:

Science driven - Maintain 3 to 10 km position, 10° attitude, and 0.5°/sec attitude rate on orbit.

Engineer driven - 100 m position, 0.1 m/s velocity, and 0.5° attitude for pre-deorbit and trim burns (all three σ).

Reliability requirements:

- CRIT-1: During deorbit, reentry, and landing phases (excluding soft landing in CRIT-2), vehicle must have 99.95 percent probability of impacting Earth within the designed footprint. Survivable impact within designed footprint is CRIT-2.
- CRIT-2: In case of abort during launch (excluding abort situations in CRIT-1), vehicle must have 99.95 percent probability of impacting in unpopulated/remote area.
- CRIT-2: On orbit (excluding systems required for controlled reentry CRIT-1), controlled reentry must have 99.95 percent probability of impacting within designed footprint or in unpopulated/remote area.

5.7.2.2 Components

5.7.2.2.1 Navigation system. The navigation system consists of the following components. The primary navigation sensor chosen was the IMU (two-fault tolerant). The secondary navigation sensor options were GPS (when available), horizon sensors, Sun sensors, Microcosm Autonomous Navigation System (MANS) (may be used to replace the horizon, Sun sensors, and GPS), and star trackers (all two-fault tolerant).

5.7.2.2.2 Control system. The control system consists of the following components.

Momentum wheels (one-fault tolerant) and ACS and deorbit jets.

The primary sensor will be used throughout the entire mission. The secondary sensors will be used to help remove positional and attitude errors accumulated in the primary sensor. See appendix D for a list of the individual avionics components.

For the 60-day elliptical orbits, Earth horizon sensors would be ineffective; star trackers are needed to update the vehicle attitude. For these orbits, the WFOV star tracker camera, developed by Lawrence Livermore National Laboratories for the Strategic Defense Initiative Organization (SDIO), has been baselined.

All mass, power and volume estimates were assessed using vendor data sheets or vendor contacts. No competitive estimates were asked for or received. All avionics systems were designed to be two-fault tolerant. This was achieved by using triple redundancy and is a worst-case scenario. However, the three-string system gives a close approximation of the avionics required for a CRIT-2 system.

Figure 5-8 indicates how the avionics components interact with the spacecraft's guidance, control, and dynamics.

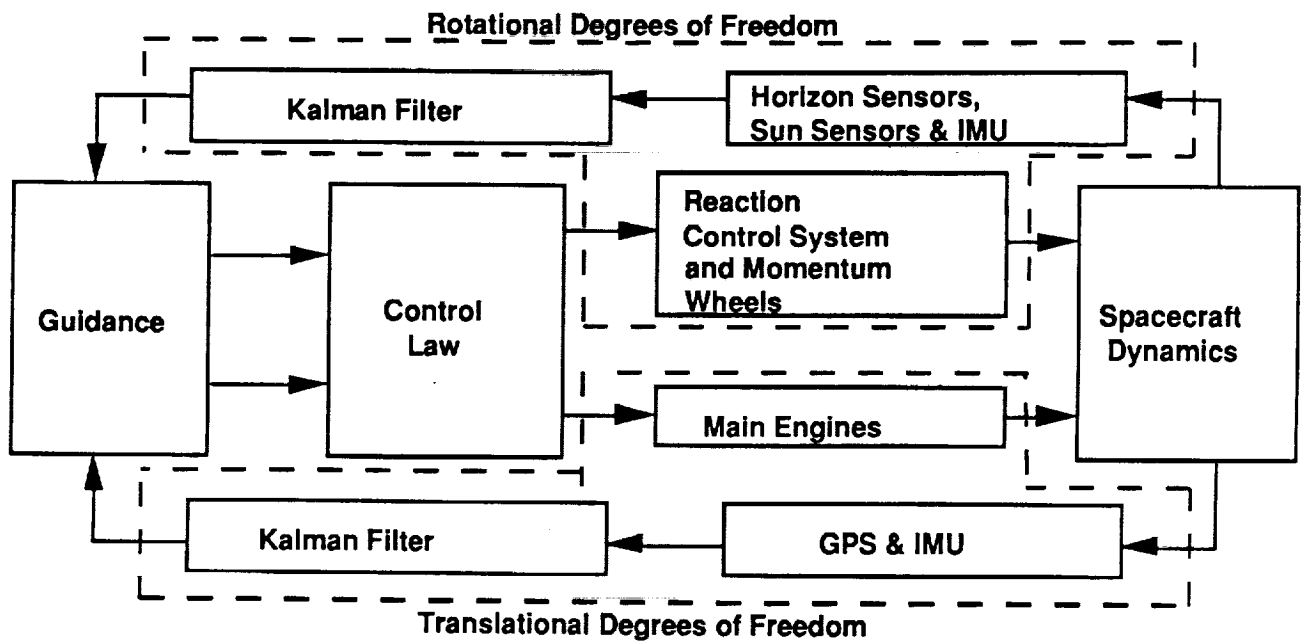


Figure 5-8. Functional Block Diagram

5.7.2.3 Architecture

Six GN&C architecture design options were investigated.

- Option 1: 3 - GG 1320 based IMUs, each with 1750A GN&C CPU
 3 - Ithaco IPS-6 horizon sensors
 3 - Adcole 18980 Sun sensors
 3 - Motorola Monarch GPS receivers
 4 - momentum wheels (3 orthogonal, 1 skewed)
- Option 2: 1 - HEXAD IMUs with three 1750A CPUs
 1 - Ithaco IPS-6 horizon sensor
 1 - Adcole 18980 Sun sensor
 1 - Motorola Monarch GPS receiver
 2 - MANS Microcosm position and attitude sensors
 4 - momentum wheels (3 orthogonal, 1 skewed)
- Option 3: 3 - Integrated Flight Management Units (IFMU) with GN&C CPU
 3 - Ithaco IPS-6 horizon sensors
 3 - Adcole 18980 Sun sensors
 4 - momentum wheels (3 orthogonal, 1 skewed)
 (See figure 5-9)

- Option 4: 3 - GG 1320 based IMUs, each with 1750A GN&C CPU
3 - WFOV star tracker cameras
3 - Motorola Monarch GPS receivers
4 - momentum wheels (3 orthogonal, 1 skewed)
- Option 5: 1 - HEXAD IMU with three 1750A CPUs
3 - WFOV star tracker cameras
3 - Motorola Monarch GPS receivers
4 - momentum wheels (3 orthogonal, 1 skewed)
- Option 6: 3 - IFMUs with GN&C CPU
3 - WFOV star tracker cameras
4 - momentum wheels (3 orthogonal, 1 skewed)

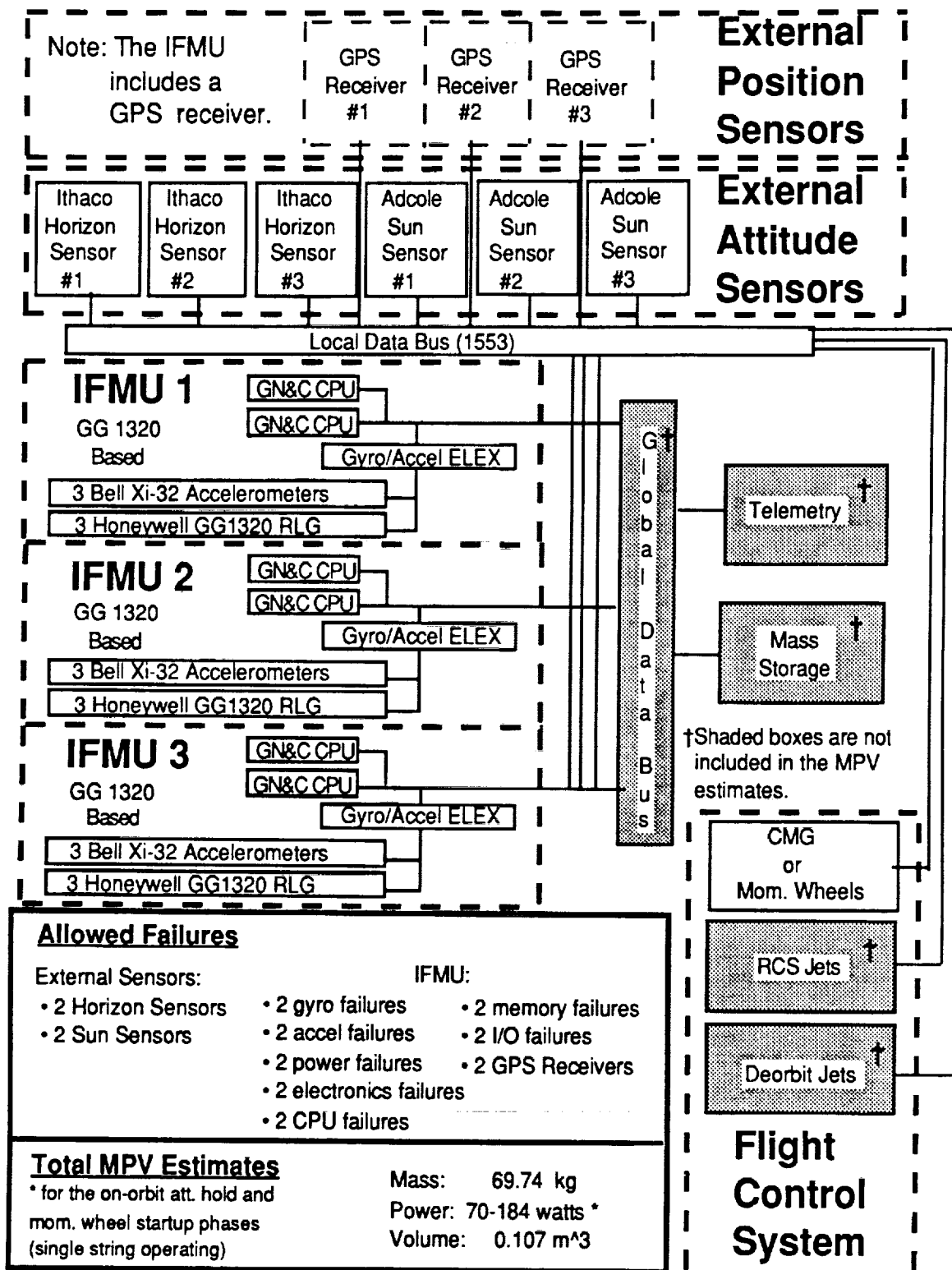
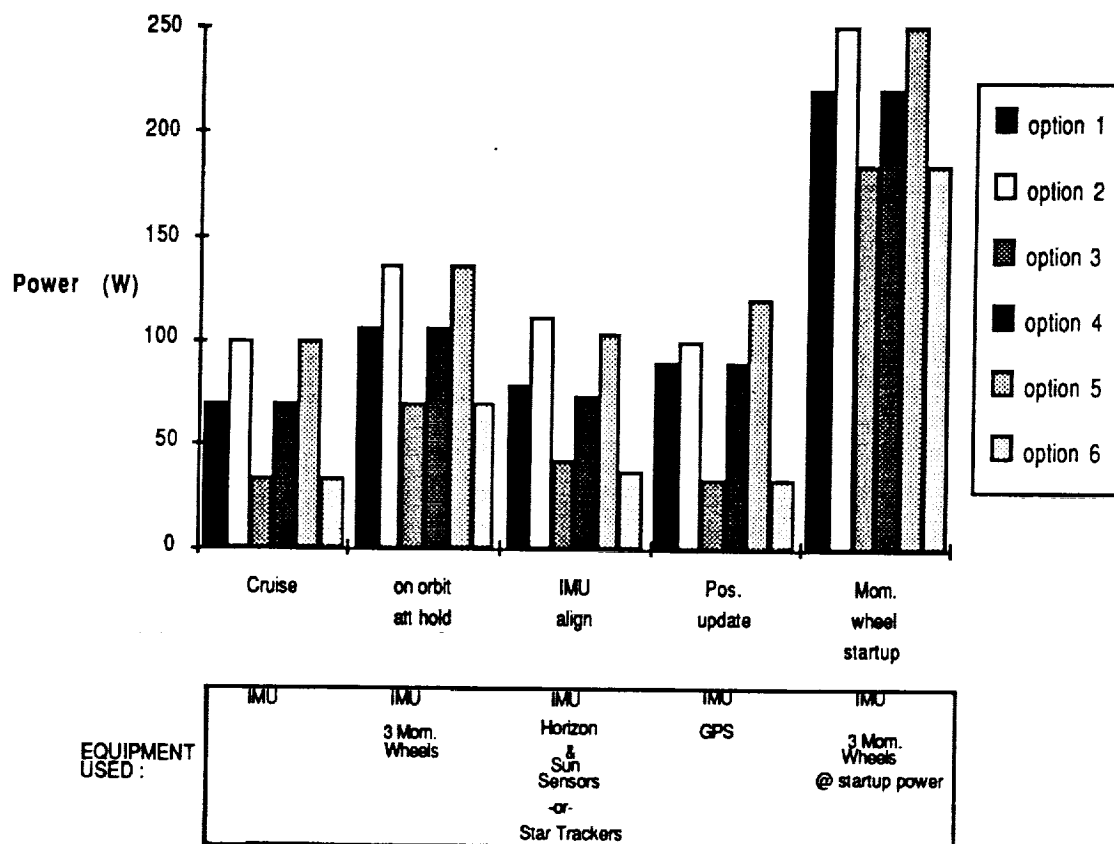


Figure 5-9. Avionics Architecture - Option 3

5.7.2.4 Power Requirements

Avionics power requirements for the cruise, on-orbit attitude hold, IMU alignment, position update, and momentum wheel startup phases of the mission are shown in figure 5-10a.



Power Requirement Time Line:

Phase	When	Frequency
Cruise	→	total duration of mission
Onorbit Attitude Hold	→	function of disturbance torques
IMU Alignment	→	once after orbit insertion once prior to deorbit burn
		TBD
Position Update	→	approx. every 6.0 hrs
Deorbit	→	from deorbit to touchdown
Mom. Wheel Start Up	→	once after orbit insertion

Figure 5-10a. Power Requirements

The momentum wheel startup phase requires maximum power. For all missions this would take place only once after orbit insertion. The majority of the

time, missions would require the power shown in the on-orbit attitude hold column.

Mass, power, and volume requirements for the different options are as follows:

	<u>Mass</u>	<u>Power*</u>	<u>Volume</u>
Option - 1	93.74 kg	106-220 W	0.121 m ³
Option - 2	75.30 kg	136-250 W	0.119 m ³
Option - 3	69.74 kg	70-184 W	0.107 m ³
Option - 4	85.40 kg	106-220 W	0.135 m ³
Option - 5	74.50 kg	136-250 W	0.116 m ³
Option - 6	62.30 kg	70-184 W	0.121 m ³

* for the on-orbit attitude hold and momentum wheel startup phases (single-string operating)

Note the integrated INS/GPS options required the least amount of power and were the least massive, and the star tracker options were slightly less massive than the horizon sensor options.

5.7.2.5 Design Conclusions and Issues

Since the WFOV star tracker is operable at all of LifeSat's proposed altitudes, ranging from the LEO circular orbits to the large elliptical orbits, it is the recommended choice for attitude determination, if a singular avionics design is preferred. The accuracy of star trackers is orders of magnitude better than that of horizon sensors (see appendix D), but may be more costly. As far as projected technology is considered, the integrated INS/GPS components (such as the IFMU) seem to be the most promising.

For a spinning vehicle (greater than 10°/sec), however, star trackers are inoperable, and a star scanner is necessary. Star scanners have not been built for spacecraft in more than 10 years, but we have listed (see appendix D) the specifications of Ball Aerospace Systems Division's Star Scanner CS-201 as typical for star scanners.

Other issues and concerns along with suggested future investigations include:

- a. Status of the HEXAD, integrated INS/GPS development
- b. Practicality of the MANS sensor for the LifeSat mission

c. Phase B shortcomings:

- (1) Redundancy: All avionics systems were designed to be two-fault tolerant. A more indepth investigation is needed to assess the various individual avionics component's reliability and lifetimes, look for trade-offs between a combination of sensors that can achieve results of singled-failed sensors, and investigate the most critical points of the avionics system design to determine a more accurate fault-tolerant system. In many instances in Phase B designs, only two strings were provided.
- (2) Power budget: One Phase B design did not include a processor for GN&C computations in its power budget. About one-third of the power required in this design is devoted to triple redundant GN&C processors.
- (3) The use of GPS for primary attitude determination: Problems with this include cycle slips (a GPS problem which has not been adequately solved), antenna baseline difficulties, and GPS availability. Many LifeSat missions carry the vehicle well beyond 6000 km, presently believed to be the upper limit for GPS coverage.
- (4) Claims of GPS achieving sub-20 meter accuracies: This is only for the encrypted form of GPS, which will not be used for LifeSat.
- (5) Use of the gravity-gradient attitude mode: The gravity-gradient torque is small in comparison to other disturbances, especially at very high orbits. This mode would make solar power generation difficult compared to a Sun-pointing attitude mode.
- (6) Phase B selection of smaller momentum wheels than this design, partially due to the Sun-pointing attitude mode, which allows aerodynamic torques to induce periodic disturbances on the vehicle.

d. The use of GPS for an orbiting vehicle is still under investigation.

5.7.3 Navigation State Integrator Model Comparison

Details of navigation state integrator model comparison can be found in appendix E.

5.7.4 Momentum Wheel Sizing

An analysis of the disturbance torques affecting the vehicle's attitude dynamics was conducted to size the momentum wheels and determine the frequency of momentum desaturation maneuvers (table 5-17). The criteria for momentum

wheel selection were to minimize g-loads to the spacecraft and minimize mass-power-volume.

The orbits investigated were 350 km x 350 km, inclination = 33.84°, and 350 km x 20,600 km, inclination = 90°. The configurations investigated were the baseline Phase B without solar panels and the Phase B with extended solar panels added. The disturbance torques investigated were aerodynamic, calculated using "flat plate" theory, and Gravity Gradient = $(\mu / R^3) * [R \times (IR)]$ (i.e. inversely proportional to R cubed). Radiation torques were assumed to be negligible. Other assumptions included center of mass and CG coincident, Sun-pointing attitude, momentum wheels on principal axes, and no effects from a fourth wheel.

TABLE 5-17. LIFESAT MOMENTUM WHEEL SIZING RESULTS

Manufacturer & Spacecraft	Mass; Power ^o ; Vol (kg ; watts ; m ³)	Frequency of Desaturation†	Jet Firing Duration Reqd. For Desat.	Angular Mom (N-m-s) (maximum per axis)	Torque (N-m)
		Roll;Pitch;Yaw (no. orbits)	For 1 jet w/ T=5 lb (seconds)		
Honeywell FSC	6.67; 6 -120 ; 0.022	9.72; 69.6 ; 120.5 9.72; 69.6 ; 120.5 For Deorbit Only	0.37	9.5	0.1
Honeywell CTS *	7.85 ; 12-50 ; 0.017	43.7 ; 186.2 ; 303.5 43.7 ; 186.2 ; 303.5 For Deorbit Only	0.79	20	0.05
Honeywell SRW	9.07 ; 10-150 ; 0.021	42.6; 182.6 ; 297.8 42.6; 182.6 ; 297.8 For Deorbit Only	0.77	20	0.29
Honeywell TDRSS	8.62 ; 12-130 ; 0.019	52.2 ; 215.4 ; 349.2 52.2 ; 195.5 ; 3504 For Deorbit Only	0.89	25	0.75
Honeywell UARS	11.79 ; 24-160 ; 0.034	234.7;842.3;Deorb.Only†† 234.7;462.5;Deorb.Only For Deorbit Only	2.33	80	0.15

* Preferred Selection

^o Power is listed as follows: Steady-State - Peak.

† Frequency of desaturation listed as follows:

Circular orbit without panels.

Circular orbit with panels.

Elliptical orbit with & without panels.

†† Equivalent to about four desaturation burns per mission
for the circular orbit without panels

The analysis showed that, largely due to drag, the circular orbits were found to drive the system to moderately sized wheels which required desaturation maneuvers of less than 1 second duration approximately every 50 orbits. Since the ACS is capable of performing such maneuvers without exceeding accelerations of $1.0\text{E-}4$ g, the microgravity payload environment is not compromised.

The analysis showed the Honeywell CTS was the preferred selection.

5.8 PROPULSION

(Prepared by Ken Kroll)

5.8.1 Introduction

The propulsion system is an integrated hydrazine system that provides three-axis attitude control and orbital maneuvering. This system was selected because of its low cost, high reliability, and avoidance of solid motor debris problems. A pulsed pressurization system minimizes the volume. An attitude change acceleration limit of 10^{-4} g is accommodated using thruster couples. The on-orbit attitude hold acceleration limit of 10^{-5} g may be difficult to meet even with thruster couples, due to plume impingement and thruster nonalignment; therefore, momentum wheels are used instead. The vehicle mass is assumed to be 4800 lbm. The vehicle diameter is 95 inches and leeward surface length is 12 inches. A 900 km circular orbit (worst case) is used for sizing.

5.8.2 Fault Tolerance

The appropriate level of redundancy for the propulsion system was much discussed, and a single-fault tolerant system was agreed upon. More information is available in reference 58.

The option was included to deorbit into an ocean in case of two faults prior to the deorbit burn. An inaccurate deorbit could be provided by the attitude control thrusters firing from alternating sides during a spin.

5.8.3 Thrust Determination

Four Hamilton Standard REA 20-4 thrusters with a thrust level of 125 lbf provide a deorbit burn time of 6.5 minutes when two of the thrusters are in standby. Usually a burn time of less than 15 minutes is desired. Since thrusters must be placed on a leeward pylon to avoid entry heating, moment arm of a thruster couple is less than usual for a vehicle this size. The thruster arrangement

shown in figure 5-10b provides a couple normally and a single thruster for a single fault.

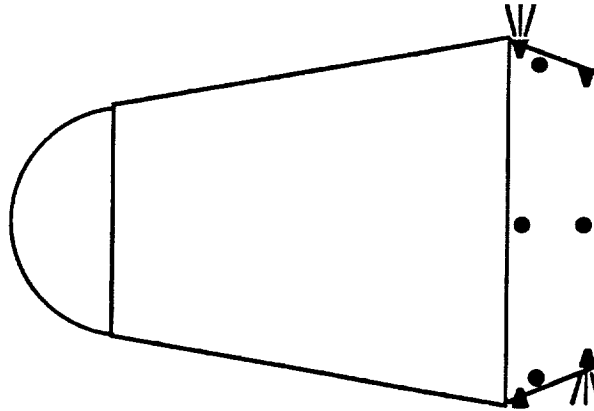


Figure 5-10b. ACS Thruster Arrangement

To cancel a CG offset of 1 inch from the centerline, which is the orbital maneuvering thrust vector, the attitude control thrusters must have at least 2.5 lbf. The closest thruster to the requirement was the 5 lbf Rocket Research MR-50K.

5.8.4 Propellant Quantity

The hydrazine thrusters have specific impulse of 232 seconds for orbital maneuvering, 220 seconds for steady-state attitude control, and 170 seconds for pulsing attitude control. Spacecraft moments of inertia were calculated assuming a uniform sphere. An attitude change precedes each on-orbit activity. The torque of the centrifuge spin-up and despin and the momentum wheel desaturation must be counteracted by the propulsion system. The propulsion system provides attitude hold before and after the on-orbit phase. Extensive orbital adjustment is needed for entry targeting. No leakage is assumed, since the strategy for external leakage is prevention. Proposed propellant usage is in table 5-18a.

TABLE 5-18a. PROPELLANT USAGE SCENARIO

<u>Maneuver</u>	<u>Engineering Requirements</u>	<u>Propellant</u>
Orbital Trim	25 ft/sec	16.1
Orbit Adjust	10 ft/sec	6.4
Deorbit	936 ft/sec	565.7
Entry Adjust	10 ft/sec	6.4
Orbital Maneuvering Reserve	5%	<u>29.7</u>
Orbital Maneuvering Total		624.3
Separation Attitude Change	5 deg/sec, 3 axes	2.0
Operational Attitude Change	5 deg/sec, 3 axes	2.0
Centrifuge Spin/Despin	400 kg, 1.5 g, 1 m dia	0.9
CMG Desaturation	376 ft lbf sec	2.3
Orbit Adjust Attitude Change	5 deg/sec, 3 axes	2.0
Deorbit Attitude Change	5 deg/sec, 3 axes	2.0
CG Offset	1 inch	17.9
Entry Adjust Attitude Change	5 deg/sec, 3 axes	1.8
Entry Attitude Change	5 deg/sec, 3 axes	1.8
Attitude Hold	12 hrs, 3 axes	0.6
Entry Spin-up	+15 RPM	1.5
Attitude Control Reserve	10%	<u>3.5</u>
Attitude Control Total		38.4
Unusable	5%	<u>33.1</u>
Grand Total		695.9 lbm

5.8.5 System Sizing

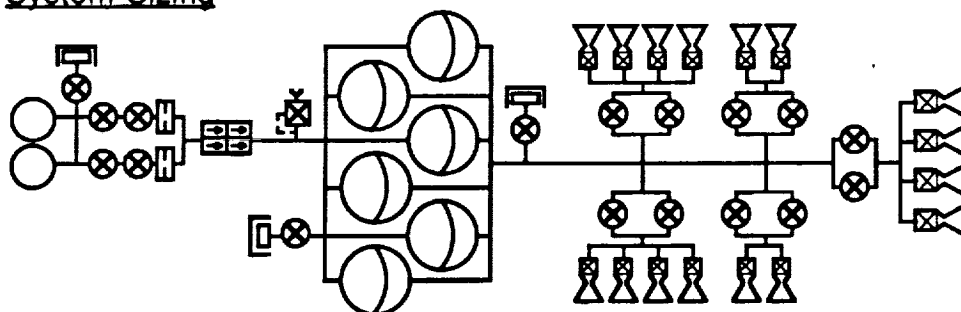


Figure 5-10c. Propulsion System Schematic

The system is single-fault tolerant, both open and closed. Each tank has a 10 percent ullage to allow a small amount of blowdown. When the pressure falls below a lower limit, pressurant tanks at 4000 psi pressurize the propellant tanks to 400 psi. Orifices control the helium flowrate. Check valves keep frozen vapor from blocking the orifices. Disconnects are required for fill.

TABLE 5-18b. PROPULSION SYSTEM MASS SUMMARY

<u>Item</u>	<u>Mass</u>	<u>Quantity</u>	<u>Total Mass</u>
Propellant	698.3	1	695.1
Propellant Tanks (0.7891 ft radius)	10.5	6	62.8
Pressurant	7.1	1	7.1
Pressurant Tanks (0.6595 ft radius)	19.9	2	39.8
Deorbit Thrusters	3.5	4	14.0
Thermal Shielding	20.0	1	20.0
Attitude Control Thrusters	1.1	12	13.0
Relief Valve	0.7	1	0.7
Valves	1.5	17	25.5
Check Valves	0.6	4	2.4
Orifices	0.5	2	1.0
Disconnect	1.0	3	3.0
Line	0.067	100.0	6.7
			891.8 lbm

5.8.6 Power

Thruster valves are open for the length of time required to deplete the usable propellant quantity. Deorbit thruster catalytic bed heating is performed five times, accounting for all orbital maneuvers listed in table 5-18a and one missed deorbit. The ACS thruster catalytic bed heating power is based off the deorbit thruster power, assuming power is proportional to the thrust to the 3/2 power. Attitude control thruster catalytic bed heating is performed 10 times. Pressurant valves are held open for a duration corresponding to replacing all the usable propellant with helium at the deorbit burn rate. Liquid valves are bistable, being opened and closed once.

TABLE 5-18c. PROPULSION SYSTEM POWER SUMMARY

<u>Item</u>	<u>Quantity</u>	<u>Power (W)</u>	<u>Time (sec)</u>	<u>Energy (kW hr)</u>
Deorbit Thruster Valves	2	30	1474.4	0.02457
Deorbit Thruster Catalysts	4	7.6	4800.0	0.04053
ACS Thruster Valves	12	9	148.6	0.00446
ACS Thruster Catalysts	12	0.167	9600.0	0.00534
Pressurant Valves	4	75	1565.1	0.13043
Liquid Valves	10	75	0.4	0.00008
Pressure Transducers	12	0.5	865632.0	1.44272
Temperature Transducers	51	0.5	865632.0	5.41020
				7.058

5.9 THERMAL PROTECTION SYSTEM

(Prepared by T. John Kowal)

This section presents analyses supporting the thermal protection required to prevent the skin temperature of the spacecraft from exceeding 300°F during the thermal soakback period. A discussion of TPS materials is in appendix F.

5.9.1 Thermal Analysis

The trajectory analyzed was for a deorbit from the 20,600 km by 350 km orbit with a vehicle weight of 3500 lbs. This trajectory was not the optimized trajectory which resulted from the entry footprint Monte Carlo analysis. From this trajectory data, the stagnation pressure and total stagnation heating were calculated. The convective stagnation heating was calculated using the Fay-Riddell equation with equilibrium shock assumptions and a radiation equilibrium wall temperature (hot wall). The radiative component of the stagnation heating was found to be 6.25 percent of the convective heating at peak heating. This 6.25 percent factor was applied throughout the trajectory to account for the radiative heating. The stagnation heating and pressure profiles are shown in figure 5-11.

One-dimensional thermal analyses were performed at three different body points on the vehicle, as shown in figure 5-12. The ratio of the local heating rate at body point 2 to the stagnation heating rate is given in reference 35. The local pressure and heating rate ratios for body point 3 are conservative estimates based on the previously assessed AFE aft environments.

Assuming a 0.1-inch thick aluminum skin, the TPS was sized to restrict the structure temperature to a maximum of 300°F. The CRAY version of the AESOP-STAB computer program was used to determine the required ablator thickness at body points 1, 2 and 3. In this preliminary analysis, only the Apollo ablative material (Avco-5026) was considered. Other more lightweight ablative materials may be considered when refining the TPS design in the future. HRSI was also considered for use on the cone (body point 2). The material analyzed was FRCI-12. For the aft region (body point 3), advanced flexible reusable surface insulation (AFRSI) was also considered. To determine the required thickness of both the fibrous refractory composite insulation (FRCI-12) material and the AFRSI material, a thermal math model (TMM) was built using the Systems Improved Numerical Differencing Analyzer (SINDA-85) computer program. The TMM automatically varied the thickness of the TPS until the maximum structure temperature was within (+0°/-2°F) of the maximum allowable temperature. A schematic of the TMM is shown in figure 5-13.

A parametric analysis was performed to determine the amount of internal insulation required to restrict the temperature of the internal components to a given value. The component temperature limit was varied from 80°F to 140°F. Again, one-dimensional analyses were performed using the AESOP-STAB and SINDA-85 computer programs. The models assumed the internal component to be a 0.1-inch thick aluminum plate. This is an extremely conservative assumption. When definite information is available on the mass and location of the various components, a more refined analysis will be performed. A schematic of the TMM is shown in figure 5-14. A natural convection coefficient between the TG-15000 and the component was calculated using an applicable Nusselt number correlation given in reference 36. This correlation assumed the distance between the TG-15000 and the component to be 2 inches and resulted in a convective coefficient of

$$h = 0.79 \frac{\text{BTU}}{\text{ft}^2\text{-Hr-}^\circ\text{F}}.$$

Radiative heat transfer between the TG-15000 and the component was also modeled. However, conduction through the air was neglected. Other factors that were parametrically varied were the recovery time (2, 3 and 4 hours); the blanket density (1, 2, and 3 pcf); and the external environment temperature (75°F and 100°F). The external environment temperature is the temperature of the surroundings to which the surface of the TPS was allowed to radiate energy. The natural and forced convection effects to the surface were neglected. This may or may not be a conservative assumption, depending on the orientation of the vehicle when it lands.

5.9.2 Results

5.9.2.1 Thermal Protection System

The results of the one-dimensional TPS sizing analysis are shown in table 5-19. Because of the extremely high peak surface temperature, an ablative TPS will be necessary on the nose region of the vehicle. However, at the nose/cone interface (body point 2), a high-temperature reusable surface insulation (HRSI) material can be used. The FRCI-12 material should be dimensionally stable at the peak temperature of 2653°F, as plasma arc jet testing has shown it to be capable of a one-mission use at temperatures up to 2900°F [37]. Although the required thickness of the ablative material is less than that of the FRCI-12 at body point 2, the cone TPS weight will be greater if the ablator is used (167 lbs compared to 128 lbs using FRCI-12). This is because of the higher density of the ablator. Also, the FRCI-12 has acceptable RF transmittance characteristics, while the ablator does not. This is an important issue in the design of the antenna system. Therefore, the FRCI-12 material has been chosen for use on the cone region of the vehicle.

An Apollo ablator thickness of 0.386 inches will be required for the base TPS, resulting in a base TPS weight of 58 lbs. The corresponding values for the AFRSI material are 0.75 inches and 22 lbs. The AFRSI material has been chosen as the TPS material for the base region because of the weight saving. However, the peak surface temperature of the AFRSI (1700°F) is only 100°F from the maximum one-mission temperature limit of the material (1800°F). If the heating increases in the future, the uncertainties in the prediction of the base heating may dictate that HRSI be used in this region.

The preliminary TPS configuration is shown in figure 5-15.

The effects of the structure temperature limit and the entry heating on the TPS weight are shown in table 5-20. Various cases were run with the structure temperature limit varying from 300°F to 250°F and 200°F, and the heating

varying from nominal to 125 percent of nominal. As can be seen from table 5-20, designing the TPS with a 25 percent margin in the heating will result in a relatively small increase in the TPS weight. The TPS weight is much more sensitive to the structure temperature limit. As will be shown in the results of the passive thermal control system (PTCS) analysis, it may be necessary to design the TPS to restrict the structure to a lower temperature to protect the interior components from thermal soakback after landing.

In the latter stages of this design phase, several additional orbits were considered. Detailed thermal analyses of the TPS requirements for reentry from these orbits were not performed. One of these orbits, the 60-day orbit, was a highly elliptical orbit which resulted in extremely high heating rates (~ 600 BTU/ft²-sec). An estimate of the TPS weight required for reentry from such an orbit was made using the non-optimized 20,600 km by 350 km orbit. A multiplicative factor of 2.0 was uniformly applied to the heating profile of this trajectory, resulting in a peak stagnation point heating rate of 604 BTU/ft²-sec. The results of this analysis are in tables 5-21 and 5-22. Note that the Apollo ablator has been sized for both the nose and the cone regions, and FRCI-12 has been sized for the base region. The FRCI-12 and AFRSI materials could not be used on the cone region and base region, respectively, as the maximum single mission temperature limits for these materials would be exceeded. The end result of having to use higher density materials on the cone and base is to increase the total TPS weight from 340 lbs to 425 lbs.

5.9.2.2 Passive Thermal Control System

The results of the PTCS parametric analysis are shown in figures 5-16 through 5-20. Figures 5-16, 5-17, and 5-18 show the amount (thickness) of TG-15000 bulk internal insulation required, as a function of the internal component temperature limit, for the nose, cone, and base regions, respectively. The results of these charts assumed a density of 2.0 pcf for the TG-15000 and an ambient temperature of 75°F. While the current baseline recovery time is 4 hours, the effect of lowering the recovery time is also shown on these charts. It is anticipated that the maximum distance between the outer structure and the interior components will be no more than 2 or 3 inches. From figure 5-16 it can be seen that the TG-15000 alone will not be adequate to maintain the internal components in the nose region below a temperature of 140°F, regardless of the recovery time. In the cone and base region (figures 5-17 and 5-18) the TG-15000 alone may be adequate if the maximum allowable component temperature is greater than ~ 110 to 120°F. Supplemental thermal control to be accomplished by active thermal control means (see paragraph 5.10.2.4).

The effect of varying the blanket density is shown in figure 5-19. While using the 1 pcf density material would decrease the blanket weight, the required thickness is unrealistically high. And although the thickness of the 3 pcf material is less than that of the 2 pcf material for a given temperature limit, the spatial benefit is not great enough to compensate for the additional weight penalty.

The effect of varying the ambient environment temperature is shown in figure 5-20. It can be seen that varying the ambient temperature from 75°F to 100°F has little effect on the required blanket thickness. In evaluating these results, it should be remembered that the surface node of the TPS was only allowed to radiate to the environment. The model did not account for any conductive or convective cooling effects from the surface. In future analyses, these effects might be considered when additional information is available to validate the modeling assumptions.

A thermal analysis has been performed to determine the preliminary TPS weight for the LifeSat vehicle. The analysis shows that a total TPS weight of 340 lbs will be required to restrict the structure to a maximum temperature of 300°F. This total weight includes 190 lbs of Apollo ablator (Avco-5026) on the nose region, 128 lbs of FRCI-12 on the cone region, and 22 lbs of AFRSI on the base region. These figures do not include weight for any incidental hardware that may be necessary to integrate the TPS design with the structure. It is suggested that an additional 20 percent be added to the weight for this purpose. Nor do the figures account for any dispersions in the flight trajectory that might increase the reentry heating. However, the sensitivity of the TPS weight to the reentry heating and the structural temperature limit has been studied. The results show that the combined effects of increasing the heating to 25 percent above the nominal and decreasing the structural temperature limit to 200°F can increase the TPS weight by more than 60 percent.

5.9.3 Conclusions

A preliminary PTCS parametric thermal analysis has also been performed. The results of the analysis show that blanket insulation alone may not be adequate to protect the internal vehicle components from the thermal soakback that occurs between landing and recovery. This analysis is very conservative in that it does not sufficiently account for the mass of the structure, which has yet to be defined. The final design of the other vehicle subsystems may also help to simplify the PTCS design. For example, the landing and recovery system may dictate that the nose region and portions of the cone be jettisoned so that the parachute and landing system can be deployed. The portions of the TPS that would be jettisoned in such a design will reduce the energy available during the thermal soakback period. Alternatively, the TPS could be oversized such that the maximum structure temperature is reduced, thereby reducing the amount of heat available to be conducted to the vehicle interior. As the vehicle design matures, an integrated thermal model will be developed to complete the design of the PTCS.

TABLE 5-19. TPS CHARACTERISTICS FOR NOMINAL HEATING
AND 300°F STRUCTURE TEMPERATURE LIMIT

Body Point	Material	TPS Thickness	Peak Surface Temperature	Surface Recession
1	Ablator	1.525	4590°F	0.238 in
2	Ablator	0.670	1856	0.001
2	FRCI-12	1.027	2653	n/a
3	Ablator	0.386	1161	0.000
3	AFRSI	0.750	1700	n/a

TABLE 5-20. EFFECT OF STRUCTURE TEMPERATURE LIMIT
AND HEATING ON TPS WEIGHT

Structure Temp Limit	Vehicle Region	Weight for Nominal Heating	Weight for 125% of Nominal Heating
300° F	Nose (ablator)	190.1 lbs.	204.5 lbs.
	Cone (FRCI-12)	128.2	139.1
	Base (AFRSI)	21.7	24.5
	Total	340.0	368.0
250° F	Nose	227.5	244.2
	Cone	154.1	166.9
	Base	24.5	27.3
	Total	406.1	438.3
200° F	Nose	283.5	301.5
	Cone	197.0	211.5
	Base	32.8	35.6
	Total	513.3	548.6

TABLE 5-21. TPS CHARACTERISTICS FOR ESTIMATED 60-DAY ORBIT
TRAJECTORY AND 300°F STRUCTURE TEMPERATURE LIMIT

Body Point	Material	TPS Thickness	Peak Surface Temperature	Surface Recession
1	Ablator	1.679	5571 ° F	1.016 in
2	Ablator	0.833	2558	0.029
3	FRCI-12	0.366	1993	0.000

TABLE 5-22. TPS WEIGHT FOR ESTIMATED
60-DAY ORBIT TRAJECTORY

Vehicle Region	Weight
Nose (ablator)	179.8 lbs.
Cone (ablator))	205.1
Base (FRCI-12)	40.4
Total	425.3

LifeSat Preliminary Entry Trajectory

22600 by 350 Km Orbit, 3500 lb Vehicle

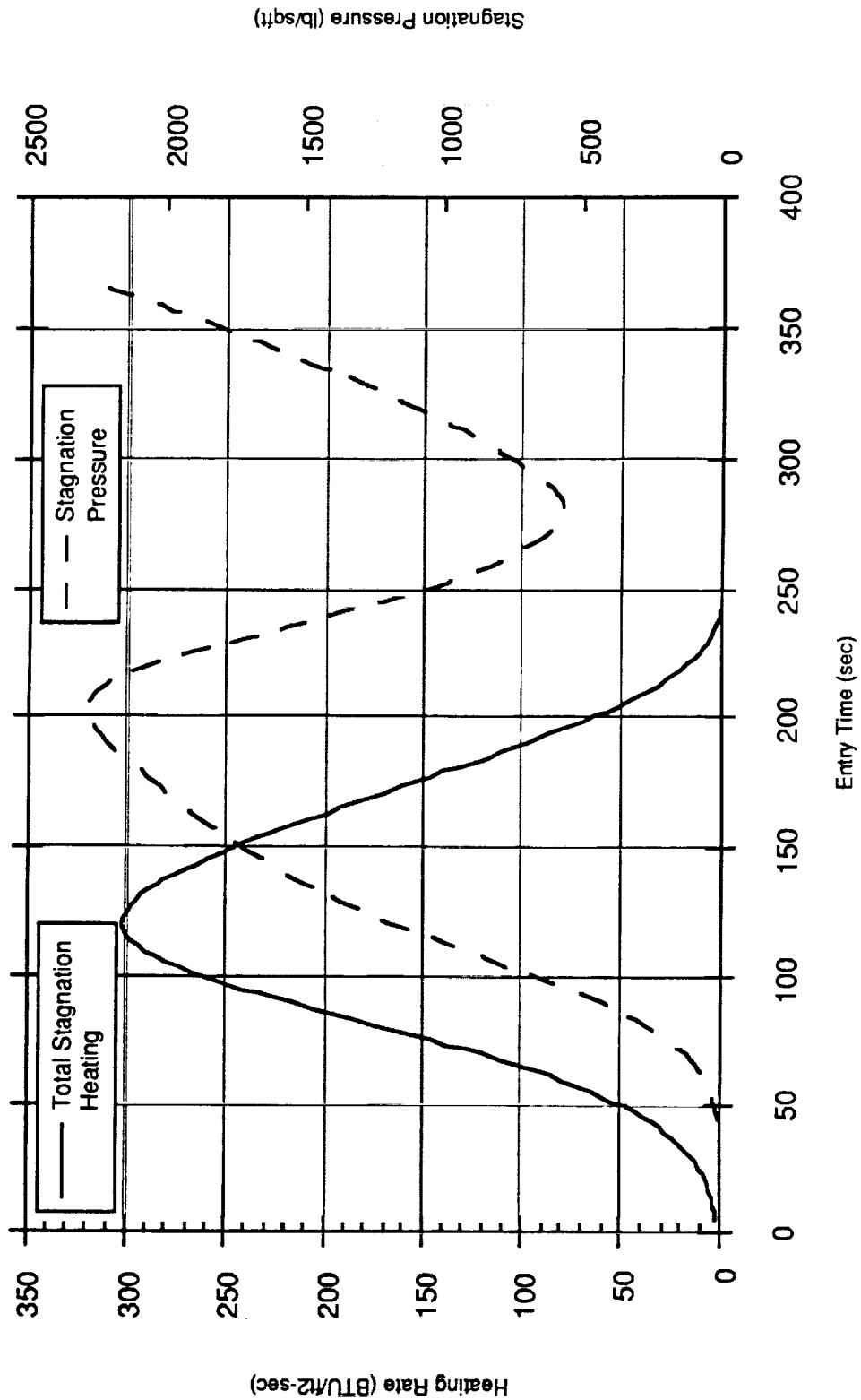


Figure 5-11. Preliminary Entry Trajectory

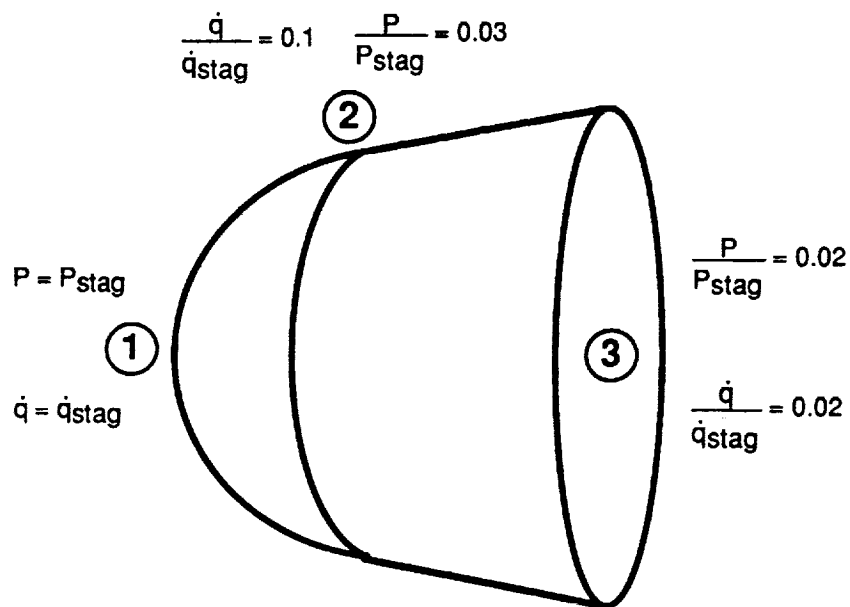


Figure 5-12. Thermal Analysis Body Point Locations

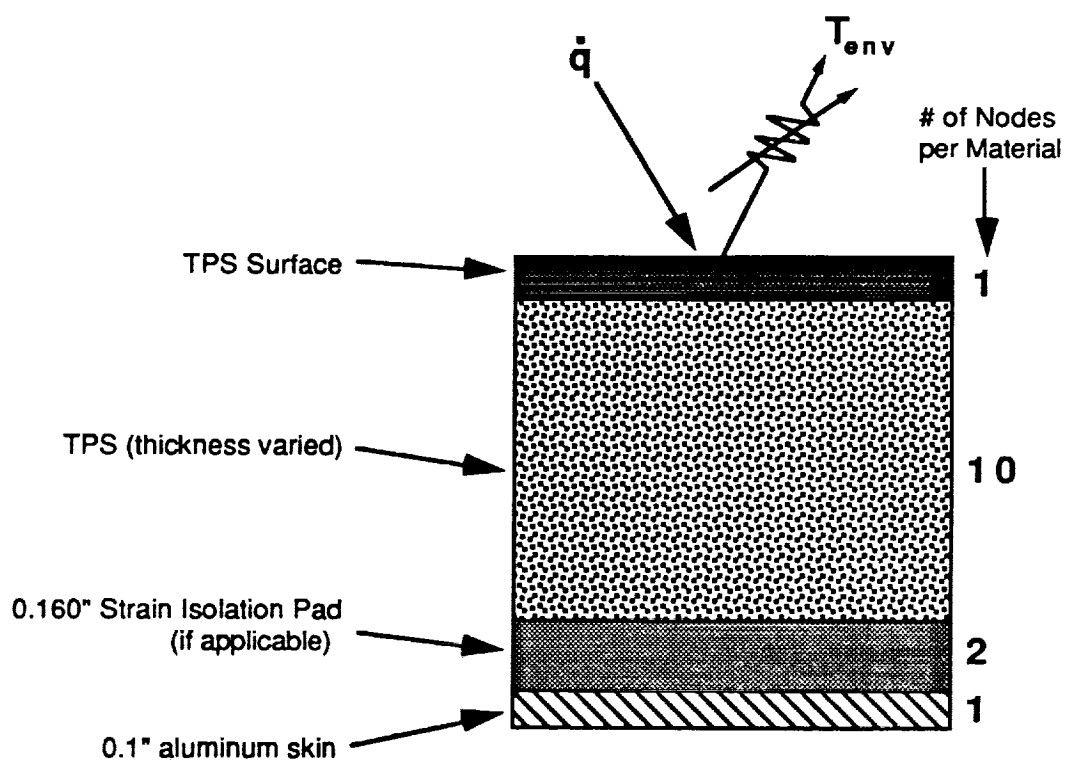


Figure 5-13. Thermal Protection System Thermal Math Model

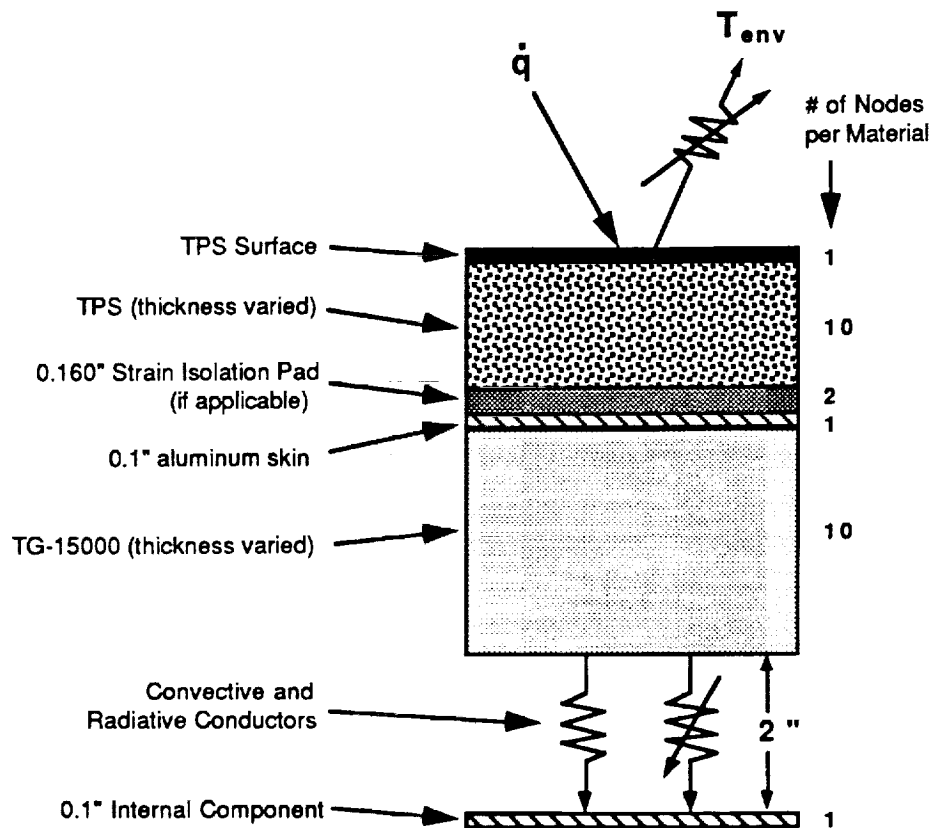


Figure 5-14. Passive Thermal Control System Thermal Math Model

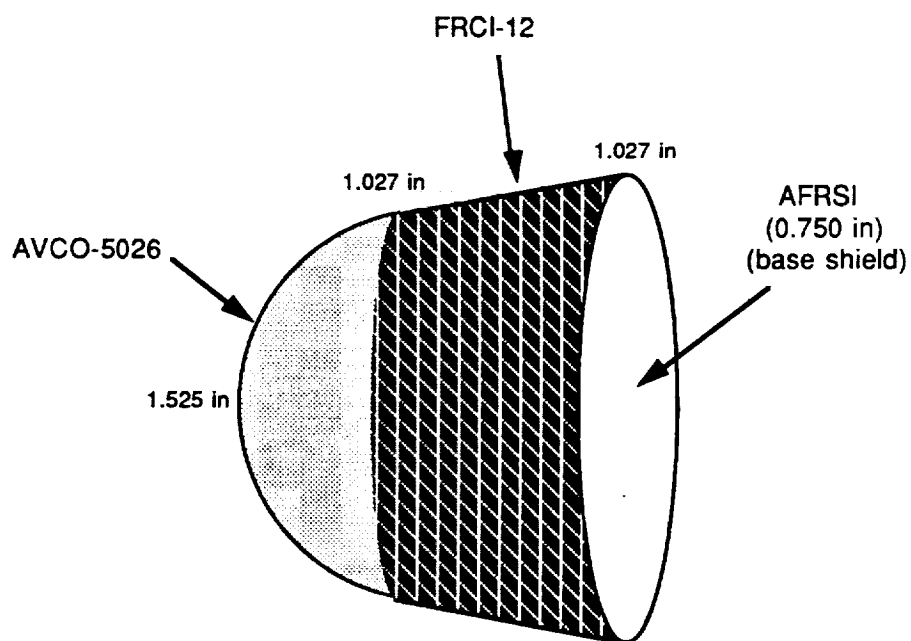


Figure 5-15. Preliminary TPS Configuration

LifeSat Internal Insulation Requirements (Nose Region)

Using 2.0 pcf TG-15000 Bulk Insulation

(assuming 75 deg F Environment)

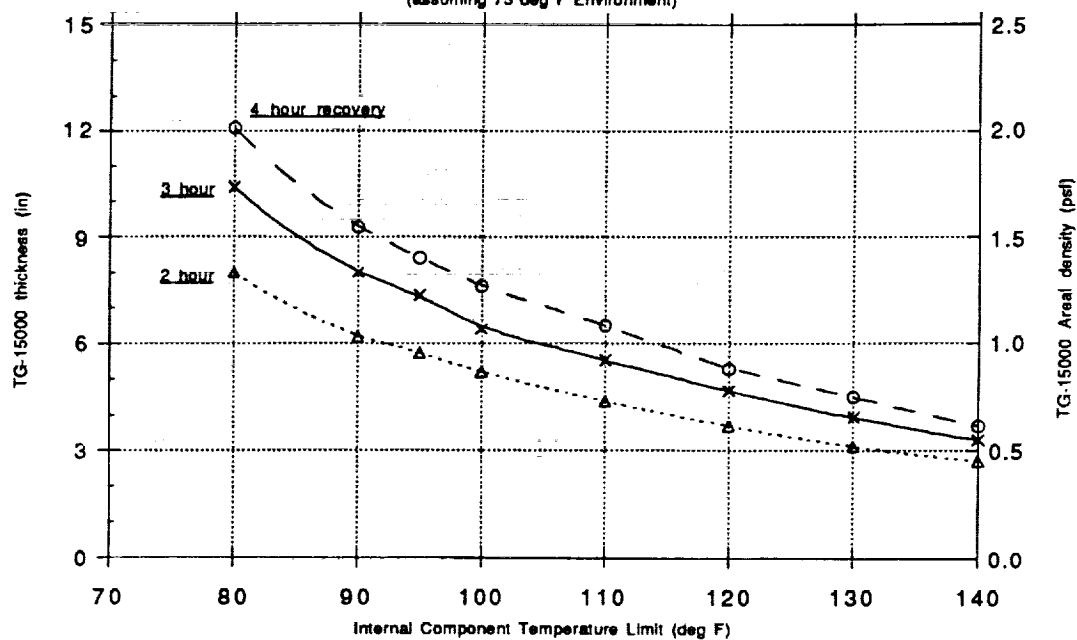


Figure 5-16. Internal Insulation Requirements (Nose Region)

LifeSat Internal Insulation Requirements (Cone Region)

Using 2.0 pcf TG-15000 Bulk Insulation

(assuming 75 deg F Environment)

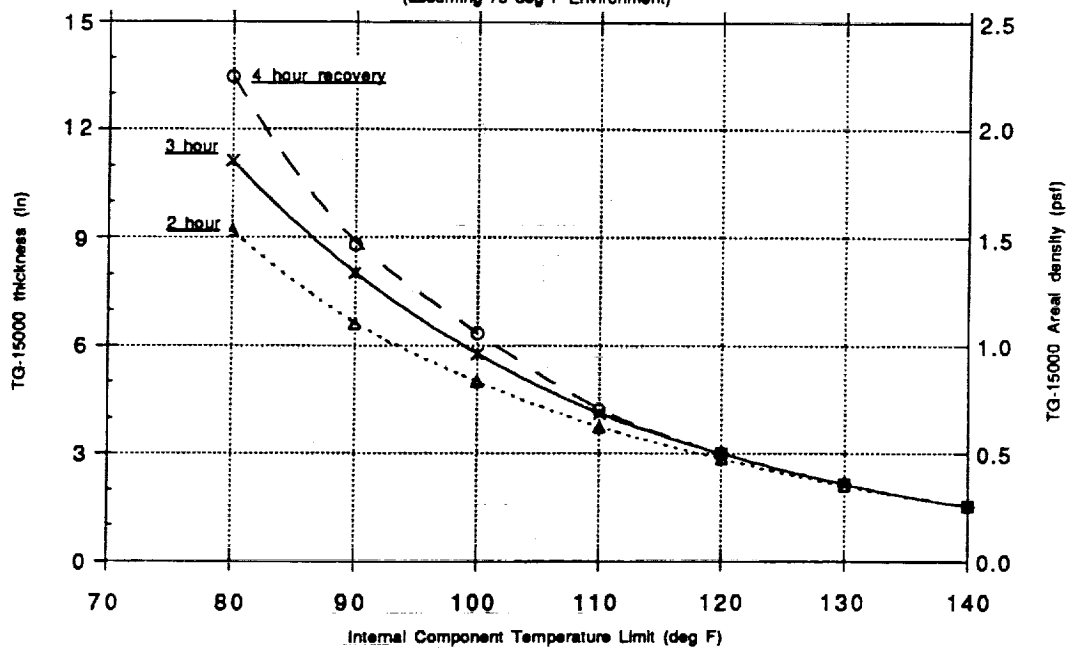


Figure 5-17. Internal Insulation Requirements (Cone Region)

LifeSat Internal Insulation Requirements (Base Region)

Using 2.0 pcf TG-15000 Bulk Insulation

(assuming 75 deg F Environment)

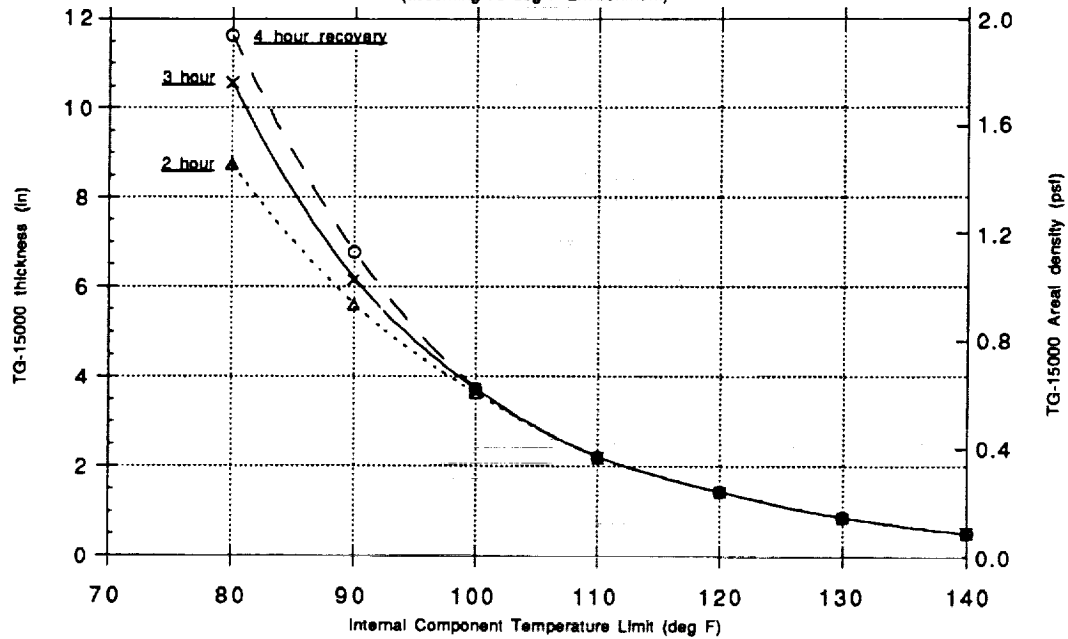


Figure 5-18. Internal Insulation Requirements (Base Region)

LifeSat Internal Insulation Requirements (Cone Region)

Effect of Varying the Density of the TG-15000 Bulk Insulation

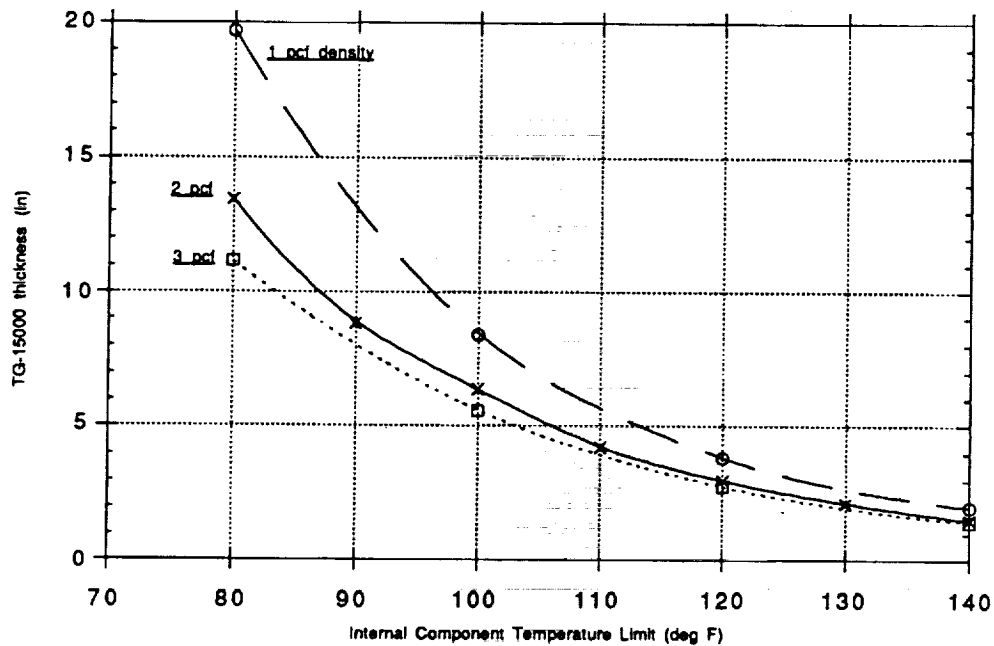


Figure 5-19. Internal Insulation Requirements (Cone Region)

LifeSat Internal Insulation Requirements (Cone Region)

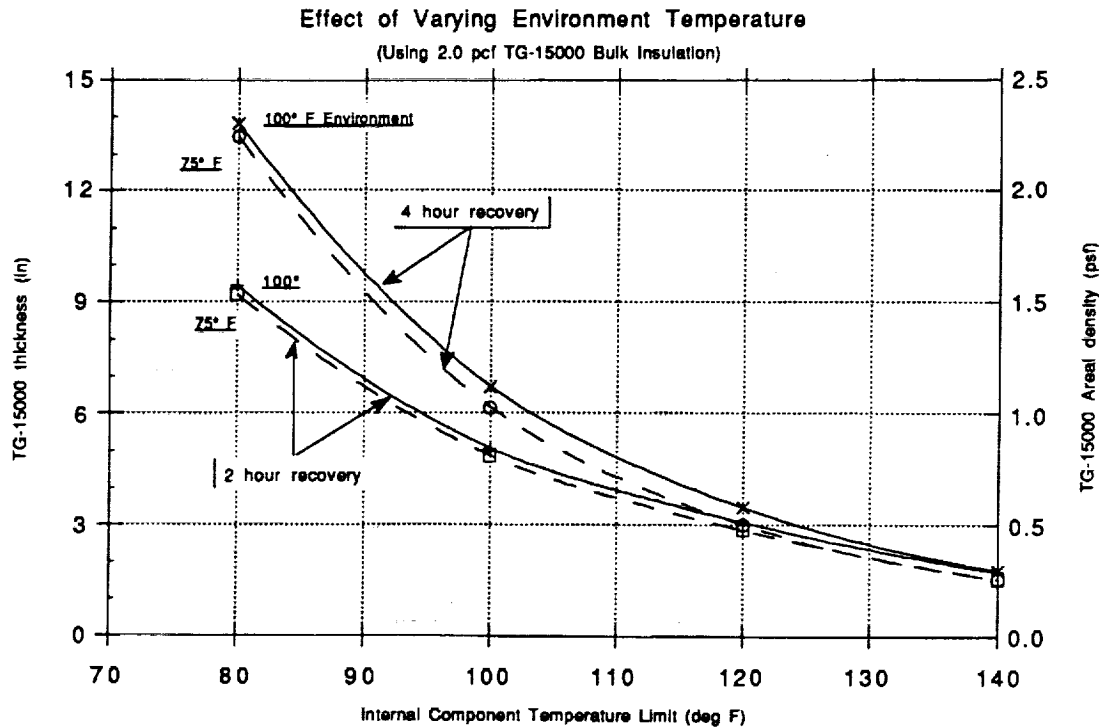


Figure 5-20. Internal Insulation Requirements (Cone Region)

5.10 THERMAL CONTROL SYSTEM

(Prepared by John Keller)

The LifeSat vehicle is a reusable orbiting platform which will examine the long-term effects of microgravity and GCR on living matter. For example, mice and plants will be placed in orbit for 60 days and subjected to extreme dosages of solar radiation. Upon completion of the mission, the vehicle will deorbit and return to Earth, and the test specimens will be retrieved for further study and evaluation.

To achieve reusability and allow Earth reentry, the entire spacecraft is covered with RSI or ablative materials. While these low conductivity materials protect the vehicle (in particular the living payload) from the heat of reentry, they have a detrimental effect on vehicle cooling. Specifically, conduction heat transfer from the inner walls to the outer surface, which radiates to deep space, is severely limited. As a result, passive payload and electronics cooling is nearly impossible, and body-mounted radiator panels in conjunction with an active cooling system must be used.

While a thermal control system (TCS) can be designed for the orbit phase of the flight, there are conditions, such as launch and landing, where radiative cooling cannot be used. Since the TPS limits passive cooling, an alternative heat rejection method must be used. For these situations, a thermal storage system, such as a wax pack or a cryogenic liquid, must be used in lieu of radiative cooling to dump the heat added to the cooling loop.

In addition to the difficulties imposed by the TPS, the cooling system design is also influenced by several additional factors such as the vehicle shape, environmental heat loads, electronic power usage and system reliability. Since this design involves many facets of vehicle performance, the TCS, including its performance requirements and goals, is described here.

5.10.1 Cooling System Requirements and Goals

While the design of a spacecraft's cooling system is based in part on the vehicle's construction and environment, the system's performance requirements are also important design factors. Typically, these requirements dictate that the electronics and the payload be maintained within a specified temperature range. In addition, system reliability and redundancy also play a role in the development process. For the LifeSat program, these requirements are still valid; however, having living organisms as payloads imposes additional constraints. After careful consideration, a list of cooling system requirements and goals has been developed.

- a. Coolant temperatures should not exceed a temperature range of -4°C to 40°C (25°F to 104°F) [9]; however, to keep the mice alive, the coolant temperature should range between 10°C and 30°C (50°F to 86°F) [10]. This temperature range should be maintained for all phases of the mission from prelaunch to recovery.
- b. The system should be able to maintain the necessary temperatures during rapid changes in heat loads.
- c. The coolant should be nontoxic and nonflammable to prevent fatalities (both human and nonhuman) in cases of coolant leaks. The coolant should be able to work within a large range of temperatures so that freezing (and, if applicable, boiling) does not occur. Finally, the fluid should not decompose during the entire mission time.
- d. The entire TCS must meet CRIT-1 redundancy (three components), since its failure will result in vehicle failure. No allowances will, however, be made for catastrophic failures, such as meteoroid punctures to fluid lines or pump disintegration.
- e. A separate payload module refrigeration system must remove 50W of heat at -20°C [9].

- f. The system should not be complex.
- g. The system should require minimal power.
- h. The system should take up a small volume and weigh as little as possible.

A cursory examination of the above requirements and goals shows that several are incompatible. For example, a two-phase system is lighter than a single-phase system; however, two-phase systems are substantially more complex, more expensive, and less reliable. Also, a system with a large volume (weight) of coolant can handle rapid fluctuations in heat load, but there is a substantial weight penalty. As evidenced, the design of the cooling system is not a straightforward task. The remainder of this report will describe a simple trade study in which an optimal cooling system was developed.

5.10.2 Development of the Cooling System

The TCS design was developed in three steps. First, a basic system was developed for the orbit phase of the mission using a numerical modeling process. Next, the additional components needed to meet the redundancy requirements were added. Finally, modifications to allow the TCS to operate during the ascent, descent, and recovery phases of the mission were incorporated.

5.10.2.1 Determination of Vehicle Heat Loads

The first step in the development of a TCS is to determine the amount of heat to be rejected so the cooling system can be sized accordingly. In general, there are two main sources of spacecraft heating: environmental (solar and Earth) and vehicle-generated (electronics, payloads).

5.10.2.1.1 Vehicle-generated heat loads. In the vehicle, heat is generated by several sources: the payload, the avionics, the Environmental Control and Life Support System (ECLSS), and the C&T equipment are the primary sources. A breakdown of their maximum power usage (which is also the heat generated) can be found in figure 5-28. As shown, 600W is a representative heat load for orbital conditions; however, to account for the inevitable increases in heat loads, 900W was used in the development of the heat rejection system.

5.10.2.1.2 Environmental heat loads. The environmental heat load experienced by the vehicle originates from two sources: the Sun and the Earth. As discussed in appendix G, the environmental heat load will be small. This approach was taken in the design of the TCS.

5.10.2.2 Development of a Numerical Model of the TCS

After the environmental and vehicle-generated heat loads were estimated, the cooling system for the orbit portion of the mission could be designed. Numerical modeling must be employed to assist in designing the system since all three modes of heat transfer (conduction, radiation, and convection) are present, and simple solutions are available. For the present system, the SINDA/FLUINT (Systems Improved Numerical Differencing Analyzer/Fluid Integrator) routine [11] was used to predict this multimode heat transfer process and (using an iterative scheme) determine the flow rates, tube sizes, and radiator design.

5.10.2.2.1 Development of the basic model. As previously determined, the cooling system must reject 900W of heat. Since earlier designs of the LifeSat cooling system [12,13] considered substantially smaller heat loads, these references will be used only as guides in the development of the current system. A schematic of the basic design is shown in figure 5-21. Here, heat exchangers or cold plates, radiator panels, control valves, and a pump all affect the thermal and hydrodynamic response of the system.

ACCUMULATOR

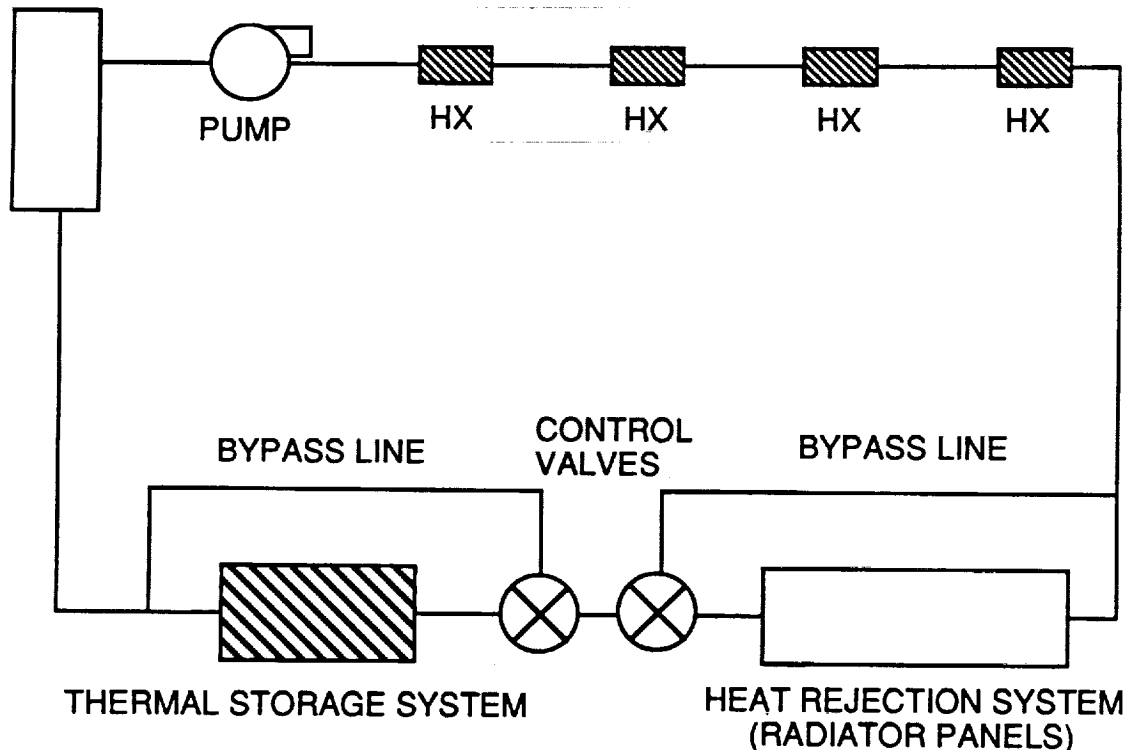


Figure 5-21. Schematic of the Flow Network

During the normal operation of the cooling system, the working fluid leaves the pump and flows through a series of heat exchangers which are used to cool the electronics and the payload. After acquiring heat from these components, the fluid flows into the radiator panels where heat is lost by radiation to deep space, in turn cooling the fluid. Next, if the radiator panels are not operating, the bypass will be open and the fluid will flow through the thermal storage system where it will reject heat. This cooled fluid then returns to the pump where the cooling process begins again. Throughout the system, control valves are used to maintain fluid temperatures, since there may be times, such as low power usage, when the radiators or the thermal storage system overcool the working fluid. The TCS also contains an accumulator to maintain system pressures and fluid levels.

Before the system of figure 5-21 could be modeled, as with any numerical model, several assumptions had to be made.

- a. Only steady-state conditions at maximum power levels will be considered, since exact power usage timelines and orbits are unavailable. This condition considers the maximum heat load and allows for worst case system sizing.
- b. Environmental heat loads will not be included, since they would be negligible if appropriate (and necessary) control measures are employed.
- c. The metal mass (thermal capacitance) of the heat exchangers will not be considered, since these devices have yet to be sized and this small amount of mass has little overall effect on system response [14]. Therefore, the heat loads can be modeled as direct heat inputs to the fluid.
- d. The pump will be modeled as a constant mass flow rate device.
- e. The thermal storage system will not be considered during this phase of the modeling.
- f. The accumulator will be modeled as a constant pressure source.
- g. The flow in each passage of the radiator panels is identical. While each flow passage could be modeled, the small gains in accuracy would be offset by substantial increases in run time [14,15,16].
- h. Since a working two-phase system has yet to be developed for any spacecraft, only a single-phase cooling loop will be considered.

With these modeling assumptions in place (a complete description of the modeling terms can be found in reference 11), a simple SINDA/FLUINT model was built; a schematic of this system is shown in figure 5-22. Here, the pump is modeled with an MFRSET (Mass Flow Rate SET) which supplies a constant flow rate to the entire fluid network. The heat exchangers are modeled as single fluid junctions (JUNC) also known as lumps, and the required heat inputs

are applied at these locations. The accumulator is modeled with the TANK option to account for its volume and with the PLEN (plenum) option to maintain constant system pressures and fluid levels. The bypass flow loop is modeled with an additional MFRSET, but for the purposes of this study, its flow rate is set to zero. Since the modeling of the radiator panels is complex, this approach is described in the next section.

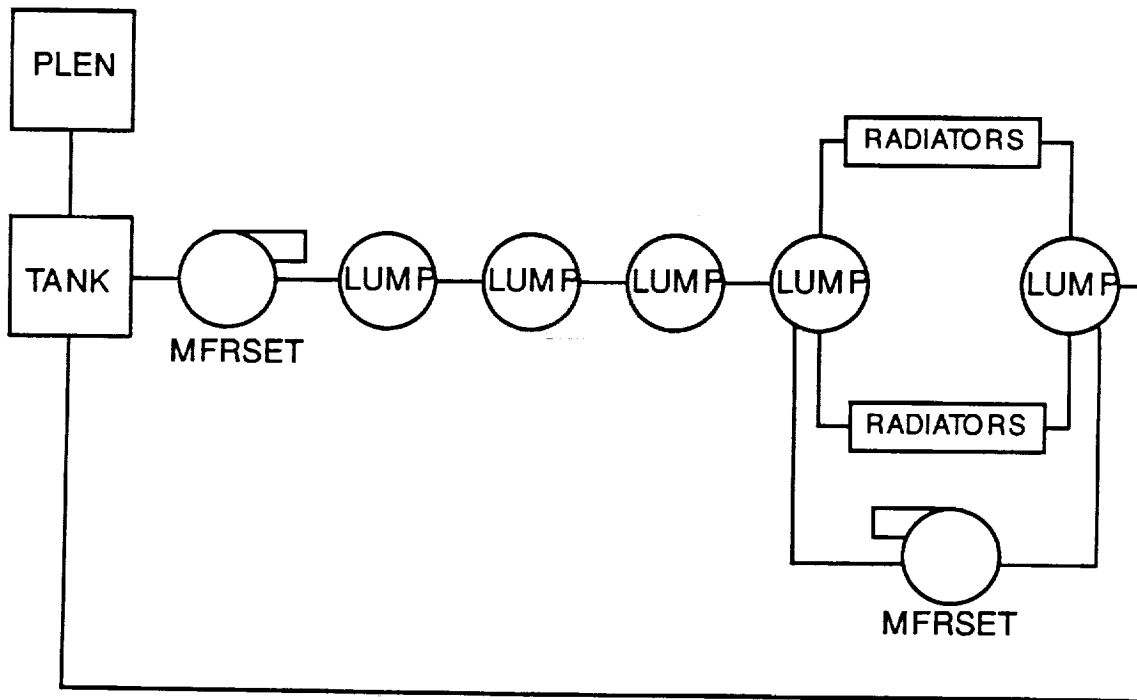


Figure 5-22. Schematic of the SINDA/FLUINT Model

5.10.2.2.2 Radiator model development. The design of efficient radiator panels is important in the overall performance of the TCS. For example, the amount of fluid required, the flow rate (pump size and power) and the overall weight and volume are all influenced by the design of the radiator panels. In addition, the vehicle's size and weight are also influenced by the construction of the panels. Therefore, to optimize the design of the TCS, it is important that the radiator panels be accurately represented in the SINDA/FLUINT model.

Typically, radiator cooling panels are an assembly of identical parallel flow passages (tubes) within a holding structure. A cutaway view of a such a system is shown in figure 5-23. Here, hot fluid within the flow channels cools by simultaneous convection and conduction to the radiator panel walls, which then radiate to deep space. This heat transfer process is governed by several parameters which include, but are not limited to, the flow passage hydraulic diameter, the number of flow channels, the fluid's thermophysical properties, the metal's material properties, the thickness from the inner wall to the outer wall, and the outer surface's coating. The backside of the panel may be insulated

with a multilayer insulation (MLI) blanket to reduce the heat gain from vehicle components.

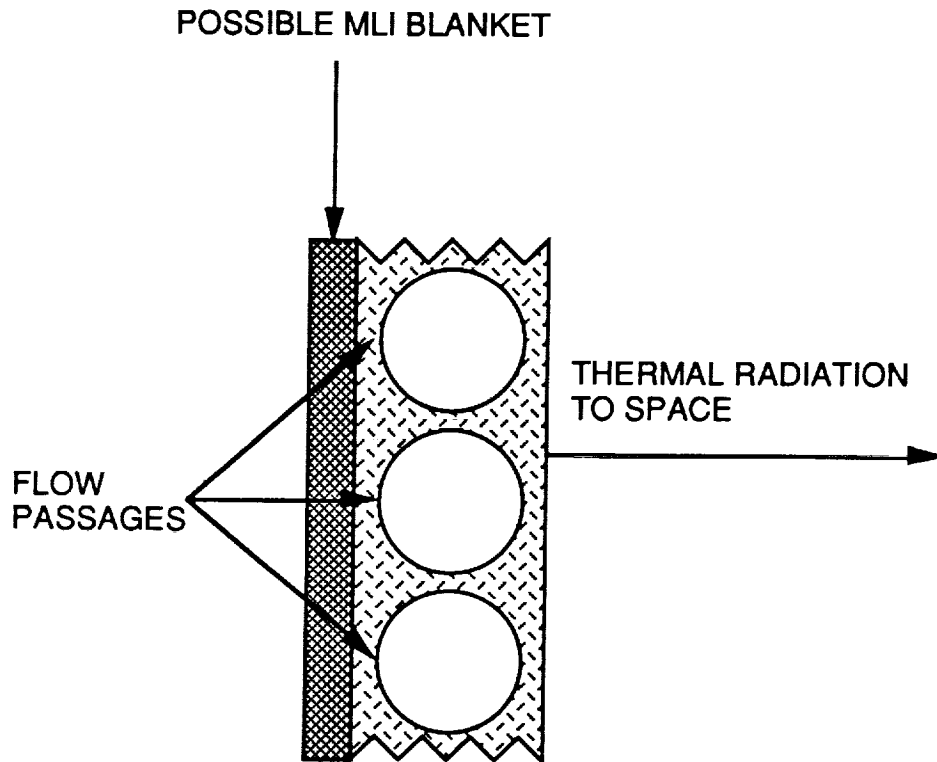


Figure 5-23. Sectional View of a Radiator Panel

To model the radiator panels, a series of eight JUNCs and TUBEs, as shown in figure 5-24, was used to represent each flow passage. This modeling approach can provide an accurate representation of the heat transfer processes within a radiator panel tube [16]. To account for these multiple and identical flow passages, the duplication options (DUPI, DUPJ, DUPL, DUPN) were used. Each fluid lump (JUNC) is then connected to the metal walls by a heat transfer tie to account for the convection with the side walls. The value of this heat transfer tie is determined internally by the SINDA/FLUINT routine and is based on the fluid velocity, number of tubes, fluid thermophysical properties, tube diameter, and tube length. The wall is represented by two SINDA nodes which are connected by a conduction conductor. The value of this connector (the conductance) can be determined by using reference 11. Lengthwise panel conduction was not considered since it can be shown that, compared to radial conduction, axial conduction is negligible. The outer surface is connected to a deep space boundary node which is held at a conservative sink temperature of -60°F by a radiation conductor, whose value can be determined using reference 5. The representative model of this simultaneous heat transfer process is shown schematically in figure 5-25.

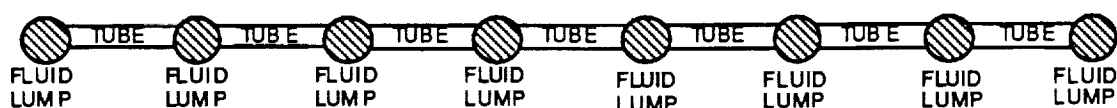


Figure 5-24. SINDA/FLUINT Representation of a Radiator Flow Passage

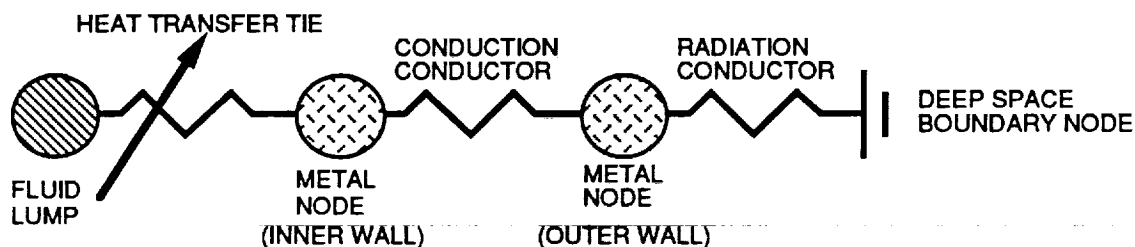


Figure 5-25. SINDA/FLUINT Representation of a Radiator Panel Wall

5.10.2.2.3 Fluid Selection. As discussed earlier, many factors influence the choice of the working fluid; however, the most important is the temperature range that the fluid will experience. That is, the fluid cannot freeze or boil for all phases of the mission, and it also must provide adequate cooling for the payloads and the electronics. Since the orbit(s) of the mission have yet to be determined, the vehicle's surface temperatures are not known, but it should be expected that the vehicle will experience temperatures similar to those of the Space Station Freedom (SSF) and the Space Shuttle (from -62°C to 27°C [16,17]). For this study, any fluid selected must be able to operate in this temperature range.

Many fluids have been used as coolants; common fluids have included water, ammonia, and low molecular weight freons [16,18]. Water is an ideal coolant, since it is nontoxic and nonflammable, but it will freeze at many of the temperatures encountered and cannot be used as a coolant. An ethylene glycol-water mixture cannot be used since there may be freezing problems. Ammonia can meet the temperature requirements, but it is toxic [19], may cause fatalities in leak situations, and also requires stainless steel components. While freons such as R-11, R-12, R-21, and R-22 can meet the requirements of the working fluid, including toxicity [19,20], these fluids may break down under the high levels of radiation experienced by the vehicle [10]. Since there are no obvious candidate working fluids, both ammonia and the freon refrigerants will be examined.

5.10.2.2.4 Results of the modeling process. Once the model of the basic system was developed, it was used in a parametric study to determine flow rates, radiator sizing and material, tube sizing, and fluid selection. Since the construction of the radiator panels is probably the most important aspect of the TCS design, a substantial portion of the iterative procedure time was devoted to this component, including determining a favorable mounting location.

A simple parametric study, using the model, revealed that the most favorable mounting location for the radiator panels is on the aft, while the least favorable location is under the TPS. A system underneath the TPS can only reject 125W of heat. A deployable system which uses approximately 40 percent less radiator area was also considered; however, this system is substantially more complex, more prone to fault, and requires a deployment mechanism (added system weight). Therefore it was eliminated as a mounting scheme.

After the iterative procedure was completed, the following design was found to describe the TCS. The recommended system should contain eight 1.0 ft x 1.75 ft (14 ft² of total radiator area) aluminum radiator panels which contain 75, 1/8-inch diameter flow passages, separated by a 1/32-inch section of aluminum. The distance from the tube walls to the outer surface should be 0.045 inch, and the backsides of the panels should be covered with MLI to reduce heat gains. The connecting hardware throughout the TCS should be 3/8-inch diameter aluminum piping, while the accumulator should have a volume of 0.1 ft³. The pump should operate at 100 psia, with a flow rate of 250 lbm/hr which will allow the fluid to cool or heat properly without any cold or hot spots in the heat exchangers or radiator panels. Finally, it was found that all the previously listed freons can provide adequate cooling, but R-12, being the least toxic, is recommended for use. If R-12 cannot be used, the modeling study also indicated that ammonia can be used as the coolant, but the system must contain all stainless steel parts and the radiator flow passages must be coated with stainless steel.

5.10.2.3 Cooling System Modifications for the Redundancy Requirements

As discussed earlier, the cooling system must meet CRIT-1 redundancy requirements, since its failure will lead to a vehicle failure and possibly endanger human life. For the current system, only the pump, the control valves, and the isolation (solenoid) valves need to meet this redundancy requirement, since the tubing is considered failure (leak) proof [21]. The heat exchangers, cold plates, radiator panels, and thermal storage system, do not need to meet this requirement, since they are essentially a collection of tubing and by the Second Law of Thermodynamics [22] which prohibits heat transfer from cold to hot regions, these passive devices cannot ever fail to transfer heat. In addition, the radiator panels, cold plates, and thermal storage system have multiple flow passages so that, in the event of a blockage, there will be little loss in system performance. The TCS will contain one accumulator, since this device is essentially a large (leak proof) tube. (A one-accumulator system is employed on the SSF [18]). Finally, the monitoring equipment for the thermal controls should meet the redundancy requirement, including interfacing to the main computer, to ensure that the proper temperatures are maintained.

Figure 5-26 shows the preliminary layout of the TCS including all redundancy requirements. Here, the pump package contains three pumps in series with their associated isolation valves. To ensure that each pump is operating correctly, three independent monitoring devices, a tachometer, a flow meter and

a downstream thermocouple examine different aspects of pump performance. The tachometer and the flow meter, directly measure pump performance, while the thermocouple indicates if fluid is being supplied to the downstream locations. An ammeter is also included in the pump system to monitor power usage and shut down the pump if it is drawing too much current. A schematic of this monitoring setup for a single pump is shown in figure 5-27.

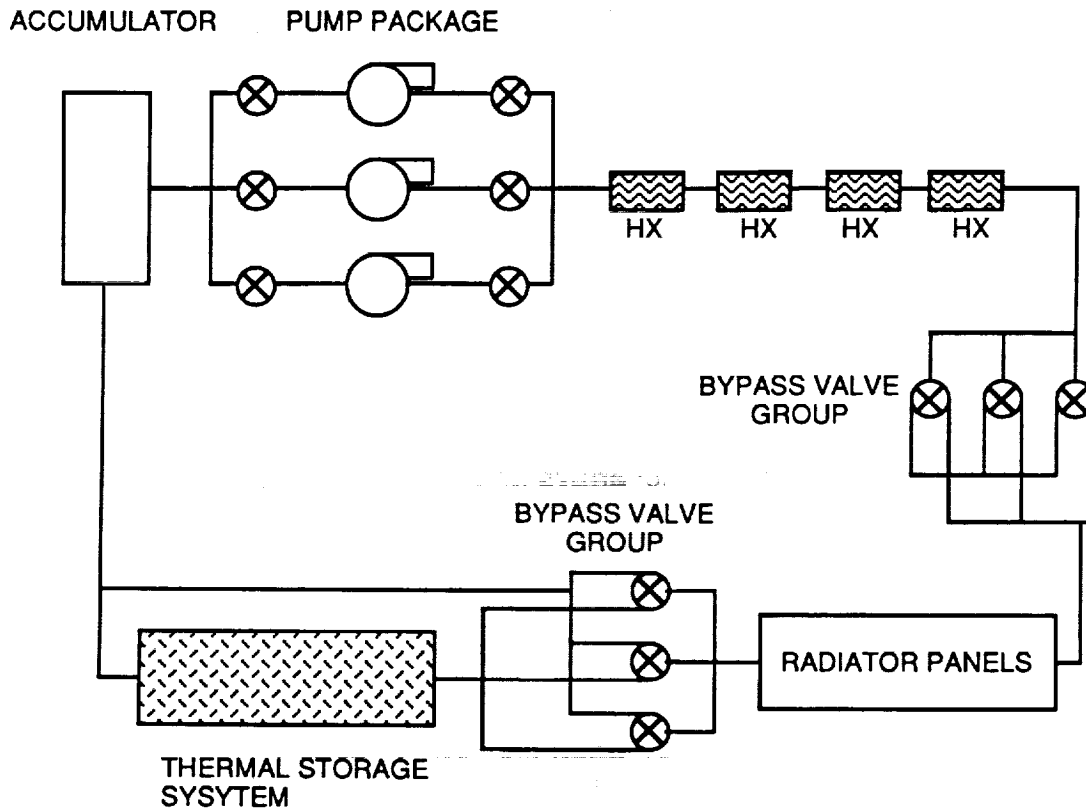


Figure 5-26. Schematic of the TCS Including Redundancy Requirements

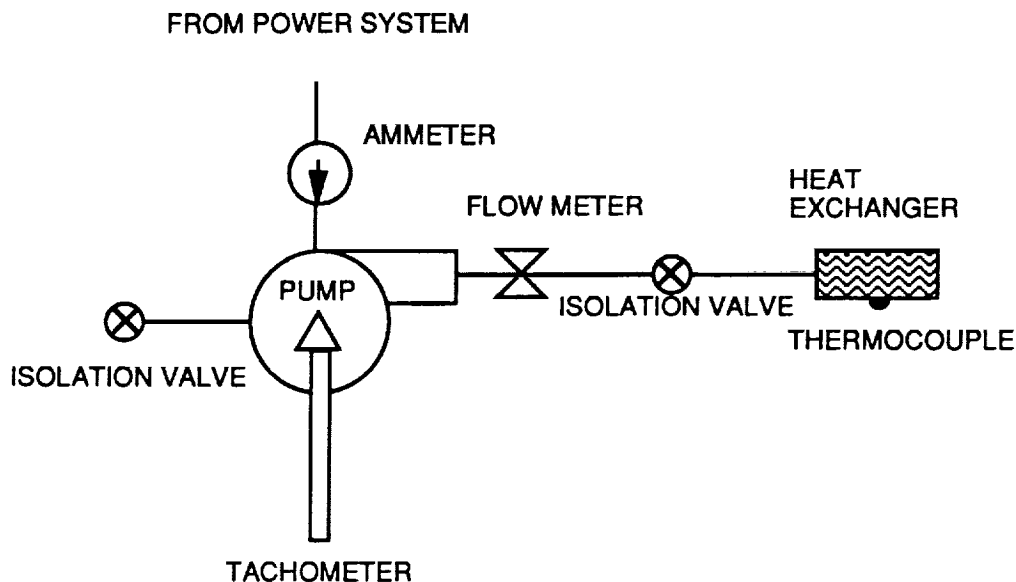


Figure 5-27. Schematic of the Pump Monitoring System

Located at the inlet to the radiator panel arrays and the thermal storage system are control valves which regulate the bypass flow. These valves are required to ensure that the correct fluid temperatures are maintained and that overcooling of the PM and electronics does not occur.

5.10.2.4 Thermal Storage System

As discussed earlier, there will be times when the radiator panels will not be able to reject heat and an alternative heat rejection (sink) source is required. While there are many methods to remove heat from a liquid, due to the weight and volume limitations imposed by the vehicle, the number of useful methods is limited. Typical thermal storage systems have considered either boiling a liquid [23] or melting a solid [24], and both methods have advantages and disadvantages. Due to the high heat of vaporization associated with boiling, these systems tend to be lightweight and compact, while solid/liquid phase systems are substantially heavier and bulkier. On the other hand, once the liquid is boiled it is not reusable, while a melted solid can be refrozen and can conceivably be used an infinite number of times. Therefore, each method will be examined as a possible thermal storage system for the LifeSat mission.

The first step in the development of a thermal storage system is to determine the amount of heat to be rejected, so this system can be sized. In general, the power loads shown in figure 5-28 indicate the amount of heat that must be rejected. A more detailed summary of the expected heat loads is shown in table G-1. As is evident, a great deal of heat can be generated especially during the prelaunch and reentry phases of the mission. Table G-2 shows the required storage masses of several candidate systems to meet the cooling requirements

for each portion of the mission. Even excluding the prelaunch phase of the mission, it is clear that only an ammonia boiler system can provide the required heat rejection at a reasonable weight.

To overcome the large mass necessary for prelaunch conditions, the following cooling scheme can be used to substantially reduce the ammonia mass. During prelaunch times, the vehicle's cooling system should be attached to an external cooling system, most likely a portable cooling system and an internal heat exchanger. Immediately before launch, this system will be disconnected and the vehicle will provide its own power and cooling. It is estimated that the vehicle will be on its internal systems for 1 hour [25]. Further reductions of the ammonia mass can be obtained by assuming that for half of the reentry time (3 hours) the radiator panels are functioning. With these assumptions, 45 lbm of ammonia is needed. Including some additional mass for increases in power, the entire system should weigh approximately 55 lbm.

5.10.2.5 PM Refrigeration System

The PM is required to supply a constant -20°C temperature source which removes 50W of heat [1]. The SINDA/FLUINT model indicates that, due to temperature limitations, the main TCS cannot meet this requirement, and a separate refrigeration unit is necessary. To meet this requirement, it is estimated that a separate cooling system weighing 40 lbm with a volume of 0.75 ft^3 [26] is needed. To make the redundancy requirements and achieve mission success, two refrigeration units are needed which will decrease the available volume and payload weight. While these weights and volumes could be incorporated into the vehicle, the power requirements of this separate refrigeration unit will be approximately 200W (50W of heat removal does not mean that one needs to put in 50W of power [26]), substantially greater than what is estimated for either the ECLSS or the PM. Since this system has a large power draw, a large volume, and a substantial weight penalty, it is recommended that it be removed from the LifeSat mission or placed on a separate mission. If this is done, there will be substantial reductions of weight, power, and occupied volume in the PM which can be used for additional scientific research.

5.10.3 Weight, Volume, and Cost Estimates

Tables G-3 and G-4 show the estimated weight, volume, and cost of the major components of the TCS for both the dry and wet (liquid filled) conditions including the redundancy requirements. Except for the radiator panels, the component weights, volumes, and costs in these tables can be found in references 27 and 28. For this equipment, it is estimated that the panels will be manufactured at a cost of \$100/hr with 10 hours of labor. The weight estimate for the TCS is 180 lbm dry and 205 lbm with the working fluid. The estimated system volume is 1.5 ft^3 . To account for risk margins, the final cost of the

cooling system is estimated to be \$80,000. These estimates do not include certification and installation costs.

5.10.4 Summary and Conclusions

A conceptual design of a TCS has been developed for the vehicle using basic heat transfer equations and a simplified SINDA/FLUINT model. Using the model in an iterative procedure, the following design was found to describe the TCS. The recommended system should contain eight 1.0 ft x 1.75 ft (14 ft² of total radiator area) aluminum radiator panels which contain 75, 1/8-inch diameter flow passages, separated by a 1/32-inch section of aluminum. The distance from the outer surface to the flow passages should be 0.045 inch, and the backsides of the panels should be covered with MLI to reduce heat gains. The panels should be mounted on the vehicle's aft. The connecting hardware throughout the TCS should be 3/8-inch diameter aluminum piping, while the accumulator should have a volume of 0.1 ft³. The pump operates at 100 psia, with a flow rate of 250 lbm/hr which allows the fluid to cool or heat properly without any cold or hot spots in the heat exchangers or radiator panels. Finally, it was found that all the previously listed freons can provide adequate cooling, but R-12, being the least toxic, is recommended for use. If R-12 cannot be used, the modeling study also indicated that ammonia can be used as the coolant; but the system must contain all stainless steel parts, and the radiator flow passages must be coated with stainless steel.

Preliminary estimates show that, if solar heating is not controlled, vehicle performance will be severely affected. Specifically, the solar cells will overheat and the radiators of the TCS will not perform effectively, if at all. To overcome these problems, the solar cells must be put into deployable arrays.

5.10.5 Recommendations for Future Work

While a preliminary design for the TCS has been developed, additional work in several other areas must be performed along with several minor changes in vehicle design. This work must be accomplished so that the exact sizing and selection of the cooling system components can be made. Specifically, the size of the radiators, the amount of fluid, the size and power requirements of the pumps, and the design of the cold plates and heat exchangers depend on information from other vehicle systems.

First, the power requirements of the various vehicle systems need to be determined, since a majority of the cooling system design, including the thermal storage system, depends on the heat generated by the electronics and the PM. The transient operation of these components is also needed to ensure that the system design can adequately control rapid changes in heat loads.

Second, the vehicle design, in particular the outer surface shape, must be agreed upon. Heat losses to the environment, the sizing of the radiators, and the heat gained from reflected solar radiation are affected by the shape of the vehicle.

Third, the expected orbits of the mission must be known. Orbital position plays an important role in the design of the cooling system, since environmental heat loads depend on orbital parameters. The amount of Earth shading also affects cooling system design, since cooling in the Earth's shadow is more efficient than in direct sunlight and the temperature controls must respond properly to avoid overcooling.

Fourth, after reentry, there may be significant environmental heat loads due to soakback from the TPS tiles. If the heat load is large, the cooling system may be undersized, and the biological payloads will die. To overcome this problem, the TPS must be sized accordingly and the inner structural walls covered with insulation; however, at this time, this analysis has yet to be conducted. Even with increased thermal protection, there will be some environmental heating and the cooling system must be modified to accommodate this added load.

After work in these areas has been completed, a more detailed thermal analysis must be conducted so the cooling system design can be optimized. This analysis will be conducted using two methods. The thermal synthesizer system (TSS) will be used to determine the environmental heat loads for a given orbit and the radiation conductors between sections of the vehicle's outer surface. Once this portion of the analysis is completed, a detailed SINDA/FLUINT model will be developed and used to predict the thermal and hydraulic response of the TCS, under transient heat loading (environmental and vehicle-generated) conditions. Using these results, the TCS can be developed, including sizing the system and the operation of the control valves.

Although not important to the design of the TCS, several additional areas should be investigated, since they may have important impact on vehicle operation.

The use of the separate refrigeration system needs to be investigated. Even though this system has a minimal effect on the design of the TCS, it causes a substantial weight, power, and volume penalty for the spacecraft. It should be determined if this system can operate at higher temperatures, such as -5°C , which will reduce all of the aforementioned problems, or if this requirement is necessary.

The thermomechanical effects of a continuously Sun-pointing surface also need to be analyzed. With one surface almost always being heated and one surface being cooled, the vehicle may experience severe thermal stresses which could create gaps in the TPS or deform the structure.

5.11 ELECTRICAL POWER REQUIREMENTS

(Prepared by David Rodriguez and Eric Darcy)

5.11.1 Introduction

This section contains an estimate of the electrical power needed by the vehicle during a typical mission. The majority of data used in this analysis was collected from JSC subsystem engineers in July 1991. Other data was taken from LifeSat requirements.

The results in this section are preliminary. Power estimates are given for the various phases of a typical LifeSat mission. All power is listed as average values. A more detailed analysis must be performed to identify the peak power requirements.

5.11.2 Assumptions

5.11.2.1 Timeline

This analysis assumed a circular orbit of 275 km for the LifeSat mission (paragraph 6-2). Although equipment operation depends on the orbit of the vehicle, duty cycles were used in an attempt to estimate the average power required per phase during either a circular or an elliptical orbit of any size.

In a small number of cases identified, a change in orbit would require a change in equipment set. For example, a highly elliptical orbit would require a high power communication amplifier. This amplifier was not scheduled to operate during the 275 km orbit mission.

The phases chosen were assumed to begin and end at the completion of particular events (table 5-23).

TABLE 5-23. DEFINITION OF LIFESAT MISSION PHASES USED IN ELECTRICAL LOAD ANALYSIS

PHASE	BEGINNING EVENT	ENDING EVENT
Prelaunch	Payload loading	Liftoff
Launch	Liftoff	Orbit insertion
Steady-State	Orbit insertion	Deorbit preparation
Landing	Deorbit preparation	Touchdown
Postlanding	Touchdown	Payload removal

5.11.2.2 Subsystems

Detailed subsystem component duty cycle assumptions can be found in the tables in appendix H. This section includes a general overview of operational assumptions on a subsystem level.

Electrical power is used by the propulsion system during engine firings. The power required is used for valve movement, pressure and temperature sensing in the lines, and thermal conditioning of hydrazine through the use of heaters. Valve movement occurs during the firing of engines, as well as when enabling and disabling the hydrazine system. Pressure and temperature sensing is maintained when the system is operable. The heater value of 10W is the estimated average power required to maintain the hydrazine at a safe temperature (40°F to 125°F) while the vehicle is in orbit.

Power required by the C&T system is used for S-Band communications, as well as for the search and rescue satellite (SARSAT) subsystem. The S-band subsystem is assumed to operate throughout most of the launch and landing phases and throughout the entire steady-state phase. The SARSAT subsystem begins operation during the landing phase and continues to operate until the vehicle is recovered.

The GN&C subsystem consists of IMUs, horizon and Sun sensors, the GPS, and momentum wheels. One IMU operates throughout the steady-state phase, and all three operate during the landing phase. Horizon and Sun sensors operate during part of the launch and landing phases, and three momentum wheels operate during the steady-state phase. One GPS unit provides updates during the steady-state phase, and two units are powered during the landing phase.

The DMS consists of a CPU, random access memory, disk drives, and accelerometers. Accelerometers to measure high-g forces operate during the launch and landing phases and during a small portion of the prelaunch and postlanding phases. Accelerometers to measure low-g forces operate throughout the entire steady-state phase. The rest of the DMS is assumed to operate during all phases of the mission.

Instrumentation used to measure radiation doses operates throughout the steady-state phase. Radiation detection was assumed to be part of the subsystem power requirements, as opposed to part of the payload power requirements.

The life support system (LSS) consists of circulation fans and waste separator fans. One circulation fan was assumed to operate during all phases of the mission, while the waste separator fan was assumed to operate only during micro-g phases of the mission.

The TCS includes circulation pumps, a refrigeration system, and associated electronics and controls. This equipment was assumed to operate during all phases of the mission.

Electrical power distribution and control (EPDC), also a user of energy, operates for the entire mission. The EPDC system on board the vehicle has an inefficiency attributed to converting DC power to AC power. The total power loss due to this inefficiency, in addition to required control power, was estimated to total 50W of average power for each phase of the mission.

Finally, LifeSat requirements allocated 150W for payload use. This average power level was scheduled during all phases of the mission.

5.11.3 Results

Based on the assumptions stated in paragraph 5.11.2, the JSC LifeSat design was analyzed to determine a representative set of average power loads which may be present during a nominal mission. The results of this analysis can be seen in figure 5-28.

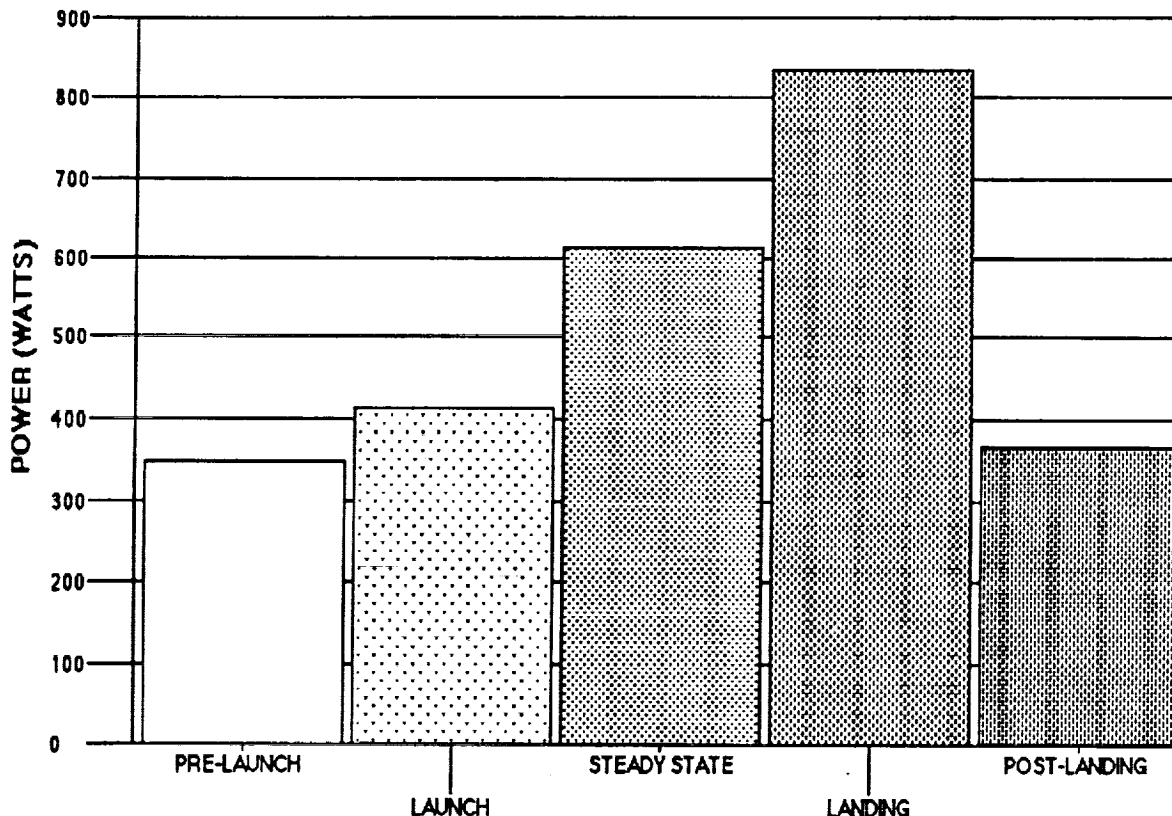


Figure 5-28. LifeSat Average Power Loads

Subsystems and payloads operating during the prelaunch, launch, landing, and postlanding phases were estimated to require 343W, 404W, 818W, and 360W, respectively. These average power levels, in conjunction with the longest duration expected for each phase, were used to size the primary battery system.

Subsystems and payloads operating during the steady-state phase were estimated to require a total of 601W. This value was used to size the solar arrays and secondary batteries.

5.11.4 Design Options

5.11.4.1 Primary Battery

Using a primary nonrechargeable battery for the entire mission's energy requirements is not practical since over 945 kWh are required. Even though such a system would be simple and reliable, it would double the weight of the vehicle. For example, at a 60-day rate, lithium carbon monofluoride batteries are projected at over 200 Wh/lb and 12.2 Wh/in³ which would result in a 4725 lb battery requiring 44.8 ft³. Other lithium chemistries, such as lithium thionyl chloride, are even heavier.

5.11.4.2 Primary Fuel Cell

A fuel system relying on cryogenic hydrogen and oxygen storage is also not practical because it would require more volume than the vehicle can provide.

5.11.4.3 Hybrid (Primary and Secondary)

There are two design-driving requirements: the on-orbit power requirement and the energy requirement for all the other phases. Recognizing that these requirements can be met with separate systems, one can conceptualize an optimum hybrid system. The on-orbit requirement can be met by a photovoltaic(pv)/rechargeable (secondary) battery system. Reliability requirements do not require this system to be one-fault tolerant, only fail-safe. The requirement of the other phases can be met by a primary battery. It must be designed to provide two-fault tolerance since it powers systems which enable launch and reentry. This concept is selected for the baseline system.

5.11.5 Baseline System

5.11.5.1 Primary Nonrechargeable Battery

The primary battery system provides power during all non-orbital phases (a total of 12 hours). This is the system which is sensitive to orbit selection since it changes the duration of the ascent and reentry phases. The system design consists of lithium bromine complex (Li-BCX) DD-cells. Thirteen 28-volt modules independently tied in parallel will meet the 7903 Wh requirement with two-fault tolerance. Each module consists of 9 DD-cells in series giving 25 Ah at 28 volts. This system offers high reliability and high energy density (125 Wh/lb, 6.2 Wh/in³). This cell is a larger version of the D cell which has flown on Shuttle since 1982. The DD-cell will be qualified for flight in 1992 for a Shuttle application. A two-fault tolerant control and distribution system will also be provided for this battery system. System mass is 78 lbs.

5.11.5.2 PV/Secondary Battery

The pv system provides the on-orbit power. It consists of 2 GaAs/Ge deployable arrays each 28 ft². This cell technology is recommended due to its proven high efficiency (16-18 percent) on several recent military spacecraft and its high radiation tolerance. Nickel/metal hydride (Ni/MH) batteries are selected due to their high energy density (30 Wh/lb) and long deep-cycle life capability. Ni/MH offers 1.8 times the energy density of Ni/Cd and is less expensive than Ni/H₂. It is new technology, but will be flown on Shuttle within 2 or 3 years. The entire system includes a control and distribution subsystem to provide power to the users. To minimize mass and volume, this system is sized as a single-string system according to a fail-safe design philosophy. System mass is 61 lbs.

5.11.5.3 Distribution and Control

The block diagram of the hybrid power system concept (figure 5-29) shows the components of the distribution and control system. The heart of the system is a power control unit which feeds power to a load controller. The load controller segregates the power to DC and AC loads as required. Note the two-fault tolerant components have redundant connections. The power control unit also controls the deployment and jettison of the solar arrays.

5.11.5.4 Estimated Cost

The complete hybrid power system is 215 lbs and will occupy 2.5 cubic feet. The projected cost for the development of this system is \$6M with a refurbishment cost of \$1M per vehicle. This cost estimate does not include any prime contractor wraps.

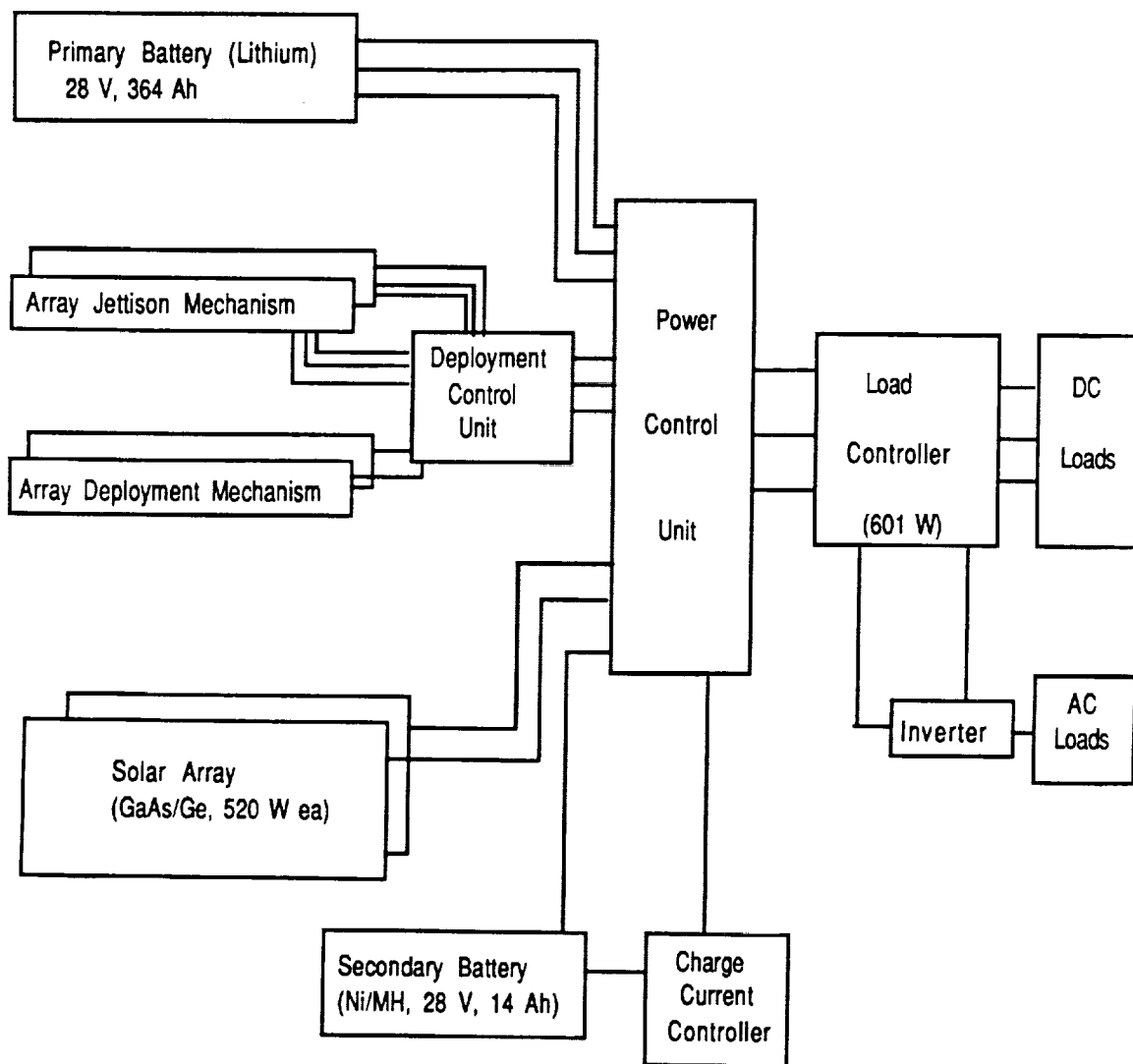


Figure 5-29. Hybrid Power System Concept

5.11.6 Conclusions

The electrical power system has been designed to provide the energy needed to operate the vehicle's subsystems and payloads for the duration of the mission. It is also assumed that this power system design would handle peak power loads. However, a more detailed analysis is required to verify that assumption.

5.12 DATA SYSTEM

(Prepared by Paul DeLaune)

5.12.1 Data Management Subsystem

The task of the DMS of the vehicle is to collect, store, format, and transmit to the ground the data collected from all of the subsystems. This includes the control of the C&T and payload subsystems as needed. The DMS also is responsible for passing all commands from the ground or the GN&C subsystem to the other subsystems as needed. This section describes the design used to meet these requirements.

5.12.2 Data Management System Components

The LifeSat vehicle requires large amounts of data to be transferred from the payload to mass storage, from mass storage to the C&T subsystem, and from C&T to all of the subsystems of the vehicle. Commands are also transferred from the GN&C subsystem to several other subsystems.

Figure 5-30 shows one string of the two-string DMS.

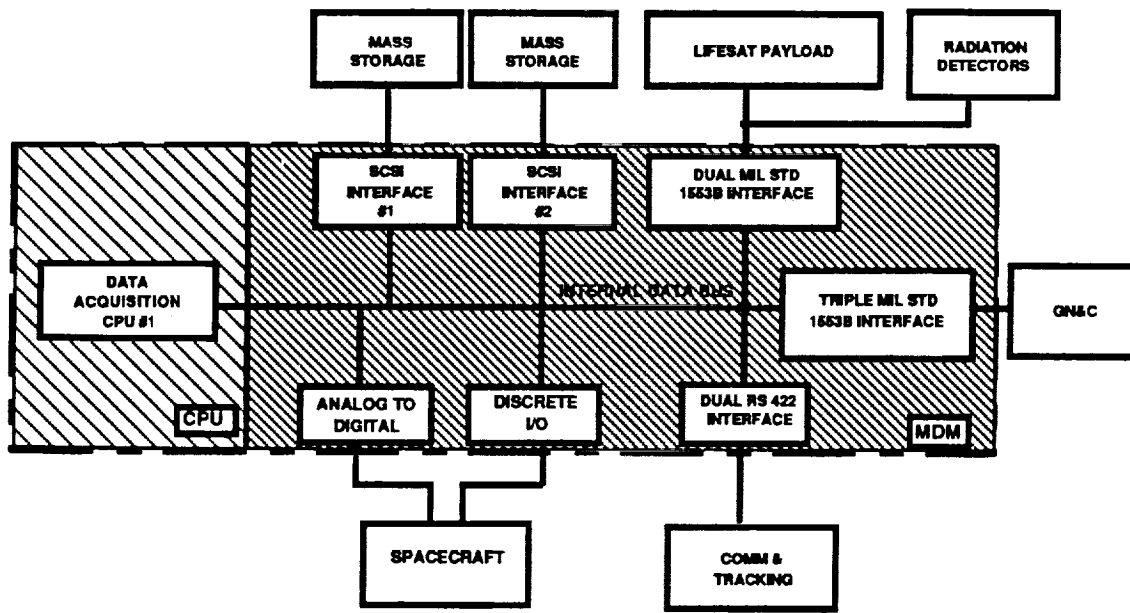


Figure 5-30. DMS Block Diagram (one string of the two-string system)

5.12.2.1 Central Processing Unit

The CPU system includes the CPU card, the local memory, and the direct memory access card. This system will allow the fast transfer of data between two subsystems without expending a large amount of CPU time. The direct memory access capability allows large amounts of data to be transferred, and the centralized DMS provides quick access to all of the subsystems. The onboard CPU is used to generate commands to the payload from "scripts" which are uploaded from the ground.

5.12.2.2 Mass Storage

The mass storage system was added to store data between daily transmissions to the ground, store commands from the ground, and store data for several days in case a transmission window was missed. A Small Computer System Interface (SCSI) bus standard system was used to interface the CPU to the mass storage system. This industry standard interface is very reliable and fast.

5.12.3 Interfaces

Each subsystem has different data rates and format requirements; therefore, each interface to the other subsystems is handled on a case-by-case basis. The following sections describe each interface to the DMS system.

5.12.3.1 Guidance, Navigation, and Control

The GN&C subsystem requires a path to the propulsion system and the C&T subsystem. The data will also be used by the CPU to control the C&T subsystem. The interface to the GN&C subsystem is designed to be a Mil Std 1553 serial interface. This interface is fast, reliable, and readily available as a commercial product. One separate bus will be provided for each of the three strings of the GN&C subsystem. Each bus will be daisy-chained (parallel) to both strings of the DMS. This will provide a redundant path for the GN&C subsystem.

5.12.3.2 Payload

The payload subsystem requires commands and large amounts of data to be transferred to and from the CPU. A lightweight dual Mil Std 1553 serial bus was chosen. The two busses will provide redundancy to the interface.

5.12.3.3 Communications and Tracking

The C&T subsystem requires the transfer from the ground of vehicle commands to the system and large amounts of data to and from the system. A dual RS422 serial channel was chosen for the link between the DMS and C&T because it will handle the 1 Mbps data rate required for transmit and receive operations, and the C&T commands can also be transferred on the same channel. C&T commands from the DMS will not need to be sent during the transmit or receive operations, therefore there is no need for a separate C&T command bus.

5.12.3.4 Radiation Detectors

The radiation detectors will be sent commands and will return data. The Mil Std 1553 interface was chosen because the designers of the radiation detectors implemented it previously. No redundancy is required for this interface.

5.12.3.5 Power and Propulsion

The power and propulsion subsystems require discrete and analog commands from the DMS and return discrete and analog data to the DMS. The interface to these subsystems requires that the DMS have input and output discretes, analog to digital converters, and digital to analog converters. The redundancy in this interface is handled by connecting one DMS string to each string of the propulsion unit. The task of adding redundant command strings to each string of the propulsion unit would add failure modes to the subsystems, so it was not attempted.

5.13 SOFTWARE

(Prepared by Gerry Roset)

5.13.1 LifeSat Flight Software Conceptual Design and Development Planning Assumptions

The philosophy adopted for the LifeSat flight software subsystems is characterized by rigorous application of sound system engineering principles and economy of design to achieve a high degree of reliability in the support of flight missions and minimize software life cycle costs. In particular, the maintenance of spacecraft flight software, after it becomes operational, has dominated software life cycle costs to the extent that initial software development costs have become a small fraction of the costs associated with maintenance of the software after it is flight-certified. Typical satellite system life cycle cost distribution allocates approximately 5 percent to the "front-end" systems engineering phase, 5 percent to the flight software development task, and the remaining 90 percent to the balance of the life cycle costs.

Since program success is measured in terms of cost, schedule, and technical performance, it is imperative that planning in the initial phases of the LifeSat program follow a unified approach that completely defines system requirements and establishes a system configuration which is proven early-on to be capable of meeting these requirements.

Once the system configuration is established, it is divided into hierarchical subsystem functional elements whose interfaces are clearly defined. This activity is then followed by the software conceptual design and development planning.

5.13.2 Purpose

The primary objective of this effort is to provide a comprehensive estimate of the LifeSat flight software implementation in terms of functional decomposition, estimated lines of C code, level of difficulty, and estimated cost for each functional element which is consistent with the goals of the LifeSat program to provide support for a reusable space-based life systems research environment to increase our knowledge base on the microgravity and cosmic radiation effects of long duration space flights.

The LifeSat software development task estimate presented in this section is bounded by other co-dependent system development life cycle phases for which a cost estimate is not presented. In particular, the software development task follows, and is dependent on, the "front-end" systems engineering phase which establishes the LifeSat functional requirements. It is then followed by the flight certification phase and the operational maintenance phase.

To provide a LifeSat software functional design, sizing and software development cost estimate consistent with economy of design, a high degree of reliability in the

support of flight missions, and minimum software life cycle costs, "off-the-shelf" software will be used when possible to lower development costs and minimize technology risk factors.

5.13.3 Software Functional Decomposition

The software functional decomposition on which the cost analysis depends, is the result of functional analysis which is a method for analyzing performance requirements and decomposing them into discrete automation tasks. It involves the decomposition of primary system functions into subfunctions at ever increasing levels of detail. Functional analysis supports mission analysis in defining functional areas, sequences, and interfaces. This approach allows hierarchical modularity within which well defined capabilities are combined until all functions and subfunctions are identified together with interface interrelationships and data flow requirements to fulfill system objectives.

The resulting flight software engineering effort and cost analysis produces a flight functional design with major CSCIs and CSCs identified under the following areas:

- LifeSat Executive
- Guidance, Navigation and Control
- Telemetry, Tracking and Control
- Failure Management
- Payload Data Acquisition and Storage

5.13.4 Cost Estimate Methodology

The "C" lines of code (LOC) estimates for identified software components are based on similar software tasks developed in-house for other programs which constitutes the corporate software development knowledge base. The accuracy of these estimates depends to a large extent on the level of in-house experience with particular areas of expertise in specific disciplines. In particular, the LOC numbers used for software components of the GN&C subsystem have a relatively high level of accuracy because of the extensive corporate experience with GN&C support of other vehicles. LOC estimates of software components that support LifeSat payload functions have a lower relative level of accuracy because the biological life system research requirements are not as well defined and the corporate knowledge base in this discipline is less complete.

The level of implementation difficulty is assessed for each software component by assigning one of three difficulty level categories (low, medium, high) each of which is associated with an average productivity figure in terms of lines of "C"

code per software engineer per week. The productivity figures used in this cost estimate represent the development implementation phase only.

<u>Difficulty Level</u>	<u>Productivity Figure</u>
Low	40
Medium	30
High	20

5.13.5 Software Estimate Abstract

The flight software sizing and development costs, based on the parameters described above, yield an estimated total cost close to \$2M. The following table is a summary breakdown by major functional area in terms of aggregate LOC estimates for each function and average component software complexity.

<u>Functional Area Estimate</u>	<u>LOC Estimate</u>	<u>Complexity</u>
System Executive	8,000	Medium
GN&C	11,000	High
Telemetry, Tracking & Control	5,050	Medium
Failure Management	5,800	High
Data Acquisition & Strength	<u>1,800</u>	Low
Total	31,650	

It is anticipated that the systems engineering effort (formal establishments of detailed requirements), additional payload software requirements, flight certification, and software life cycle maintenance costs could result in a total LifeSat software life cycle cost amounting to three or four times as much as the estimated cost for the LifeSat flight software development phase presented in this section. Detailed LOC and complexity estimate is in appendix I.

5.14 LIFE SUPPORT SYSTEM (Prepared by Marybeth Edeen)

5.14.1 Requirements

The life support system requirements for LifeSat were poorly defined at the end of the phase B studies. The science requirements document did not specify if the vehicle was to provide the life support system or if this was to be a payload

responsibility. Another problem was that the payloads were defined only as black boxes. For life support, this level of definition is unacceptable for conceptual design. After numerous discussions with the science working group, it was decided that a centralized life support system would be most advantageous for the rodent module but not in the best interest of the cellular bioreactors or the other payloads which had not yet been identified. The requirements used for the life support system design are provided in table 5-24 along with their source.

The life support system designed was as responsive to the science working group as possible. A decision was made for the cell biologists to design and maintain their own life support systems for several reasons. Cell bioreactors require very stringent control of temperature, oxygen level, carbon dioxide level, and other environmental parameters and are normally designed as self-contained units. In contrast, the rodents have much wider control bands, have requirements similar to humans, and have classically been designed to be integrated with human life support systems. Conceptual design for the undefined payloads was impossible because of lack of information on design requirements.

TABLE 5-24. RODENT MODULE DESIGN REQUIREMENTS

Parameter	Requirement	Source
Vehicle Requirements		
Circulation	1 volume exchange/minute	(1)
CO ₂ level	$\leq 1\%$	(1)
O ₂ level	20 % \pm 2 %	(1)
Diluent gas	Nitrogen	(1)
Humidity level	40 - 70 %	(1)
Temperature	4 - 40 ° C \pm 1 ° C	(1)
Total pressure	14.7 psia	(1)
Trace Contaminant Control		(2)
Ammonia	Control level	(2)
Hydrogen sulfide	Control level	(2)
Carbon monoxide	Control level	(2)
Ethylene	Control level	(2)
Ozone	Control level	(2)
Specialty Gases	Helium	(1)
Mouse Requirements		(3)
Food	4.0 grams/day	(3)
Water	8.0 grams/day	(3)
Oxygen	3.8 grams/day	(4)

The engineering requirements self-imposed on the design are relatively few and very simple. Of most importance is that the system be simple and use existing technology whenever possible to lower cost. Also, two levels of redundancy are to be designed when necessary since the system is necessary for mission success but is not CRIT-1.

5.14.2 Life Support System Conceptual Design

The life support system conceptual design, shown in figure 5-31, was designed for 50 mice for 60 days. After numerous discussions with the scientists, it was decided that waste removal would best be accomplished at the individual cage and that the life support system would not be responsible for urine and feces removal. The initial processor in the system is a small fan/separator which is used to remove any stray waste particles that get out of the cages. Then, the air is sent through a cabin circulation fan which provides circulation at the rate of 1 volume exchange per minute. Following this, the air splits and a side stream goes through eight combination lithium hydroxide/charcoal beds which remove carbon dioxide and some trace contaminants.

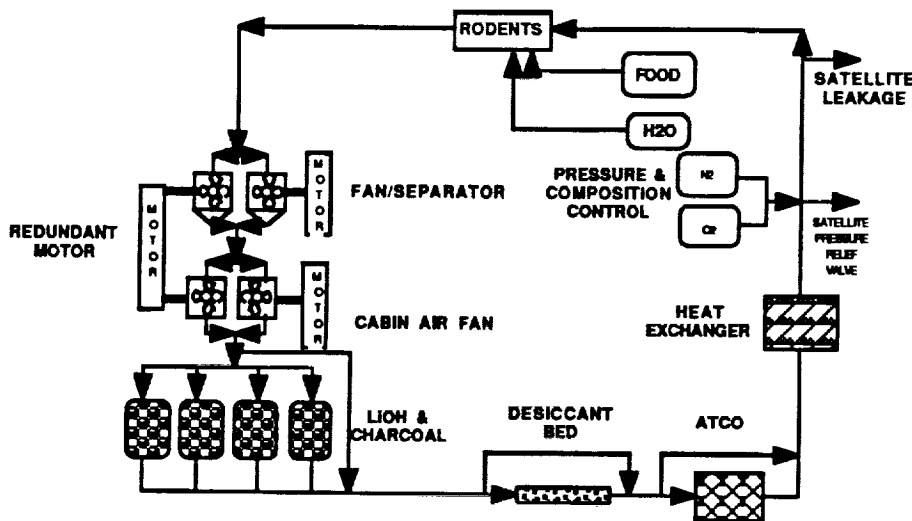


Figure 5-31. Conceptual Design of the LifeSat Life Support System

The water generated in the LiOH reaction and the small amounts of respiratory water produced by the mice are removed in the desiccant bed which is next in the circulation loop. After that, an even smaller side stream is sent through an ambient temperature catalytic oxidizer (ATCO) which removes the remaining trace contaminants. The ATCO may have to be run at slightly higher than ambient temperatures if ethylene is established as an important trace contaminant. Next, the air goes through a heat exchanger to remove the sensible heat from the fans, other equipment, and rodents' metabolic loads.

Following this, oxygen and nitrogen are injected to bring the partial and total pressures to their correct levels, replacing the oxygen metabolized by the rodents and oxygen and nitrogen that are lost to leakage. Finally, the air stream is recombined and returned to the rodents. Food is supplied at each cage, and water provided from a common storage tank through redundant lines to each cage. The weight, power, and volume requirements for each subsystem are shown in table 5-25.

TABLE 5-25. WEIGHT, POWER, AND VOLUME REQUIREMENTS

Item	Weight kg	Power watts	Volume cm ³
Life Support System			
LiOH canisters	11.6	0	33235
Circulation fan	2.1	0	4825
Redundant fan	2.1	0	4825
Circulation fan motor	1.2	50	347.5
Redundant motor	1.2	0	347.5
Desiccant bed	9	0	13500
Fan/separator	2.5	0	3785
Redundant fan	2.5	0	3785
Fan/separator motor	1.1	40	347.5
Ambient temperature	1.5	0	2790
Catalytic oxidizer			
N ₂	0.5	0	in tank
N ₂ storage	1.3	0	2840
Payload Requirements			
H ₂ O	12	0	in tank
H ₂ O storage	4	0	21000
Food	4.8	0	in tank
Food storage	2.4	0	3700
O ₂	4.8	0	in tank
O ₂ storage	11.6	0	26160
Urine	7.2	0	in tank
Urine storage	2.4	0	12600
Feces	8.4	0	in tank
Feces storage	4.2	0	6500
He	TBD	0	in tank
He storage	1.3	0	2820
Total	99.7	90	143407.5

5.14.3 Water Vapor Removal Options

A trade study was done to determine if a condensing heat exchanger or a dehumidification membrane and non-condensing heat exchanger should be used in place of the desiccant bed and the non-condensing heat exchanger. The weight comparison is shown in table 5-26.

TABLE 5-26. WATER VAPOR REMOVAL
COMPARISON

System Choice	Weight (kg)
Desiccant Bed/Heat Exchanger	10.6
Condensing Heat Exchanger	20.1
Membrane/Heat Exchanger	6.6

Although the membrane/heat exchanger combination is lighter, the membrane technology is relatively new and has not had previous applications in space hardware. Because of the new technology, the cost to develop the hardware for space applications was thought to be prohibitive. The difference in weight between the condensing heat exchanger and the desiccant bed/heat exchanger combination is small. However, the condensing heat exchanger requires a slurper to remove the condensed water from the air stream. Since the vehicle may be spun during some missions and not during others, this slurper may have to be designed to operate under both conditions. Also, the slurper could become clogged and free water could end up floating in the PM. Because of the uncertainty of the types of mission required and the higher possibility of failure, the desiccant bed/heat exchanger combination was chosen for water vapor removal.

SECTION 6 MISSION DESCRIPTION

(Prepared by Nancy Wilks)

6.1 DESIGN REFERENCE MISSIONS

The LifeSat Project Office and the LSSWG defined several candidate design reference missions (DRMs). The goal of these missions is to satisfy the requirements listed in the LifeSat Facility Science Requirements Document [29]. A 275 km circular orbit was proposed as the minimum exposure mission because studies showed that the proton exposure of the 275 km orbit was less than that of the 350 km circular orbit. (NOTE: Proposed orbit only. The baseline low orbit was 350 km per project requirements document (PRD).)

The discussion which follows of the timeline in the proposed 275 km circular orbit is divided into several mission phases: prelaunch, launch, steady-state, landing, and postlanding. These activities and operations are typical of all LifeSat missions and may be approximated for the other missions using the relationships given in the timeline tables in the discussions of each phase.

6.2 LIFESAT TRAJECTORY OVERVIEW

The RRS is launched from the Eastern Test Range (ETR) directly into a 275 km circular orbit with a 34° inclination. The satellite coasts in this orbit for approximately 60 days, performs a deorbit burn, and then parachutes to a touchdown at WSMR.

6.3 OPERATIONAL PHASES

Each mission phase begins and ends with specific events as described.

- The prelaunch phase begins with the spacecraft mating to the upper stage and continues until launch.
- The launch phase begins at launch and continues until the spacecraft acquires the Sun-pointing attitude after orbit insertion.
- The steady-state phase begins when the satellite acquires the Sun-pointing attitude and continues until deorbit preparations.
- The landing phase begins with the deorbit preparations and terminates with the RRS touchdown at WSMR.
- The postlanding phase begins with the RRS touchdown and ends with the payload removal.

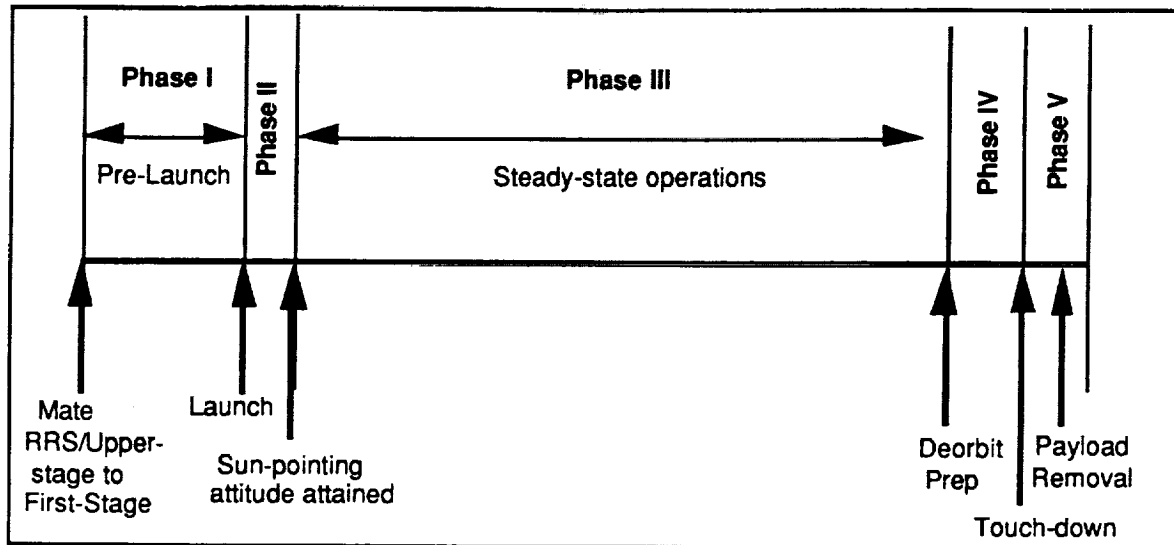


Figure 6-1. An Event Overview of the Phases

Figure 6-1 shows an overview of the five phases and the major events which indicate the beginning or the end of each phase.

6.4 PRELAUNCH PHASE

The prelaunch phase begins 6 days before the launch with the mating of the RRS to the Delta II in the missile service tower (MST) cleanroom at the launch site. During this phase, verification tests are performed on the RRS and the ELV, the propellant is loaded, and the RRS batteries are charged.

The prelaunch operations were derived from a three-stage Delta II configuration timeline listed in the Commercial Delta II Payload Planners Guide (DPPG) and begin on Day L-6 (L-0 is launch day.) with the mating of the RRS to the Delta II in the MST cleanroom on the launch pad. Table 1 in appendix J lists the Delta II vehicle preparations from Day L-6 through launch. Access to the RRS is limited on Days L-4 and L-2 for Delta II vehicle ordnance installation and propellant loading, respectively. For more detailed launch vehicle operations, refer to the DPPG.

Any RRS subsystems that are powered ON from Day L-5 through separation with the Delta II launch vehicle are required to participate in the L-0 Day simulation and the Power ON Stray Voltage Test on Day L-5. All data is monitored for electromagnetic interference (EMI) and radio frequency interference (RFI). RRS support of these two vehicle systems tests takes priority over any required spacecraft testing. The RRS prelaunch timeline is moved to appendix J, table 2.

The RRS is mated to the Delta II upper stage on L-8 Day. A handling can is assembled around the RRS/upper stage on L-7 Day after final upper stage

preparations. On L-6 Day, the RRS is transported to the launch site, uncanned, and mated to the upper stage. Also, on L-6 Day, RRS operations begin at 1300 (hours) continue until 2100 with an optional hour and a half shroud installation beginning at 1300. It is assumed that the RRS propellant is loaded before the RRS/upper-stage mating.

The LSS is turned on 30 minutes before loading the experiments into the PM (if the specimens have not already been loaded). This allows for a thorough system checkout before the specimen loading. After the experiments are loaded, the LSS will maintain the necessary experimental environment while the RRS is in the launch configuration.

Instrumentation monitors the vehicle and payload status prior to launch. The DMS is connected to ground equipment using an umbilical and transmits any required data pertaining to the status of the RRS, its payload, and any system checkout data.

After the removal of the MST cleanroom at approximately L-7 hours, adequate thermal regulation for the scientific payload and the RRS propellant tanks is supplied using both insulation and ground-based cryogenic cooling to guard against the launch pad environment.

The RRS is switched to internal power 1 hour before liftoff. The IMU is then realigned and the RRS completes a final vehicle checkout.

6.5 LAUNCH PHASE

These timelines were developed using 11/30/96 19:00:00 GMT as a launch time. The launch vehicle is propelled initially by the first-stage main engines and the solid motors. The second-stage engine ignites and places the vehicle into a Hohmann transfer to the final orbit. A second ignition of the second stage circularizes the orbit, and the second stage then maneuvers away from the RRS. A detailed listing of the launch phase mission elapsed time (MET) event times is in appendix J.

Figure 6-2 shows the Delta II 7920 mission profile. The main engine and six of the nine solid rocket motors ignite at liftoff. As the six solid motors burn out, the main engine continues to burn. Six seconds later the last three solid motors ignite and the six solid motors are jettisoned three at a time. A short time later, the last three solid motors burn out and are jettisoned. Following a brief coast period after main engine cutoff (MECO), the separation bolts between the first and second stages are blown. The second stage ignition begins 13 seconds later and is followed by the fairing separation. Stage two engine cutoff (SECO) occurs almost 9 minutes into the mission and places the vehicle in a Hohmann transfer trajectory to the 275 km orbit. Final orbit circularization is accomplished by a second burn of Delta II second stage. The Delta II second stage also controls the RRS terminal velocity, RRS final orientation, and separation

maneuvers. Separation of the RRS and the second stage occurs approximately 4 minutes after SECO 2.

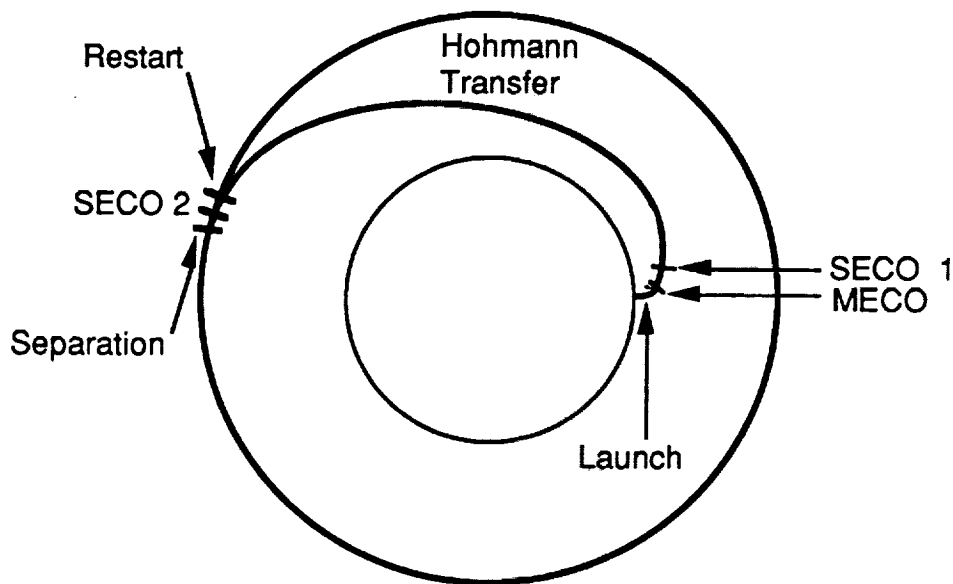


Figure 6-2. A Delta II 7920 Mission Profile

The Sun and horizon sensors are used to realign the IMU, and then the RRS performs any necessary orbital error correction maneuvers. The RRS acquires the Sun-pointing orientation approximately 45 minutes after liftoff. Table 3 in appendix J shows the timeline for these activities.

The maximum steady-state axial acceleration occurs at the end of the first-stage burn and will typically be between 6 and 7 g's. At liftoff and during transonic flight, there will also be sinusoidal, random, and acoustical vibrations. In a two-stage configuration, the aft end of the RRS is typically exposed to higher acoustic levels due to the fairing configuration. The maximum shock response occurs when the RRS and the final Delta stage separate. Additional launch environment detail can be acquired from the DPPG and the Delta Program Office.

Battery power provides the necessary power to the RRS from 1 hour before launch until the RRS assumes the Sun-pointing attitude. The electrical umbilicals are unplugged by automatic mechanism at liftoff.

It is assumed that the C&T system is used only after orbit insertion.

Two accelerometers measure the g's experienced by the payload. Each measures a particular spectrum of accelerations. Accelerometer #1 measures the "high" g-loads during launch and landing, and accelerometer #2 measures the micro-g accelerations.

The LSS maintains the environment as required by the science requirements. Initial requirements are listed in the PRD. The fan/separator is activated after SECO 1.

The LifeSat propulsion system is not used during the launch phase if the Delta II orbit insertion and attitude orientation are totally successful. The timeline reflects times for an orbital trim maneuver and an attitude adjustment; these are placeholders for fine-tuning the orbit and attitude of the RRS.

The GN&C data processing will be handled by CPU #1 which operates continually throughout the launch.

A second CPU (CPU #2) will be responsible for all other data processing and is turned on only when required by the other systems. During launch, the payload is monitored and records the launch accelerations, radiation exposure, and payload environment. The payload environmental measurements include temperature, pressure, humidity, and atmospheric composition.

6.6 STEADY-STATE OPERATION PHASE

After the the Sun-pointing attitude is attained, the solar panels are deployed and the steady-state operations begin. No significant maneuvers are performed during the steady-state operations. The science community requires 10^{-5} g environment for 95 percent of the flight with the maximum accelerations not exceeding 10^{-4} g for the remaining 5 percent of flight.

The GN&C controls the attitude and orbit of the RRS. The GN&C will maintain a Sun-pointing attitude during the steady-state phase using control moment gyros (CMGs). No desaturation of the CMGs is planned during the steady-state phase. The state vector will be maintained on board and propagated using CPU #1.

The GN&C will also provide the Principal Investigator (PI) attitude and position data during radiation spectrometer data sampling. The GPS updates the IMU hourly to meet the accuracy requirement of the PI. The GPS update will last approximately 30 seconds.

During the steady-state phase, the TCS is responsible for maintaining the proper temperature of subsystem components and the PM. Insulation will protect the Sun-pointing RRS from exposure to the extremes of the space environment. The LSS maintains the proper environmental conditions as specified by the PI. The environmental conditions are listed in the PRD.

The necessary spacecraft power will be generated using deployable solar panels on the sides of the RRS. Rechargeable batteries will supplement the power supplied by the solar cells during the day/night cycle and peak loads.

The C&T system provides the mechanism for ground command, control, and monitoring of the RRS. Two S-band antennas will be on board with only one antenna operating at a given time. The RRS communicates with the DSN.

After the Sun-pointing attitude has been attained and RRS health and status have been verified, the C&T downloads the data accumulated during the launch phase. Throughout the steady-state portion of the mission, the C&T system will download the PI's data and other RRS health data during communication opportunities with the DSN network.

The PI requires PM environmental measurements at a rate of 1 sample per minute during the steady-state operations and during any mode change. Sampling includes radiation spectrometry, atmospheric conditions, pressure, temperature, and humidity. Concurrent magnetometer readings, RRS attitude and position readings are required when recording the radiation spectrometer data.

6.7 LANDING PHASE

The landing phase begins with the start of the deorbit activities, the IMU is realigned, and the deorbit attitude is attained using the ACS. After the deorbit burn, the RRS descends into WSMR on a ballistic trajectory. Parachutes are deployed and the RRS lands in the WSMR. The time of touchdown is assumed to occur during daylight at least 4 hours before sunset. Table 4 in appendix J lists the landing phase operations and activities.

The timelines in the appendix assume no special accommodation for ground visibility or communication during preparation for deorbit and reentry.

Landing operations begin with the GPS updates occurring every 30 seconds. The centrifuge is turned off, the CMGs are desaturated if necessary, and the IMU is realigned. If orbital phasing is required for the WSMR landing, the RRS altitude is adjusted to accomplish the phasing. The RRS attains the proper deorbit attitude using the ACS thrusters. The deorbit burn occurs at a transfer angle of 180° from the landing site. A velocity residual trim maneuver is performed 2 minutes after the deorbit burn if necessary.

The high-g accelerometer is activated before the deorbit burn and the low-g accelerometer is switched off. The DMS continues to collect data at a rate of 1 sample per minute and during any mode change.

The solar panels are ejected prior to the deorbit burn, and the RRS switches to battery power.

The LSS fan/seperator is turned off after the deorbit burn since it is designed for zero-g operation. The LSS continues to maintain the environment required by the PI without the aid of the TCS radiators.

Fifteen minutes before the entry interface (EI) at 400,000 ft, an EI error correction maneuver is performed, if necessary. Prior to EI, the RRS is spun up to remove any aerodynamic anomalies caused by the asymmetric ablation of the heat shield. After EI the RRS is spun down and the SARSAT beacon is switched on. When the Mach number equals 1.5, the drogue parachute is deployed. The three main parachutes are deployed at 10,000 mean sea level (MSL), and the RRS touches down at WSMR elevation (4000 ft).

A more detailed discussion of the landing phase is included in section 8.

6.8 POSTLANDING PHASE

After touchdown, the RRS is located, recovered, safed, and transported to a nearby processing facility. Table 5 in appendix J shows the postlanding phase timeline.

All subsystems are turned off except the SARSAT beacon, the DMS, and the LSS. The RRS is powered and cooled as it was in the landing phase.

After recovering and safing the RRS, GSE is connected to provide power and cooling. The helicopter transport device is attached, and the RRS is moved to the PI's location.

SECTION 7 FLIGHT DYNAMICS

7.1 BALLISTIC ENTRY DYNAMICS (Prepared by Mike Tigges)

7.1.1 Entry Profile Dynamics

LifeSat is a ballistic entry vehicle. The term "ballistic" entry means an unguided entry, much like the trajectory of a bullet fired from a gun. There is no vehicle control authority available to remove entry flight dispersions. As the ballistic vehicle descends into the atmosphere, the interaction of the vehicle with the atmosphere decides the in-flight aerothermodynamic trajectory conditions and ultimately the vehicle landing point.

Many factors affect where the entry vehicle lands within the available landing area. For example, atmosphere, wind, aerodynamics, mass properties, and vehicle systems such as navigation, control, and parachute all affect landing accuracy. The attitude dynamics and stability of the ballistic LifeSat entry vehicle affect the vehicle aerodynamic properties and therefore also landing accuracy and thermal protection system requirements. Off nominal aerodynamics and mass properties can cause lift accelerations that rapidly push the vehicle out of the available landing area. This effect is known as lift vector non-averaging. A despun vehicle with an aerodynamic trim misalignment of 5 degrees can miss the target site by up to 60 nm. To counteract this effect, the LifeSat vehicle is spun up to a predetermined rate before atmospheric entry. The vehicle spin rate greatly reduces the effect of lift vector non-averaging during the entry phase and causes the vehicle to follow a spiral trajectory about the nominal trajectory down to the altitude of parachute deploy.

But a spin rate coupled with aerodynamic forces and torques can cause dynamic gyroscopic effects. One gyroscopic effect is a resonance condition that occurs when the vehicle roll rate "locks-in" with the natural longitudinal pitch frequency. Large deviations in the trim angle of attack can result, with body angular rates and accelerations that affect vehicle stability. Other undesirable effects are possible. For example, a stable motion can occur where the vehicle roll rate and precession frequency align. If this occurs, the vehicle shows the same meridian, or face, to the wind. This type of motion is called "Lunar" (analogous to the Moon always showing the same side to the Earth). Lunar motion exposes the heat shield to increased probability of asymmetric ablation, asymmetric heating, and roll resonant lock-in. Asymmetric ablation increases the potential for undesirable body and wind-fixed moments. These moments can become large and cause roll perturbations that spin up, spin down, or even roll reverse the vehicle spin. Vehicle spin-up is undesirable to the LifeSat biological payload, and spin-down and roll reversal are undesirable for landing accuracy. Therefore, conditions that cause roll resonant lock-in with Lunar

motion should be avoided during entry flight, and vehicle and trajectory designers should be aware of conditions which increase the likelihood of these gyroscopic conditions.

7.1.2 Analysis

Entry gyroscopic resonance conditions have received extensive analytic and numeric investigation over the past 30 years. Intercontinental ballistic missile trajectory design and analysis stimulated much of the early work in this area, and identified the major sensitivities and proposed and tested corrective systems and flight techniques. Therefore, the analytical development of this topic is quite mature. However, to ease understanding of gyrodynamic motions possible with a LifeSat type of vehicle design, three processors were linked together to provide numerical, graphical, and animation capabilities (figure 7-1).

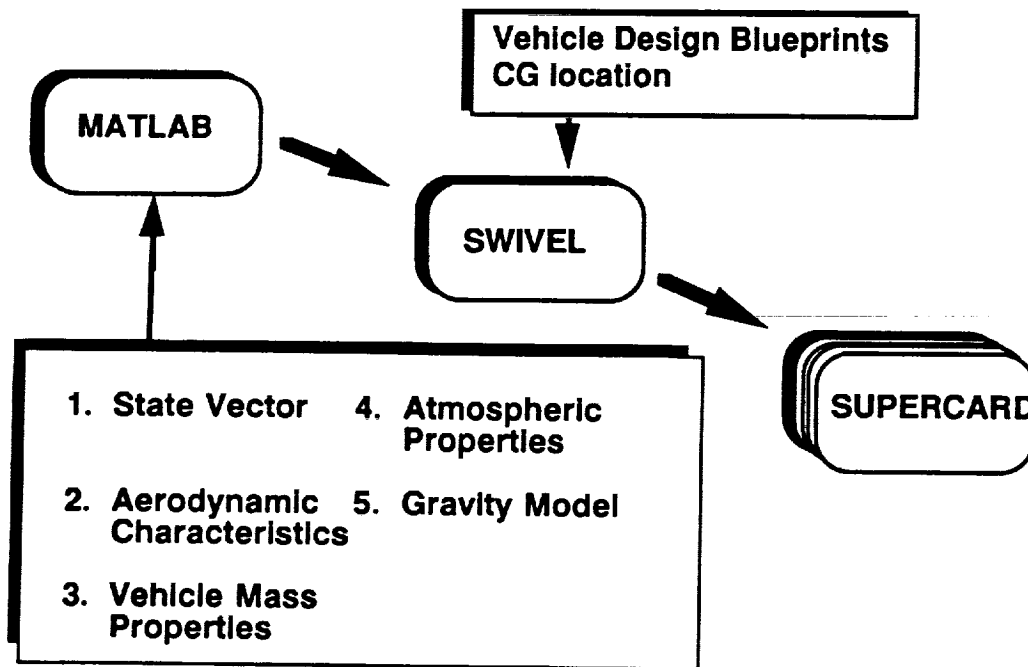


Figure 7-1. Processor Analysis Flow

To provide a numerical test-bed for evaluating the validity of analytical expressions and for accurately modeling gyroscopic effects on entry vehicle performance, a six degree-of-freedom (6-DOF) simulation was created in MATLAB (a C-based interpretive language with vector/matrix capability). The 6-DOF program numerically simulates the trajectory and attitude dynamics during the LifeSat ballistic entry phase. The MATLAB program also provides detailed plots of important trajectory parameters. The numerical output from

MATLAB was then transferred into SWIVEL, a graphics program which uses a 3-dimensional depiction of the LifeSat vehicle to generate 3-dimensional snapshots of the vehicle at each timestep of the entry trajectory. This graphical output was then linked into SUPERCARD, which displays the LifeSat animation. The animation provides a tool for assessing the actual body attitude and motion during atmospheric flight. The effect of transient and resonant phenomena due to a set of user-defined vehicle and trajectory initialization parameters can be analyzed real time from a realistic 3-dimensional perspective.

7.1.3 Results

Figure 7-2 shows a prospective LifeSat vehicle configuration. Note that the vehicle is symmetrical about the body x-axis. The vehicle is spun about this principle axis before entry at the rate $\dot{\phi}$ shown. Measurement of the total angle-of-attack is about this axis. As shown, this angle is measured directly from the wind relative velocity to the body x-axis. For a nominal entry profile, the angle-of-attack is kept small throughout entry. The aerodynamic coefficients are computed from knowledge of angle-of-attack. The General Electric MOSES vehicle configuration, which has a symmetric design very similar to that used for LifeSat, provided the aerodynamic tables used for this analysis. These tables provide the axial, lateral, and normal force aerodynamic coefficients as a function of angle-of-attack. For small angles-of-attack, only the axial force coefficients for computing vehicle drag force are non-zero. Therefore, for nominal entries where the angle-of-attack is kept small, the lateral and normal accelerations that compute the lift acceleration are zero, and the total aerodynamic acceleration is along the vehicle symmetry axis. This is the best case for minimizing landing dispersions due to aerodynamics. The rolling moment coefficient for this symmetrical design analysis was zero since no viscous drag effects were modeled.

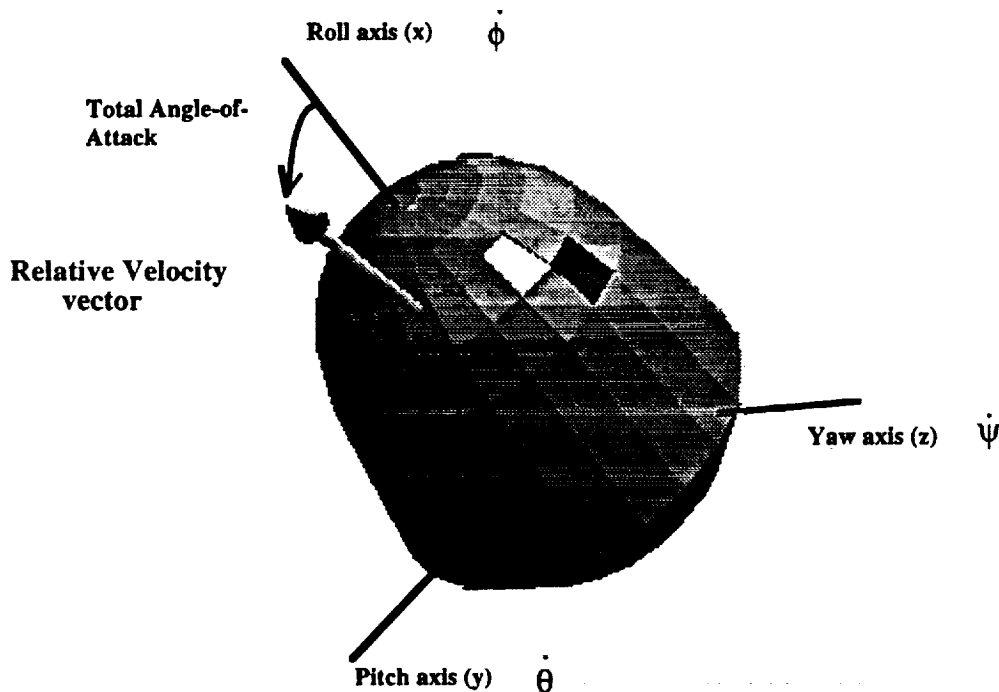


Figure 7-2. LifeSat Orientation Parameters

Tables 7-1 and 7-2 contain the vehicle aerodynamic coefficients and mass properties. These parameters were used for all entry dynamic attitude simulations and analysis. It will be stated here, and again later, that gyrodynamic resonance conditions are strongly a function of initial conditions. This analysis shows the possibility of encountering undesirable gyroscopic conditions with a realistic LifeSat vehicle design. This should not raise a major concern. It should be possible to either passively avoid gyroscopic resonances by proper design of initial conditions (such as entry velocity, spin rate, etc.) or actively control the vehicle away from undesirable resonance conditions via aerodynamic dampers, reaction impulse, CG control, thermal shield winding techniques, or other control devices and techniques.

TABLE 7-1. AERODYNAMIC FORCE COEFFICIENTS

alpha (deg)	Axial (CA)	Normal (CN)
0.0	0.66512	0.0
5.0	0.66446	0.10033
10.0	0.66249	0.19762
15.0	0.65865	0.29228
20.0	0.65178	0.38773
25.0	0.64165	0.48259

TABLE 7-2. MASS PROPERTIES

mass (kg)	1422.2
lxx (kg-m ²)	865.3
lyy (kg-m ²)	1167.2
lzz (kg-m ²)	1228.3
Rcg (m)	-0.682 , 0.0 , 0.0
cbar (m)	2.0067
Reference Area (m ²)	3.1587

Figure 7-3 shows a set of plots for a nominal LifeSat entry from a 900 km apoapsis orbit. Clockwise are shown the vehicle roll angle, dynamic pressure, total angle of attack, and body roll rate and pitch rate. The vehicle body x-axis is perfectly aligned with the entry relative velocity vector. Note that the maximum offset in trim angle-of-attack is less than 3 degrees throughout the entry phase. The roll rate is 25 deg/sec and the pitch rates reach no higher than about 5 deg/sec. The landing site miss from a zero-spin ideal entry simulation was 0.02 km.

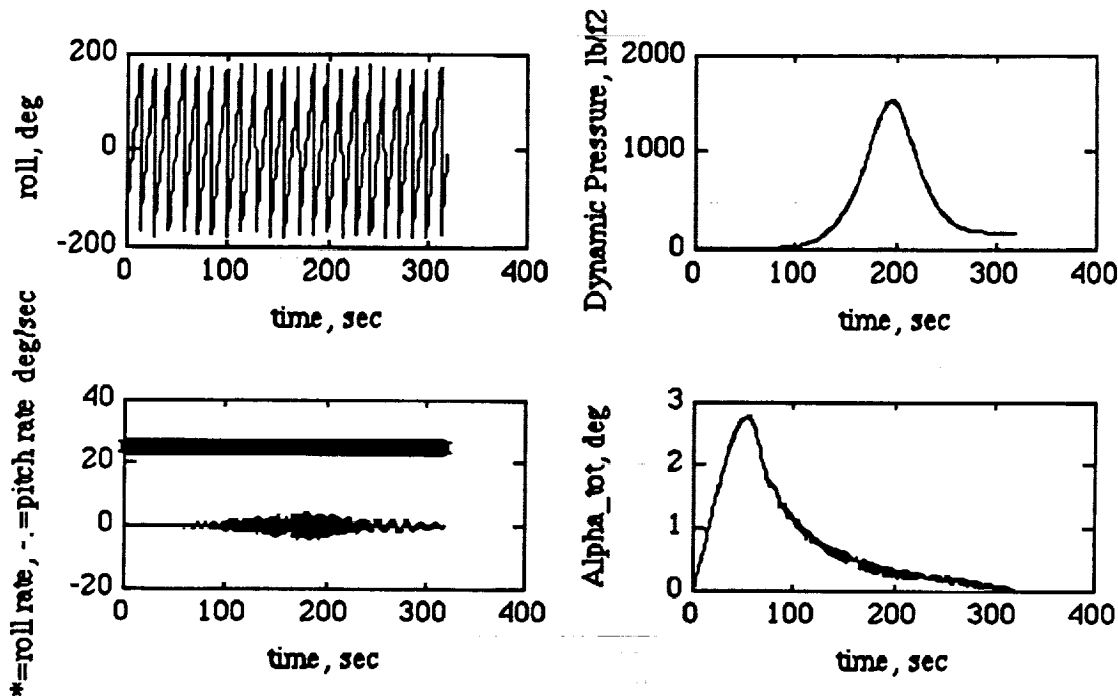


Figure 7-3. Nominal Entry Trajectory Plots

Figure 7-4 shows a set of similar plots for a vehicle with a dispersed CG. All other initializations were unchanged. The CG was displaced 2 inches off the vehicle centerline. This case displayed a pitch roll resonance with Lunar motion. The resonance began at high altitude and, although not severe, caused an angle-of-attack divergence of about 15 degrees with pitch rates approaching 25 deg/sec. The Lunar motion is not suggested from these plots, but began at about peak dynamic pressure and continued down to chute deploy. The landing site miss was only 1.1 km. So the appearance of resonance and Lunar motion phenomena does not degrade landing site performance. However, as was stated earlier, these conditions can lead to deterioration in shield integrity that can aggravate vehicle dynamics and stability.

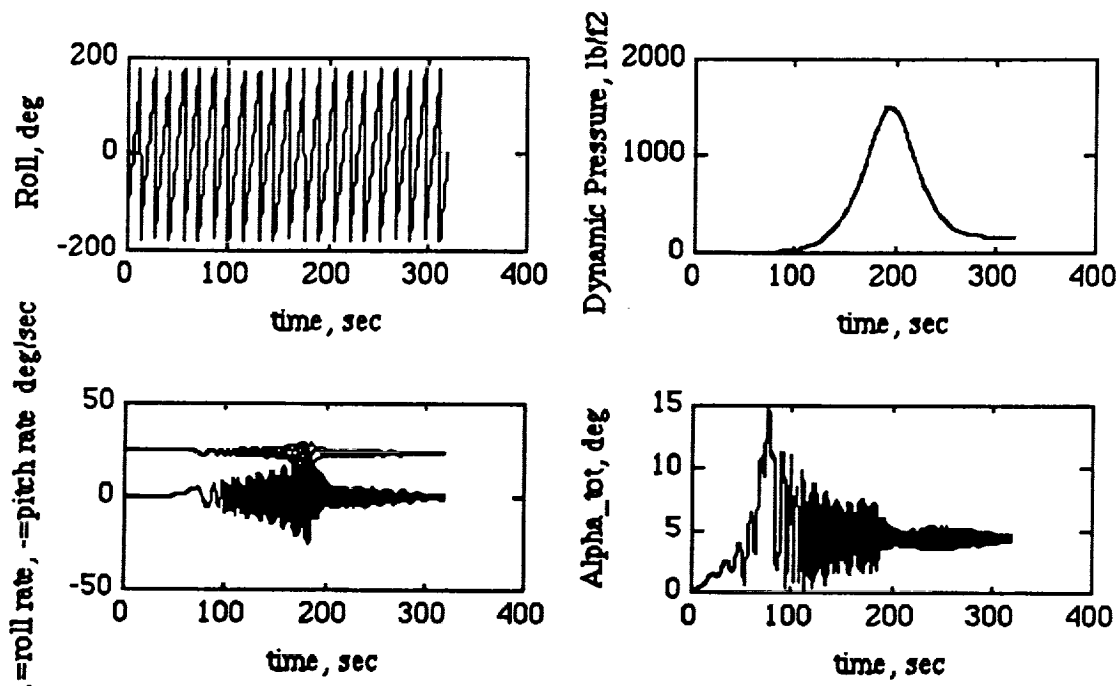


Figure 7-4. Dispersed CG Trajectory

7.1.4 Conclusions

LifeSat stability and resonance phenomena have been shown to occur naturally with entry conditions in the operational range. These conditions do not affect landing site accuracy but do affect vehicle spin rate and accelerations and are conducive to unstable motion amplification and heat shield degradation. These phenomena are of concern if not recognized during vehicle and trajectory design, but can be minimized using either active, passive or combined methods of control.

7.2 CENTRIFUGE DYNAMICS (Prepared by Lisa Ling)

7.2.1 Effects of the Moving Mice on the Centrifuge

The LifeSat centrifuge cultural facility consists of 2 counter-rotating centrifuges of equal mass each containing 12 chambers in which the walls of the chambers extend radially. A 25g mouse resides in each chamber, with an assumption that each mouse is restricted to move only in the radial direction. The movements of the mice in each chamber may cause an imbalance and, thus, a CG offset in the centrifuge. The moving mice may also cause a change in the angular velocity of the LifeSat ($d\omega_{sat}$). Therefore, an analysis was essential to determine the worst case CG offset for a centrifuge and the effects of the moving mice on the angular velocity of the LifeSat.

7.2.1.1 Worst Case CG Offset

The centrifuge has a radius of 0.5 m. Each mouse can move freely at a radial distance between 0.25 m and 0.3125 m inside its chamber. Figure 7-5 shows the configuration of the mice which will yield the worst case CG offset. The CG location calculated for the worst case was 5.844×10^{-5} m.

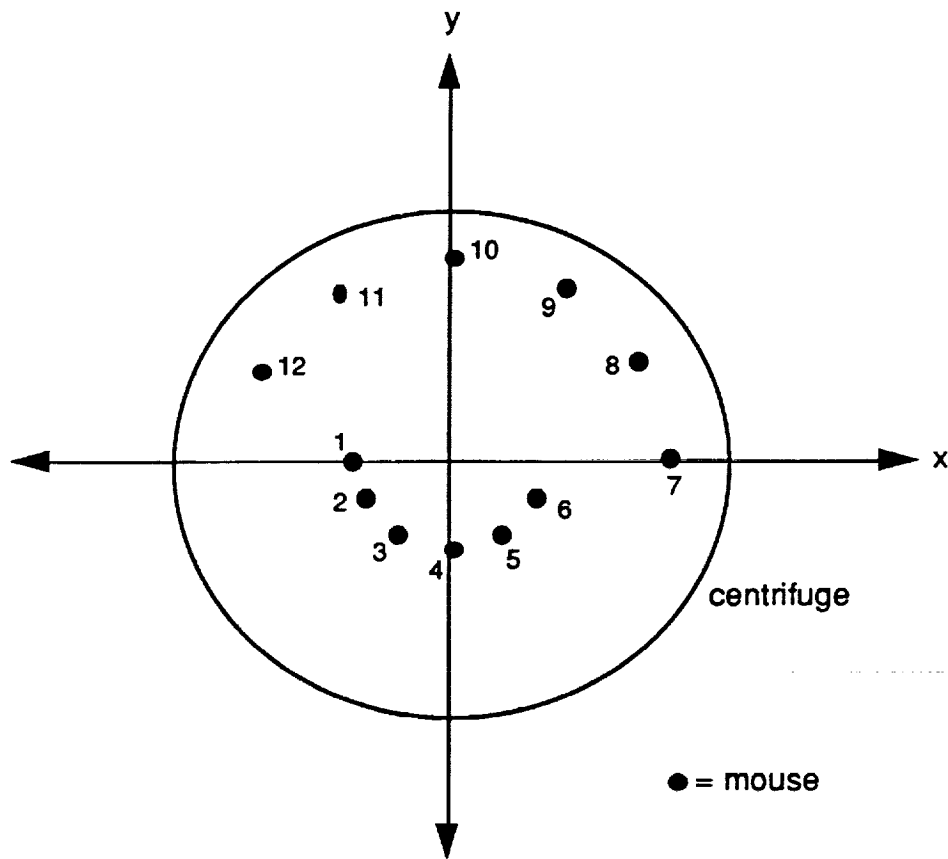


Figure 7-5. Scenario for Worst Case CG Offset in Centrifuge

7.2.1.2 Effect of Moving Mice on LifeSat Angular Velocity

The mass of the centrifuge is 103 kg. The mass moment of inertia for one centrifuge is $12.875 \text{ kg}\cdot\text{m}^2$. The mass moment of inertia for the 12 mice is $0.0293 \text{ kg}\cdot\text{m}^2$ at a radial distance of 0.3125 m. The mass moment of inertia for the LifeSat (I_{sat}) is $799.752 \text{ kg}\cdot\text{m}^2$. The angular velocity of each centrifuge (ω_c) is 5.112 rad/sec. The above data were obtained from the Space Biological Sciences Group at the Jet Propulsion Laboratory (JPL).

To obtain the maximum change of angular momentum, assume that all 12 mice moved the maximum distance of 0.3125 m in each centrifuge. Let the mice in the top centrifuge run inward, while the mice in the bottom centrifuge run outward. Note that if the mice in both centrifuges ran in the same direction, the change of angular momentum in the centrifuges would then cancel so that the total change of angular momentum would be zero ($dH_T=0$).

The change of angular momentum in the centrifuge may be transferred to the LifeSat to cause a change in the angular momentum of the LifeSat (dH_{sat}). To obtain the maximum change in the angular velocity of the LifeSat, assume that momentum transferred to the motor of the centrifuge is transferred to the satellite ($d\omega_c = 0$). The following results are obtained:

For the centrifuge:

$$dH_T = -0.1208 \text{ kg}\cdot\text{m}^2/\text{s}$$

$$d\omega_c = 0 \text{ rad/sec}$$

For the LifeSat:

$$dH_{\text{sat}} = 0.1208 \text{ kg}\cdot\text{m}^2/\text{s}$$

$$d\omega_{\text{sat}} = \frac{dH_{\text{sat}}}{I_{\text{sat}}} = 1.51 \times 10^{-4} \text{ rad/sec}$$

To obtain the maximum change in the angular velocity of the centrifuge ($d\omega_c$), assume that there is frictionless bearing such that no momentum is transferred to the satellite. All the change in angular momentum (dH_T) from the moving mice goes into changing the angular velocity of the centrifuge ($dH_c=0$). The following are then obtained:

For the centrifuge:

$$dH_T = 0 \text{ kg}\cdot\text{m}^2/\text{s}$$

$$|d\omega_c| = 9.34 \times 10^{-3} \text{ rad/sec}$$

For the LifeSat:

$$dH_{\text{sat}} = 0 \text{ kg}\cdot\text{m}^2/\text{s}$$

$$d\omega_{\text{sat}} = 0 \text{ rad/sec}$$

7.2.2 Vibration Analysis for an Unbalanced Centrifuge

When CG offset occurs in the rotating centrifuge, vibration will result. The vibration is transferred to the LifeSat and will affect other experiments carried on board. Some g-load sensitive experiments have micro-g constraints which may be violated as a result of the vibration. Therefore, vibration analysis was essential in determining the vibration responses of the centrifuges and the LifeSat caused by the imbalance in the centrifuge.

Two approaches for obtaining the vibration response equations for the centrifuge and the vehicle were used. The conventional approach using simple substitution of steady-state harmonic motion for the responses allows a quick look at the magnitudes and frequencies of the steady-state responses. A rather detailed modal analysis approach yields the magnitudes, frequencies, phase angles, and directions of the vibration responses with given initial conditions. For the modal analysis, two cases were examined. The first case is free response with initial conditions where the centrifuge has no force input. The second case is forced response where the centrifuge experiences a force input as a result of the imbalance. The solutions obtained for forced response from the two approaches were compared and found to be compatible.

A solution to minimize or eliminate the effects of the imbalance in the centrifuge using a vibration absorber was also examined. The vibration absorber is formed by attaching a spring-mass system to the centrifuge. The vibration absorber will effectively absorb the vibration so that the centrifuges, the vehicle, and the g-load sensitive experiments will experience minimum or no vibration as the result of an imbalance in the centrifuge.

7.2.3 Conclusions

The following system characteristics were used in the analysis:

centrifuge mass (m_c) = 103.0 kg
vehicle mass (m_{sat}) = 1589.0 kg
length of CG offset (L) = 6.0×10^{-5} m
centrifuge angular velocity (ω_c) = 5.112 rad/s
spring constant (k) = 100,000.0 N/m
damping coefficient (c) = 120.0 N•s/m

The values for m_c , m_{sat} , and ω_c were obtained from the Space Biological Sciences Group at JPL. The CG offset, L , was obtained from paragraph 7.2.1.1. The values for k and c were chosen rather arbitrarily and are in no way representative of the true values. It was determined that, with the system characteristics listed previously, a system with damping will not cause the g-load transferred to the vehicle to exceed 10 micro-g's. Therefore, g-load sensitive experiments with a 10-micro-g constraint will not be damaged as a result of an imbalance in the centrifuge. For a system without damping ($c = 0$), the maximum g-load transferred to the vehicle will be approximately 73 micro-g's.

For the vibration absorber, a mass of 1 kg was chosen arbitrarily. It was determined that for a centrifuge operating at the design frequency of 5.112 rad/sec, the vibration will be totally eliminated. For such case, no g-load will be transferred to the vehicle. The vibration absorber will continue to perform satisfactorily for an operating frequency which differs slightly from 5.112 rad/sec.

For a $\Delta\omega_c$ of ± 0.01 rad/sec, the g-load transferred to the vehicle will not exceed 10 micro-g's. It was determined in paragraph 7.2.1.2 that the movements of the mice in the centrifuge will not be significant enough to cause a $\Delta\omega_c$ greater than ± 0.01 rad/sec. Therefore, the vibration absorber is a practical solution for the vibration problem caused by the imbalance in the centrifuge. The details of the vibration analysis can be obtained in reference 44.

7.3 TAPE DRIVE DYNAMICS

7.3.1 Tape Drive Start Up and Stop Transient Effects in Microgravity

Two disk drives will be installed in the vehicle. The angular acceleration during the power up or power down of the disk drives will generate momentum. Assume that all the momentum is transferred to the vehicle for the worst case. The momentum transferred will perturb the angular velocity (ω_{sat}) and angular acceleration ($\dot{\omega}_{sat}$) of the vehicle. This will then affect the g-loads of the payloads carried on board. An analysis was therefore performed to determine the tape drive start up and stop transient effects in micro-g. The derivations can be obtained in reference 43.

7.3.1.1 Characteristics of Tape Drives and Vehicle

The mass moment of inertia for all the spinning components of a disk drive (I_d) is approximately 1.609×10^{-4} kg·m². The rotation speed of the spinning components of the disk drive is 4500 rpm. The typical start time or stop time for a disk drive is 15 seconds. The disk drives will be started or stopped one at a time. The mass moment of inertia for the vehicle was assumed to be 800 kg·m². The properties of the disk drives, other than I_d , were obtained directly from a specification summary provided by the manufacturer of the disk drives. The mass moment of inertia for the disk drive was determined by making approximate mass and radius measurements of all the spinning components of a similar disk drive.

7.3.1.2 Effects on the Micro-g of Experiment

The following values were used to determine the effects of the disk drives for an LVLH attitude satellite:

$$R = h + R_{EARTH} = 400 + 6378.15 = 6778.14 \text{ km}$$

$$\bar{R} = 6778.14 \hat{X} \text{ km}$$

$$\omega_{\text{sat}} = \sqrt{\mu/R^3} = 1.131 \times 10^{-3} \text{ rad/sec}$$

$$\ddot{\omega}_{\text{sat}} = 1.131 \times 10^{-3} \text{ }^{\Delta}\text{rad/sec}$$

$$\dot{\omega}_{\text{sat}} = 0 \text{ rad/sec}^2$$

$$P = 0.01 \text{ km}$$

where h is the vehicle altitude, \bar{R} is the inertial position vector for the vehicle; and \bar{P} is the position vector of the experiment relative to the vehicle's coordinate system as shown in figure 7-6. The values for \bar{R} and P were chosen rather arbitrarily. Maximum diameter inside the vehicle is 2.4 meters.

The disk drives will have parallel spin axes but opposite directions of rotation. Then the resulting angular momentum of the disk drives during operation will exactly cancel. Still, five cases need to be considered.

- a. starting up the first disk drive while the second is at rest
- b. operating the first disk drive while the second is at rest
- c. starting up the second disk drive while the first is operating
- d. stopping the second disk drive while the first is operating
- e. stopping the first disk drive while the second is at rest

In addition to these five cases, the orientations of the disk drives and the experiment with respect to the vehicle's coordinate system need to be considered as well. The disk drive spin axis was aligned to each of the three axes of the vehicle to yield three orientations for the disk drives. For each orientation of the disk drive spin axis, the experiment was placed in the x-z, x-y, and y-z planes within a radius of 10 m from the vehicle CG. The g-load contour for the experiment is then plotted for each plane. This was done for each of the five cases mentioned above, plus a case where both of the disk drives are at rest.

7.3.1.3 Results

In table 7-3 the rows display the five cases plus the case where both of the disk drives are at rest. The columns show the orientation of the disk drive spin axis with respect to the vehicle's coordinate system. The maximum g's for the worst and optimal cases are also listed for each orientation of the disk drive spin axis, and the corresponding orientation of the experiment for each case is given. Figure 7-7 shows the g-load contour for case d (one operating, second

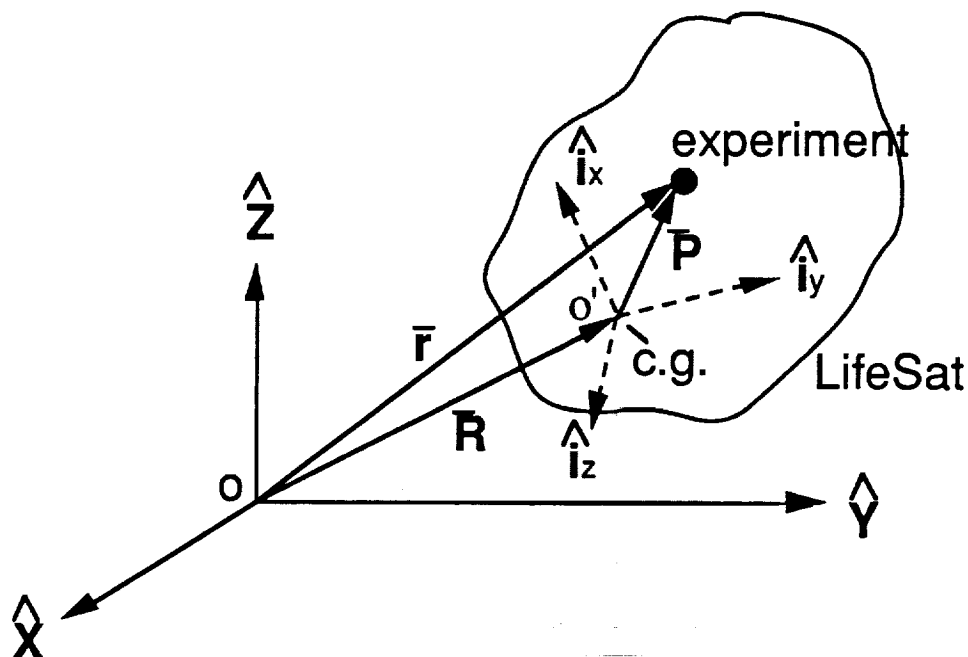


Figure 7-6. Inertial and Relative Coordinate Systems for the Vehicle and Experiment

stopping) where the disk drive spin axes are aligned to the \hat{i}_y -axis and the experiment is in the x-z plane. This figure shows the worst case, which is placing the experiment at $\pm P \cos 45^\circ (\hat{i}_x + \hat{i}_z)$.

7.3.1.4 Conclusions

With the \bar{R} , $\bar{\omega}_{\text{sat}}$, and $\dot{\bar{\omega}}_{\text{sat}}$ chosen for this study, table 7-3 indicates that the optimal case can be achieved by aligning the disk drives to the \hat{i}_y -axis, placing the experiment along the \hat{i}_y -axis, and placing the experiment as close to the vehicle's CG as possible. At 10 m away from the vehicle's CG, the experiment will experience micro-g's ranging from 0 to 0.1. This would be even less for a distance less than 10 m.

The worst case occurs when:

- The disk drives are aligned to the \hat{i}_y -axis.
- The experiment is placed in the x-z plane at 45° from both axes.
- The experiment is placed as far away from the vehicle's CG as possible.

At 10 m away from the vehicle's CG, the experiment will experience micro-g's ranging from 2.9 to 9.2.

TABLE 7-3. RESULTS OF DISK DRIVES MICRO-G ANALYSIS

Disk Drives		Disk Drive Spin Axis Aligned to I_x -axis		Disk Drive Spin Axis Aligned to I_y -axis		Disk Drive Spin Axis Aligned to I_z -axis	
		Worst Case	Optimal Case	Worst Case	Optimal Case	Worst Case	Optimal Case
① off ② off	Max g (micro-g's)	2.919	0	2.919	0	2.919	0
	Orientation of Experiment	$\pm P \cos \frac{\pi}{4} (I_x \pm I_z)$	along I_y	$\pm P \cos \frac{\pi}{4} (I_x \pm I_z)$	along I_y	$\pm P \cos \frac{\pi}{4} (I_x \pm I_z)$	along I_y
① starting ② off	Max g (micro-g's)	7.128	3.916	9.151	0	8.629	1.305
	Orientation of Experiment	$\pm P \cos \frac{\pi}{4} (I_y \pm I_z)$	$\pm P I_x$	$\pm P \cos \frac{\pi}{4} (I_x \pm I_z)$	along I_y	$\pm P \cos \frac{\pi}{4} (I_x \pm I_z)$	$\pm P I_z$
① on ② off	Max g (micro-g's)	2.967	0.001	2.924	0.109	2.778	0.210
	Orientation of Experiment	$\pm P \cos \frac{\pi}{4} (I_x \pm I_z)$	$\pm P I_y$	$\pm P \cos \frac{\pi}{4} (I_x \pm I_z)$	$\pm P I_y$	$\pm P \cos \frac{\pi}{4} (I_x \pm I_z)$	$\pm P I_y$
① on ② starting	Max g (micro-g's)	7.128	3.917	9.151	0.109	8.583	1.305
	Orientation of Experiment	$\pm P \cos \frac{\pi}{4} (I_y \pm I_z)$	$\pm P I_x$	$\pm P \cos \frac{\pi}{4} (I_x \pm I_z)$	$\pm P I_y$	$\pm P \cos \frac{\pi}{4} (I_x \pm I_z)$	$\pm P I_z$
① on ② stopping	Max g (micro-g's)	7.128	3.917	9.151	0.109	8.583	1.305
	Orientation of Experiment	$\pm P \cos \frac{\pi}{4} (I_y \pm I_z)$	$\pm P I_x$	$\pm P \cos \frac{\pi}{4} (I_x \pm I_z)$	$\pm P I_y$	$\pm P \cos \frac{\pi}{4} (I_x \pm I_z)$	$\pm P I_z$
① stopping ② off	Max g (micro-g's)	7.128	3.916	9.151	0	8.629	1.305
	Orientation of Experiment	$\pm P \cos \frac{\pi}{4} (I_y \pm I_z)$	$\pm P I_x$	$\pm P \cos \frac{\pi}{4} (I_x \pm I_z)$	along I_y	$\pm P \cos \frac{\pi}{4} (I_x \pm I_z)$	$\pm P I_z$

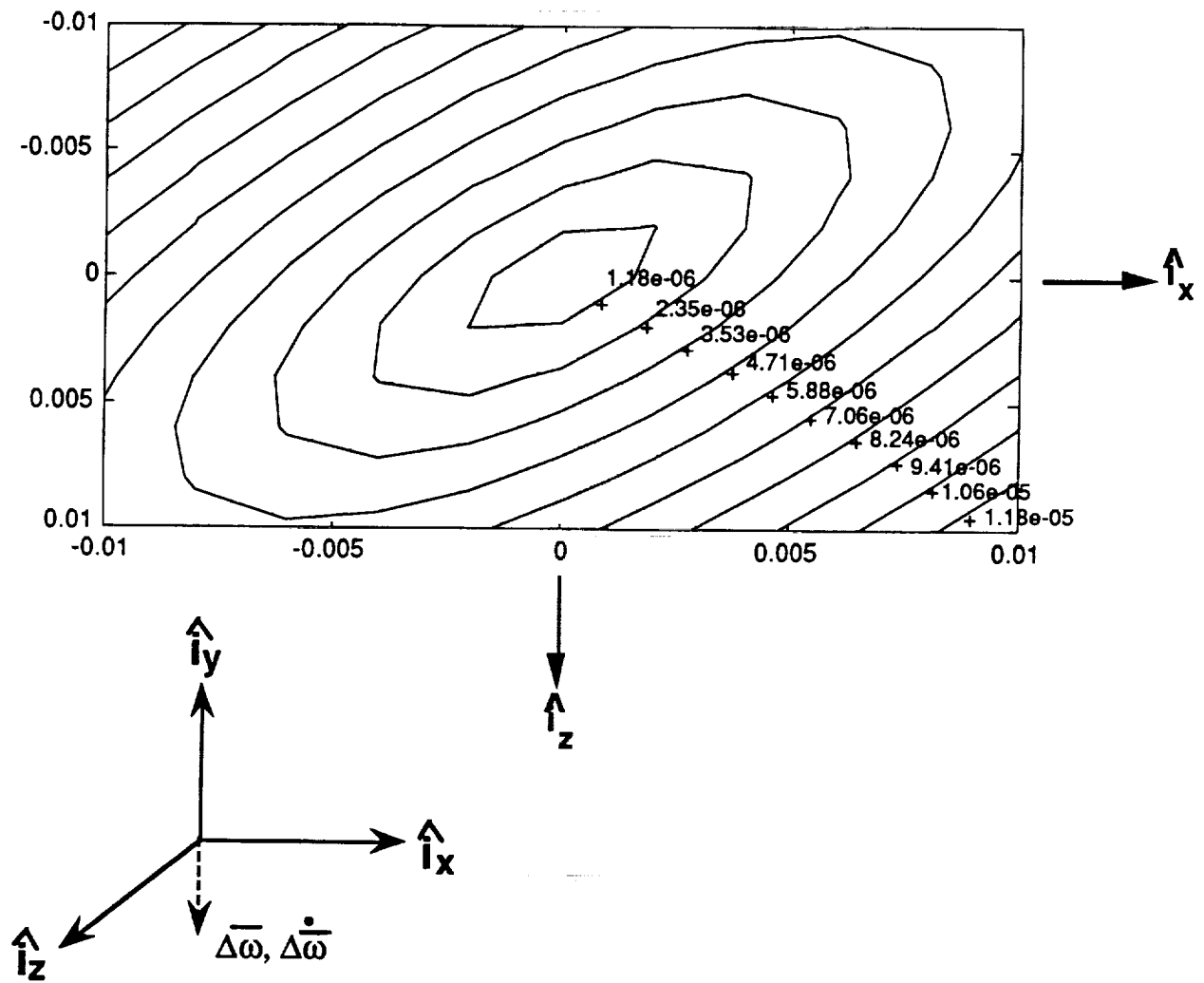


Figure 7-7. G-load Contour for Case d

SECTION 8 LANDING ANALYSIS

8.1 LANDING OPPORTUNITIES FROM CIRCULAR ORBITS

(Prepared by Tim Crull)

A brief study investigated landing opportunities from circular orbits at ~34 degrees inclination. The major goal was to determine landing opportunity availability throughout a 65-day mission, to allow recovery of the payload if the mission needed to be terminated early. Landing opportunity availability was investigated as a function of additional orbital maneuvering propellant. Other items investigated were the effect of different landing site latitudes on landing opportunity availability and lighting at the landing site throughout the mission.

8.1.1 Assumptions and Background

It was assumed that required adjustments to position the groundtrack over the landing site were made only with orbital altitude adjustment maneuvers. Plane change maneuvers were not considered. The altitude adjustment approach typically involves timing a maneuver into an elliptical orbit. The maneuver also needs to be timed to orient the line of apsis so deorbit is done at apogee (to minimize the burn magnitude). This approach requires no additional propellant if a single retrograde maneuver is used to lower perigee. The deorbit perigee is simply achieved in two steps versus one. Additional propellant becomes necessary if posigrade burns, or two retrograde burns, are used. The latter case comes into play once perigee is lowered to the limiting value for stable orbital flight. At that point, apogee must then be lowered to achieve further change in the orbital period. It was assumed that orbital altitudes could not be lowered below 194.5 km (105 nm).

Important parameters for landing opportunity availability are the size of the altitude adjustment and the amount of time in the adjusted orbit. The lowest proposed orbit (275 km) was therefore studied, as it results in the smallest single retrograde adjustment to reach the minimum orbital altitude (and hence the smallest difference between the period of the original and adjusted orbit). Therefore, this orbit will define the lowest landing opportunity availability for no additional propellant.

It was assumed that only 24 hours could be spent in the adjusted orbit. Longer periods result in increased landing opportunity availability for the same propellant. However, periods longer than 24 hours were assumed to be undesirable, since the study was addressing early mission terminations due to some failure.

It was assumed a groundtrack that passed through the landing site in either an ascending or descending direction, i.e., before or after (respectively) reaching the peak groundtrack latitude, was acceptable.

8.1.2 Methodology

The empirical portion of the study involved first defining the amount of groundtrack shift possible for various levels of additional orbital maneuvering propellant. Figure 8-1 illustrates the scenario for the maximum shift possible with zero additional propellant.

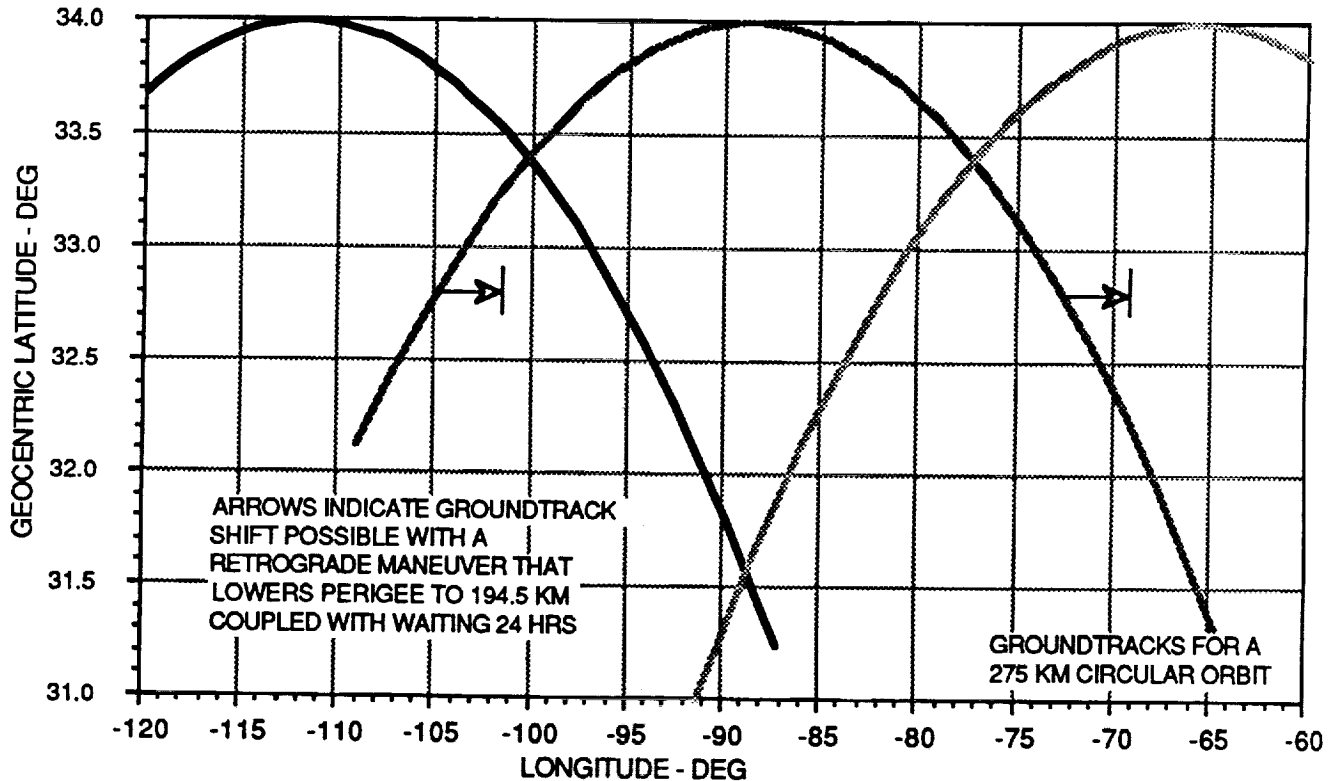


Figure 8-1. Possible Groundtrack Shifts for a 275 km Orbit

A 275x194.5 km orbit has an orbital period 48 seconds shorter than the original 275x275 km orbit. Accumulating that difference over 16 revolutions (24 hours) translates into 3.2 degrees less of earth rotation angle. The groundtrack is therefore shifted east by that amount. Additional shifts to the east are possible by using additional propellant to lower apogee; if the second maneuver is properly phased for deorbit, the additional propellant requirement is the amount used to lower apogee. Shifts to the west are possible by maneuvering into an elliptical orbit with an apogee greater than 275 km; if the maneuver is properly phased for deorbit, the additional propellant requirement is the amount used to raise apogee.

Maximum crossrange values were then defined for the possible groundtrack shifts. For this study, maximum crossrange values were defined since the available landing opportunity propagator used crossrange (the parameter of interest for a nonballistic vehicle such as shuttle). Limiting crossrange values

were defined for different latitudes, as a given shift in longitude translates into a different crossrange for each latitude. A landing opportunity propagator that uses longitudinal offset of the groundtrack from the landing site would simplify the process for ballistic vehicles.

Daily landing opportunities to sites in the WSMR area were then generated for two hypothetical 65-day missions: one with an initial ascending node of 150 degrees west longitude, the other with an initial ascending node of 144 degrees west longitude. Days with available landing opportunities were then defined by comparing crossranges for opportunities to the limiting values for different levels of additional propellant.

8.1.3 Empirical Results

The results for one hypothetical mission are presented in figure 8-2. The data show a peak in availability if the landing site is positioned two or three tenths of a degree below the peak groundtrack latitude. For no additional propellant, ~30 percent of the days (19 of the 65 days) have a landing opportunity available which passes close enough to the landing site so that 24 or less hours in an orbit between 275x275 km and 275x194.5 km can eliminate the crossrange. These results assume the landing may occur anytime (day or night) at a single site.

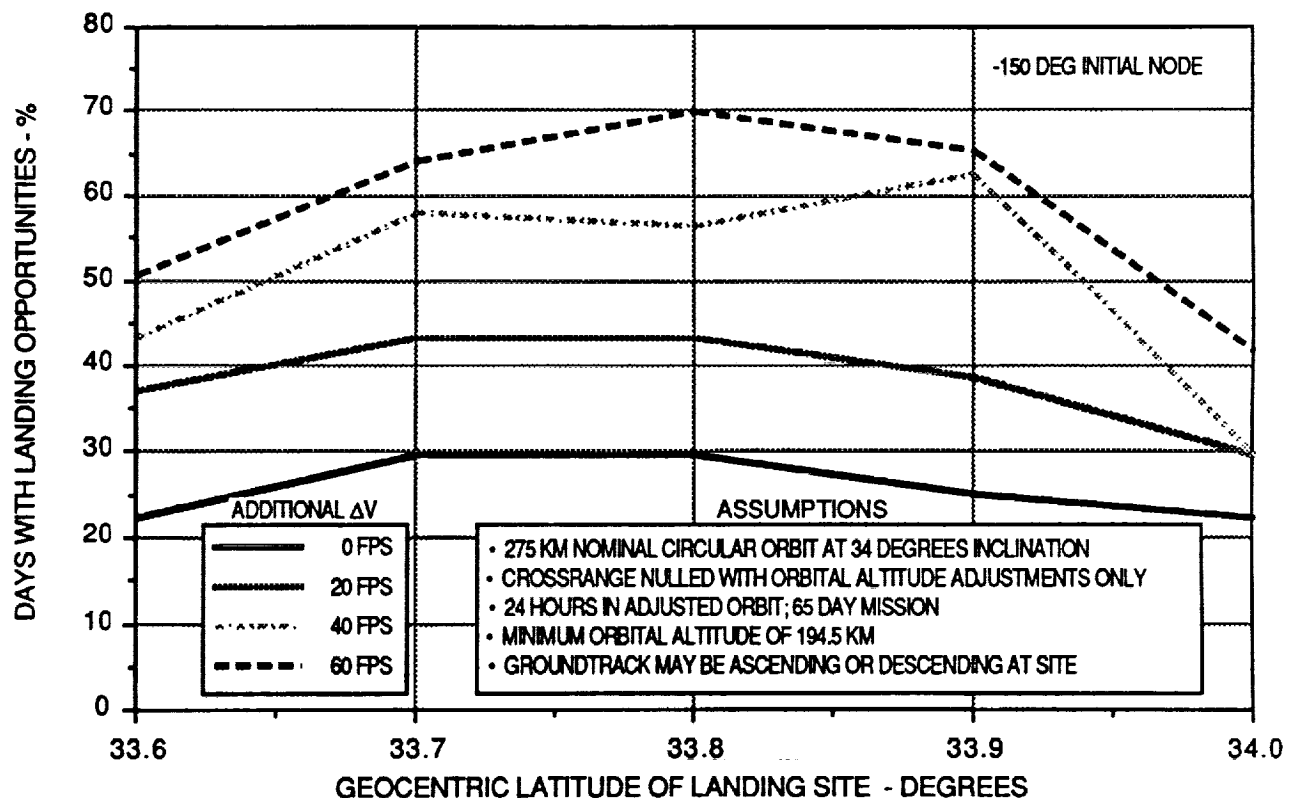


Figure 8-2. Landing Opportunity Availability for One Hypothetical Mission

A site is needed in both the northern and southern hemisphere to have daylight landings throughout the mission, due to nodal regression of the orbit. Since the ascending node of the orbit considered in this study regresses 360 degrees in inertial space every ~50 days, a site will have daylight landing opportunities for 25 days, on the average, followed by 25 days of night landing opportunities.

Figure 8-3 shows potential lighting conditions for WSMR landings. This particular cycle is obtained by launching from KSC about an hour before sunset. This allows landings early and late in the mission to be in daylight.

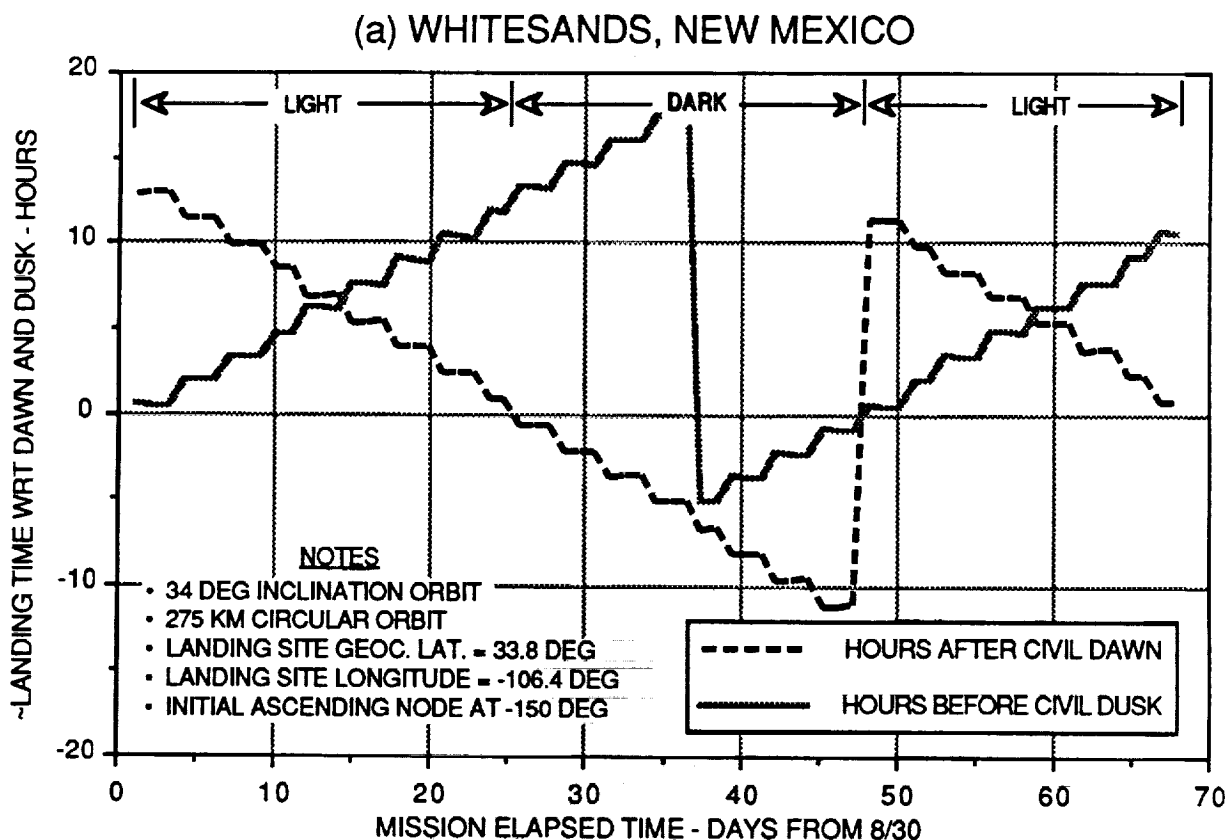


Figure 8-3. Lighting Conditions for WSMR Landings

Adding a site in the southern hemisphere will allow daylight landings during the middle portion of the mission (figure 8-4). The discontinuities in the curves are produced by shifts to an earlier revolution in the day. The flatter portions of the curves (typically spanning 3 days) indicate landings that are occurring on the same revolution of a mission day. Landings shift to an earlier revolution in the day as the mission progresses.

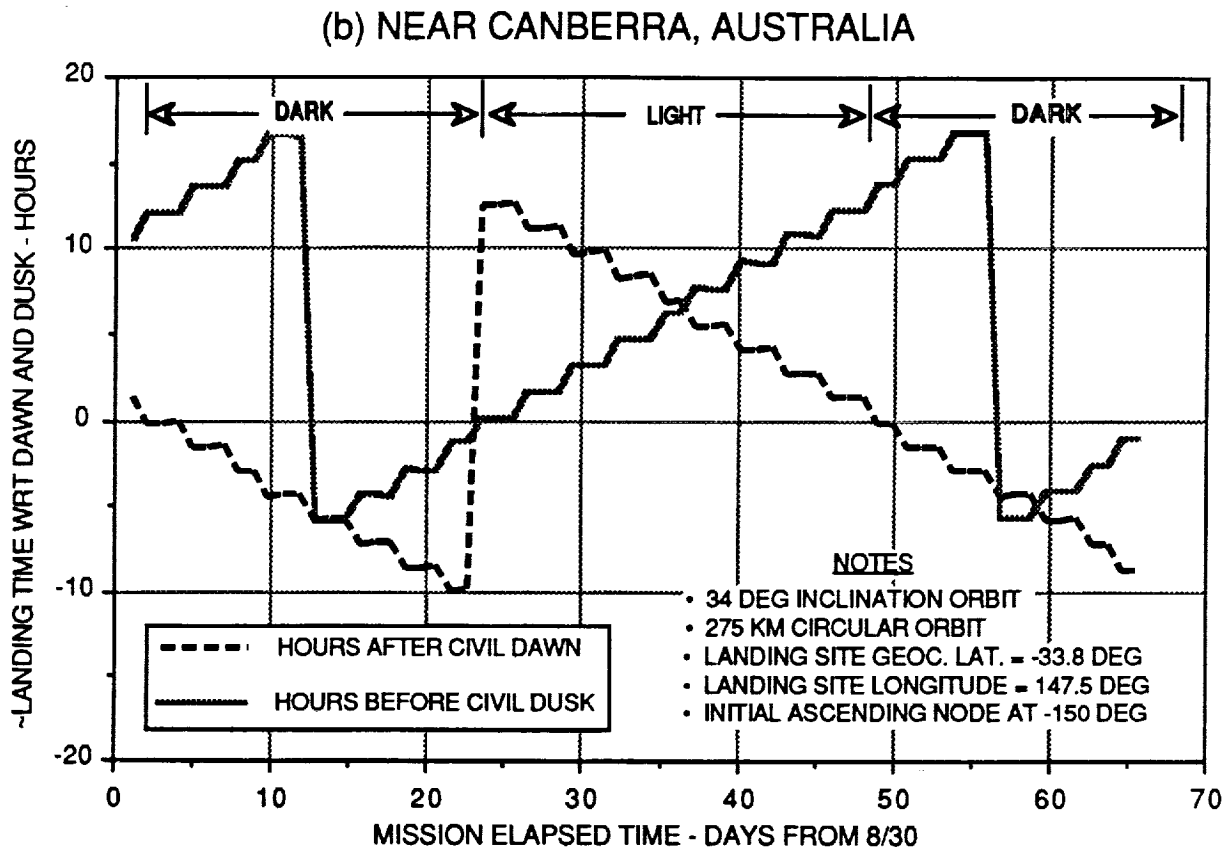


Figure 8-4. Lighting Conditions for Landings Near Canberra, Australia

Figure 8-5 presents an approximate relationship for landing opportunity availability as a function of additional propellant. The data are from the two hypothetical missions, assuming a landing site at 33.7 or 33.8 degrees geocentric latitude. The data show that landing opportunity availability can be doubled if ~40 fps of propellant is budgeted for that purpose. The data scatter indicates some sensitivity to the initial orbital orientation and landing site location. Landing opportunities for this orbital altitude have crossranges that are repetitive over a several day cycle, producing a somewhat discrete distribution of specific landing opportunity crossrange values over a 65-day period. Some conditions produce opportunities that are achievable with a given amount of propellant, while others may have a landing opportunity pattern that requires a bit more propellant to achieve the same level of availability. The next section will discuss an approach to determining the expected, or average, value of availability for a given propellant level.

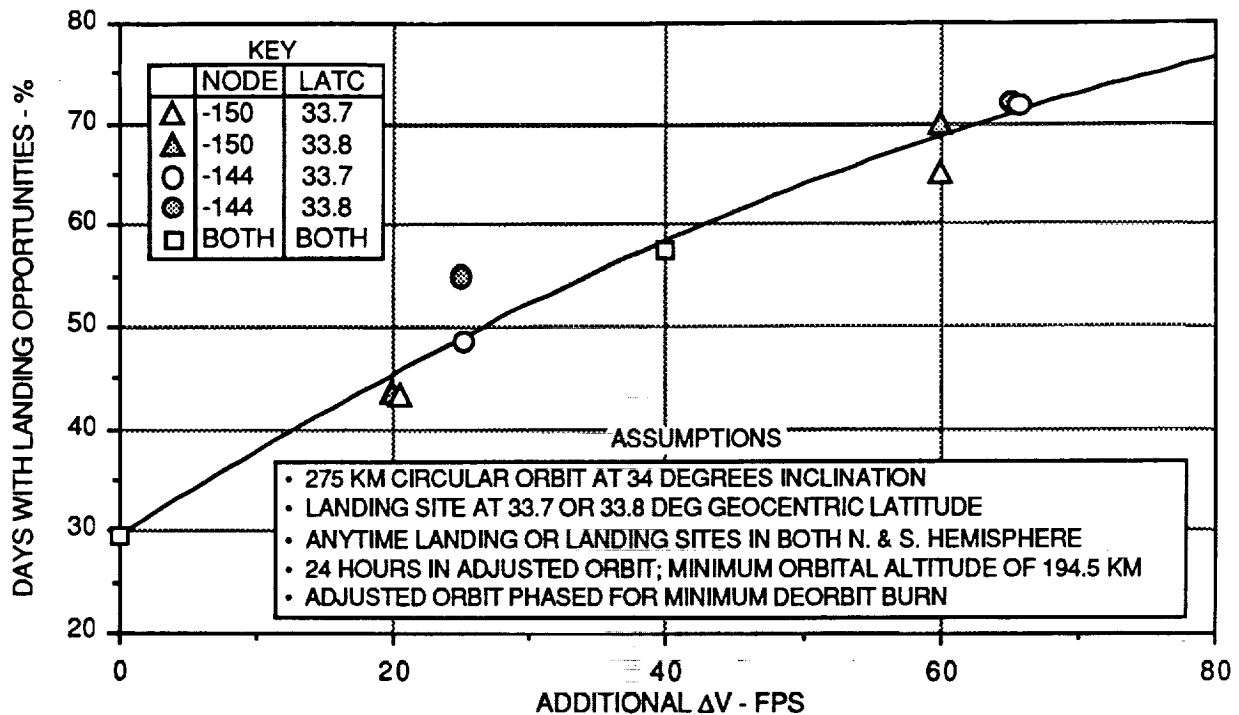


Figure 8-5. Landing Opportunity Availability as a Function of Additional Propellant

8.1.4 Theoretical Discussion

The expected, or average, value of landing opportunity availability for a given orbit may be obtained by considering the groundtrack shift possible for a given propellant level. This discussion will address the the case for no additional propellant. However, the approach can be easily extended to other conditions.

Figure 8-1 previously presented the maximum groundtrack shift for no additional propellant (about 3.2 degrees). Considering that a 275 km orbit circles the earth 16 times per day and an ascending and descending pass to most site latitudes is possible each revolution, the total daily longitudinal coverage equals $16 \times 2 \times 3.2$ degrees, or 102.4 degrees. This translates into a 28.4 percent probability of having a landing opportunity available on any given day: $(102.4/360) \times 100$ percent. This probability is halved if a site latitude can only provide one unique band of longitudinal coverage per revolution, e.g., the peak groundtrack latitude or a latitude where the groundtracks intersect. This latter condition is illustrated on figure 8-1 at 33.4 degrees latitude. Only one band of longitudinal coverage is available per revolution, since the band for the ascending pass of one revolution corresponds to the descending pass for the next.

The empirical data of figure 8-2 was extended to lower latitudes to verify the theory (figure 8-6). There appears to be an average availability of ~28 percent for latitudes where the longitudinal coverage for the ascending and descending pass is unique. Also, the availability decreases to half that value at the latitude where the groundtracks intersect (33.4 degrees).

The empirical data at the peak groundtrack latitude is a little higher than expected because both hypothetical missions with a 34-degree latitude site had a number of days (5 or 6) with opportunities of 0.1 nm crossrange. These opportunities would require additional propellant to position the groundtrack exactly over the landing site; however, the opportunities were considered acceptable by rationalizing that the recovery zone was big enough to accommodate the miss distance. This situation was only encountered at the peak groundtrack latitude, where small crossranges occur more frequently due to the flat nature of the groundtrack.

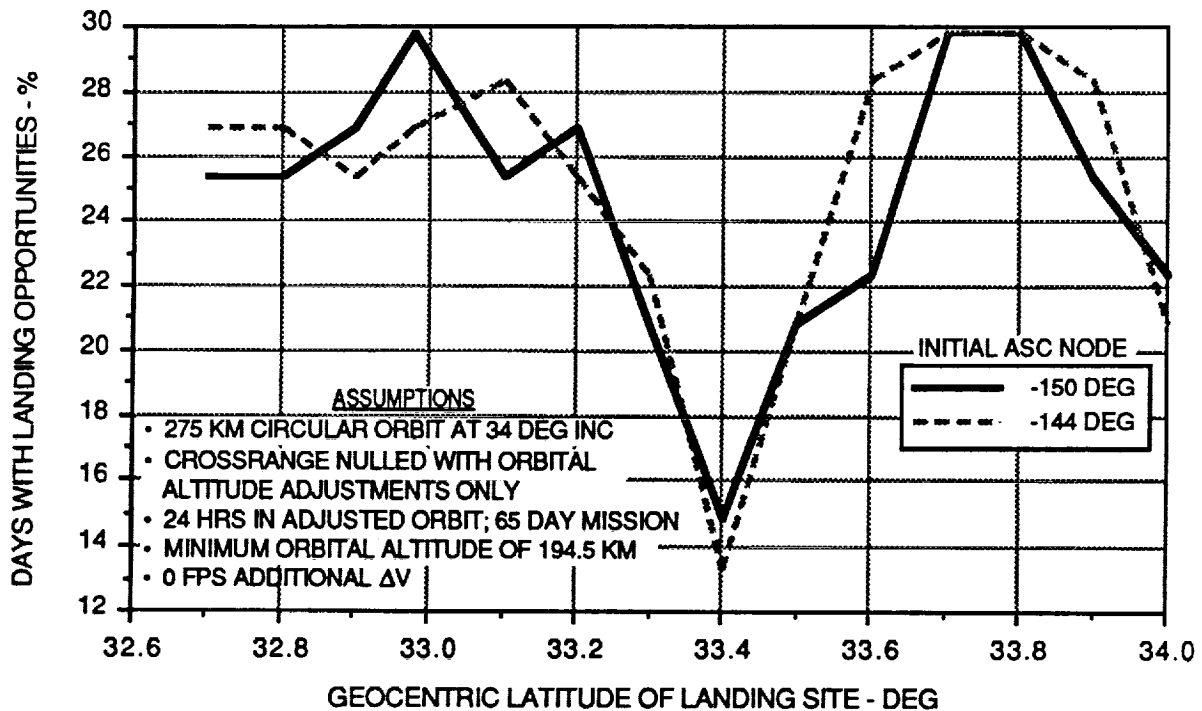


Figure 8-6. Landing Opportunity Availability for Sites to 32.5 Degree Latitude

For a 900 km circular orbit and similar assumptions, a daily landing opportunity is available with no additional propellant, regardless of the landing site location. The difference in orbital period between the 900 km circular orbit and a 900x194.5 km elliptical orbit is 443.7 seconds. This equates to 27.7 degrees of groundtrack shift for a 24-hour loiter in the adjusted orbit. 27.7x15 revolutions per day equals 416 degrees of longitudinal coverage per day (or 100+ percent availability), using just the ascending or descending pass to a landing site.

8.1.5 Conclusions

With no additional propellant, a landing opportunity should be available for ~28 percent of the days for the 275 km, low inclination orbit, provided the inclination and landing site latitude are selected properly. The site latitude, or inclination, needs to be selected to maximize longitudinal coverage from possible shifts in the groundtrack (obtained by loitering in an elliptical orbit with the lowest possible perigee). Longitudinal coverage is maximized if the site is positioned away from the peak groundtrack latitude, or away from latitudes where the groundtracks intersect, so that two distinct bands of longitudinal coverage are obtained for each revolution: one on the ascending pass through the site latitude, the other on the descending pass. Positioning the site at a point of groundtrack intersection will cut landing opportunity availability in half, since the longitudinal coverage for the ascending pass of a revolution is duplicated by the descending pass of the next revolution. Budgeting ~40 fps of additional propellant will allow additional altitude adjustment maneuvers that will approximately double landing opportunity availability.

The above conclusions assume a landing can be made during the day or night at a single site. If day only landings are mandated, a site is required in both the northern and southern hemisphere to avoid an approximate 25-day period of landing opportunity unavailability due to the effects of orbital node regression.

As orbital altitude increases, landing opportunity availability will also increase. Greater longitudinal coverage is possible due to the bigger difference between the period of the circular orbit period and the period of an elliptical orbit with apogee at the circular altitude and perigee at the minimum value. For a 900 km circular orbit, a daily landing opportunity is available with no additional propellant, if it is acceptable to loiter for up to 24 hours prior to deorbit in a 900x194.5 km orbit.

8.2 ENTRY FOOTPRINT ANALYSIS

(Prepared by Bret McCleary)

Atmospheric perturbations, uncertainties in the vehicle aerodynamics, and other unknown environmental and vehicle parameters, if uncontrolled during entry, cause variations in the vehicle's touchdown location. The vehicle maintains a zero angle-of-attack during entry with no closed loop atmospheric guidance to control its final landing position. Thus, the only landing position control for LifeSat is reentry steepness controlled by the deorbit burn guidance. The reentry steepness is traditionally characterized as the flight-path angle at EI but since the LifeSat is unguided during entry, steepness can also be defined as the nominal peak g-load encountered. A steeper entry causes a higher peak g-load while a shallower entry results in a lower peak g-load. A steeper entry also decreases the uncertainty in the landing location or footprint size while a shallower entry increases the footprint.

The purpose of the entry footprint analysis is to determine the expected peak g-loads that are encountered by the vehicle during atmospheric entry to provide a 99.73 percent reliability (3σ) of touchdown within a pre-defined target area. The target area was selected for all mission scenarios from ground maps of the WSMR. This section describes the mission scenarios, the footprint analysis assumptions, and the footprint analysis results.

8.2.1 Mission Scenarios

The landing footprint for the vehicle was determined for four mission scenarios, which can be separated into two categories: deorbit from a circular orbit at 34° inclination and deorbit from an elliptical orbit entering the Earth's atmosphere with a 90° inclination. A typical entry timeline is shown in table 8-1. The mission scenario categories investigated are shown pictorially in figure 8-7.

TABLE 8-1. TYPICAL ENTRY TIMELINE (900 km CIRCULAR ORBIT)

<u>Event</u>	<u>Time From EI</u> <u>(min:sec)</u>
EI	0:00
Peak Heat Rate	2:43
G-Load Exceeds 8 g's	2:49
Peak G-Load	3:10
G-Load Drops Below 8 g's	3:30
Drogue Chute Deployment	4:08
Main Chute Deployment	6:26
Touchdown	9:56

In the category 1 mission scenario, the vehicle coasts in a circular orbit at an altitude well below the GPS constellation. Just before deorbit, the onboard navigation state is updated via GPS. After the deorbit burn is initiated, guidance logic corrects the deorbit burn direction and duration for proper entry targeting. The vehicle is spun just before EI until parachute deployment to null any unwanted lift during entry. Drogue chute deployment occurs at Mach 1.5 at an altitude of approximately 55,000 ft. The three main chutes are deployed at approximately 10,000 ft. Touchdown occurs with a relative velocity of about 25 ft/sec with the three nominal main chutes.

The category 2 mission scenario's on-orbit trajectory coasts well above the GPS constellation at apogee. Because of the altitude and geometry of the constellation, GPS coverage is limited to below 6000 km. Thus, a GPS update is performed below 6000 km as the vehicle coasts toward apogee. An altitude of 4000 km was chosen to update the vehicle's state since a finite amount of time is required to acquire accurate state information and update the navigated position and velocity. A deorbit burn is performed at apogee, then a GPS

update is performed at 4000 km before reaching EI. At least one trim burn is necessary before the vehicle reaches EI to correct the actual vehicle state to the desired nominal state. Once the vehicle enters the Earth's atmosphere, the sequence of events is essentially the same as the category 1 mission scenario.

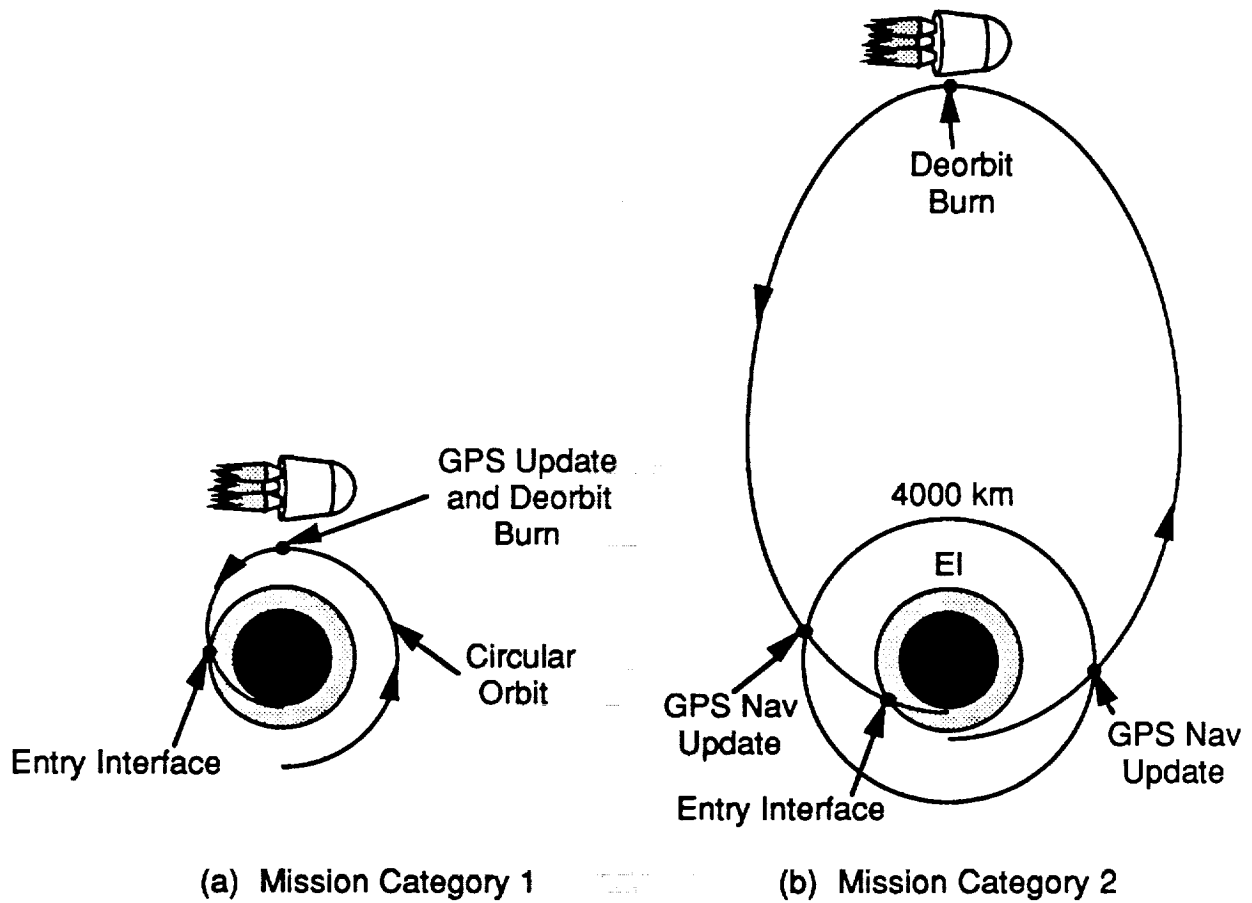


Figure 8-7. LifeSat Mission Scenario Categories for Footprint Analysis

8.2.2 Footprint Analysis Assumptions

To determine the entry footprint, a Monte Carlo technique was used. This section describes the error source magnitude assumptions made to determine the footprint. The vehicle and environment models used in the trajectory simulation are shown followed by the dispersions used in the Monte Carlo analysis.

8.2.2.1 Vehicle and Environment Assumptions

This section describes the vehicle mass and aerodynamics as well as the drogue and main parachute aerodynamics. A brief description of the atmosphere and wind model used in the analysis is also given.

The vehicle is modeled as nearly ballistic with only a small amount of lift. The parachutes are simply modeled with a constant coefficient of drag. Table 8-2 shows the values of lift and drag coefficients at ± 5 degrees angle-of-attack. The resulting drag coefficient is normalized as a function of reference area (A).

TABLE 8-2. VEHICLE AND PARACHUTE AERODYNAMIC COEFFICIENTS

<u>Aerodynamic Parameter</u>	<u>Angle-of-Attack (deg)</u>		
	-5.0	0.0	5.0
Vehicle drag coefficient (C_d)	0.671	0.665	0.671
Vehicle lift coefficient (C_l)	-0.042	0.0	0.042
Drogue chute drag coefficient (C_d)	0.55	0.55	0.55
Main chute drag coefficient (C_d)	0.8	0.8	0.8

Thus,

$$C_d = \frac{C_{d1}A_1 + C_{d2}A_2 + C_{d3}A_3 + \dots}{A_1 + A_2 + A_3 + \dots}$$

The vehicle weight is assumed to be 3500 lb before the deorbit burn. The mass at EI varies slightly with the steepness of the trajectory.

The atmosphere and winds were modeled using the 1988 version of the Global Reference Atmospheric Model (GRAM-88) [2]. GRAM generates atmospheric density, pressure, and temperature given the local time (month, day, year, hour, minute, second), altitude, latitude, and longitude. GRAM also produces north and east wind component magnitudes. Either a mean or dispersed atmosphere and wind can be produced using GRAM. The dispersed atmospheres and winds were used in the Monte Carlo analysis.

8.2.2.2 Monte Carlo Dispersions

Five vehicle and environmental parameters are dispersed in the Monte Carlo analysis. Atmosphere and wind data are dispersed by GRAM-88 as discussed earlier. The initial vehicle state is dispersed at EI through a state covariance matrix. Vehicle and parachute aerodynamics are normally dispersed via drag coefficient and reference area variations. Paragraph 8.2.3.4 discusses the individual contributions of all dispersed parameters to the total downrange and

crossrange dispersion for the 900 km orbit. Table 8-3 shows the standard deviation values for the aerodynamic and mass dispersions.

TABLE 8-3. AERODYNAMIC AND MASS DISPERSION MAGNITUDES

<u>Error Source</u>	Dispersion (3σ)	
	<u>Magnitude</u>	<u>Percent</u>
Vehicle Drag Coefficient	0.0333	5.0
Drogue Chute Drag Coefficient	0.0275	5.0
Main Chute Drag Coefficient	0.04	5.0
Drogue Chute Reference Area	0.442 sq. ft.	1.0
Main Chute Reference Area	5.515 sq. ft.	1.0
Vehicle Mass (Uniformly Distributed)	+/-55 lbm	+/-1.7

The vehicle aerodynamics are also dispersed by uniformly varying initial angle-of-attack ± 5 degrees. Note that the vehicle is spun about the velocity vector at a constant rate of 4.2 rpm to cancel the effects due to lift.

The Monte Carlo results presented in this paper are based on 1109 dispersed cases. A binomial distribution is used when statistical data is presented. The binomial distribution is based on the premise that a case either passes or fails. In this study, "pass" or "fail" means the touchdown location is either inside or outside the desired landing area. To ensure at least 95 percent confidence of 99.73 percent reliability (3σ), 1109 samples are needed. If all 1109 pass, there is a 95 percent confidence that the probability of the vehicle landing within the target zone is 99.73 percent.

8.2.3 Footprint Analysis Results

8.2.3.1 Proposed Landing Areas

The size and shape of the available landing area greatly influences the entry trajectory. A steep entry reduces the landing footprint at the cost of higher g-loads and vehicle heating. Since the selection of the landing area is a critical part of the entry trajectory design, a description of each landing zone with limitations to size of each site is described in this section.

WSMR has been selected as the landing site for the vehicle. Figure 8-8 is a sketch of WSMR which is about 33 nm in width east to west and about 100 nm in length north to south. An extension zone, requiring 30 days prior notice, extends the range northward another 32 nm at approximately the same width. The entire range, however, cannot be used for vehicle landing operations. The San Andres mountain range runs northeast to southwest and then north to south through a large part of WSMR. Obviously, landing the vehicle in a mountain range would severely increase vehicle recovery time. A number of airstrips are also located throughout the range thus limiting the number and size of acceptable landing zones.

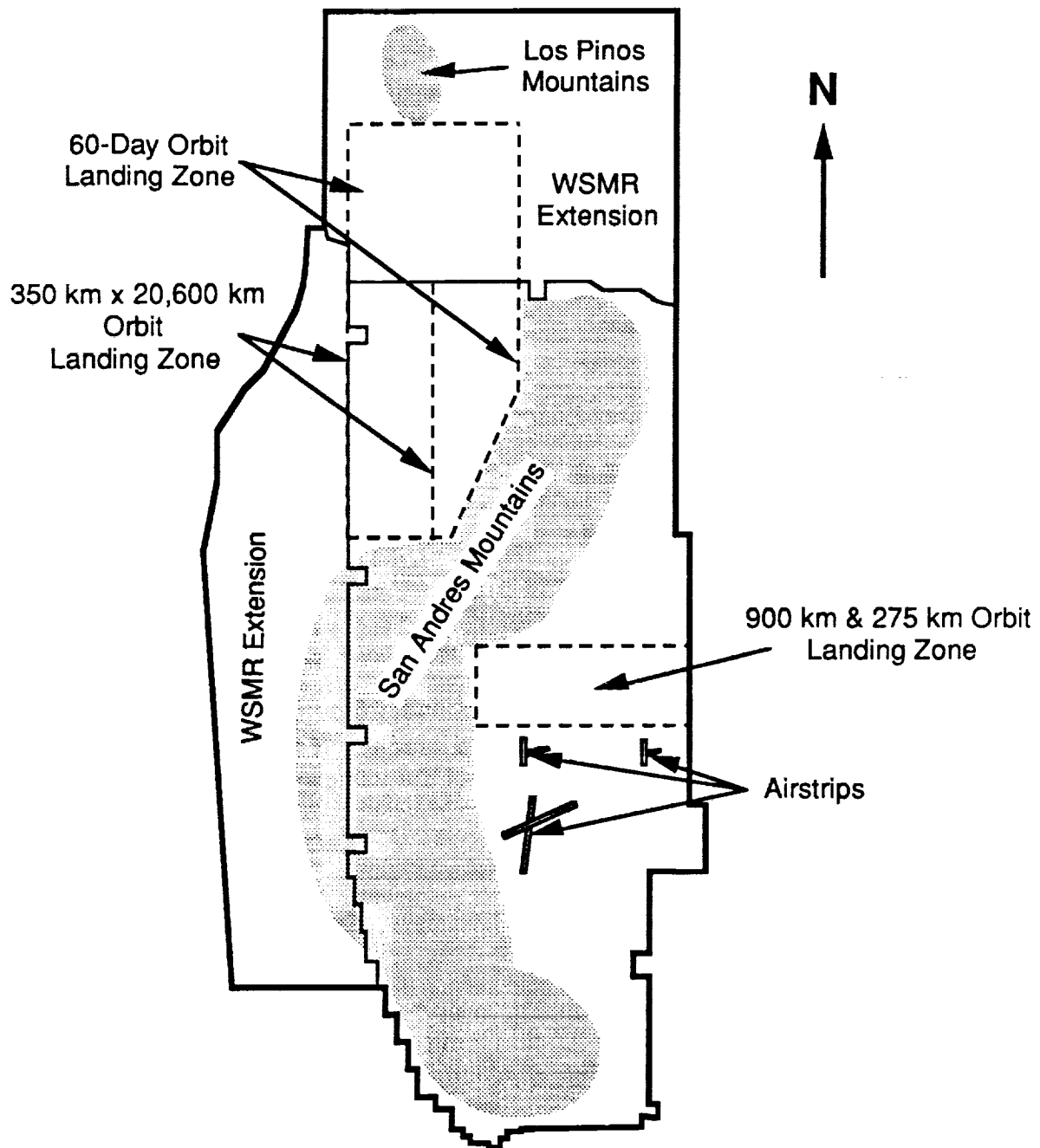


Figure 8-8. Sketch of White Sands Missile Range

The assumed landing sites within WSMR were chosen based on mission scenario and inclination. The landing site for the 34° inclination missions was chosen in the eastern portion of the range. This landing area is approximately 23 nm east to west and about 8 nm north to south. The site is bounded on the east by the WSMR boundary and on the west by the San Andres mountain range. Two airstrips lie about 1 nm to the south of the proposed landing zone.

The northwest corner of the zone is also bounded by the mountain range. The landing site could be increased at least another 5 nm to the north on the eastern half of the zone since the mountain range extends southwest to northeast.

The landing zone for the 90° inclination, 350 km by 20,600 km orbit, was chosen in the northwest portion of WSMR. This landing area is about 8 nm east to west and 25 nm north to south. The site is limited on the west and north by the boundaries of the missile range. The south side and southeast corner of the proposed area are bounded by the San Andres mountain range. The landing site could be widened by 9 nm to the east in the north half of the proposed area since the mountains run southwest to northeast and only constrain the southwest corner of the zone.

The 60-day elliptical orbit is unique in that a 30-day notice before landing can be given to WSMR personnel. Assuming the extension zone can be used, a much larger landing area can be provided for this mission. The proposed landing area for this mission runs 40 nm north to south and 17 nm east to west. The east boundary narrows to 8 nm at the south edge of the zone. The WSMR boundary limits the landing area to the west, the Los Pinos mountains limit the area to the north, and the San Andres mountain range bounds the area on the east and south.

8.2.3.2 Monte Carlo Analysis

A series of Monte Carlo sets were run with each set using varying EI flight-path angles. The purpose of running these Monte Carlo cases is to determine the reentry steepness needed to touchdown within the desired landing zone. An example of the touchdown locations from a Monte Carlo analysis of the 900 km orbit mission is shown in figure 8-9. The entry steepness is proportional to the peak g-load encountered during entry. A steep reentry causes high peak g-loads and a smaller downrange landing footprint. Figure 8-10 shows the downrange distance of the landing footprint plotted versus the nominal peak entry g-load for all four missions.

The nominal g-load is obtained by entering the atmosphere at a specific flight-path angle while simulating no dispersed conditions during entry. The downrange limit of the landing site is shown in the figure as a horizontal line. The g-load corresponding to the downrange limit of the landing area gives the lowest nominal entry peak g-load to land within the target area. Since the sample size of the Monte Carlo was relatively low, the results are accurate to within about ± 1 g. Thus, the desired nominal entry steepness was chosen to the nearest 1 g. Ten g's was chosen for the 275 km orbit mission, 11 g's was chosen for the 900 km orbit mission, 12 g's for the 60-day orbit mission, and 14 g's for the 350 km by 20,600 km orbit mission.

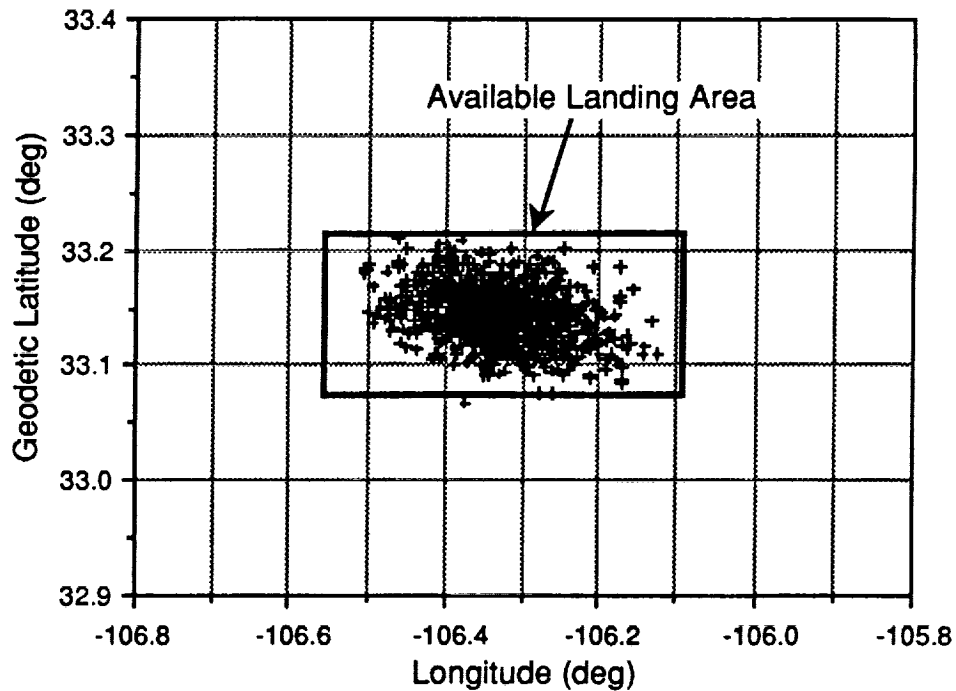


Figure 8-9. Example of Monte Carlo Landing Locations for 900 km Mission

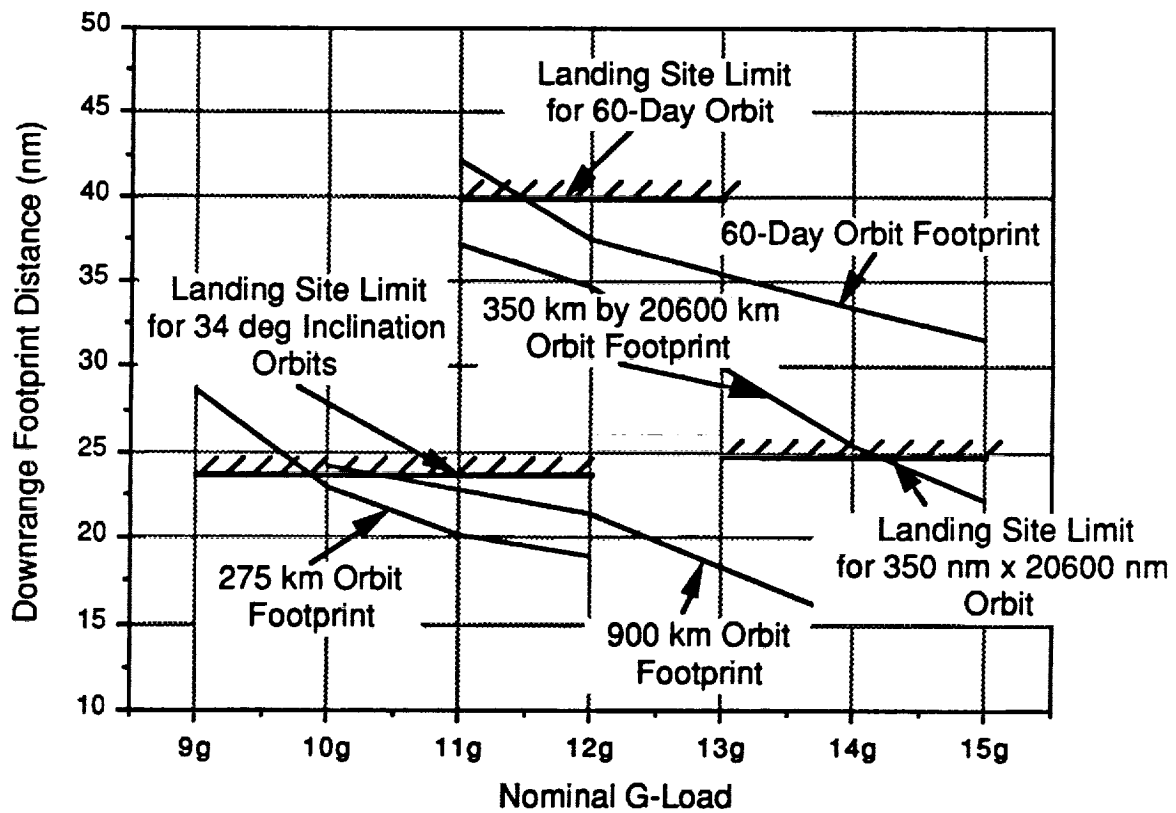


Figure 8-10. Total Footprint Downrange Distance Versus Nominal Entry G-Load

Only the downrange component of the footprint can be controlled since the LifeSat vehicle has no active guidance during entry. The crossrange component of the footprint is essentially unaffected by reentry steepness. The crossrange deviation is almost entirely caused by wind variations after the parachutes are deployed. The post-chute deployment vehicle trajectory is not significantly affected by reentry steepness because of the low vehicle velocity. Thus the vehicle "drifts" according to wind speed and direction leading to a crossrange variation at touchdown.

Generally, a higher transfer orbit energy leads to a higher entry g-load. The 60-day orbit mission had the highest orbital energy but had a relatively low 12 g entry because of the increase in size of the available landing area. This mission seems more viable from an entry point of view as opposed to the 350 km by 20,600 km mission because the extension zone at WSMR can be used.

Because of variations in the environment and uncertainties in vehicle aerodynamics, mass, and EI state, an off-nominal peak load factor and heat rate are likely during reentry. The Monte Carlo analysis also helped quantify variations in g-load and heat rate. Table 8-4 shows variations in peak g-load (a), heat rate (b), and time above 8 g (c) for all four missions. The g-load varies within ± 1 g of the nominal peak value. The heat rate varies within about ± 8 percent of the nominal value. Note that the heat rate values were computed using Chapman's heating equation (convective heating, cold wall assumption) with a nose radius of 2.78 ft. The heat rate shown for the elliptical orbits may be even higher since radiative heating was not included in the computation.

A LifeSat payload requirement limits to 60 seconds the duration the vehicle is above an acceleration level of 8 g's. The table shows the nominal, minimum, and maximum duration the vehicle is above 8 g's. Note that the 60-day orbit exceeds 60 seconds at an 8 g or higher acceleration level.

8.2.3.3 Nominal Atmospheric Entry

The footprint analysis discussed in the previous section showed the peak g-load required during entry to land within the target landing area. Given an initial orbital velocity, this g-load constraint defines the EI conditions. For example, the inertial entry conditions for a deorbit from a 900 km circular orbit are -3.7° flight-path angle at a velocity of 26,224 ft/sec.

The nominal trajectories are shown from EI to touchdown at WSMR located at 4000 ft altitude above sea level (figure 8-11). Nominal peak g-loads and heat rates were given for all mission scenarios in table 8-4.

Parachute deploy occurs at Mach 1.5 at an altitude of about 55,000 ft. The simulation used to produce figure 8-11 assumes a constant drag coefficient of 0.665 throughout atmospheric flight. Data from the Apollo vehicle, however,

TABLE 8-4. MONTE CARLO NOMINAL AND DISPERSED PERFORMANCE

(a) Peak G-load

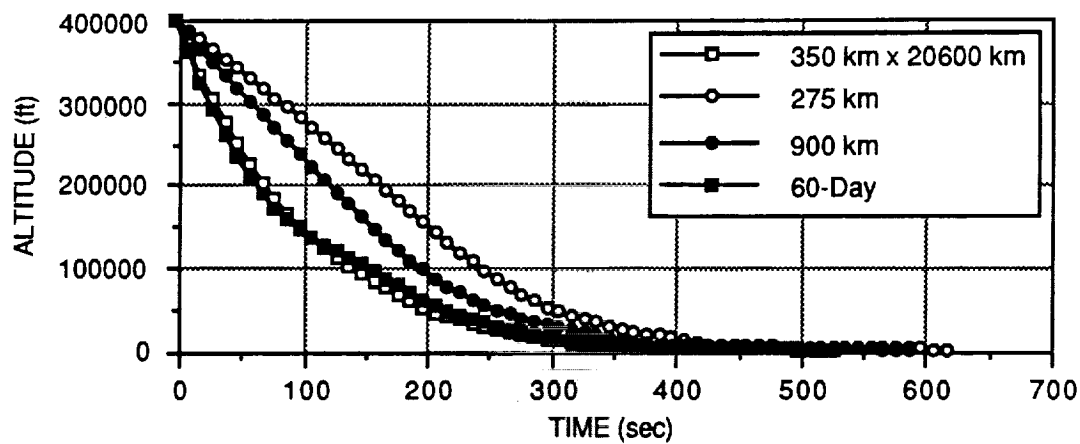
<u>Mission</u>	<u>Peak G-Load (g's)</u>		
	Nominal	Minimum	Maximum
900 km	11.0	10.5	11.7
275 km	10.0	9.5	10.6
350 km x 20,600 km	14.0	13.4	15.0
60-Day	12.0	11.7	13.0

(b) Peak heat rate

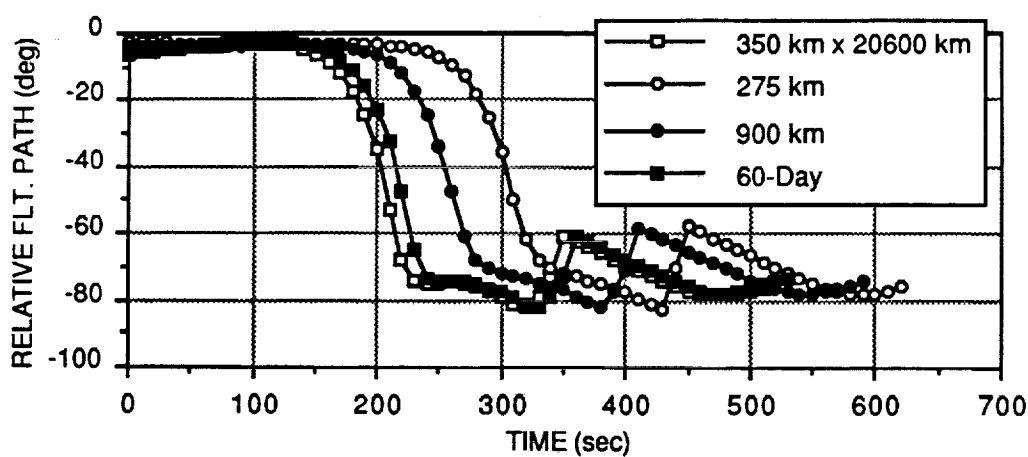
<u>Mission</u>	<u>Peak Heat Rate (BTU/ft²-sec)</u>		
	Nominal	Minimum	Maximum
900 km	203	193	216
275 km	193	183	208
350 km x 20,600 km	494	474	525
60-Day	619	601	658

(c) Duration vehicle is above 8 g's

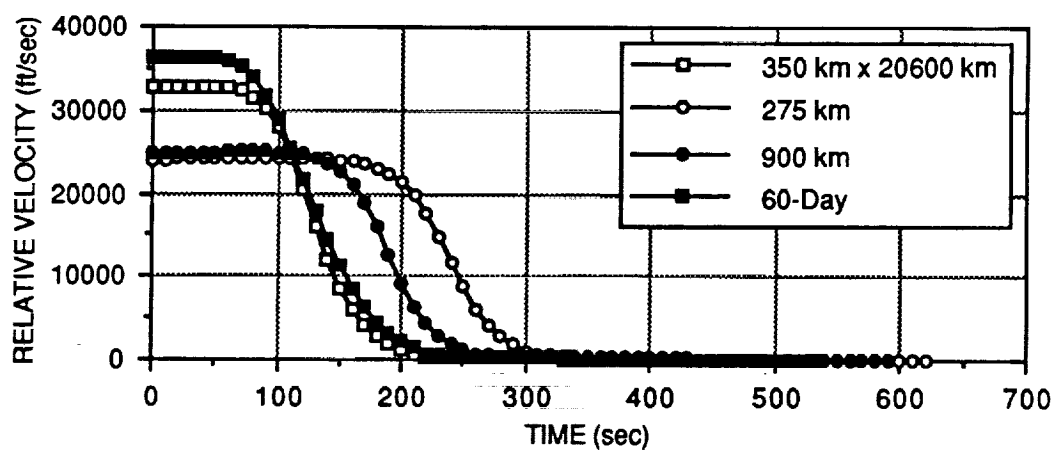
<u>Mission</u>	<u>Time Above 8 g's (sec)</u>		
	Nominal	Minimum	Maximum
900 km	38.4	35.6	41.1
275 km	35.4	30.7	38.6
60-Day	68.8	65.0	73.6



(a) Altitude (ft)

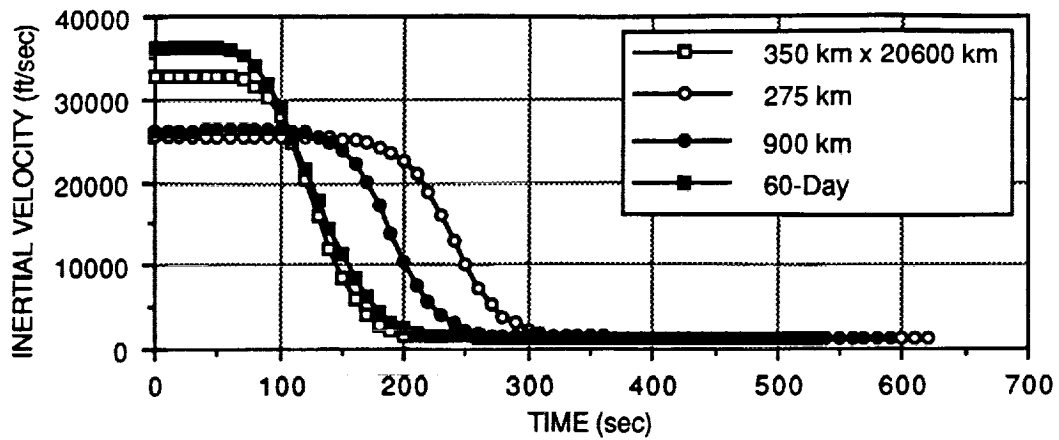


(b) Relative flight-path angle (deg)

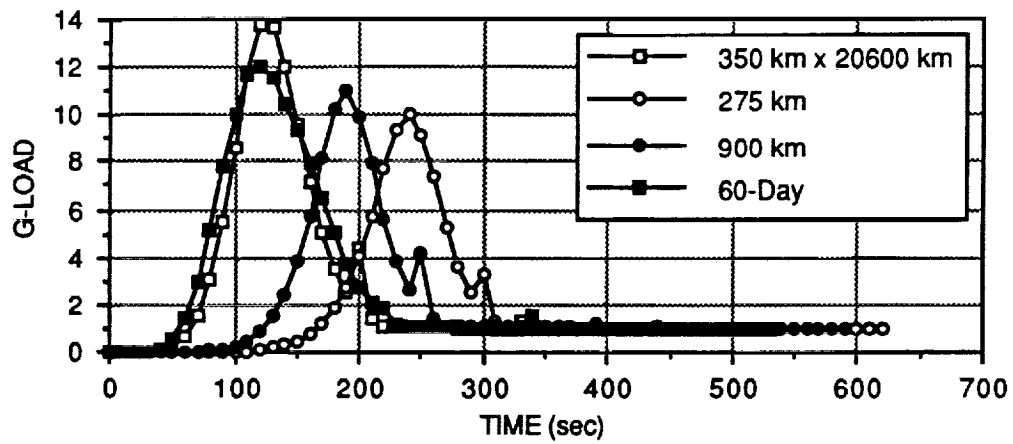


(c) Relative velocity (ft/sec)

Figure 8-11. Nominal entry trajectories (Page 1 of 2)



(d) Inertial velocity (ft/sec)



(e) Load factor (g's)

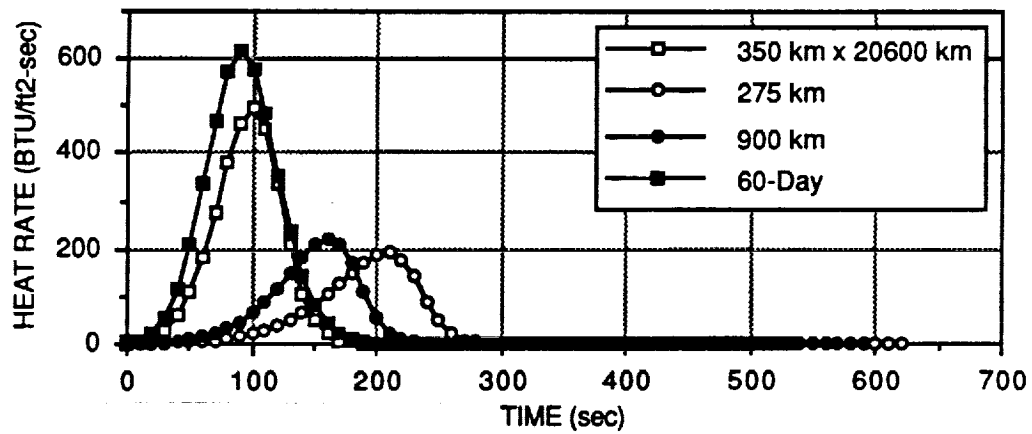


Figure 8-11. Nominal entry trajectories (Page 2 of 2)

indicates the drag coefficient should decrease by 40 percent at parachute deploy as compared with the drag at hypersonic velocities [6]. Therefore, the drogue chute deploy is expected to occur at lower altitudes.

The three main chutes are deployed in three reefed stages. The first reef stage is modeled as 8 percent of the total chute reference area. The chute opens to 25 percent of its total area after 6 seconds and is fully deployed about 16 seconds after the vehicle has reached an altitude of 10,000 ft.

8.2.3.4 Landing Footprint Sensitivities

The entry footprint is affected by a number of errors or uncertainties that were modeled in the Monte Carlo analysis. The uncertainties were atmospheric density, winds, aerodynamics, vehicle mass, and initial EI state. Each uncertainty affects the footprint size to a varying degree. All uncertainties affect the footprint downrange but only wind perturbations significantly affect the footprint crossrange. Table 8-5 shows the contribution each uncertainty has on the downrange and crossrange footprint distances for the 900 km mission. Dispersions in atmospheric density and uncertainties in EI state are the largest contributors to the size of the footprint followed closely by wind dispersions. The uncertainty in EI state is caused by the small uncertainty in state after the GPS update prior to the deorbit burn. These small errors in the vehicle state increase as the vehicle coasts toward EI. The vehicle aerodynamic and weight dispersions also significantly affect the footprint. The footprint is relatively insensitive to uncertainties in parachute drag coefficient and small errors in reference area. The individual downrange errors root-sum-squared (RSS) were about 2.9 nm lower than the actual Monte Carlo results.

TABLE 8-5. CONTRIBUTORS TO FOOTPRINT
MAGNITUDE - 900 km MISSION

<u>Error Source</u>	<u>Total Downrange Variation (nm)</u>	<u>Total Crossrange Variation (nm)</u>
Atmospheric Density (GRAM-88)	11.0	0.1
Initial Entry State	11.5	0.3
Winds (GRAM-88)	9.7	9.0
Aerodynamics	6.6	0.1
Parachute Aerodynamics	0.1	0.0
Vehicle Weight	2.2	0.0
RSS	19.9	9.0

Some uncertainties such as the deorbit burn attitude and burn duration were not modeled in the Monte Carlo simulation since the vehicle has a deorbit guidance which can correct for these errors. If no closed loop deorbit guidance

is used, these errors would substantially affect the footprint. Table 8-6 shows the miss distance for each of these errors in the deorbit burn assuming no closed loop guidance.

TABLE 8-6. MISS DISTANCE SENSITIVITIES, OPEN LOOP DEORBIT GUIDANCE - 900 km MISSION

<u>Error Source</u>	<u>Miss Distance Sensitivity</u>
Deorbit Burn Magnitude	8.3 nm/ft/sec
Deorbit Burn Attitude (In-Plane)	53.3 nm/deg
Deorbit Burn Attitude (Out-of-Plane)	1.7 nm/deg
Initial Orbital Altitude	120 nm/nm
Burn Ignition Delay	3.3 nm/sec

This table shows a small error in the deorbit burn magnitude and attitude which, if uncorrected, results in significant miss distances at touchdown. A 1 nm error in the initial orbital altitude causes about a 120 nm target miss. The deorbit burn attitude, if uncorrected by deorbit guidance, causes about a 8 nm miss for every 1 ft/sec of deorbit delta-velocity error. Target misses of 53 nm and 1.7 nm in downrange and crossrange result from 1 degree uncertainties in the in-plane and out-of-plane thrust direction. These errors were computed assuming a 3500 lbf vehicle and a total deorbit thrust of 250 lbf.

8.2.4 Conclusions

Four mission scenarios were investigated to determine the feasibility of landing the LifeSat vehicle within a pre-defined area at the WSMR. The mission scenarios include deorbit from a 275 km circular orbit, a 900 km circular orbit, a 350 km by 20,600 km elliptical orbit, and direct entry from an elliptical orbit with a 60-day period. A Monte Carlo technique was used to determine feasibility and compute the required entry steepness to ensure 99.73 percent reliability of landing within a prescribed target area.

The analysis results presented throughout paragraph 8.2 assume GPS navigation updates are available just prior to the deorbit burn for the two circular orbit missions. The results also assume a trim burn is performed after the deorbit burn for the elliptical missions to correct the actual vehicle state to within GPS accuracy at EI. A previous study showed a trim burn is necessary for the elliptical missions to ensure landing within the desired target area [49].

The footprint analysis results indicate landing within designated areas at WSMR is feasible for all missions investigated. The required nominal g-load encountered during entry for all missions is extreme, however, ranging from 10g's to 14g's (table 8-4). Vehicle heating is also extreme in all cases and may raise design issues for the high-speed entry elliptical missions.

SECTION 9 REFERENCES

1. deleted
2. Justus, C.G., Alyea, F.N., Cunnold, D.M., Blocker, R.S., Johnson, D.L., "GRAM-88, Improvements in the Perturbation Simulations of the Global Reference Atmosphere Model", Marshall Space Flight Center, ES44-11-9-88, November 1988.
3. deleted
4. deleted
5. deleted
6. Cerimele, C.J., Peterson, W.L., Ross, B.P., Stagnaro, M.J., "A Conceptual Design of a Crew Emergency Return Vehicle", JSC-23103, NASA-Johnson Space Center, August 1988.
7. Lees, Lester, "Laminar Heat Transfer Over Blunt-Nosed Bodies at Hypersonic Flight Speeds," The Ramo-Wooldridge Corporation, Los Angeles, and the California Institute of Technology, Pasadena, California, January 26, 1956.
8. Murray, L.P., and Tillian, D.J., "Over-Temperature Tests of Aeroassist Flight Experiment (AFE) Thermal Protection Materials," JSC-22993, Houston, Texas, April 1988.
9. RRS Requirements Document, April 1991.
10. Personal communications with B. Minden, August 1991.
11. Cullimore B.A., SINDA '85/FLUINT User's Manual, Version 2.3, 1991.
12. Reusable Reentry Satellite Final Report, GE Aerospace, Document No. 90SDS2129, (NAS 9-18201) 21 September 1990.
13. Reusable Reentry Satellite Phase B Final Report, SAIC, 1990.
14. Keller, J.R., "Techniques for Reducing CPU Run Times of SINDA85/FLUINT Models," LESC-28955, December 1990.
15. Keller, J.R., Reduction in CPU Run Time and Oscillatory Behavior for SINDA85/FLUINT Models," LESC-27581, November 1989.

16. Keller, J.R., "Conversion of the Space Shuttle Active Thermal Control System Models from SINDA/SINFLO to SINDA85/FLUINT," LESC-27826, December 1989.
17. Galate, J.W., and Purvis, K.L., "Space Station Freedom Thermal Environment Database A Comparison of Flux Cube Data for Equipment Thermal Analysis," LMSC-EVA-EV-100, March 1990.
18. Keller, J.R., and Welch, M.J., "Development of the LMSC Ground Test Unit Model," LESC-28205 April 1990.
19. ASHRAE Handbook, 1981 Fundamentals, American Society of Heating, Refrigerating and Air Conditioning Engineers Inc., Atlanta, 1985.
20. McHale, E.T., Habitable Atmospheres which do not Support Combustion - Final Report," Prepared for the US Army Research Office Contract No. DAHC 19-71-C-002.
21. Loral Group Discussions, LifeSat August Meeting.
22. VanWylen, G.J., and Sonntag, R.E., Fundamentals of Classical Thermodynamics, 3rd Edition, John Wiley and Sons, New York, 1986.
23. Bacala, P.A., "Space Shuttle Systems Handbook," Vol. 1., Revision E, December, 1990.
24. Personal communications with J. Galate of LMSC Life Sciences Lab, August 1991.
25. Personal communications with E. Darcy of NASA August 1991.
26. NESLAB Product Bulletin, 1990.
27. Grainger Product Catalog, 1990.
28. McMaster's Product Catalog, 1990.
29. LifeSat Facility Science Requirements Document (SRD), March 8, 1991.
30. LifeSat Project Requirements Document (Draft) (PRD), October, 8, 1991.
31. Commercial Delta II: Payload Planners Guide (DPPG), (MDC) H3224B), McDonnell Douglas Commercial Delta Inc., December, 1989.
32. "LifeSat Micro-g Analysis," 1991.
33. "Tape Drive Start Up and Strop Transient Effects in Micro-g," 1991.
34. Ling, Lisa, "Vibration Analysis for the LifeSat Centrifuge," 1991.

35. Glover, L.; "Effects on Roll Rate of Mass and Aerodynamic Asymmetries for Ballistic Re-Entry Bodies," Applied Physics Laboratory, Johns Hopkins University; J. Spacecraft, April 1965.
36. Price, D.A. Jr.; "Sources, Mechanisms, and Control of Roll Resonance Phenomena for Sounding Rockets", Lockheed Missiles & Space Co., J. Spacecraft, November, 1967.
37. Platus, D.H.; "Ballistic Re-entry Vehicle Flight Dynamics," The Aerospace Corporation, AIAA Journal 82-4019, July, 1981
38. Platus, D.H.; "Angle-of-Attack Convergence and Windward-Meridian Rotation Rate of Rolling Re-Entry Vehicles," The Aerospace Corporation, AIAA Journal, Vol 7., No.12, January, 1969.
39. Personal communications with J. Kowal, July 1991.
40. Williams, S.D., and Browning, R.E., "Pathfinder Thermophysical Property Data - Thermal Protection Materials for High Energy Aerobraking Vehicles - Volume 1," LESC-27438, August 1989.
41. Incropera, F.P., and DeWitt, D.P., Fundamentals of Heat and Mass Transfer, John Wiley and Sons, New York, 1985.
42. Personal communications with J. Jue of LMSC Sunnyvale, August 1991.
43. Henniger, J.H., Solar Absorptance and Thermal Emittance of Some Common Spacecraft Thermal-Control Coatings," NASA Reference Publication 1121, April 1984.
44. Siegel, R., and Howell, J.R., Thermal Radiation Heat Transfer, Hemisphere Publishing Co. Washington, 1981.
45. Thermal Radiation Analyzer System (TRASYS) User's Manual, JSC-22964, LEMSCO-22641, April 1988.
46. Howell, J.R., A Catalog of Radiation Configuration Factors, Mc-Graw Hill Book Co. 1982.
47. Spencer, Jose L.: "Use of a Non-singular Gravitational Potential" McDonnell-Douglas Technical Services Co., Inc., JSC Internal Note No. 75-FM-29, JSC-09661, May 27, 1975.
48. Lear, William M.: "Kalman Filtering Techniques" TRW Inc., Mission Planning and Analysis Division, JSC Internal No. 85-FM-18, JSC-20688, Sept. 1985.
49. Bryant, L., McCleary, B., Hood, L., Engler, J., "Landing Accuracy Analysis," Unpublished, September 1991.

- 50. See 39.
- 51. See 40.
- 52. See 41.
- 53. See 42.
- 54. See 43.
- 55. See 44.
- 56. See 45.
- 57. See 46.
- 58. Kroll, Ken, "Lifesat Propulsion Fault Tolerance" August 8, 1991.

Additional Documentation

- [1] "A Conceptual Design Study of the Reusable Reentry Satellite," NASA TM 101043, October, 1988.
- [2] See 12.
- [3] "SAIC Reusable Reentry Satellite (RRS) System Design Study" (RRS-037; DRL 07), contract # NAS 9-18202, 26 February 1991.
- [4] "Reusable Reentry Satellite Final Report: Rodent Module Trade Study and Preliminary Design" (LMSC - F408581), Lockheed Missiles and Space Company Inc., 14 September 1990.
- [5] See 31.
- [6] Mission Planner's Guide for the Atlas Launch Vehicle Family (Revision 2), General Dynamics Commercial Launch Services Inc., 10 July 1990.
- [7] See 6.
- [8] "Design Mass Properties: Guidelines and Formats for Aerospace Vehicles" (JSC-23303), NASA/JSC Engineering Directorate, Advanced Programs Office, Systems Definition Branch, March 1989.

APPENDIX A
LIFESAT ENGINEERING BASELINE REQUIREMENTS
FOR VEHICLE PERFORMANCE
(Prepared by Chuck Miller)

SCOPE

This section will be limited to the LifeSat vehicle engineer performance requirements assumed in this study.

DESCRIPTION OF REFERENCE MISSION DESIGN REQUIREMENTS

The LifeSat vehicle must support the DRMs listed in table 5-1. For the vehicle to perform its intended purpose, the following requirements must be satisfied.

- a. Fly a minimum of six missions projected over the life of the program.
- b. The vehicle must be capable of:
 - Reuse after it has been refurbished.
 - Dual launches of identical spacecraft aboard the same launch vehicle.
 - A controlled descent and spin-stabilized reentry to recovery at WSMR within a footprint of 22.5 nm by 7.5 nm for orbits at an inclination of 34° and 24 nm by 9 nm for polar orbits.
 - Successful reentry following a call down at the next available opportunity after any credible system fault.
 - Delivering, supporting while on orbit, and safely returning a payload consisting of up to 400 kilograms of experiments and radiation measurement equipment to a circular orbit of 350 nm.
 - Conducting communications through the DSN.
- c. The vehicle must consist of an RRS which will contain and support a PM.
- d. The vehicle will be certified for flight immediately before release to the launch system integrating authority. This certification will include a final all up mass, moments of inertia, and CG determination as well as final system verification.
- e. The vehicle must provide:
 - Sufficient data transmission capability to allow ground control to ascertain its health and status.

- Sufficient data uplink capability to allow uplink of RRS and/or PM work around procedures and flight software patches.
 - A microgravity environment of 10^{-5} g shall be provided while on orbit for 95 percent of the mission exclusive of PM-generated perturbations. Any maneuvering required for attitude adjustment will not exceed 5 percent of the mission time and will not degrade the microgravity environment to more than 10^{-4} g. The microgravity environment quality requirement will be relaxed when degradation of this environment is due to the operation of any payload system contained within or housed outside the PM. In these cases, the microgravity environment will be 10^{-5} g plus/minus the delta caused by the payload perturbation.
- f. The vehicle must accommodate small radiation sources not to exceed 100 millicurie of radioisotope tracer substances and sealed calibration sources within the PM.
 - g. The vehicle must be maintained, recovered, and refurbished by the designer/fabricator.
 - h. The LifeSat mission must:
 - Use Delta II ELVs.
 - Use the ETR as the launch site.
 - Use WSMR for the landing site.
 - Provide payload exposure to GCR of 50-2000 Megaelectron volts per nucleon while maximizing the ratio of GCR to trapped protons and electrons, and provide an exposure of GCR of sufficient duration to permit statistically significant radio-biology experiments.
 - Have different orbits to provide experiments radiation exposure between 1 and 2 Gray of protons or minimum exposures of less than 0.1 Gray of protons over the duration of the 60-day mission.

PERFORMANCE REQUIREMENTS

The following LifeSat performance requirements must be satisfied for successful mission completion.

Structure

The RRS Structure, defined here as all load-bearing components comprising the basic vehicle, must satisfy the following requirements.

- Withstand thermal cycles of the planned missions (60-day missions).
- Provide standard interfaces to attach the RRS to the launch vehicle and provide mil-standard structural interfaces to attach the PM to the RRS.
- No launch vehicle loads shall be carried by the RRS. Loads expected during the DRM will not damage the spacecraft structure nor compromise the experiments.
- Be refurbishable without requiring structural repairs or modifications of the structure for subsequent missions.
- All dimensions must be metric.
- All project hardware must be transportable by standard over-the-road cargo vehicles.
- Structure must be designed not to generate on-orbit debris.
- The bulk of the payloads will be contained and supported within a pressure vessel (the PM).
- Late access to PMs must be provided. The RRS structure must allow a limited amount of experimental specimens to be installed into the PM while on the launch pad immediately prior to the t-12 hour point in the launch countdown. Maximum dimensions on these samples will be 6 inches by 6 inches by 4 inches. The installation of these samples shall be accounted for in the certified spacecraft mass, moments of inertia, and CG.
- Provide radiological viewing access unhampered by any major structural component and mounting provisions external to the PM for equipment to monitor external radiation sources.
- With the exception of the dual spacecraft launch fittings, launch vehicle standard services will not be exceeded during any and all integration activities.
- The RRS and PM must be designed to an appropriate factor of safety for the structural, dynamic, and vibro-acoustic loading environment.
- Density, mass, location, and material composition must be provided for all as-built RRS components and for the PM housing and structure.

Payload Module

To achieve successful mission completion, the PM shall:

- Contain racks and support connections to accommodate up to three Shuttle middeck lockers with associated support fittings and connections as well as structural mounts. Two of the locker volumes may be configured as a dual middeck locker.
- Provide mounting provisions to accommodate additional experiment packages or ballast in open spaces around the locker volumes within the PM.
- Accommodate a minimum internal volume of 1 cubic meter with an internal unobstructed diameter of 1 meter over a minimum axial length of 30 centimeters.
- Be capable of being cleaned, inspected, and loaded by a 95-percent American male, without the aid of special equipment.
- Not have sharp corners with inaccessible crevasses and fixtures.
- Include instrumentation to measure vibration, noise, pressure, temperature, radiation, and acceleration.
- Provide a second PM, ground control experiment module (GCEM), for each flight article which will be a ground-based analog to the orbiting PM. Support requirements for these modules shall be the same as for the flight article including environmental requirements. Four-hour battery backup for all systems within the ground modules will be provided throughout the duration of the ground-based experiments.

Thermal Control

- a. The RRS must provide thermal control and conditioning to the PM.
- b. The RRS must transport from the PM as much as 50W of heat throughout the 60-day mission, so as to maintain a volume within the PM at $-20^{\circ}\text{C} \pm 2^{\circ}$. Power consumption to provide this capability shall be included in the payload power budget.
- c. Sufficient heat sink must also be provided to reject excess heat created by electronics, animals metabolic processes, and experiment processes.
- d. The temperature must be banded in the range of 18°C to 28°C , capable of being set to a set-point that can be deviated by $\pm 2^{\circ}\text{C}$ on the launch pad and $\pm 3^{\circ}\text{C}$ on launch, entry and recovery.

- e. In event of multiple failures, the temperature shall not exceed 30°C for more than 0.5 hour. At no time will the temperature exceed 35°C.
- f. The active thermal control system must:
 - Meet CRIT-1 redundancy.
 - Use nontoxic and nonflammable coolant. During nominal operation, the coolant must not boil or freeze and it should not decompose.
 - Be able to maintain the necessary temperatures during rapid changes in heat load.
 - Use single-phase coolant and existing technology.
 - Be able to reject 900W of heat.
 - Coolant temperatures in contact with the payload heat exchangers and electronics cold plates must not exceed a temperature range of 4 to 40°C. If mice are included in the experiments, the coolant temperature should range between 18 and 28°C. This temperature should be maintained for all phases of the mission, from prelaunch to recovery, which in some cases may require ground support equipment (GSE).

Electrical

The RRS electrical system must satisfy the following requirements throughout the 60-day mission.

- Provide and use Mil-Standard interfaces and practices to receive/supply power.
- Be reliable and provide sufficient redundancy for a 95-percent mission success.
- Provide sufficient power so that communications and tracking, thermal conditioning, experimentation needs, monitoring and data collection, and life support functions can be accomplished with some reserve to compensate for system reconfiguration and emergency needs.

All power connections to experiment packages contained within the PM shall be compatible with standard Shuttle middeck locker interfaces.

The spacecraft shall provide an average of 150W of electrical 28 volts direct current +/-2 volts direct current power with a maximum surge capability of 500W and a 30-minute maximum load of 225W during any 2-hour period. Total payload mission power consumption will be 216 kilowatt-hours during a 60-day mission. This requirement shall be satisfied over and above that power

required for the ECLSS and other mission support activities unless required otherwise.

GSE power shall be available to the PM within 2 hours after landing.

Instrumentation

Instrumentation shall include, but not be limited to, equipment to measure vibration, noise, pressure, temperature, radiation, acceleration, RRS health and safety, and receipt and dispersion of RRS-provided consumables.

Data Management

The following data management requirements must be satisfied by the RRS during a 60-day mission.

- Support uplink and distribution of payload commands, flight software updates, and data tables.
- Format spacecraft data packets for downlink.
- Process and transmit to the ground 25 Megabits per day of biological experiment data and an additional 80 Megabits per day of radiological data.
- Record PM environmental data consisting of temperature, pressure, humidity, and acceleration levels continuously at 1-minute intervals for daily shipment to the ground, in addition to spacecraft position and attitude data.
- Manage a budget of spacecraft health and safety data sufficient to accurately determine RRS and payload status.
- Store and relay for activation, preprogrammed commands as well as ground transmitted commands to aid in real-time diagnosis and resolution of payload anomalies.
- Use data connections to experiment packages contained within the PM that are compatible with standard Shuttle middeck locker interfaces.
- Generate and utilize a master timing signal.
- Provide the master timing signal to the PM.

Data downlink for the RRS will accept information from its subsystems and the PM in analog, serial, digital, and bi-level digital form; convert the analog and bi-level information to serial digital form; and arrange all information in an appropriate format for the time multiplexing transmission to Earth. A typical data handling design will collect all data and provide a complete ground dump at

least once a day. However, for redundancy, several days onboard storage must be accommodated.

Unique RRS events, such as parachute deployment, memory storage initiation, etc., will have time-tagged identifications for mission profile reconstruction, environmental atmospheric composition, pressure, temperature relative to absolute humidity, and acceleration levels. A number of sensor locations may be used for any given parameter. Typically, steady-state measurements at 1-minute intervals will be required and measurements during all periods of state/mode change. During certain missions, limited still-frame data will also be captured. A minimum average data generation for the biological portion of the payload is estimated to be 25 Megabits per day. Radiation spectrometry information will average an estimated minimum 80 Megabits per day. Additional allowance must be made for RRS information.

Communication and Tracking

To satisfy C&T requirements during the 60-day mission the RRS must:

- Use the DSN.
- Support uplink and downlink data and commands.
- Provide sufficient data uplink capability to allow uplink of work around procedures and flight software patches.
- Provide data in CCSDS format.
- Have a Bit Error Rate of 10^{-5} or better with a link margin of 3 decibels for the communications links (uplink and downlink).
- Have downlink that will provide telemetry for necessary spacecraft data for operation and fault detection and isolation and science/payload data.
- Have antennas designed for solar inertial attitude and a spacecraft spinning at up to 42 revolutions per minute.
- Provide state vectors on orbit to the spacecraft from the C&T subsystem via uplink from the ground or an onboard tracking subsystem.
- Provide state vector updates during reentry in order to be within the footprint.
- Provide a system to locate the satellite on landing.

- Provide a communication subsystem that will:
 - (a) Radiate a signal of sufficient coverage, strength, and stability to enable acquisition by downlink telemetry station(s) during both the orbital and recovery phases.
 - (b) Acquire an uplink signal and receive commands while the vehicle is randomly oriented in orbit.
 - (c) Radiate a signal to serve as a tracking beacon during the orbital phase.
 - (d) Acquire an uplink terminal homing signal from the ground after the vehicle has deployed the recovery parachute.
 - (e) Radiate a signal of sufficient strength to serve as a homing beacon during the recovery process.

All uplink, downlink, and vehicle command and control capabilities will be compatible with capabilities at the Goddard Space Flight Center Mission Control Center. Communication formatting for the downlink and uplink will conform with protocols established by the JPL-managed DSN.

Life Support Equipment

To satisfy life support requirements during the 60-day mission, the life support system must:

- Provide thermal control and other life supporting environments.
- Provide the space and interfaces for oxygen, nitrogen, and one specialized gas taken from a qualified list.
- Maintain pressurized environments to levels ranging from 0.952 to 1.013 Newtons per square meter. Pressure relief capability must be supplied in the RRS package.
- Provide mil-standard gas and fluid interfaces at all interfaces.
- Provide fluid connections to experiment packages contained within the PM that are compatible with standard Shuttle middeck locker interfaces.

- Remove the following substances from the atmosphere at the following generation rates for 50 mice.

carbon dioxide	5 grams/mouse
water vapor	2.8 grams/mouse
ammonia	TBD
carbon monoxide	TBD
hydrogen sulfide	TBD
ethylene	TBD
ozone	TBD

- Provide the following substances at the following rates for 50 mice.

oxygen	3.8 grams/mouse
water	8 grams/mouse
food	4 grams/mouse

- Maintain the following environmental conditions in the mouse habitat at all times.

Air composition:	nitrogen and oxygen
Total pressure:	14.7 +/- .2 pounds per square inch atmospheric
Partial pressure:	
Oxygen	20 +/- 2 percent
Carbon dioxide	<= 1 percent
Air temperature:	selective between 18 and 28°C
Launch pad and on orbit:	+2/-3°C from set point
Launch, entry, and recovery:	+3/-4°C from set point
Air circulation:	one volume change per minute
Relative humidity:	55 +/- 15 percent
Contaminant quality:	remove particulates, contaminants, and microbes

- Meet CRIT-2 redundancy since failure will result in loss of mission but not loss of vehicle.
- Use existing technology.
- Not introduce any materials harmful to people or mice.
- Control humidity to prevent condensation.
- Set the air flow to maintain atmospheric conditions, but in no case will it be less than 1 exchange per minute. Particles and liquid entrained in the air will be removed along with certain trace contaminants.

- Accommodate the storage and high pressure transfer of up to two special gases.
- Have a trace contaminant monitor and disposal system.

The spacecraft shall be capable of supporting the experiments in a viable condition for as long as 4 hours after landing. The spacecraft will have provisions for rapid field connection of support equipment to continue to sustain the experiments in a viable condition until the spacecraft reaches a suitable facility for off-loading of the experiments.

The PM atmosphere will be maintained by the ECLSS contained in the RRS. The atmosphere will be comprised of oxygen at a concentration regulated to 20 percent +/- 2 percent and nitrogen as the dilution. Carbon dioxide shall be removed by the ECLSS and shall not exceed 1 percent. The air temperature will be set prior to launch to a value between 4 and 40°C.

The PM shall receive the primary atmosphere from the RRS at a flow rate necessary to maintain desired environmental conditions. The flow must be at least equivalent to one exchange per minute, however. The total pressure and gas composition will be controlled by the RRS. Some trace contaminants produced by the payloads will be removable by the ECLSS.

The production rate of trace contaminants shall not exceed the removal rate at the maximum allowable concentration selected for the flight.

Up to two specialty gas penetrations will be available to the PM. Regulation and control of these gases will be performed within the PM.

Control of particulates, waste products, and liquid shall be accomplished at the experiment unit.

The experiment shall be designed to accommodate the potential growth of microbes within its containment.

Thermal Protection

The RRS thermal protection system must be adequate to protect all internal elements from heating during aerodynamic decelerating.

Attitude Control

- a. The vehicle must provide either solar inertial or local vertical/local horizontal attitude control, depending on the mission, throughout the duration of the mission.

- b. Attitude control dead-bands must be sufficient to maintain microgravity levels while continuing to satisfy RRS housekeeping requirements.
- c. The RRS shall correct launch errors in the orbital parameter and adjust the parameters to be compatible with the recovery site requirements.

Attitude Control System

The RRS must perform attitude correction, stabilization, and control functions as required throughout the orbital phase of a mission. Launch orbit error corrections shall be performed and implemented to adjust the orbital parameters to be compatible with the recovery site requirements.

The ACS must meet CRIT-2 requirements.

Landing

- a. The RRS must be oriented for deorbit and reentry via verifiable ground commands, RRS sequence programmer commands, or signals generated from onboard events.
- b. The deorbit, reentry, and terminal maneuvers are required to be sufficiently accurate and controlled so as to allow a near-vertical descent from an altitude of at least 18 kilometers with a three sigma probability of a landing footprint within a crossrange dispersion of ± 6 kilometers and a downrange dispersion of ± 30 kilometers.
- c. The reentry decelerating shall not exceed 15 g's axial and TBD lateral. Engineering must study this requirement further.
- d. The RRS ground impact decelerating shall not exceed 10 g's along any axis. Engineering has not determined that this is an acceptable requirement.

Launch

- a. LifeSat shall use the ETR as the launch site.
- b. The vehicle will be launched by ELV on separate missions into different orbits.

Reliability and Maintainability

- a. Vehicle systems must be checked out sufficiently to allow for 95 percent probability of successful start of on-orbit operations after a successful launch.
- b. All project hardware shall perform within specification when exposed to all natural, prelaunch, launch, and on-orbit environments encountered.
- c. Vehicle systems must be of sufficient robustness and redundancy to provide for a 95 percent probability of successful mission completion following one single credible failure during on-orbit operations. Vehicle operations must degrade gracefully (that is, provide for continued operations although in a degraded mode) following multiple vehicle system failures.
- d. The spacecraft contractor shall provide observers to all PM integration and loading operations, but they will not participate in actual loading operations. When delivered for experiment loading, the PM will be clear of all visible contaminants when viewed with the naked eye.
- e. The RRS structure shall permit easy removal/replacement of RR subsystem components and inspection and repair of the structure for damage during the refurbishment process.

REFERENCE DOCUMENTS

The following documents are applicable to the extent specified herein.

- a. Badhwar's Radiation Manual (TBD)
- b. LifeSat Facility Science Requirements Document, 8 March 1991
- c. Space Debris Document (TBD)
- d. OSSA Metrication Policy, NASA Headquarters Bulletin, September 1990
- e. Reliability and Maintainability Plan (TBD)
- f. Safety Plan (TBD)
- g. Quality Assurance Plan (TBD)
- h. Goddard Space Flight Center Document (TBD)
- i. Commercial Delta II User Manual, MDC H3224A, dated July 1989
- j. ESMCR 127-1 Range Safety Requirements

- k. WSMR Safety Requirements (TBD)
- l. Draft of LifeSat Project Requirements Document (PRD) dated 8 October 1991
- m. LifeSat Mission Requirements, 29 May 1991, Charles Miller, Lockheed Engineering and Sciences Company
- n. Review of LifeSat Program Requirements Document drafted 9 August 1991, 30 August 1991, Laura Hood
- o. Deep Space Network/Flight Project Interface Design Handbook, 810-5, Revision D
- p. LifeSat Communications and Tracking Subsystem Performance Requirements, 11 October 1991, Laura Hood
- q. C and T Issues Related to LifeSat Requirements Document, 18 June 1991, Laura Hood
- r. LifeSat Program Requirements Document Draft **Reply Note of 29 May 1991 PRD, 30 August 1991, P. Jan McCoy
- s. System Performance Requirements for Life Support and Thermal Systems, 8 November 1991, Marybeth Edeen
- t. ECLSS Paragraph, 11 September 1991, David Kissinger
- u. LifeSat Mission Timeline: 275 kilometers circular orbit at 34° inclination, 8 November 1991, Nancy Wilks

CHANGES TO THE REQUIREMENTS

Additions or modifications to these requirements will be incorporated into this baseline only through a formal process.

APPENDIX B

FUNCTIONAL DECOMPOSITION

BACKGROUND

Functional decomposition is a system analysis and design procedure/tool which allows the orderly development of sequentially lower-tiered system requirements. These requirements, when satisfied, will result in a system that will achieve the stated objectives. Functional decomposition does not represent a substitute for the design process nor for the trade studies which must be conducted for any design effort. Rather, it presents an orderly format within which these activities may be conducted and tracked, and it will provide the requirements traceability matrix necessary to any design effort.

The original intent of the LifeSat requirements functional decomposition was to provide a basis for the development of the SOW for the LifeSat phase C/D contract. It must be pointed out here that a functional decomposition of requirements is not normally used to develop a SOW, but rather, to develop the system which will satisfy the requirements of the SOW. In this case, however, it was decided to use functional decomposition to develop the SOW because of the drastic changes that had taken place in the original mission requirements for the LifeSat vehicle and because of the short lead time available to develop the SOW.

The LifeSat functional decomposition presented here was used to develop the initial system requirements set for the LifeSat program. These, in turn, were decomposed to arrive at the requirements that each of the vehicle components would have to satisfy to achieve mission success. As with any functional decomposition, conflicts in the initial program requirements were unearthed and refined to develop the final vehicle performance requirements set presented in appendix A of this report. The functional decomposition process was then used to flow the vehicle performance requirements down to the component subsystems and to define the interfaces between the components.

A set of LifeSat component design teams was originally constituted about the functionally decomposed requirements to determine the subsystem level requirements which had to be satisfied in any proposed system intended to fill the LifeSat roll. These design teams were also formed into joint multi-disciplined working groups to assess the various interfaces between the subsystems as defined by the functional decomposition.

During this requirements definition effort, management decided to develop an in-house design which would:

- a. Produce a candidate system against which responses could be judged.
- b. Further develop the subsystem requirements teams so they could efficiently produce an SOW.

- c. Flush out requirements incompatibilities as presented by the end user, the LifeSat radiation science community.

The decomposed requirements served as the skeleton for the resulting trade studies that produced the in-house vehicle design presented in this document.

FUNCTIONAL DECOMPOSITION SYMBOL CONVENTIONS

The following conventions were used throughout this functional decomposition. The actual functional decomposition was performed using the accompanying functional flow charts and their attendant N**2 charts which present the component interfaces.

FUNCTIONAL FLOW CHARTS

Functional flow charts contain the information necessary to describe the interrelationships of functions necessary to the process being analyzed. Only the functions being performed are presented in these charts. Thus, the function performed in block 4.0 in figure B-1 is presented as Perform LifeSat Experiments.

Outside Organizations

Functions performed by outside organizations are presented in a simple box. An example, as shown in figure B-1, is the Present Operational Requirements function. This function is performed by the science community which is outside the functions to be performed by the total LifeSat system.

Interface Functions to Outside Organizations

Interface functions to outside organizations are depicted as in the box labeled 1.0 in figure B-1. Note that the bottom line segment in the function box Manage LifeSat has a break in it. This depicts that the function is an external interface while being part of the functional flow described.

Interface Functions to Other Functional Flows

Interfaces with other functional flows are depicted as shown in figure B-2. An example of an outside functional flow is 3.0, Communicate With LifeSat. Here, the box represents a flow which is part of the overall LifeSat system but which only interfaces with the flow under consideration in the figure. It is depicted by a box with a large break in the bottom line.

Functions Internal to the Functional Flow

Functions internal to a particular functional flow are depicted by boxes with solid lines as shown by function 4.0, Perform LifeSat Experiments, as shown in figure B-1.

Flow Conventions

Flow conventions are normally depicted as moving from left to right. Therefore, interfaces are shown as arrows which exit the right side of a function and enter the next function from the left.

N**2 CONVENTIONS

N**2 charts present the information passed between components which perform the functions in the functional flow charts. In these charts, the interfaces are described in a clockwise fashion. Therefore, in the N**2 chart shown in figure B-3, the level one component, LifeSat Communications (which performs the function of Communicate with LifeSat) in block 3.0 puts out commands to the vehicle (which performs LifeSat experiments) in block 4.0. The LifeSat vehicle, in turn, outputs LifeSat data and state vectors to LifeSat communications. This convention is followed through increased levels of detailing in each of the lower tiers of the functional decomposition. At the lowest level of the functional decomposition, parametric data handed off between components is described.

LIFESAT FUNCTIONAL DECOMPOSITION

Only the first two levels of the LifeSat functional decomposition are presented here. For the sake of brevity, this discussion will be limited to the areas necessary to describe the functional flow for the LifeSat vehicle. Again, for the sake of brevity, interfaces to components will not be discussed if they have been described in the course of depicting another component or system.

LIFESAT LEVEL ONE VEHICLE FUNCTIONAL FLOW DESCRIPTION

The LifeSat communications network passes vehicle commands to the spacecraft as depicted in figure B-1 by the arrow moving from area 3.0 to area 4.0. This service is provided during all phases of mission operations which include vehicle checkout on the launch pad, on-orbit operations, and entry.

During operations on the launch pad and during the boost phase of the mission, the launch vehicle provides mechanical and structural interfaces and connections, and electrical and data connections in addition to the structural

accelerations experienced during the ascent phase. This is depicted by the arrow from 5.0 in figure B-1, to the vehicle area.

The LifeSat vehicle preparation facility (6.0) in figure B-1, provides refurbishment services to the spacecraft in addition to the prepared LifeSat PM. This facility will also provide checkout and certification of the vehicle subsystems in preparation for certification for flight.

The vehicle will provide health and status data via telemetry to the communications network. It will also provide the necessary structural and electrical interfaces as well as data interfaces to the launch vehicle. During vehicle preparation, the RRS will provide support to the PM, which includes structural, data, and life support interfaces, as well as system and component test results to the vehicle preparation facility. After landing, the vehicle will provide data interfaces and ground support interfaces to the recovery facility as well as a viable PM.

LIFESAT LEVEL TWO FUNCTIONAL DECOMPOSITION

For a depiction of the LifeSat level two functional flow and interfaces as they were derived for the vehicle, refer to figures B-3 and B-4. Again, for the sake of brevity, level one functions and interfaces depicted in these figures will not be presented here even though they are depicted in the figures.

Once commands are received by the vehicle communications system, they are forwarded to the RRS data processor where they are directed to the various vehicle components including the LSS, the ACS, the science module via the PM support interface, the power generation system, the navigation system, and the reentry system as appropriate. Onboard commands stored by the RRS data processor are also routed to these components as required by either previously stored commands or upon command from the ground. The RRS data processor receives PM data from the PM via the PM support interface and forwards the data to the communications subsystem for transmission to the ground. The onboard data processor accepts data from the other onboard systems including the ACS, the LSS, the power generation system, and the navigation system. The data are then routed to the communications system for transmission to the ground. The onboard data processor also uses the data to control the respective systems, thereby providing onboard housekeeping.

The PM support system transmits accelerations and torques to the structure and transmits power and heat to the PM to maintain the PM in a viable state. This system accepts power and heat from the LSS and power generation systems, respectively. It receives structural support and accelerations from the spacecraft structure. It also receives waste heat from the PM as well as data from the experiments housed within the PM.

The RRS reaction control system provides forces and moments to the RRS structure and in turn receives forces and moments from the structure. This

system also receives power from the RRS power generation system and environmental conditioning from the environmental control system within the LSS.

The ECLSS provides environmental conditioning to all of the RRS components and in turn receives power from the RRS power generation system.

The power generation system provides power to all the components of the RRS. It, in turn, receives commands from the onboard data processor and environmental conditioning.

The navigation system receives forces and torques from the spacecraft structure and develops the data necessary to determine the spacecraft state vector. This is forwarded to the onboard data processor along with health and status data. When a GPS is installed on the RRS, the state vector is also forwarded to the onboard data processor from this component of the navigation system.

The reentry system transmits forces and heat during reentry to the structure. In turn, this system receives structural support from the RRS structure.

The RRS structure provides structural support to all of the spacecraft system components. It also receives forces and moments from these components.

The PM houses the science experiments during the time that the module is installed in the RRS. This component receives structural, data, and life support from the RRS components via the science module support system.

ADDITIONAL PRODUCTS FROM THE LIFESAT FUNCTIONAL DECOMPOSITION

Several collateral products were provided to the LifeSat Project Office as a result of the requirements functional decomposition. These included a requirements traceability matrix, a functional flow for payload ground processing, a hierarchical tree for the project functions, and a draft SOW for the vehicle.

REQUIREMENTS TRACEABILITY MATRIX

One of the major advantages of functional decomposition is that a requirements traceability matrix is produced as a matter of course in the process. The matrix produced for LifeSat was maintained throughout the vehicle design effort. The final matrix was forwarded to the LifeSat Project Office and was incorporated into the draft SOW.

FUNCTIONAL FLOW FOR PAYLOAD GROUND PROCESSING

A functional flow was developed for payload ground processing. This was forwarded along with the bulk of the functional decomposition and was used to analyze and verify requirements for land-based recovery in WSMR.

HIERARCHICAL TREE

A hierarchical tree of the LifeSat requirements was generated and forwarded to the LifeSat Project Office. This tree formed the basis of the LifeSat work breakdown structure (WBS). If the project had continued, the WBS would have been the basis for the assignment of specific areas of responsibility throughout the life of the project.

DRAFT STATEMENT OF WORK

A draft SOW was generated for the spacecraft element of the LifeSat project. This document was based on the mission requirements as they had been functionally decomposed. As with the other products of the functional decomposition, this document was also forwarded to the LifeSat Project Office for its use in generating of the project SOW.

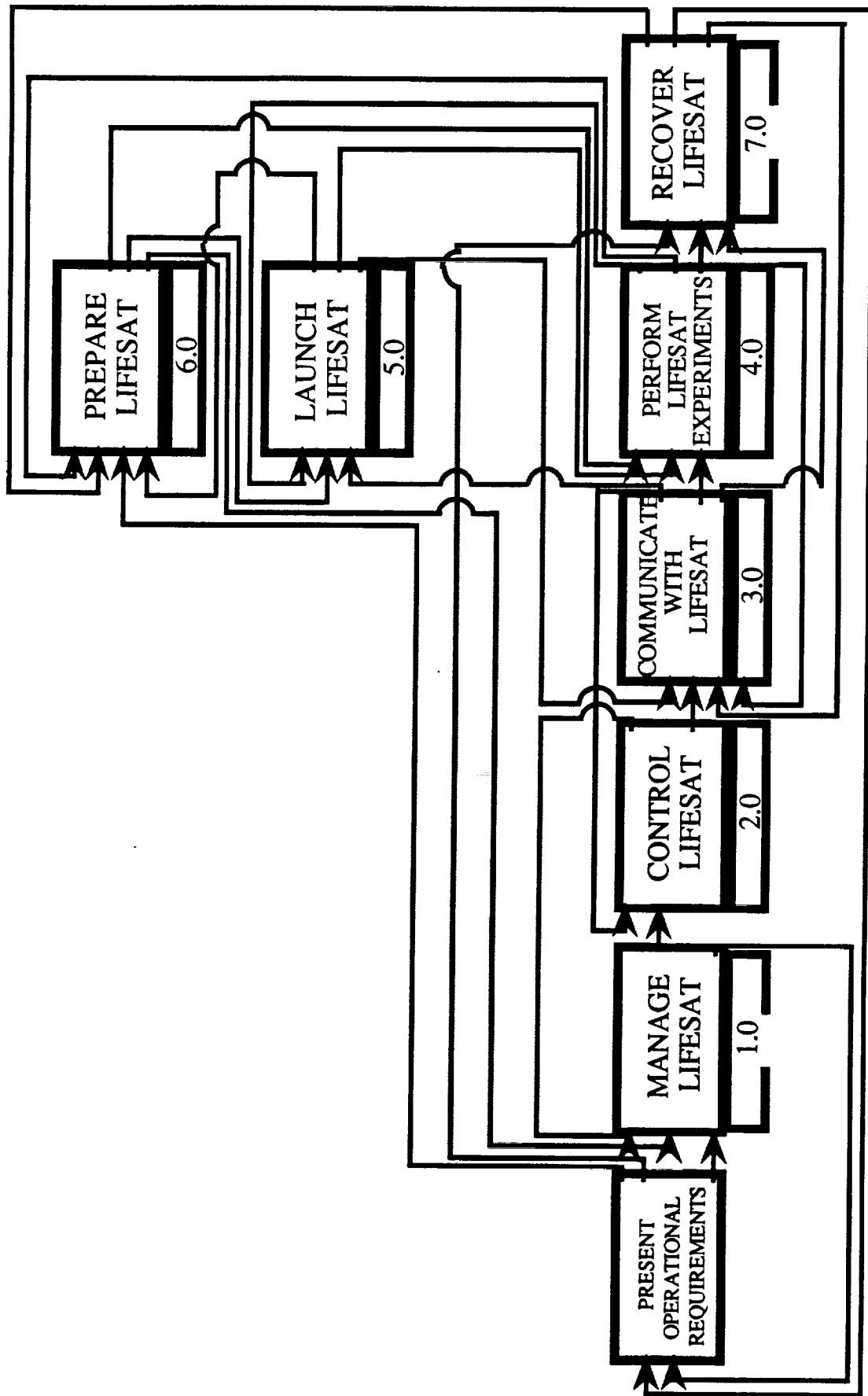


Figure B-1. LifeSat Level One Functional Flow

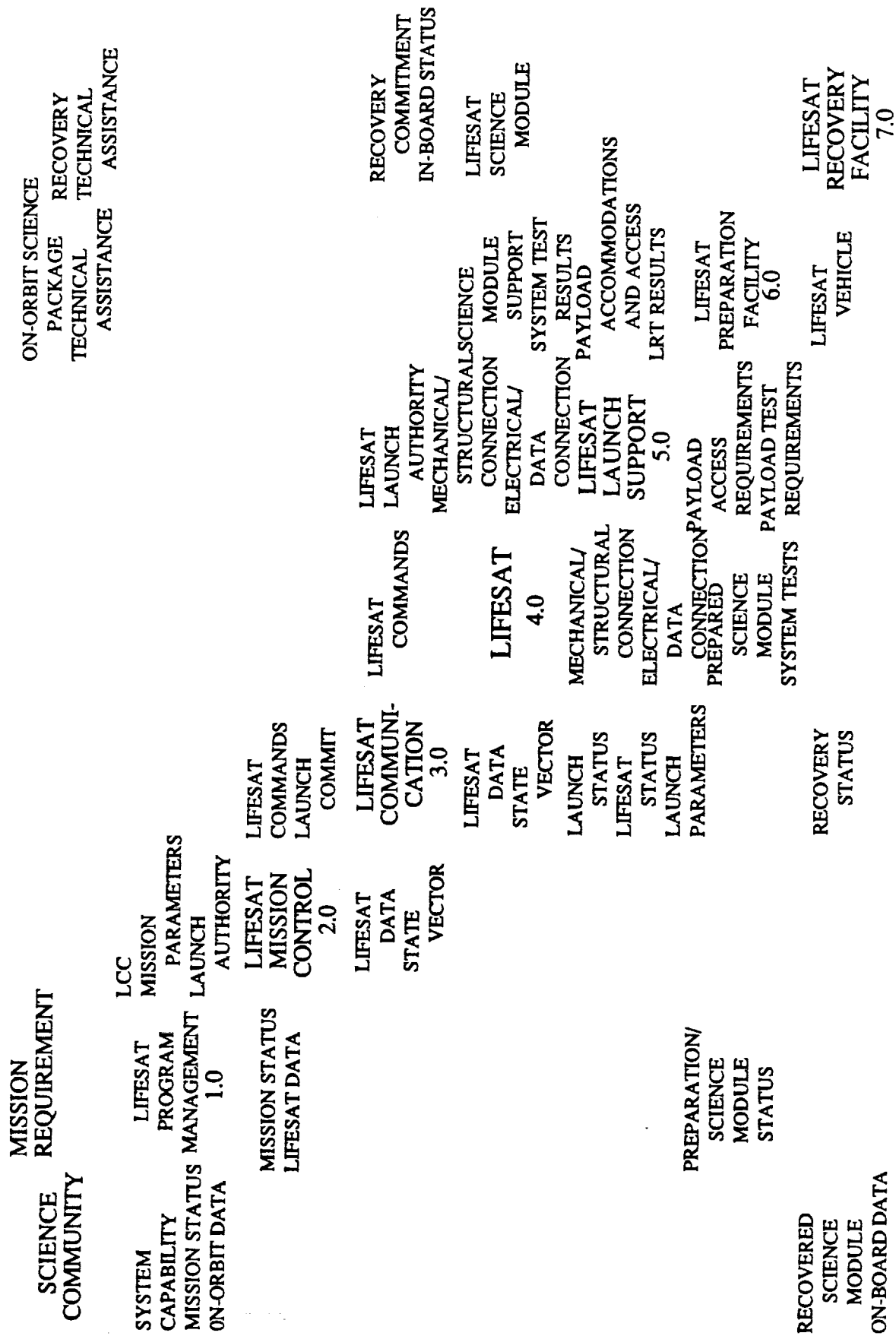
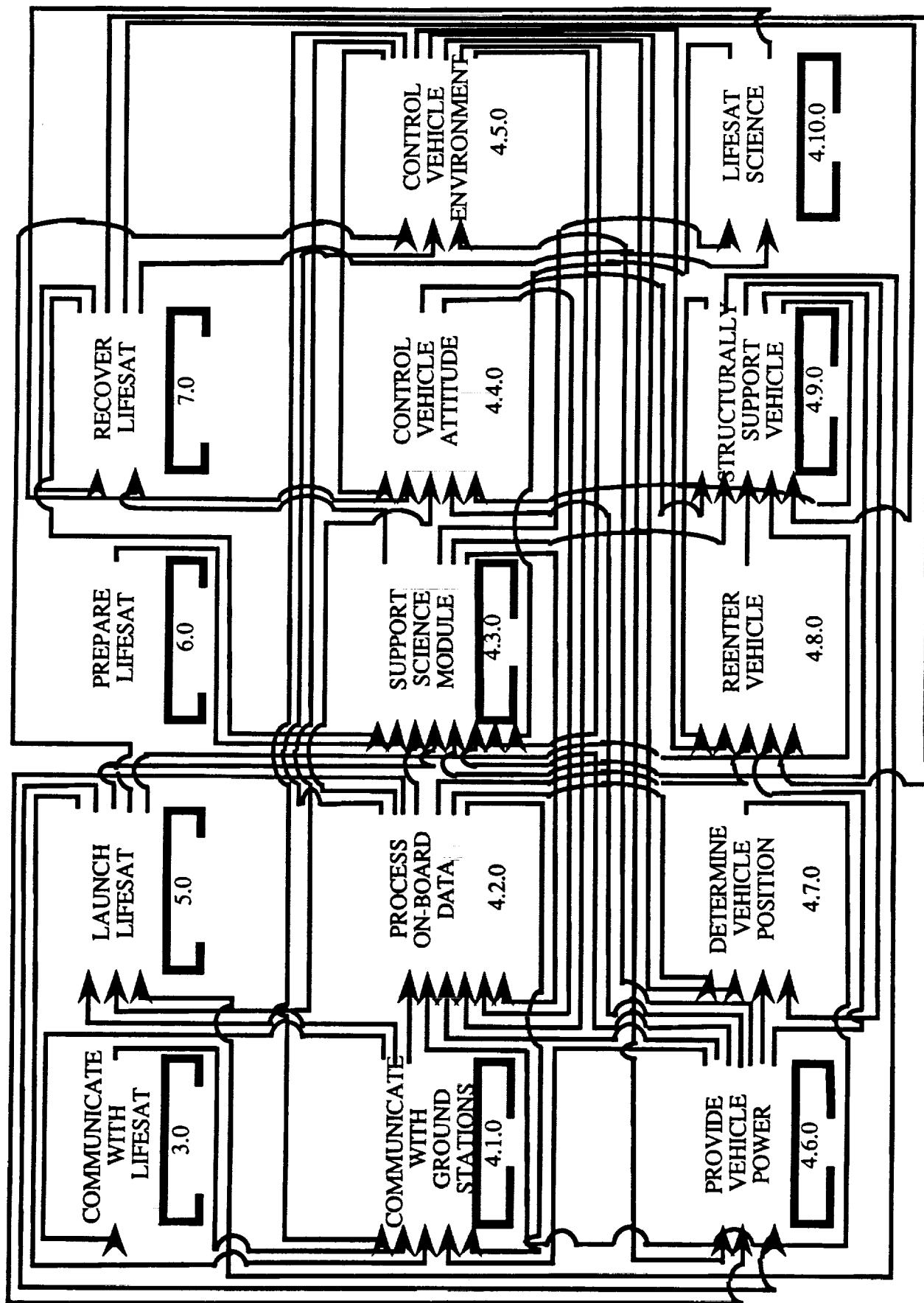


Figure B-2. LifeSat Level One Functional Interface N**2



* DOES NOT INCLUDE REFURBISHMENT COMPONENTS OR RECOVERY SERVICES. SEE 6.0 AND 7.0 FLOWS, RESPECTIVELY

Figure B-3. LifeSat Level One Functional Flow

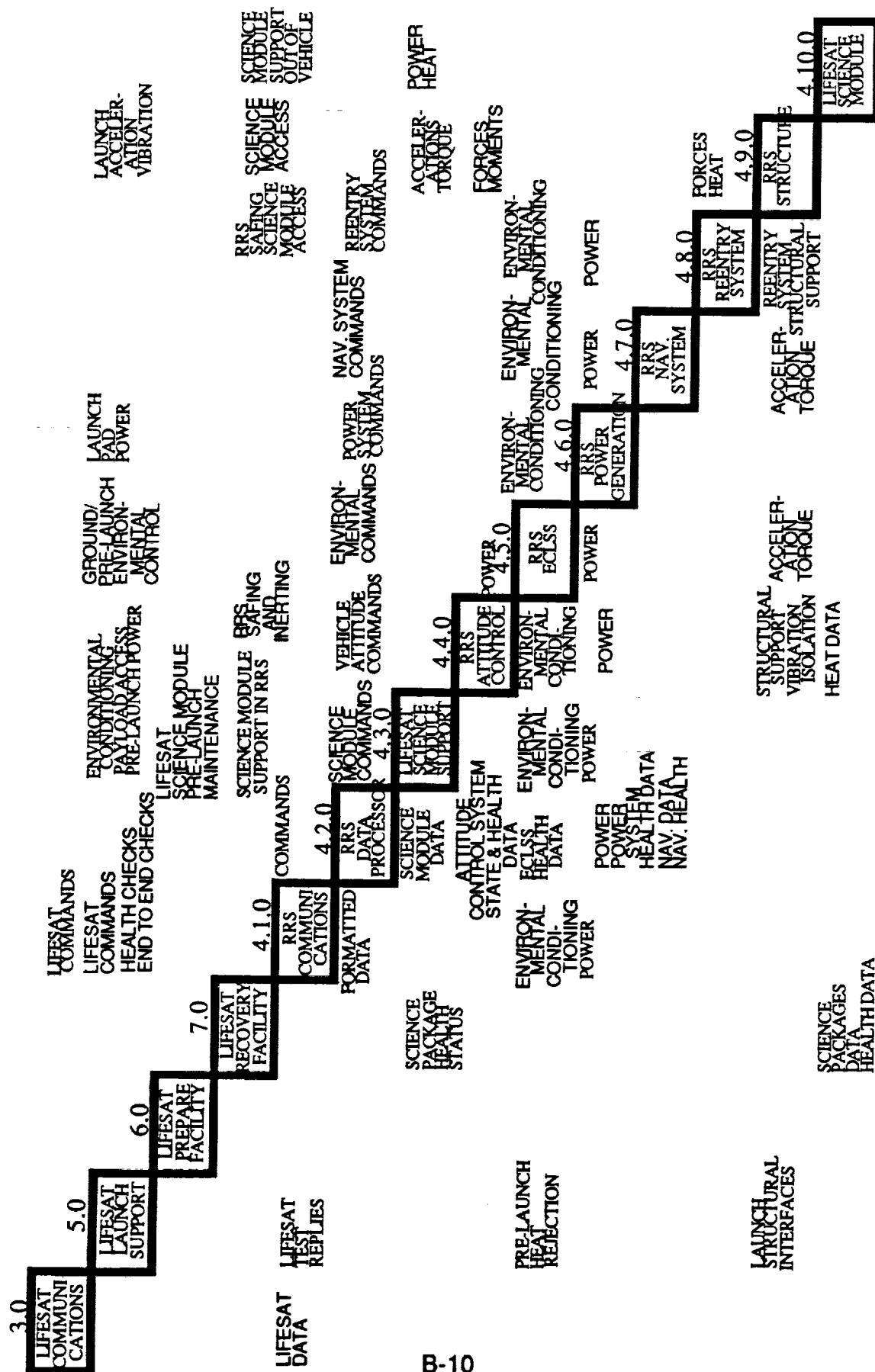


Figure B-4. LifeSat Level One Functional Interface N**2

APPENDIX C MASS AND DESIGN DETAILS

RRS	MASS (lbs)	No	Comments
SUBSYSTEM:			
1.0 Structure:	624.0		Contact Edward Robertson x36615
Primary Body Structure	624.0		Est. uses JSC baseline dimension data and areal density (lbs/ft ²)
Primary Structure	624.0	1	3.0 lbs/ft ² areal density, 208.0 ft ² wetted area
			Obtained from Heineman Body Structure plot ESTFOR14, min. manned
Subsystem Mounting Structure (info only)	328.8		Mounting and Installation mass summed from the subsystem data

RRS	MASS (lbs)	No	Comments
SUBSYSTEM:			
2.0 Protection:	444.1		Contact John (T.J.) Kowal x38871
Thermal Protection System (TPS)	444.1		
Spherical Nose Heat Shield	190.1	1	32 lb/ft ³ density ablator; 1.525" thick at nose, 1.027" thick at cone int.
Frustum Heat Shield	122.0	1	12 lb/ft ³ density FRCI-12 tile; 1.027" thick (uniform)
Base Heat Shield	57.9	1	0.386" thick
Attach hardware	74.0		20% of TPS mass
Insulation	0.0		Insulating blankets for the interior are being sized

RRS	MASS (lbs)	No	Comments
SUBSYSTEM:			
3.0 Propulsion:	227.0		Contact Ken Kroll, x39011, IMLEO = 4800 lbm assumed
Orbital Maneuvering System	211.5		SFT for engine firing/pressurant supply & propellant leakage
Deorbit Thrusters	14.0	4	Hamilton Standard REA 20-4, 125 lbf thrust, 232 sec ISP
Hydrazine Propellant Tanks	63.1	6	400 psi operating pressure, FS = 2, 0.7891 ft radius
Helium Pressurant Tanks	39.9	2	4000 psi operating pressure, FS = 2, 0.6595 ft radius
Thermal Shielding	20.0	1	
Plumbing	39.3	n/a	Relief/check valves, lines, orifices, disconnects for OMS & ACS
Mounting and Installation	35.2	n/a	20% of OMS subsystems. Includes brackets, fittings, etc.
Attitude Control System	15.6		
Thrusters	13.0	12	Rocket Research MR-50K, 5 lbf thrust, 220/170 sec ISP (steady/pulse)
Mounting and Installation	2.6	n/a	20% of ACS subsystems. Includes brackets, fittings, etc.

RRS	MASS (lbs)	No	Comments
SUBSYSTEM:			
4.0 Power:	215.0		Contact Eric Darcy x39055
Generation	172.0		
GaAs/Ge Solar Photovoltaic Array	45.7	2	Two deployable arrays, 28 ft ² per array, 0.951 ft ³
Array Deployment Mechanism	0.0		Deployment mechanism under study
Primary Batteries	78.0		0.951 ft ³ Lithium; sized for 6 hours of launch, descent and recovery
Secondary Batteries	19.6		0.275 ft ³ ; sized for on-orbit light/dark cycle (2:1 ratio) in a 90 min orbit
Mounting and Installation	28.7		20% of battery mass. Includes fittings and brackets.
Electrical Pwr Dist. & Control (EPDC)	43.0		DOES NOT include EPDC within other subsystems, 0.421 ft ³
EPDC Hardware	35.8		Estimated as 25% of power generation figure without mounting hardware
Mounting and Installation	7.2		

RRS SUBSYSTEM:	MASS (lbs)	No	Comments
6.0 Avionics:	376.1		Contact Paul Delaune 333-6808
<u>Guidance, Navigation and Control (GNC)</u>	208.6		117W of power for the on-orbit phase
Inertial Measurement Unit	84.1	3	Honeywell Lins GG1320-based, 1750A CPU
Horizon Sensor	6.3	3	Ithaco IPS-6 sensor
Horizon Sensor Electronics	10.3	3	Ithaco IPS-6 electronics
Sun Sensor	0.9	3	Adcole Model 18980 sensor
Sun Sensor Electronics	2.9	3	Adcole Model 18980 sensor electronics
Momentum Wheels	69.3	4	Honeywell - CTS, three orthogonal, one skewed
Mounting and Installation	34.8		
<u>Data Management System (DMS)</u>	80.4		
CPU System	24.0	2	8.0W
Disk Drive	4.0	2	6.0W
Multiplexer/Demultiplexer (MDM)	24.0	2	19.0W
Cabling	15.0	n/a	
Mounting and Installation	13.4		
<u>DMS Bay Enclosures</u>	10.0	2	Radiation protection for data acquisition & internal data bus
<u>Instrumentation</u>	14.4		
Accelerometers	12.0	2	
Mounting and Installation	2.4		
<u>Communications</u>	62.6		Contact Laura Hood/EE74 (x30121)
Transponder (Near-Earth, 2.5W RF)	14.4	2	Includes diplexer; 7.0W receive / 24.0W xmit & receive
RF Group	16.8	1	2.0W pulse during switching
GPS Receiver	20.0	2	Motorola Monarch GPS receiver, 15.0W
SARSAT Beacon System	1.0	1	26.0W peak, 7.0W standby
Mounting and Installation	10.4		20% of subsystem hardware mass

RRS SUBSYSTEM:	MASS (lbs)	No	Comments
7.0 Environment:	245.6		Contact Marybeth Edeen x39122
<u>Life Support System (LSS)</u>	95.6		
Circulation Fan	9.3	2	One redundant fan
Circulation Fan Motor	5.3	2	One redundant fan motor
Desiccant Bed	9.0	1	
ATCO	3.3	1	
Heat Exchanger	7.3	1	
O2 Storage Tank	25.6	1	
N2 Storage Tank	2.9	1	
He Storage	2.9	1	
H2O Storage Tank	8.8	1	
Food Storage	5.3	1	
Mounting and Installation	15.9		
<u>Thermal Control System</u>	150.0		Contact John Keller (333-6573)
Pumps and Motors	15.0	3	
Radiator	25.0	8	
Isolation valves	15.0	6	
Thermal Control Valves	15.0	6	
3/8" Tubing	10.0	1	200 feet
Accumulator	10.0	1	
Heat Exchangers (Air/Liquid)	20.0	4	
Flow Meters	5.0	3	
Tachometers	5.0	3	
Thermocouples	0.0	3	
Ammonia Pressure Vessel	5.0	1	
Mounting and Installation	25.0		Used a 20% figure rather than the 20 lbm given as input

RRS SUBSYSTEM:	MASS (lbs)	No	Comments
8.0 Other:	475.3		Contact Rob Meyerson x34629
<u>Landing and Recovery System</u>	475.3		
Parachute Assembly	217.0	1	
Impact & Recovery System	179.1	1	
Mounting Structure	79.2		20% of L&R subsystem hardware

RRS SUBSYSTEM:	MASS (lbs)	No	Comments
9.0 Growth:	391.1		15% of Dry Subsystem Masses
1.0 Structure	93.6		
2.0 Protection	66.6		
3.0 Propulsion	34.1		
4.0 Power	32.2		
6.0 Avionics	56.4		
7.0 Environment	36.8		
8.0 Other	71.3		

RRS DRY MASS	2,998	(lbs)
--------------	-------	-------

RRS SUBSYSTEM:	MASS (lbs)	No	Comments
10.0 Non-Cargo	148.8		Estimate by Ken Kroll x39011
<u>Reserve and Residual Fluids</u>	73.8		
OMS Propellant Reserves	29.7	6	
OMS Propellant Residuals	31.2	6	
ACS Propellant Reserves	3.7	6	
ACS Propellant Residuals	2.0	6	
OMS/ACS Tank Pressurant	7.1	3	
<u>Active Thermal System Fluids</u>	75.0		
Thermal System Fluid (R21)	25.0	n/a	Estimate provided 08/26/91 by John Keller (333-6573)
Ammonia	50.0	n/a	

RRS SUBSYSTEM:	MASS (lbs)	No	Comments
11.0 Cargo	883.0		Multi-payload capability, LSSWG req't for 400 kg allocation 50 kg estimated for pressure vessel, primary structure 200 kg allocation as given in requirements document Calculated to complete 400 kg (883 lbm) payload allocation Freezer as defined by John Keller
<u>General Biology Module</u>	883.0		
Pressure Vessel	110.4		
Centrifuge	441.6		
Middeck Lockers	78.8		
Freezer	80.0		
Radiation Detector/Carousel	15.0	1	
Interior/Exterior Radiation Detectors	10.0	2	
Mounting and Installation	147.2		
			20% of hardware mass

RRS INERT MASS	4,030	(lbs)
----------------	-------	-------

RRS SUBSYSTEM:	MASS (lbs)	No	Comments
12.0 Non-Propellant (Consumables)	57.3		Contact Marybeth Edeen x39122
Gaseous O2	10.2		
Gaseous N2	1.1	n/a	
Gaseous He	1.0	n/a	
LiOH Cannisters	18.6	4	
Liquid H2O	26.5	n/a	

RRS SUBSYSTEM:	MASS (lbs)	No	Comments
13.0 Propellant	631.6		Contact Ken Kroll, x39011.
OMS Propellant	594.6	6	
ACS Propellant	37.0	6	

RRS GROSS MASS	4,719	(lbs)
----------------	-------	-------

APPENDIX D LIFESAT GN&C AVIONICS COMPONENTS

		Mass	Power	Volume
NAVIGATION:				
IMU - Honeywell Lins GG1320 based	(1) ->	12.70 kg	70.0 W	0.260 X 0.216 X 0.165 m
IMU - Honeywell Lins HEXAD	(2) ->	27.20 kg	100.0 W	0.193 X 0.315 X 0.584 m
IMU/GPS - Honeywell IFMU	(3) ->	10.00 kg	34.0 W	0.180 X 0.193 X 0.274 m
Earth Sensor - Ithaco IPS-6	(4) ->	0.95 kg +1.55 kg	4.0 W 4.0 W	0.102 X 0.076 dia. (sensor) 0.152 X 0.178 X 0.076(elec)
Sun Sensor - Adcole Model 18980	(5) ->	0.14 kg +0.44 kg	incl. below 0.3 W	0.051 X 0.065 X 0.034(sens) 0.089 X 0.076 X 0.083(elec)
Radar Alt.	(6) ->	2.0 kg	25.0 W	0.079 X 0.188 X 0.097 m
GPS Receiver - Motorola Monarch	(7) ->	5.0 kg	20.0 W	0.140 X 0.175 X 0.203 m
Att/Pos Sensor - MANS Microcosm	(8) ->	1.25 kg +3.06 kg	incl. below 10.0 W	est. .0007 m ³ (sensor) est. .003 m ³ (elec)
Star Tracker - LLNL WFOV (9)	->	0.30 kg	3.2 W	0.180 X 0.180 X 0.250 m
Star Scanner - BASD CS-201	(10) ->	2.95 kg	1.9 W	0.495 X 0.457 X 0.356 m
CONTROL:				
Mom Wheel	(11) ->	7.85 kg	12.0 W	0.017 m ³

NOTES:

(1) - Accuracy (3 sigma): Accelerometer: misalignment = 12 arc sec, bias = 50 micro-g, scale fac = 175 ppm
 - Accuracy (3 sigma): gyro drift = .015 deg/hr, gyro scale factor = 30 ppm, random walk = .006 deg/hr
 - R&D activity will potentially reduce size from .009m³ to .005m³, mass from 12.7kg to 5kg, and power to 50 W

(2) - Two-fault tolerant. Reliability: 0.999978 for 100 hr mission. Space certified ?

(3) - MTBF: 3500 hrs. 1320 or 1308 IMU's. Includes optional P-Code, C/A Code GPS

(4) - Accuracy: .05° GEO to .1° LEO

(5) - Accuracy: .5° or less. FOV - 180° fan. MTBF: 4.4 E06 hrs. Max. spin rate 100 rpm.

(6) - Shuttle type.

(7) - Accuracy 50m/.07m/s (1-sig) C/A-code, 15m/.03m/s (1-sig) P-code. Parts level S. 6 channel. Cost approx. \$800k

(8) - Accuracy: 2 Sensors- after 1 sec Pos=5 km, Att=.05 deg; after 10 sec Pos=1.5 km, Att=.03 deg (3-sig) Targets Earth, Sun, and Moon. Pos requires Moon availability. Algorithms verified by CSDL. To be flight tested in 92. MTBF of 900,000 hours advertised for Barnes sensor in MANS.

(9) - Accuracy 40 arc sec, FOV 28° by 44°, star visual magnitude $m_v = 4.5$ or brighter needed for detection max. rot.rate 10 deg/s

(10) - Accuracy 10 arc min

(11) - Nominal power = 12 watt AC. Startup requires 50 watts AC. MTBF of 5 years advertised.

(1-10) 28 volt DC power source.

APPENDIX E

NAVIGATION STATE INTEGRATOR MODEL COMPARISON

ORBIT MODELS

The appropriate order of math model truncation was investigated for certain orbit-predicting programs. The simple math models compared with the TRAJ2 orbit were a J2 model, a 4 x 4 model, and a 6 x 6 model, while the integrator used was an NLZ66/stepsize of 60 seconds (assumed updates of 1 minute were often enough). Assuming no initial error, the desired accuracy was to be within 3 km as long as possible. A 350 km circular and 350 x 20,600 km elliptical orbit were analyzed. The reference orbit was generated by TRAJ2, a high fidelity orbit-predicting program. Models used by the reference were a 12 x 12 earth gravity model, Jacchia atmosphere, Sun/Moon perturbations, and solar radiation (for the elliptical orbit only). See reference 47 for details of the math models studied.

The analysis yielded the following speed/accuracy comparison of the math models.

<u>Math Model</u>	<u>Relative Time Between Updates</u>	<u>Hours before Error Exceeds 3 km -- (circular case)</u>
J2	1	4
4 x 4	11.25	8
6 x 6	21.25	9.2

For the elliptical case, errors associated with a J2 model are well within 1 km after 12 hours.

Since the 4 x 4 model can maintain the same accuracy as the J2 model for twice as long, it is a superior choice despite being 11 times as slow in CPU time. Because the 6 x 6 model maintains the same accuracy as the 4 x 4 for only 1.2 hours longer, and it is twice as slow in CPU time, the 4 x 4 model is the better choice. Because of the accuracy and CPU time requirements, the 4 x 4 model is the recommended choice for the circular orbit.

SELECTING AN INTEGRATOR

The following algorithms for integrators were compared: super g (sg), Runge-Kutta 3rd order (rk), Nystrom-Lear 3rd order (nlz33), Nystrom-Lear 6th order (nlz66). The stepsizes were varied for the integrators. To see how accurately the algorithm performed, the simple two-body gravity model (which has an analytical solution--thus the error in the integrator can be found) was used as the math model to integrate. See reference 48 for details of the state integrators studied. The testing yielded the results in table E-1.

TABLE E-1. INTEGRATOR/STEPSIZE COMPARISONS
(IN ORDER OF SPEED--FASTEST TO SLOWEST)

Integrator	Stepsize	Relative Time to Finish Integrating Over a Certain Delta t	Max. Error After 6 Hour Propagation (m)
nlz66	60	1.00	0.015 45
nlz66	30	2.00	0.000 266
sg	10	2.71	2 977.0
nlz33	10	2.76	122.9
rk	10	5.03	2 779.0
sg	5	5.42	838.9
nlz33	5	5.52	15.4
nlz66	10	6.00	1. 6 E-06
rk	5	10.06	347.6
nlz66	5	12.00	6.92 E-09
sg	1	27.09	36.6
nlz33	1	27.61	0.122 9
rk	1	50.32	2.782
nlz66	1	60.00	5. 8 E-07

The two fastest integrators/stepsize combinations (nlz66/stepsize 60 and nlz66/stepsize 30) are very accurate and either one is highly desirable. The only others that are more accurate are over three times as slow. Therefore, it is recommended that nlz66/stepsize 60 or nlz66/stepsize 30 be selected when knowledge of the state vector is not needed more often than once in 60 seconds or 30 seconds.

APPENDIX F

THERMAL PROTECTION SYSTEM

The TPS materials that have been used on reentry space vehicles fall in two major categories: ablative and reusable surface insulation (RSI). Ablative materials, or ablators, are high density, low conductivity materials that rely on the energy absorption which takes place during the chemical reaction of the material with the high temperature boundary layer gases to insulate the vehicle from the severe reentry heating. The first reaction, charring, occurs when the material reaches the charring temperature, which varies for the different ablative materials available. It is usually on the order of 1000°F. This reaction creates a layer of lower density material comprised mostly of carbon. The second reaction, surface recession, occurs when the charred material reacts with the oxygen in the flowfield to create gaseous by-products which are carried away in the flow.

Again dependent on the material, this process will begin when the temperature reaches approximately 2000°F. The rate of this reaction is directly related to the surface temperature of the material. As the surface temperature increases, the recession rate will increase, thus eroding more and more material. In addition to the low conductivity of the ablator and the energy absorbed by the chemical reactions, a third condition exists which serves to insulate the vehicle structure. The gaseous by-products entering the boundary layer impede the convective heating to the material's surface. The ablative materials can be used in environments resulting in surface temperatures up to ~6000°F.

There are many examples of RSI which were developed for and are currently in use on the orbiters. These include tile materials such as Lockheed Insulation (LI-900 and LI-2200) and FRCI-12, and exterior blanket insulation materials such as flexible reusable surface insulation (FRSI) and AFRSI. The tile materials are low density, amorphous, non-isotropic ceramic materials consisting mostly of silica fibers. The high porosity of the material makes radiation the primary heat transfer mode through the thickness of the material. This, coupled with the low thermal conductivity of the silica and the air within the tile, results in a material with a very low effective thermal conductivity. The HRSI tiles are coated with the reaction cured glass (RCG) coating, which consists of black borosilicate glass. The high emittance of the RCG coating allows the tile to re-radiate much of the absorbed energy. The HRSI tiles have been certified to 2300°F for 100 missions for the Space Shuttle Program. However, ground testing has shown the material to be capable of a one-mission use up to 2900°F, at which point the RCG coating begins to erode and the material becomes dimensionally unstable.

The FRSI and AFRSI materials are soft, flexible blanket materials which can be used on multimission vehicles. FRSI is Nomex felt-coated with a thin silicone elastomeric film. It has a multimission temperature limit of 750°F and a single mission limit of 900°F. AFRSI is comprised of a 4 pcf composite, fibrous, silica

batting sewn between two layers of white silica fabric. It has a multimission temperature limit of 1500°F and a single mission limit of 1800°F.

APPENDIX G ENVIRONMENTAL HEAT LOADS

Environmental heat loads originate from two sources: the Sun and the Earth. The solar portion is constant and can be easily determined. On the other hand, Earth-induced heat loads are not as easily determined and are strongly dependent upon orbital position and attitude. Since solar heating is substantially greater than Earth heating and the vehicle has a continuously Sun-pointing surface, the complexity of the problem is reduced.

ESTIMATION OF THE SOLAR HEAT LOADS

To estimate the solar heating, attention is directed to figure G-1, which shows a cutaway view of the Sun-pointing surface of the vehicle. Here, this surface is covered by a series of felt, TPS (exact material is not known at this time [50]), and solar cells. Since both the felt and the TPS are low conductivity materials ($k \approx 0.01$ Btu/ft-hr-R [51]), it should be expected that conduction (or the environmental heat load) through this insulating layer is small.

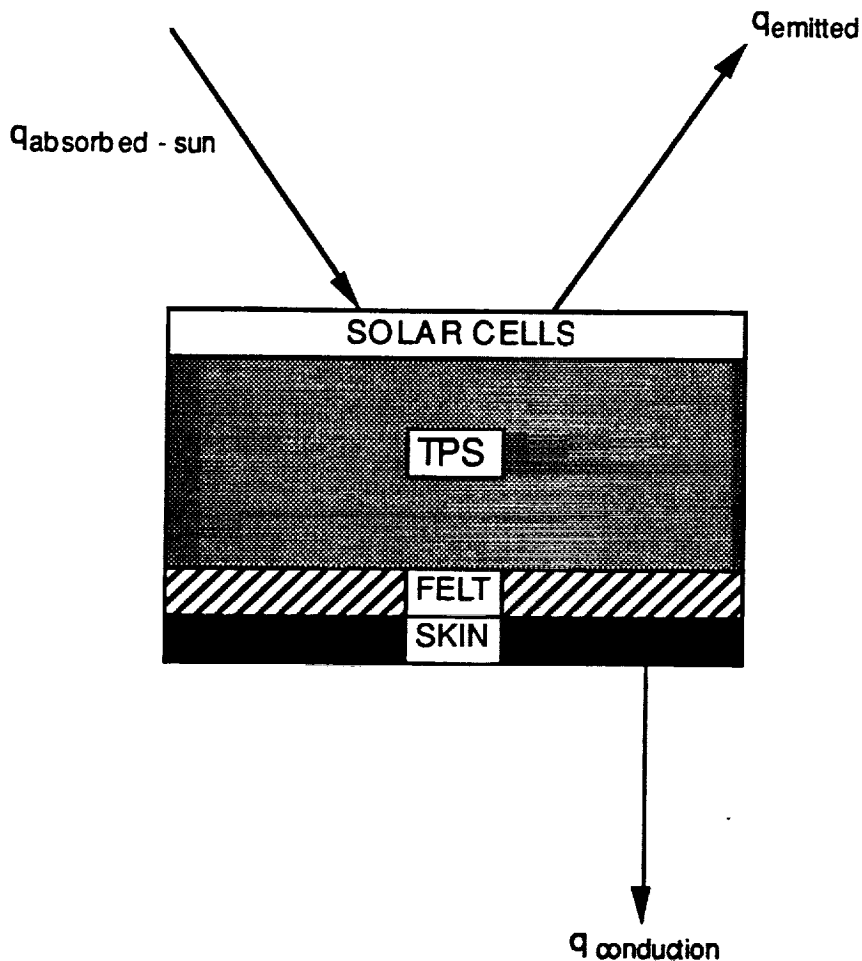


Figure G-1. Sectional View of the Vehicle

Using figure G-1 as a guide, an energy balance on a unit area basis yields the following equation for the solar environmental heat load,

$$Q_{\text{absorbed - sun}} = Q_{\text{emitted}} + Q_{\text{conduction}} \quad (1)$$

where $Q_{\text{absorbed - sun}}$ is the absorbed solar energy, Q_{emitted} is the reradiated vehicle energy, and $Q_{\text{conduction}}$ is the conductive heat flux to the vehicle's inner surface. Rewriting equation (1) in terms of the appropriate temperature relationships found in Reference 41 gives,

$$\alpha Q_{\text{solar}} = \epsilon \sigma T_s^4 + k(T_s - T_{\text{int}})/L \quad (2)$$

where α is the surface absorptivity of the solar radiation, Q_{solar} is the solar flux, ϵ is the emissivity, σ is the Stefan-Boltzmann constant, T_s is the surface temperature, k is the conductivity, L is the thickness and T_{int} is the desired internal temperature. In writing equation (2), it is assumed that the Sun-pointing surface is always perpendicular to the incoming solar radiation, that the vehicle reflected radiation is negligible, and that the system has reached steady-state conditions. For the LifeSat vehicle, with $\alpha = 0.64$ [6,7], $Q_{\text{solar}} = 462.0 \text{ Btu/hr-ft}^2$ [55], $\epsilon = 0.8$ [54], $\sigma = 0.1718 \times 10^{-8} \text{ Btu/ft}^2\text{-hr-R}^4$ [55], $k = 0.01 \text{ Btu/ft-hr-R}$ [51], $L = 0.75 \text{ inch}$ [50], and T_{int} held at 70°F , the Sun-pointing surface surface temperature is estimated to be 210°F . Using the conduction portion of equation (2), $k(T_s - T_{\text{int}})/L$, an area of 34 ft^2 , and the surface temperature of 210°F , the environmental heat load is estimated to be 760 Btu/hr (225W).

While the solar heat load is relatively small and controllable, the high backside temperature can create several problems. First, solar cells will not operate efficiently at temperatures over 200°F [42]. Second, if the radiator panels are located near this high temperature source, radiative heat transfer will be severely reduced. To avoid these problems, the solar cells should be relocated in deployable arrays (this has been done, see paragraph 5.10), which allows their backside to efficiently reject heat by radiation, and the Sun-pointing surface should be coated with a low absorptivity, high emissivity material ($\alpha/\epsilon < 0.175$, several materials of this type may be found in Reference 43). If these changes are made, the temperature of the solar cells and the Sun-pointing surface will be 100°F and 0°F , respectively, and the solar heat load will be negligible.

ESTIMATION OF THE EARTH HEAT LOADS

The thermal radiation a vehicle receives from the Earth consists of a solar component and an Earth-emitted component. The emitted component is due to typical thermal emissions and consists primarily of long wavelength radiation, while the solar component is reflected sunlight and consists primarily of short wavelength radiation. Since the absorption process is wavelength dependent [44], any analysis of the Earth-induced heat load must account for these

variations in absorption. For this system, the percentage of solar energy absorbed is given by the absorptivity, while the percentage of Earth-emitted energy absorbed is given by the emissivity [45].

The Earth-induced heat load can be determined using the same approach as that used for the Sun-pointing surface of the vehicle. That is, an energy balance, again using figure G-1 as a guide, can be performed on the outer wall. This analysis leads to the following equation

$$Q_{\text{absorbed - Earth}} = Q_{\text{emitted}} + Q_{\text{conduction}} \quad (3)$$

where $q_{\text{absorbed - Earth}}$ is the absorbed energy coming from the Earth, q_{emitted} is the reradiated vehicle energy, and $q_{\text{conduction}}$ is the conductive heat flux to the vehicle's inner surface. Writing equation (3) in terms of temperature for steady-state conditions gives,

$$F_{ij}(\epsilon q_{\text{Earth}} + \alpha a q_{\text{solar}}) = \epsilon \sigma T_s^4 + k(T_s - T_{\text{int}})/L \quad (4)$$

where the new terms F_{ij} , a , and q_{Earth} denote the view factor, albedo, and Earth emission, respectively. For the Earth viewing section of the vehicle, $a = 0.8$ [6,7], $q_{\text{solar}} = 462.0 \text{ Btu/hr-ft}^2$ [44], $\epsilon = 0.8$ [43], $\sigma = 0.1718 \times 10^{-8} \text{ Btu/ft}^2\text{-hr-R}^4$ [44], $k = 0.01 \text{ Btu/ft-hr-R}$ [40], $L = 1.0 \text{ inch}$ [39], α is 0.3 [45], F_{ij} is 0.85 (as determined from reference 46, using a minimum altitude of 170 miles), and q_{Earth} is 77 Btu/hr-ft^2 [45]. When the internal temperature, T_{int} , is held at 70°F , the surface temperature of the forward section is estimated to be 75°F , producing an environmental heat load of 100 Btu/hr (30W).

SUMMARY OF THE ENVIRONMENTAL HEAT LOAD DATA

Preliminary estimates show that Earth-induced heat loads have a negligible effect in the design of the thermal control system; however, solar heat loads are important. If solar heating is not controlled, vehicle performance will be severely affected. Specifically, the solar cells will overheat and the radiators of the thermal control system will not perform effectively, if at all. To overcome these problems, the solar cells must be put into deployable arrays and the Sun-pointing surface of the vehicle coated with a high emissivity, low absorptivity material. With this simple design, the solar cells will be well below their maximum operating temperature, and the radiator panels will perform efficiently.

TABLE G-1. LIFESAT NONORBIT HEAT BUDGET

	Prelaunch	Ascent	Reentry	Recovery
Payloads	150W	150W	150W	150W
Avionics	35W	50W	290W	35W
ECLSS	110W	120W	150W	110W
Propulsion	0W	5W	140W	0W
Comm and Track	0W	30W	40W	20W
Electrical Losses	50W	50W	50W	50W
Environmental	0W	0W	?	?
Total	345W	405W	820W	365W
Time	5 days	3.0 hr	6.0 hr	4.0 hr
Total Heat Removal	41400W-hr	1215W-hr	4920W-hr	1460W-hr

TABLE G-2. THERMAL STORAGE SYSTEM WEIGHTS

Cooling Method	Prelaunch	Ascent	Reentry	Recovery
Wax pack	1770lbm	52lbm	210lbm	65lbm
Liquid N2 Boiler	940lbm	27lbm	111lbm	20lbm
Ammonia Boiler	256lbm	7.5lbm	30.5lbm	10lbm

**TABLE G-3. WEIGHT, VOLUME AND COST ESTIMATES
FOR THE LIFESAT VEHICLE**

Main TCS

Item	Number	Weight (lbm)	Volume (ft3)	Cost (\$)
Pumps	3	15	0.3	1500
Radiator Panels	8	25	0.5*	8000
Isolation Valves	6	15	0.15	1000
Thermal Control Valves	6	15	0.15	3000
3/8" Tubing	200ft	10	0.5	1000
Accumulator	1	10	0.1	2000
Heat Exchangers	4	20**	0.20	1000**
Flow Meters	3	5	0.1	500
Tachometers	3	5	0.1	500
Thermocouples	3	0	0.0	0
Mounting Hardware	?	15	0.2	1000
Subtotal (DRY)		135	1.80	19500
(WET)		160	1.80	21500

Thermal Storage System

Ammonia		50		1000
Pressure Vessel	1	5	1.40	2000
Subtotal		55	1.40	3000
System Total (DRY)		180	3.20	23500
(WET)		205	3.20	24500

* External Volume

**Will be less if cold plates are used

**TABLE G-4. PAYLOAD MODULE REFRIGERATION
SYSTEM ESTIMATES**

Item	Number	Weight (lbm)	Volume (ft3)	Cost (\$)
Refrigerator	2	80	1.5	10000
Mounting Equipment	?	10	0.15	1000
Total		90	1.65	11000

APPENDIX H
SUBSYSTEM COMPONENT DUTY CYCLE ASSUMPTIONS

	PWR (W)	SPEC	DUTY CYCLES				
			PRE- LAUNCH	LAUNCH	STEADY STATE	LANDING	POST- LANDING
PROTECTION							
PROPULSION							
OTHER							
Liquid Valve	75	1	0	0	0	0	0
Liquid Valve	75	2	0	0	0	0	0
Liquid Valve	75	3	0	0	0	0	0
Liquid Valve	75	4	0	0	0	0	0
Liquid Valve	75	5	0	0	0	0	0
Liquid Valve	75	6	0	0	0	0	0
Liquid Valve	75	7	0	0	0	0	0
Liquid Valve	75	8	0	0	0	0	0
Liquid Valve	75	9	0	0	0	0	0
Liquid Valve	75	10	0	0	0	0	0
Liquid Valve	75	11	0	0	0	0	0
Liquid Valve	75	12	0	0	0	0	0
Liquid Valve	75	13	0	0	0	0	0
Liquid Valve	75	14	0	0	0	0	0
Liquid Valve	75	15	0	0	0	0	0
Liquid Valve	75	16	0	0	0	0	0
Liquid Valve	75	17	0	0	0	0	0
Liquid Valve	75	18	0	0	0	0	0
Pressure Transducer	0.5	1	0	0	0.1	1	0
Pressure Transducer	0.5	2	0	0	0.1	1	0
Pressure Transducer	0.5	3	0	0	0.1	1	0
Pressure Transducer	0.5	4	0	0	0.1	1	0
Pressure Transducer	0.5	5	0	0	0.1	1	0
Pressure Transducer	0.5	6	0	0	0.1	1	0
Pressure Transducer	0.5	7	0	0	0.1	1	0
Pressure Transducer	0.5	8	0	0	0.1	1	0
Pressure Transducer	0.5	9	0	0	0.1	1	0
Pressure Transducer	0.5	10	0	0	0.1	1	0
Temp. Transducer	0.5	1	0	0	0.1	1	0
Temp. Transducer	0.5	2	0	0	0.1	1	0
Temp. Transducer	0.5	3	0	0	0.1	1	0
Temp. Transducer	0.5	4	0	0	0.1	1	0
Temp. Transducer	0.5	5	0	0	0.1	1	0
Temp. Transducer	0.5	6	0	0	0.1	1	0
Temp. Transducer	0.5	7	0	0	0.1	1	0
Temp. Transducer	0.5	8	0	0	0.1	1	0
Temp. Transducer	0.5	9	0	0	0.1	1	0
Temp. Transducer	0.5	10	0	0	0.1	1	0
Temp. Transducer	0.5	11	0	0	0.1	1	0
Temp. Transducer	0.5	12	0	0	0.1	1	0
Temp. Transducer	0.5	13	0	0	0.1	1	0
Temp. Transducer	0.5	14	0	0	0.1	1	0
Temp. Transducer	0.5	15	0	0	0.1	1	0
Temp. Transducer	0.5	16	0	0	0.1	1	0

			DUTY CYCLES				
	PWR (W)	SPEC	PRE-LAUNCH	LAUNCH	STEADY STATE	LANDING	POST-LANDING
Temp. Transducer	0.5	17	0	0	0.1	1	0
Temp. Transducer	0.5	18	0	0	0.1	1	0
Temp. Transducer	0.5	19	0	0	0.1	1	0
Temp. Transducer	0.5	20	0	0	0.1	1	0
Temp. Transducer	0.5	21	0	0	0.1	1	0
Temp. Transducer	0.5	22	0	0	0.1	1	0
Temp. Transducer	0.5	23	0	0	0.1	1	0
Temp. Transducer	0.5	24	0	0	0.1	1	0
Temp. Transducer	0.5	25	0	0	0.1	1	0
Temp. Transducer	0.5	26	0	0	0.1	1	0
Temp. Transducer	0.5	27	0	0	0.1	1	0
Temp. Transducer	0.5	28	0	0	0.1	1	0
Hydrazine Heater	10	1	0	0.5	1	0.5	0
ACS							
ACS Thruster Valve	9	1	0	0	0.1	0.1	0
ACS Thruster Valve	9	2	0	0	0.1	0.1	0
ACS Thruster Valve	9	3	0	0	0.1	0.1	0
ACS Thruster Valve	9	4	0	0	0.1	0.1	0
ACS Thruster Valve	9	5	0	0	0.1	0.1	0
ACS Thruster Valve	9	6	0	0	0.1	0.1	0
ACS Thruster Valve	9	7	0	0	0.1	0.1	0
ACS Thruster Valve	9	8	0	0	0.1	0.1	0
ACS Thruster Valve	9	9	0	0	0.1	0.1	0
ACS Thruster Valve	9	10	0	0	0.1	0.1	0
ACS Thruster Valve	9	11	0	0	0.1	0.1	0
ACS Thruster Valve	9	12	0	0	0.1	0.1	0
ACS Thruster Valve	9	13	0	0	0.1	0.1	0
ACS Thruster Valve	9	14	0	0	0.1	0.1	0
ACS Thruster Valve	9	15	0	0	0.1	0.1	0
ACS Thruster Valve	9	16	0	0	0.1	0.1	0
ACS Thruster Catalyst	0.2	1	0	0	0	0.3	0
ACS Thruster Catalyst	0.2	2	0	0	0	0.3	0
ACS Thruster Catalyst	0.2	3	0	0	0	0.3	0
ACS Thruster Catalyst	0.2	4	0	0	0	0.3	0
ACS Thruster Catalyst	0.2	5	0	0	0	0.3	0
ACS Thruster Catalyst	0.2	6	0	0	0	0.3	0
ACS Thruster Catalyst	0.2	7	0	0	0	0.3	0
ACS Thruster Catalyst	0.2	8	0	0	0	0.3	0
ACS Thruster Catalyst	0.2	9	0	0	0	0.3	0
ACS Thruster Catalyst	0.2	10	0	0	0	0.3	0
ACS Thruster Catalyst	0.2	11	0	0	0	0.3	0
ACS Thruster Catalyst	0.2	12	0	0	0	0.3	0
ACS Thruster Catalyst	0.2	13	0	0	0	0.3	0
ACS Thruster Catalyst	0.2	14	0	0	0	0.3	0
ACS Thruster Catalyst	0.2	15	0	0	0	0.3	0
ACS Thruster Catalyst	0.2	16	0	0	0	0.3	0

	PWR (W)	SPEC	DUTY CYCLES				
			PRE- LAUNCH	LAUNCH	STEADY STATE	LANDING	POST- LANDING
Pressurant Valve	75	1	0	0	0	0.1	0
Pressurant Valve	75	2	0	0	0	0.1	0
Pressurant Valve	75	3	0	0	0	0.1	0
Pressurant Valve	75	4	0	0	0	0.1	0
Pressurant Valve	75	5	0	0	0	0.1	0
Pressurant Valve	75	6	0	0	0	0.1	0
Pressurant Valve	75	7	0	0	0	0.1	0
Pressurant Valve	75	8	0	0	0	0.1	0
Pressurant Valve	75	9	0	0	0	0.1	0
OMS							
Deorbit Thruster Valve	30	1	0	0	0	0.2	0
Deorbit Thruster Valve	30	2	0	0	0	0.2	0
Deorb Thruster Catalyst	7.6	1	0	0	0	0.55	0
Deorb Thruster Catalyst	7.6	2	0	0	0	0.55	0
Deorb Thruster Catalyst	7.6	3	0	0	0	0.55	0
Deorb Thruster Catalyst	7.6	4	0	0	0	0.55	0
Deorb Thruster Catalyst	7.6	5	0	0	0	0.55	0
STRUCTURE							
POWER							
DISTRIBUTION							
Elec. Power Dist. & Cntrl	50	1	1	1	1	1	1
CONTROL							
AVIONICS							
GN&C							
IMU-Honeywell GG1320	70	1	0	0	1	1	0
IMU-Honeywell GG1320	70	2	0	0	0	1	0
IMU-Honeywell GG1320	70	3	0	0	0	1	0
Ithaco IPS-6 Hbr. Sens.	4	1	0	0.5	0	0.2	0
Ithaco IPS-6 Hbr. Sens.	4	2	0	0.5	0	0.2	0
Ithaco IPS-6 Hbr. Sens.	4	3	0	0.5	0	0.2	0
Horiz. Sens. electronics	4	1	0	0.5	0	0.2	0
Horiz. Sens. electronics	4	2	0	0.5	0	0.2	0
Horiz. Sens. electronics	4	3	0	0.5	0	0.2	0
Sun Sens-Adcole 18980	0	1	0	0.5	0	0.2	0
Sun Sens-Adcole 18980	0	2	0	0.5	0	0.2	0
Sun Sens-Adcole 18980	0	3	0	0.5	0	0.2	0
Sun Sensorelectronics	0.3	1	0	0.5	0	0.2	0
Sun Sensorelectronics	0.3	2	0	0.5	0	0.2	0
Sun Sensorelectronics	0.3	3	0	0.5	0	0.2	0
GPS Receiver-Motorola	20	1	0	0	0.05	1	0
GPS Receiver-Motorola	20	2	0	0	0	1	0
GPS Receiver-Motorola	20	3	0	0	0	0	0

			DUTY CYCLES				
	PWR (W)	SPEC	PRE- LAUNCH	LAUNCH	STEADY STATE	LANDING	POST- LANDING
Honeywell - Mom. Wheel	12	1	0	0	1	0	0
Honeywell - Mom. Wheel	12	2	0	0	1	0	0
Honeywell - Mom. Wheel	12	3	0	0	1	0	0
Honeywell - Mom. Wheel	12	4	0	0	0	0	0
DMS							
Central Processing Unit	10	1	1	1	1	1	1
Random Access Mem.	5	1	1	1	1	1	1
Disk Drive	8.4	1	1	1	1	1	1
Disk Drive	8.4	2	1	1	1	1	1
Accelerometer	6.1	1	0	0	1	0	0
Accelerometer	6.1	2	0.1	1	0	1	0.1
GN&C Processing Unit	15.8	1	0	0	0	0	0
INSTRUMENT							
Rad. Detector/Carousel	20.5	1	0	0	1	0	0
Int./Ext. Radi. Detector	20	1	0	0	1	0	0
Int./Ext. Radi. Detector	20	2	0	0	1	0	0
C&T							
S-Band Transponder	19	1	0	1	0.4	1	0
High Power Amplifier	125	1	0	0	0	0	0
S-Band Transmitter	35	1	0	0	0	0	0
S-Band Receiver	8.4	1	0	1	1	1	0
Switch Assembly	2	1	0	1	1	1	0
SARSAT Transmitter	17	1	0	0	0	0.5	1
ENVIRONMENT							
LSS							
Circulation Fan Motor	50	1	1	1	1	1	1
Circulation Fan Motor	50	2	0	0	0	0	0
Fan/Separator Motor	40	1	0	0.2	1	0.9	0
TCS							
Pump & Motor Assembly	10	1	1	1	1	1	1
Pump & Motor Assembly	10	2	0	0	0	0	0
Refrigeration System	50	1	1	1	1	1	1
Controls	1	1	1	1	1	1	1
OTHER							
PAYLOAD							
Payload	150	1	1	1	1	1	1
GROWTH							
TOTAL POWER (Watts)			343	404	601	818	360

APPENDIX I
DETAILED LOC AND COMPLEXITY ESTIMATE

LIFESAT FLIGHT SOFTWARE DEVELOPMENT SPREADSHEET

The following spreadsheet provides a detailed estimate of the LifeSat flight software implementation in terms of functional decomposition, estimated lines of C code, and level of difficulty for each software component identified to satisfy currently known requirements and allocated to system functions and sub-functions identified above.

<u>LifeSat FLIGHT S/W</u>	<u>LOC</u>	<u>Lvl.</u>
<u>LifeSat EXECUTIVE</u>		
<u>INTERRUPT PROCESSING (Supplied by O. S.)</u>	500	High
<u>CUSTOM PAYLOAD DEVICES SERVICE PROCESSING:</u>	1000	High
Initialization	300	Medium
Power-up Configuration	300	Medium
<u>OPERATING SYSTEM SERVICES (Supplied by O.S.):</u>	2500	High
<u>TASK SCHEDULER (Supplied by O. S.):</u>	2500	High
<u>MODE CONTROL:</u>		
Mode Selection	500	Medium
Stand-by Mode Processing	200	Medium
Mode Transition	200	Medium
EXECUTIVE LOC Est. SUBTOTAL:	8000	
<u>GUIDANCE, NAVIGATION & CONTROL</u>		
<u>GN & C FUNCTION MANAGEMENT:</u>	300	High
<u>GN & C REDUNDANCY MANAGEMENT:</u>	1100	High
<u>VEHICLE HEALTH & SAFING:</u>	700	High

<u>ATTITUDE DETERMINATION:</u>		
Vehicle Spin Rate Determination	200	High
Star Tracker Device Service & Processing	800	Medium
Angular Rate Estimator	200	Medium
Horizon Sensor Interface Processing	200	High
Sun Sensor Interface Processing	300	High
<u>ATTITUDE CONTROL:</u>		
Attitude & Rate Control Law processing	200	Medium
On-Orbit Attitude Correction processing	300	High
Spin-up/De-spin Command processing	200	High
On-Orbit Spin Rate Correction Processing	200	High
Reaction Control System I/F Processing	100	High
Momentum Wheels I/F Processing	300	High
<u>NAVIGATION:</u>		
Inertial Measurement Unit I/F Processing	200	High
Global Positioning System I/F Processing	300	High
Kalman Filter Processing	700	Medium
Precision Orbit Determination	600	Medium
Precision Location Determination	800	High
<u>GUIDANCE:</u>		
Precision Re-entry Control	1600	High
Pre-Deorbit Processing Processing	500	High
Deorbit/trim Burn Processing	400	High
Main Engines Interface Processing	300	High
Pre-entry Processing	300	High
Main Chute Deployment Interface Processing	200	High
GN&C LOC Est. SUBTOTAL:		11000

<u>LifeSat TELEMETRY, TRACKING & CONTROL</u>		
<u>TELEMETRY:</u>		
Downlink Data Gathering	1000	Low
Downlink Data Packetizing	1000	Medium
Downlink Data Transmission	200	Medium
Uplink Command Receiving	200	Medium
<u>TRACKING</u>		
Antenna Selection	300	High
Beacon Transmission	150	High
<u>CONTROL</u>		
Uplink Command Decoding	500	Medium
Uplink Command Validation	200	Medium
Uplink Command Execution	1500	High
TELEMETRY, TRACKING & CONTROL SUBTOTAL:		5050
<u>LifeSat FAILURE MANAGEMENT</u>		
<u>CYCLIC FAILURE MONITORING:</u>		
CPU Monitor	300	Medium
Payload Monitor	300	High
Propulsion Control System Monitor	300	High
Communications Control System Monitor	300	High
Power System Monitor	300	Low
Thermal Control System Monitor	300	High

<u>FAILURE PROCESSING:</u>		
Failure Analysis	1000	High
Failure Recording	500	Low
Failure Recovery Processing	1000	High
<u>FAILURE RESETS:</u>	1500	High
FAILURE MANAGEMENT LOC Est. SUBTOTAL:	5800	
<u>LifeSat DATA ACQUISITION & STORAGE</u>		
<u>RADIATION DETECTOR DATA I/F PROCESSING:</u>	200	Medium
<u>PROPULSION DATA I/F PROCESSING:</u>	150	Medium
<u>MISSION DATA BASE MANAGEMENT:</u>	300	Low
<u>PAYLOAD MODULE DATA INTERFACE PROCESSING:</u>	1000	Low
<u>ACCELEROMETER DATA INTERFACE PROCESSING:</u>	150	Low
DATA ACQUISITION & STORAGE Est. SUBTOTAL:	1800	
<u>Flight S/W Est. TOTALS:</u>	31650	

APPENDIX J

TABLE J-1. DELTA II PRELAUNCH ACTIVITIES

Day	Tasks
L-6	Transportation to the launch site and erection Mating of the RRS/upper stage to the Delta II lower stage
L-5	ELV flight program verification test F-0 Day simulation (minus count, launch mode, and plus count Power ON stray voltage test
L-4	Delta II vehicle ordnance installation and connection Preparations for fairing installation
L-3	RRS final preparations prior to fairing installation Delta II upper stage closeout Preparations for propellant servicing Fairing installation
L-2	Delta II propellant loading of the second stage
L-1	Tasks include Delta II vehicle system checkout Delta II and RRS vehicle arming Final fairing preparations for MST removal Delta II final vehicle preparations
L-0	Gantry removal Final arming Terminal sequences Launch

TABLE J-2. THE RRS PRELAUNCH TIMELINE

Event (duration)	MET (d:hh:mm:ss)
Mate RRS/upper stage to lower stage	- 06:07:00:00
Uncan RRS (2 hours)	- 06:14:30:00
<i>Begin RRS operations (place holder)</i>	- 06:11:00:00
Begin shroud installation (optional)	- 06:11:00:00
End shroud installation	- 06:09:30:00
<i>End RRS operations (place holder)</i>	- 06:03:00:00
Begin F-0 Day simulation	- 05:16:30:00
End F-0 Day simulation	- 05:15:00:00
Communication check (15 minutes)	- 05:15:00:00
Minus count (1.5 hours)	- 05:14:45:00
RRS in launch mode	- 05:12:00:00
Plus Count (1.5 hours)	- 05:11:30:00
Power ON (30 minutes)	- 05:09:45:00
Power ON Stray Voltage Test (2 hours)	- 05:09:00:00
Begin shroud removal (optional)	- 03:20:00:00
End shroud removal	- 03:19:00:00
Begin fairing installation	- 03:15:00:00
Fairing Air ON	- 03:13:00:00
End fairing installation	- 03:11:30:00
Load mice (45 minutes)	- 00:17:30:00
Turn on CPU #1	- 00:17:30:00
Turn on circulation fan	- 00:17:30:00
MST removal	- 00:12:45:00
Switch to internal power	- 00:01:00:00
Final systems check (10 minutes)	- 00:00:45:00
Turn on GN&C CPU and align IMU	- 00:00:30:00
Turn on accelerometer #1	- 00:00:01:00
Unplug ground-based cryogenic cooling, power, and data umbilicals	- 00:00:00:00

TABLE J-3. THE RRS LAUNCH TIMELINE

Event	Relative Timing	MET (d:hh:mm:ss)
ETR Launch (2:00 pm local time)		00:00:00:00
Main solid motor ignition (6 solids)		00:00:00:00
Solid motor burnout (6 solids)		00:00:00:57
Solid motor ignition (3 solids)		00:00:01:03
Solid motor separation (3/3 solids)		00:00:01:05
Solid motor burnout (3 solids)		00:00:02:00
Solid motor separation (3 solids)		00:00:02:05
MECO		00:00:03:44
Stage II ignition		00:00:03:57
Fairing separation		00:00:04:27
SECO 1		00:00:08:49
Turn on centrifuge		00:00:09:00
Turn on fan/separator		00:00:09:00
Stage II engine restart		00:00:16:17
SECO 2		00:00:16:40
Spacecraft separation	Sep	00:00:20:50
Separation attitude change (if necessary)	Sep + ~14 min	00:00:34:50
Separation maneuver	Sep + ~15 min	00:00:35:50
Sun and horizon sensor realignment	Sep + ~15 min	00:00:35:50
IMU alignment	Sep + ~20 min	00:00:40:50
Orbital trim maneuver (if necessary)	Sep + ~21 min	00:00:41:56
Acquire proper attitude	Sep + ~25 min	00:00:45:56
Deploy solar panels	Sep + ~26 min	00:00:46:56

TABLE J-4. THE RRS LANDING PHASE TIMELINE

Event	Relative Timing	MET (d:hh:mm:ss)
Start GPS update every 30 sec.	Burn-(1 rev + 30 min)	59:18:08:02
Turn off centrifuge	Burn-(1 rev + 25 min)	59:18:13:02
CMG desaturation (if necessary)	Burn-(1 rev + 20 min)	59:18:18:02
Update horizon and sun sensors	Burn-(1 rev + 15 min)	59:18:23:02
Orbit adjust attitude change	Burn - 1 rev	59:18:38:02
Orient attitude for deorbit	Burn - 10 min	59:19:58:02
Turn on accelerometer #2	Burn - 1 min	59:20:07:02
Turn off accelerometer #1	Burn - 1 min	59:20:07:02
Eject solar panels	Burn - 1 min	59:20:07:02
Deorbit burn ignition	Burn	59:20:08:02
Deorbit burn cutoff	Cutoff	59:20:13:36
Turn off fan/separator	Cutoff + 30 sec	59:20:14:00
Velocity residual trim man. (if nec.)	Cutoff + 2 min	59:20:15:36
EI error correction (@ 15 min.)	EI - 1 min	59:20:23:30
Entry spin-up (21 sec. duration)	EI - 30 sec	59:20:24:00
Entry interface	EI	59:20:25:23
Turn off radiation detectors	EI + 30 sec	59:20:26:00
Spin-down (21 sec. duration)	EI + 1.5 min	59:20:27:00
Turn on SARSAT Beacon	EI + 2.5 min	59:20:28:00
Drogue deployment	M = 1.5	59:20:29:39
Seal propellant system		59:20:30:00
Parachute deployment (10K ft MSL)	altitude = 10 K ft MSL	59:20:31:16
Touchdown (8:34 am local time)	TD	59:20:34:00

TABLE J-5. THE RRS POSTLANDING PHASE TIMELINE

Event	Relative Timing	MET (d:hh:mm:ss)
Turn off COMM system except SRSAT Beacon	TD + 1 min	59:20:35:00
Turn off GN&C	TD + 1 min	59:20:35:00
Locate and recover RRS	TD + 15 min	59:20:49:00
Safe vehicle	TD + 20 min	59:20:54:00
Attach transport device and cryogenic cooling	TD + 40 min	59:21:14:00
Helicopter transport to PI	TD + 120 min	59:22:34:00
Turn off circulation fan, DMS, & internal power	Remove - 1 min	59:22:48:30
Remove payload module	TD + 135 min	59:22:49:00
Sunset		59:29:35:00

REPORT DOCUMENTATION PAGE			Form Approved OMB No. 0704-0188	
Public reporting burden for this collection of information is estimated to average 1 hour per response, including the time for reviewing instructions, searching existing data sources, gathering and maintaining the data needed, and completing and reviewing the collection of information. Send comments regarding this burden estimate or any other aspect of this collection of information, including suggestions for reducing this burden, to Washington Headquarters Services, Directorate for Information Operations and Reports, 1215 Jefferson Davis Highway, Suite 1204, Arlington, VA 22202-4302, and to the Office of Management and Budget, Paperwork Reduction Project (0704-0188), Washington, DC 20503.				
1. AGENCY USE ONLY (Leave blank)		2. REPORT DATE July 1992		3. REPORT TYPE AND DATES COVERED Technical Memorandum
4. TITLE AND SUBTITLE LifeSat Engineering In-House Vehicle Design			5. FUNDING NUMBERS	
6. AUTHOR(S) Robert Spann, et al				
7. PERFORMING ORGANIZATION NAME(S) AND ADDRESS(ES) Systems Engineering Division National Aeronautics and Space Administration Johnson Space Center Houston, Texas 77058			8. PERFORMING ORGANIZATION REPORT NUMBER S-685	
9. SPONSORING / MONITORING AGENCY NAME(S) AND ADDRESS(ES) National Aeronautics and Space Administration Washington, D.C. 20546-001			10. SPONSORING / MONITORING AGENCY REPORT NUMBER NASA-TM-104752	
11. SUPPLEMENTARY NOTES				
12a. DISTRIBUTION / AVAILABILITY STATEMENT AVAILABLE ONLY WITH APPROVAL OF ISSUING OFFICE: R.Spann JSC/IA Subject Category 15			12b. DISTRIBUTION CODE	
13. ABSTRACT (Maximum 200 words) The LifeSat program was initiated to research the effects of microgravity and cosmic radiation on living organisms. The effects of long-term human exposure to free-space radiation fields over a range of gravitational environments has long been recognized as one of the primary design uncertainties for human space exploration. A critical design issue in the radiation biology requirements was the lack of definition of the minimum radiation absorbed dosage required to produce statistically meaningful data. The Phase A study produced a spacecraft conceptual design resembling a Discoverer configuration with a total weight of approximately 2800 pounds that would carry a 525-pound payload module (45 inches in diameter and 36 inches long) and support up to 12 rodents and a general biology module supporting lower life forms for an on-orbit duration of up to 60 days. The Phase B conceptual designs focused on gravitation biology requirements and only briefly addressed the design impacts of the shift toward radiobiological science that occurred during the latter half of the Phase B studies.				
14. SUBJECT TERMS long-term human exposure, Discoverer configuration, payload module, general biology module, free-space radiation fields, gravitational environments			15. NUMBER OF PAGES	
			16. PRICE CODE	
17. SECURITY CLASSIFICATION OF REPORT Unclassified	18. SECURITY CLASSIFICATION OF THIS PAGE Unclassified	19. SECURITY CLASSIFICATION OF ABSTRACT Unclassified	20. LIMITATION OF ABSTRACT SAR	